ULTRASTRUCTURE OF CEPHALIC MALE CILIA OF *CAENORHABDITIS ELEGANS*: DEVELOPMENT AND SPECIALIZATION

By

MALAN SHARANGA SILVA

A dissertation submitted to the

Graduate School-New Brunswick

and

The Graduate School of Biomedical Sciences

Rutgers, The State University of New Jersey

In partial fulfillment of the requirements

For the degree of

Doctor of Philosophy

Graduate Program in Microbiology and Molecular Genetics

Written under the direction of

Maureen M. Barr, Ph.D.

And approved by

_____

_____

_____

_____

New Brunswick, New Jersey

May 2017

ABSTRACT OF THE DISSERTATION

Ultrastructure of cephalic male cilia of *Caenorhabditis elegans*: development and specialization

By MALAN SHARANGA SILVA

Dissertation Director: Maureen Barr, Ph.D.

Cilia are ubiquitous eukaryotic organelles. The medical importance of cilia is underscored by the growing list of diseases caused by cilia defects, called ciliopathies. In the past several decades, researchers uncovered the basic molecular machinery required to build all cilia. Despite the fact they they're built by the same "core" set of proteins, cilia exhibit a plethoric diversity of morphology, structure and function. How this ciliary diversity is generated is not well understood. To address this question I used serial transmission electron microscopy and electron tomography to reconstruct cephalic male (CEM) cilium in wild-type *Caenorhabditis elegans* and mutants that altered CEM cilia shape and function.

I found that CEM cilia contain a novel and specialized microtubule arrangement (Chapter 1). Inner core of most cilia contains microtubule doublets (dMT), each composed of a complete A-tubule and an incomplete B-tubule. In CEM cilia, these doublet microtubules splay to form A- and B-tubule singlet microtubules (sMT) that are attached to each other at their ends, forming a splayed doublet, a structural feature partially conserved in mammalian sperm flagella. I found that a cell specific alpha tubulin isoform TBA-6 is required for the splayed doublet microtubule

architecture in CEM cilia. In *tba-6* loss of function mutants, doublet A- and B- tubules remain associated with each other, thereby defaulting to their commonly observed state in other cilia types. Loss of CEM cilia-specific microtubule ultrastructure correlates with perturbation of certain ciliary proteins' localization, of shedding rate, composition and signaling of cilia-derived extracellular vesicles, and of cilia-specific coordination of ciliary microtubule-based motors. We conclude that the splayed dMTs are a specific architectural feature of CEM cilia axoneme that regulates ciliary shape, motor-based transport and EV protein composition. In addition, formation of this CEM cilia-specific ultrastructure requires a specific isoform of alpha tubulin TBA-6.

To understand how the splayed dMT is generated, I characterized CEM cilia ultrastructure undergoing development in larval males (Chapter 2). I found intact (fully fused) dMT in developing CEM cilia up to the adult stage. This suggests that the splayed dMT architecture is achieved by splaying of the intact doublets rather than coming together of separate sMTs. I also discovered that some of ciliary dMTs are formed in the absence of visible basal body microtubules. In the absence of visible basal body, CEM ciliary dMTs are established by first forming the complete A-tubule and subsequent addition of the incomplete B-tubules. I found that length and volume of CEM cilia are established at different rates: while the length of CEM cilia are established by few pioneering microtubules by larval stage 4, generation of adult CEM ciliary volume occurs later, during larval-adult transition, and coincides with fully formed ciliary microtubule core and sexual maturation of the male. Together, these findings may provide novel insights in interpreting microtubule ultrastructure phenotypes in pathological cilia.

To summarize part I of this dissertation (Chapters 1 and 2), ultrastructural characterization of adult CEM cilia revealed a novel aspect of ciliary specialization – remodeling of doublet microtubules in ciliary microtubule core as well as novel features of ciliogenesis: progressive addition and asynchronous extension of microtubule doublets to the growing ciliary axoneme in the absence of visible basal body microtubules. Changes in CEM cilia-specific microtubule ultrastructure in *tba-6* mutants coincide with the loss of ciliary specialization, illustrating the role of a specific tubulin isoform in determining specialized ciliary structure and function.

Part II of this dissertation consists of major collaborative studies. They are arranged chronologically.

In chapters three and six, I describe the discovery of posttranslational microtubule glutamylation as a second genetic mechanism to generate splayed doublet architecture and B-tubule singlets in CEM cilia. In chapter four, I reexamined the data from chapter three (O'Hagan *et al.* 2011) and conducted additional TEM studies to conclude that the splayed doublet architecture of CEM cilia requires a "Goldilocks" level of posttranslational glutamylation. With excessive polyglutamylation (in *ccpp-1* mutants), B-tubules completely separate from the A-tubules; while without glutamylation (in *ttll-11* mutants), B-tubules remain oddly attached to their A-tubule partners. These phenotypes are not CEM-specific In amphid channel cilia microtubule doublets are present in distal region of *ttll-11* mutants, where only A-tubule singlets are found in wild type. Together, these results demonstrate that glutamylation-based regulation of ciliary B-tubule architecture may be a common mechanism to define specialized ciliary structural identity.

In chapter four, my TEM studies extended the previous observations by Natalia Morsci to resolve polycystin accumulations at CEM cilia base. My ultrastructural data showed that PKD-2::GFP accumulations seen under light microscope were discrete vesicles trapped in the lumen outside the cilium. In wildtype CEM cilia, these vesicle-based accumulations were rare, but present. In mutants isolated in Young Bae's screen for defects of ciliary targeting of PKD-2::GFP (Cil phenotype), these vesicles accumulated upwards of ten-fold compared to wild type. Additionally, my serial section TEM and electron tomography-based characterization of multiple *cil* mutants reveled the existence of two types of vesicles populations in CEM sensilla: smaller-sized EVs at the level of the axoneme that may be released to the outside environment, and larger-sized EVs that are found in the lumen surrounding the cilia base. Wang *et al*. 2014 established CEM cilia as a model to study extracellular vesicle (EV) biology. My TEM and tomography data provided corroborating ultrastructural evidence and insight to the otherwise vague phenotype of PKD-2::GFP accumulation in distal dendrite/cilia region observed using light microscopy.

TEM results summarized in Chapter Five are one of the many mutants that I fixed, sectioned and characterized (at low resolution). These mutants were chosen based on the RNAseq experiments by Dr. Maureen Barr and included: *lov-1*, *pkd-2*, *trf-1*, *trf-2*, *tag-232*, and *pmk-1*. *pmk-1* was chosen because it has the "reverse Cil" phenotype: level of PKD-2::GFP at the ciliary base is reduced (rather than increased) compared to wild type. My TEM results corroborated these observations and additionally revealed that *pmk-1* mutants have less than nine dMTs in CEM transition zones. Together with TEM characterization of the developing CEM axoneme, these

findings formed the empirical basis of the hypothesis that CEM cilia phenotype of *pmk-1* mutants is immature (underdeveloped) cilia phenotype, rather than degeneration phenotype. Moreover these findings illustrate that cilium development could be genetically uncoupled from organism development.

To summarize part II of this dissertation (Chapters 3 to 6), I discovered that balanced level of tubulin glutamylation is required for specific B-tubule architecture of ciliary axoneme in two different cilia types (CEM and amphid channel). My serial TEM and tomography-based characterization of the complete CEM sensillum revealed that it contains two different populations of extracellular vesicles based on size and location.

How are cilia specialized? My thesis work based on CEM cilia revealed cilia-specific axoneme microtubule architecture and its role in contributing to cilia-specific functions. TEM studies of CEM cilia revealed that cell-specific tubulin alpha tubulin isotype six is required for splayed doublet ultrastructure in CEM cilia. Posttranslational glutamylation regulates the architecture in both CEM and Amphid cilia via regulating the stability of B-tubules. Therefore mechanisms that regulate B-tubule architecture contribute to ciliary structural and functional specialization.

List of Abbreviations

CEM	cephalic male
CEM sensillum	CEM cilia containing sensillum
Cil	ciliary localization defective
dMT	doublet microtubule
ET	electron tomography
EV	extracellular vesicles
HPF	high pressure freeze fixation
MT	microtubule
PCMC	periciliary membrane compartment
sMT	singlet microtubule
SEM	scanning electron microscopy
TEM	transmission electron microscopy
TZ	transition zone

Acknowledgments

Thank you, Maureen, Dave, and Abbi, for believing in me, supporting me, and challenging me through the years. I am forever grateful.

Chris and Barth for their generosity and insight.

Charles and Johanna Busch Fellowship (2012-16), and University and Louis Bevier Dissertation fellowship (2016-17).

Barr Lab, for being my home for the past six years; Juan and Bob for advice and support.

Hall Lab, for being my second home for the past five years; Ken for being a patient and supportive EM guru!

Diane Murano, and those who have had my back through the years-I am grateful!

Natalia, for supporting me and continuing to infuse me with an ever-positive attitude, I couldn't have made it without you.

To my Amma and Thaththa, love.

Table of Contents

Index of Figures

Chapter 5

Chapter 6

Introduction

What are cilia?

Cilium (plural, cilia) is derived from the Latin word for eyelash and aptly describes the morphology of the most commonly found cilia type in human body: primary cilia (Figure 1a). Primary cilia are found in most non-dividing human cells and protrude away from the cell surface; much like an eyelash from an eyelid. Cilia are membrane-covered protuberances with a microtubule inner core. These are eukaryotic organelles that are ubiquitously found from protozoan to mammalian phyla (Vincensini, Blisnick, & Bastin, 2012). Despite the simple morphology of a primary cilium, cilia are morphologically diverse and highly specialized sensory organelles of a cell that house a variety of signaling molecules required for receiving and transmitting extracellular signals.

Cilia and human health

Cilia are of profound medical interest (Pan, Wang, & Snell, 2005). Thanks to the extensive research in the past several decades, cilia have been promoted from the status of a "vestigial organelle" to the "site of focused cellular reception – a cellular antenna of sorts". Fast-forward to the present day, when the recognition of cilia's importance in human health is driven by an ever-growing list of human diseases caused by cilia dysfunction and therefore collectively called ciliopathies (Waters & Beales, 2011). In mammals, cilia are required for development; complete loss of cilia results in embryonic arrest (Ref). Thus, ciliopathies are caused by mutations in a fraction of all possible ciliary genes, only those that allow for embryonic survival.

Ciliary scaffold: tubulins, microtubule singlets, doublets, and triplets

Microtubules are indispensible for eukaryotes. They constitute a major portion of cellular cytoskeleton that is the basis of many cellular processes including growth and maintenance of cilia (Barisic & Maiato, 2016; Cearns, Escuin, Alexandre, Greene, & Copp, 2016; Kapitein & Hoogenraad, 2015). Microtubules are composed of α- and β-tubulin heterodimers arranged into protofilaments that form cylinders (Figure 2a) (Dutcher, 2001; Wade, 2009). There are two schools of thought regarding how these cylinders form. One stipulates that microtubules are helical polymers, and that tubulin heterodimers are helically added to the growing polymers (Desai & Mitchison, 1997). The alternative hypothesis is that a microtubule is formed by inwardly curved lattice sheath of tubulin heterodimers. (Pampaloni & Florin, 2008). Given the intermediate structures seen in ciliary microtubules (Chapter 1 Figure 1, Chapter 6 Figure 7), and for the purposes of this dissertation, microtubules are considered to be curved lattices.

Microtubules also form higher-order structures such as doublets (commonly found in cilia) and triplets (found in centrosome-derived basal body) (Figure 2b). A microtubule doublet is composed of a 13-protofilament "A" tubule and, fused to it, 10 or 11-protofilament "B" tubule. How the number of protofilaments within A- and B- tubules of a doublet microtubule is determined is not well understood. However, tubulin isotype composition (Raff, Fackenthal, Hutchens, Hoyle, & Turner, 1997) and tubulin posttranslational modifications such as acetylation (Topalidou et al., 2012) are known to affect the protofilament numbers in cytosolic singlet microtubules.

The ciliary axoneme: all cilia share conserved structural features

The ciliary axoneme, a microtubule core ensheathed by ciliary membrane, is stereotypical for all cilia (Figure 3). When viewed at a cross-section of cilia base, the axoneme consists of nine microtubule doublets arranged in a circle and anchored to the ciliary membrane via Y-shaped multi-protein structures aptly named Y-links. This region is called the transition zone (TZ) and serves as a selective entryway to ciliary plasma. Depending on the type of cilium, there may also be a variable number of singlets in the middle of the ring formed by doublets at the TZ (Doroquez et al., 2014). These singlets are called "the inner singlets" and are of unknown function in sensory cilia. In motile cilia, such as in *Chlamydomonas* flagella, these singlets function in motility and are found in two per axoneme (Ringo, 1967). Moving towards the middle of the cilium, microtubule doublets lose the Y-links that restrain them to the membrane and, perhaps as a consequence, lose their cylindrical arrangement. This region of a cilium is called "the doublet region" or "the middle segment". Middle segment doublets extend to the tip of the cilium and, in some cilia types, A-tubules of the dMTs extend to form distal singlet region while B-tubules unravel from one of the seams and terminate thus marking the end of the doublet region (Figure 3).

Cilia are functionally and structurally diverse

Cilia are perhaps the most diverse cellular organelle of all (Figure 1). As a whole, all cilia are sensory organelles. Cilia are sub-specialized to sense physical pressure, temperature, many different types of soluble or volatile chemicals, oxygen, and light. Ciliary morphological diversity parallels their functional diversity. For example, primary

cilia have simple morphology: long flexible thread-like cylinders protruding from the cell surface. Other types, like rods and cones that detect specific wavelengths of light in human retina, have more complex morphology with many membrane stacks regularly shed (Figure 1). Some cilia can also function to direct fluids across cell surfaces or as cellular propellers. Long mono or bi cilia that propel unicells across fluids, such as those found in *Chlamydomonas* and in mammalian sperm, are called flagella. Cilia that rhythmically beat to move fluids along cellular surfaces, such as on human airway epithelium, are called motile cilia. It should be noted that both motile cilia and flagella are essentially sensory cilia with an additional kinetic specialization.

Historically, ciliary axonemes were viewed as one of either of the two classes: 9+2 for motile cilia/flagella, and 9+0 for sensory cilia. These numbers indicate the number of circularly arranged microtubule doublets + the number of inner singlets when viewed in cross section at the cilia base. These designations were primary based on detailed ultrastructural characterization of *Chlamydomonas* flagella, a classical 9+2, and primary cilia in cultured cells that have 9+0 configuration. In light of the growing body of serial TEM data on a variety of cilia types that do not neatly sort into either 9+0 or 9+2 class, I propose that this nomenclature has since become outdated.

All cilia share a conserved cohort of proteins for their formation and maintenance

Despite the diversity in form and function, all cilia depend on one core group of conserved proteins called intraflagellar transport (IFT) complex that consists of microtubule motors and cargo adaptors required for transport of ciliary proteins and construction of cilia (Cole et al., 1998; Cornils et al., 2016). The IFT complex consists of

biochemically, genetically, and functionally separable IFT-A and IFT-B particles (Cole et al., 1998; Piperno, Siuda, Henderson, & Segil, 1998). These IFT particles are transported anterogradely towards cilium tip by kinesins, and retrogradely towards the cilia-base by dyneins. Heterotrimeric kinesin II, the core IFT motor, is required for formation of all cilia and is deeply conserved. In higher order taxa, and in cilia of distinct morphology and function, anterograde transport is modulated by additional accessory kinesins (Mukhopadhyay et al., 2007).

Although it was previously thought that IFT motors could not differentiate between axonemal microtubule tracks, recent reports show that kinesin II-driven anterograde transport in *Chlamydomonas* flagella is restricted to B-tubules, while retrograde dynein-driven transport uses A-tubules of microtubule doublets(Pigino et al., 2009; Stepanek & Pigino, 2016). Heterotrimeric kinesin II is the sole anterograde IFT motor in *Chlamydomonas*. These results complement findings in cells with additional accessory anterograde kinesins, such as in *C. elegans* amphid channel cilia. In these cilia, heterotrimeric kinesin II is restricted to the doublet region while accessory kinesin OSM-3 transports IFT particles into the distal A tubule-based singlet region (Perkins, Hedgecock, Thomson, & Culotti, 1986; Scholey, 2012).

The tubulin code

Microtubules that make up ciliary axoneme are biochemically distinct. According to tubulin hypothesis, the primary mechanism of generating these distinctions is the combinatorial use of different tubulin isotypes (Cleveland, 1987; McKean, Vaughan, & Gull, 2001). These tubulins can be further modified via post-translational modifications (PTMs):

transient or stable addition of glutamate, acetyl, tyrosine, glycine, palmitoyl, and phosphate groups (Westermann & Weber, 2003). Tubulin PTMs can be erased by tubulin-modifying enzymes such as cytosolic carboxypeptidase deglutamylases that remove glutamylates from microtubules (Mukai et al., 2009). Tubulin code posits that specific tubulin isoforms and their PTMs represent a molecular code that can be read and interpreted by cellular factors to coordinate microtubule ultrastructure, signal transduction and regulation of microtubule motors within a cell (Janke, 2014; Roll-Mecak, 2014; Verhey & Gaertig, 2007) (Yu, Garnham, & Roll-Mecak, 2015).

C. elegans CEM cilia as a model to study ciliary specialization

Cilia are generally indispensible for vertebrate embryonic development. The model organism *C. elegans* can develop and live without cilia in laboratory conditions. Thus, *C. elegans* is uniquely suited for genetic interrogation of the relationship between ciliary structure and function. In *C. elegans,* cilia are only found in the context of the nervous system, but nonetheless are morphologically diverse and perform a variety well-characterized sensory functions (Doroquez et al., 2014). Cilia of cephalic male-specific (CEM) neurons have several unique specific features: CEMs have genetically-regulated stereotypic sinusoid shape (Figure 4), express an additional cell type-specific ciliary kinesin-3 KLP-6 and α-tubulin TBA-6, and also release extracellular vesicles (EVs) in IFT-dependent manner (Hurd, Miller, Núñez, & Portman, 2010; Peden & Barr, 2005; J. Wang et al., 2014).

Novel specialized MT feature of CEM cilia axoneme

CEM cilia have a distinctive microtubule ultrastructure that requires alpha tubulin six (TBA-6). In CEM, the ciliary axoneme has a modified doublet microtubule region: A- and B-tubules of the nine microtubule doublets splay to form a region of 18 microtubule singlets consisting of nine A-tubule and nine B-tubule singlets. In the past, B-tubule singlets have been observed in the the flagella tips of mammalian spermatozoa (Figure 6), suggestive of a conserved but unexplored ciliary feature (Afzelius, Dallai, Lanzavecchia, & Bellon, 1995; L I Binder, 1975; Woolley & Nickels, 1985). My discovery of this structure in *C. elegans* allowed dissection of the molecular mechanism driving this ciliary specialization (Chapters 1-3 and 6).

What is the function of splaying MT doublet architecture in CEM cilia?

In Chapter 2, I describe the axonemal ultrastructure of wild type CEM and identification of α-tubulin isotype TBA-6 as a requirement for splaying doublets. CEM cilia of *tba-6* mutants lack splayed microtubule doublets. Instead, *tba-6* CEM cilia contain a longer doublet region at the distal end of which B-tubules discontinue. To test the consequences of these changes in axonemal ultrastructure on ciliary function, we tested three processes as readouts of CEM cilia specialization and function: 1) localization of ciliary gene products (Barr et al., 2001) (Maguire et al., 2015; J. Wang et al., 2015), 2) coordination of IFT motors and particles (Morsci, 2011), and 3) composition, release, and bioactivity of CEM cilia-derived extracellular vesicles (EVs) (J. Wang et al., 2014). We found that the core ciliary processes are affected to a lesser degree while processes specific to CEM cilia are grossly affected (see chapter 2 for more details). These results suggest that

tba-6 is required for CEM ciliary specialization aspects which include axonemal ultrastructure, localization of ciliary proteins, cilia specific IFT motor-cargo interactions, and EV biology.

Existing models of ciliogenesis

In cycling cells, cilium projects from the daughter centriole (Sorokin, 1962) during the S-phase of the cell cycle. Currently, there are two established models of ciliogenesis (Williams et al., 2011). Both of these models suggests that centrosomal microtubules template all nine axonemal microtubule doublets simultaneously, and that cilium growth and final length is established via synchronous extension of all nine axoneme microtubules from the base to the tip of the cilium. These models are based primarily on ultrastructural studies in Chlamydomonas and in ex vivo and in vitro cultured cells. These two models, although widely accepted, may not be universal. For example, cilia in C. elegans are not associated with centrioles in adult animals (Doroquez et al., 2014). Although there is some ultrastructural evidence to suggest that nascent cilia are associated with centrioles (wormatlas.org), whether or not this is definitive for all worm cilia remains unresolved.

A study of CEM cilia development

In Chapter 2, I examined CEM axoneme ultrastructure in younger larval stages and concluded that development of CEM ciliary axoneme deviates from the two well-established ciliogenesis in several aspects. First, larval CEM cilia begin with fewer than 9 microtubule doublets in the axoneme, progressively adding more doublets as the organism develops. Second, new axonemal doublets appear despite the visible absence

of centriolar microtubules. Third, these doublets extend along cilium asynchronously and do not have the structural dMT splaying feature seen in adult CEM cilia. Fourth, CEM cilium reaches full (adult) length before it generates the splayed microtubule feature seen in adult CEM cilia (see Chapter 2 for details). My data suggests that splayed microtubule doublet ultrastructure of CEM cilia is established by first generating intact doublets, and then partially unzipping them in the middle to generate A- and B-tubule singlets. Fifth, the inner singlet microtubules are absent in developing axoneme, suggesting that they are a feature of mature cilia. Perhaps these unexpected results are due to the inherent characteristics specific to CEM cilia development. Alternatively, the intermediate ciliogenesis steps seen in CEM cilia may reflect sub-steps of ciliogenesis present in all cilia, but that may have missed due to the shorter ciliogenesis timeline in other models. CEM neurons have an extended developmental gap between nascent and mature cilia. My data suggest that although CEM cilia are born at larval stage 2, they become structurally complete and functional only in adults.

Summary

In summary, this dissertation work utilizes *C. elegans* model to investigate the role of axonemal microtubules in cilia specialization. Using TEM and electron tomography, I discovered a novel axonemal microtubule arrangement in CEM cilia where doublet microtubules splay to from A- B-tubule singlets, and identified alpha tubulin TBA-6 (Chapter 1) and microtubule polyglutamylation (Chapters 3 and 6) as requirements for this arrangement. I discovered that posttranslational glutamylation is required B-tubule

ultrastructure of doublet microtubules in both CEM and amphid cilia. By looking at CEM cilia in larval animals using TEM and tomography, I provide data in support of sub-steps in ciliogenesis that maybe useful in interpreting defective axonemes in pathological conditions. By generating and characterizing serial TEM and tomography volumes of wild type CEM sensilla, I provided critical insight into the discovery that established CEM cilia as a model to study extracellular vesicle biology (Chapter 4 and 5), and discovered that there are two distinct populations of extracellular vesicles within CEM sensilla (Chapter 2).

Figures

Figure 1

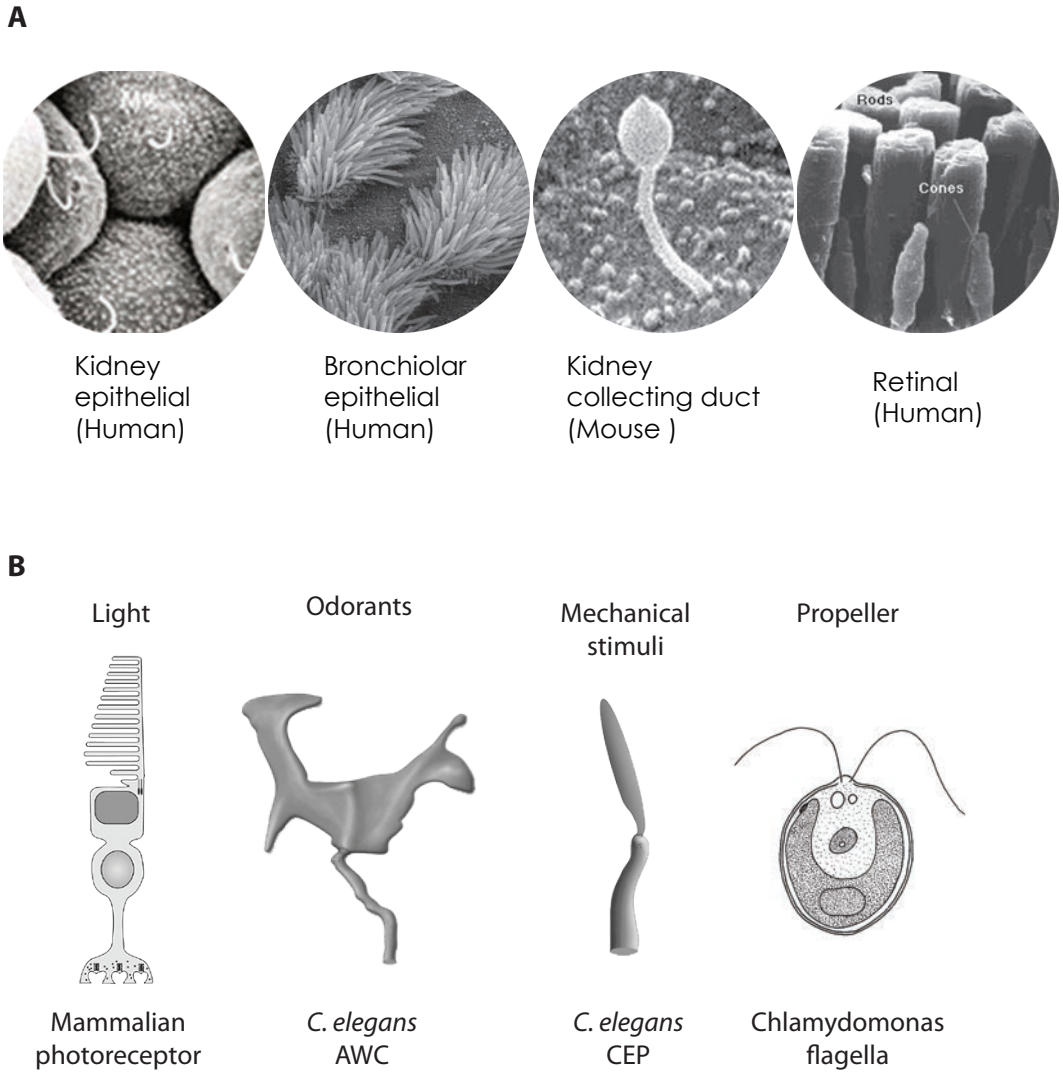

Figure 1 Cilia are morphologically and functionally diverse

A SEM micrographs of mammalian cilia depicting their morphological diversity (Images are from multiple sources)

B Cartoons of functionally distinct cilia depicting their morphological diversity (Images are from multiple sources including wormatlas.org)

Figure 2

A
Microtubules are composed of tubulin heterodimers that form curved lattices

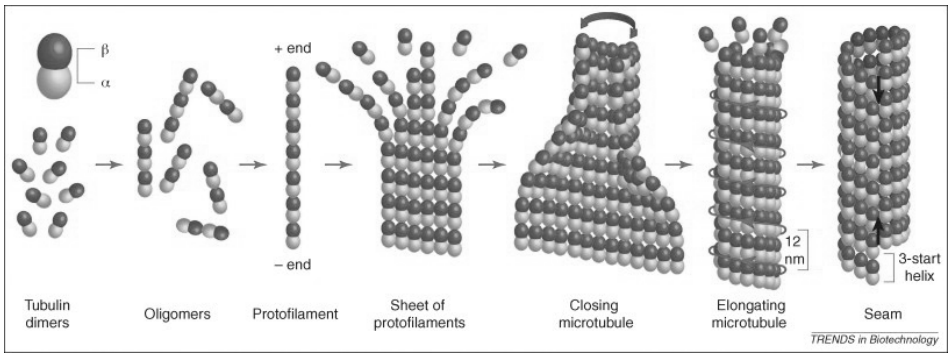

Modified from Pampaloni *et al*. 2008

B
Microtubules (MTs) form higher-order structures such as doublets and triplets

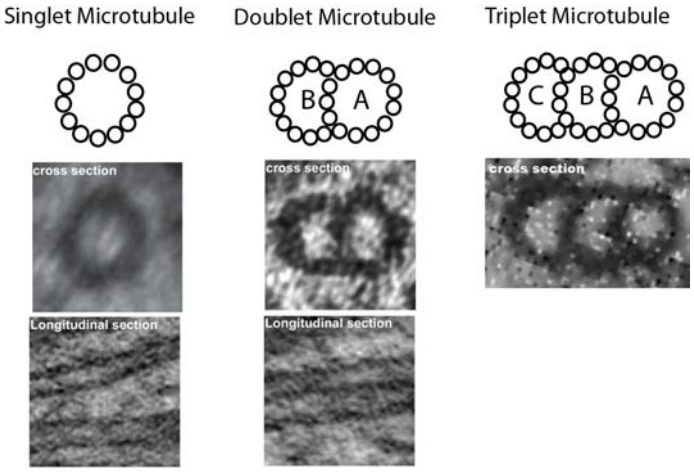

Figure 2 Ultrastructure of microtubules

A Formation of microtubules from alpha and beta tubulins. Alpha and beta tubulins from heterodimers that are assembled into protofilament that fro sheets of protofilaments. These protofilament sheets close to from curved lattices that are microtubules.

B Cartoon cross section (top row), TEM cross section (middle panel), and longitudinal view taken from electron tomogram, depicting singlet, doublet and triplet microtubules. (TEM image of the triplet was from online source)

Figure 3

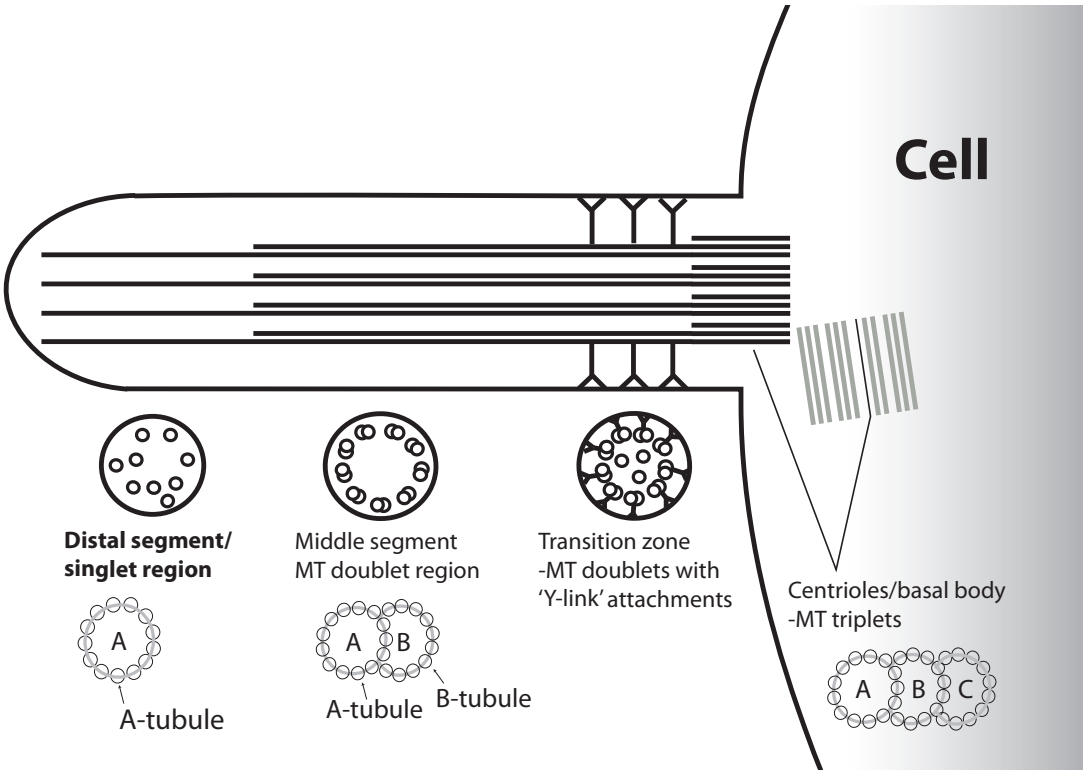

Figure 3 Ciliary axoneme microtubule ultrastructure

All cilia share conserved structural features. Cartoon of a cilium protruding from a cell surface depict ciliary axoneme and axoneme microtubule architecture. Ciliary axoneme is nucleated from centrosome-derived basal body. Basal body composed of triplet microtubules. Microtubule triplets consists of complete A-tubule and incomplete B- and C-tubules. At the base of the ciliary axoneme are a ring of doublet microtubules composed of complete A-tubule and incomplete B- tubule. These doublets are attached to the membrane via Y links. (Y-likes are visible in TEM cross section of the cilia. In TEM length-wise view Y-links appear as lines. In this cartoon they are dramatize to denote the transition zone). Transition zone give rise to the region of doubles devoid of Y-links. Doublet region give rise to a region of distal singlets. Distal singlets are formed

continuation of doublet A-tubules. At the end of the doublet region B-tubule become discontinuous.

Figure 4

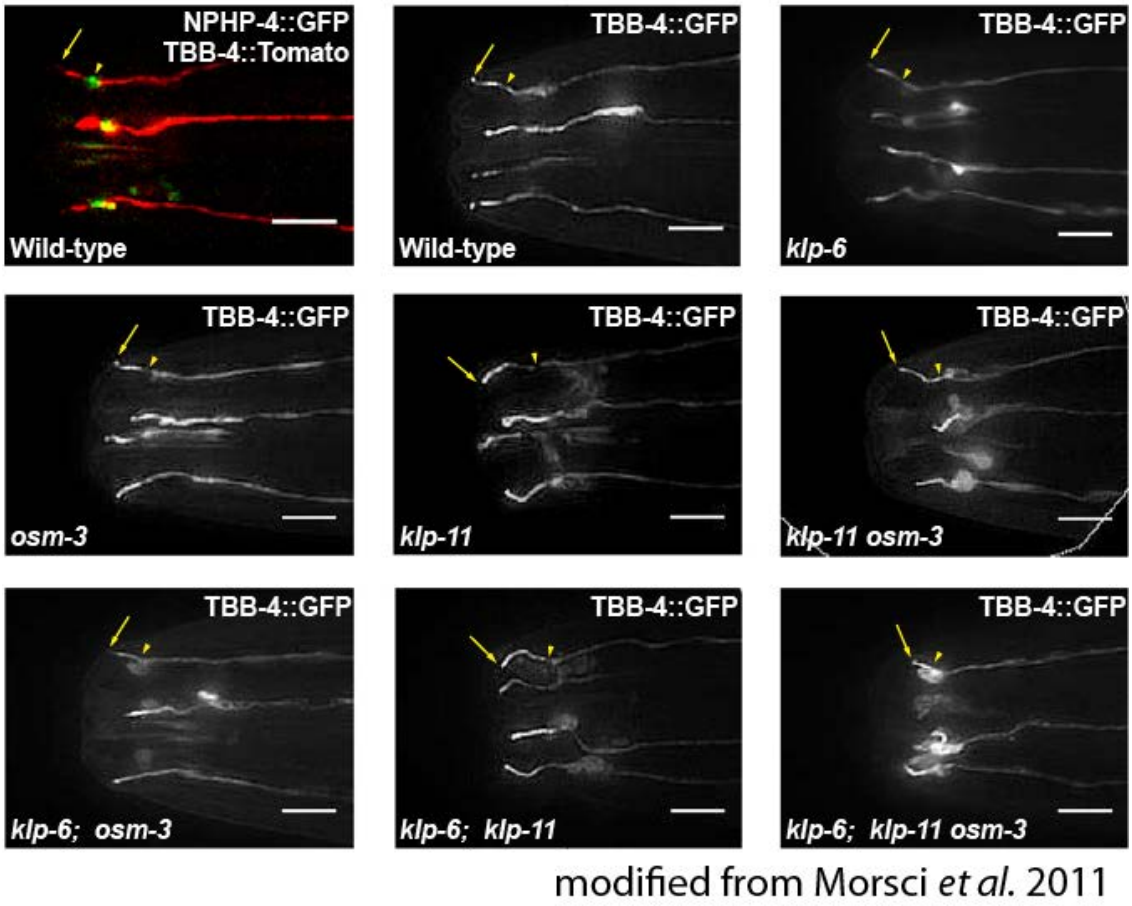

Figure 4 CEM cilia shape is genetically regulated

Wild field fluorescence images of CEM cilia are double labeled with TBB-4::tdTomato and transition zone maker NPHP-4::GFP (top left panel). All other panels use TBB-4::GFP reporter to demonstrate that in wild type CEM shape is altered in some mutant backgrounds. These are: kinesin 3 *klp-6*, heterodimeric kinesin 2 *osm-3*, heterotrimeric kinesin subunit *klp-11*. Modified from Morsci *et al.* 2011

Figure 5

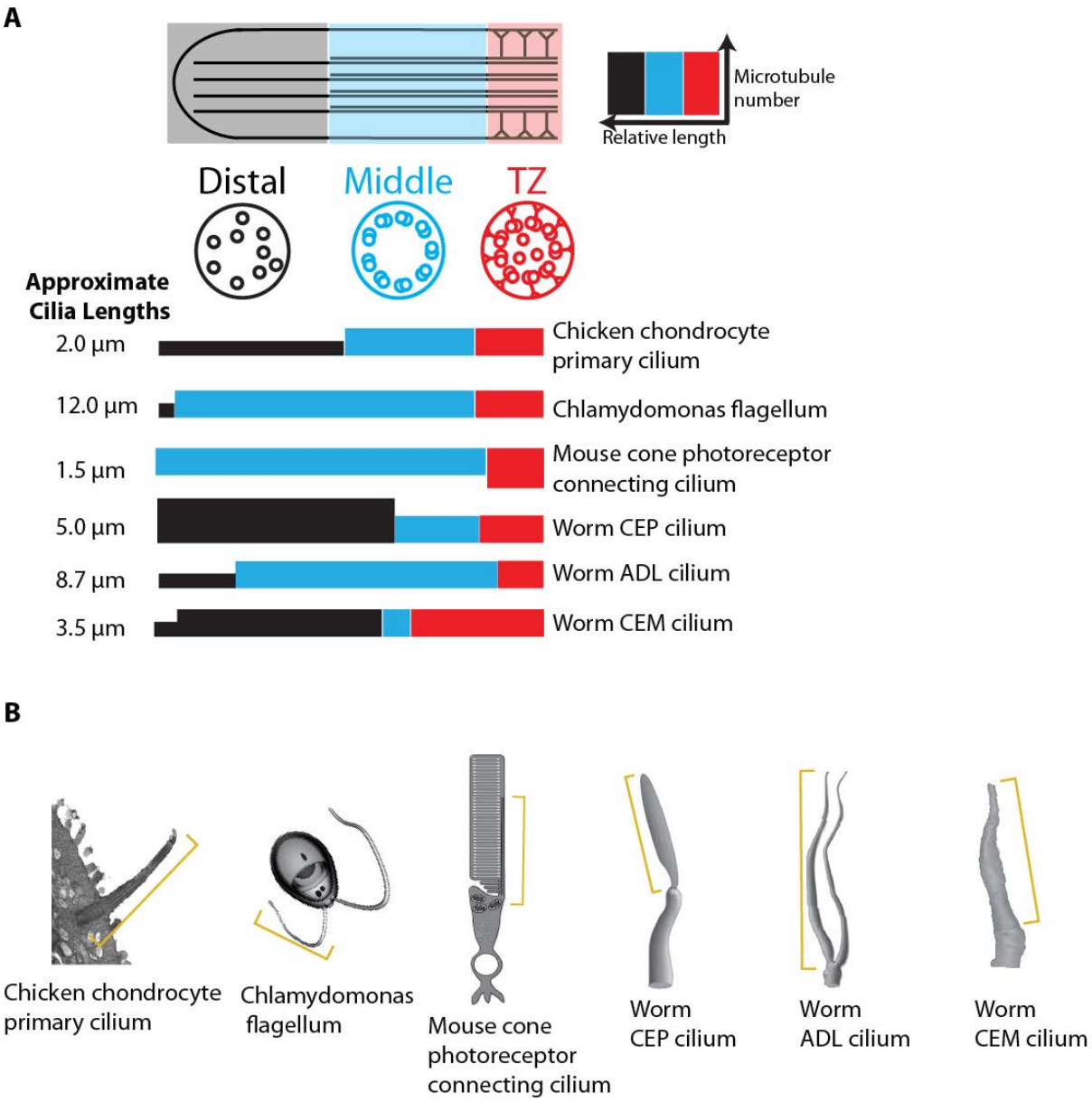

Figure 5 Ciliary microtubule spans differ in cilia of distinct morphology

A Color-coded transition zone (red), middle segment/ doublet region (blue), and distal segment/singlet region (black) in cilia of distinct morphology. Span of ciliary segments are presented as a fraction of ciliary length.

B Representative SEM images and cartoons of the cilia used in the graph

Figure 6

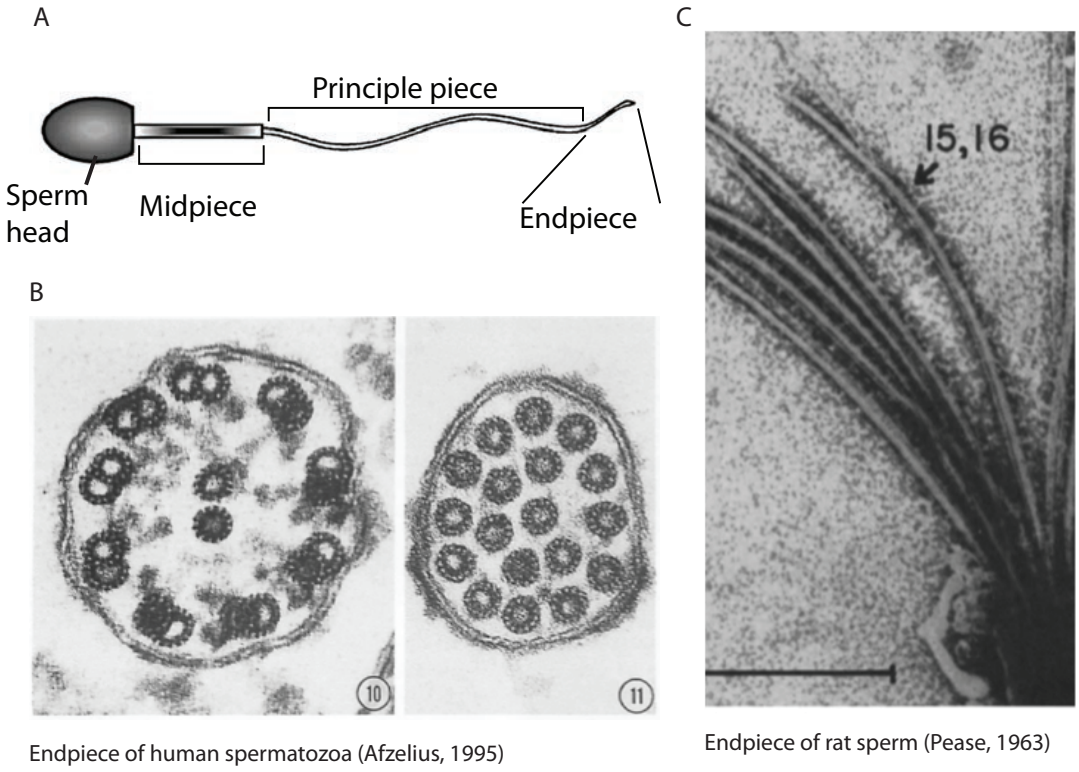

Endpiece of human spermatozoa (Afzelius, 1995)

Endpiece of rat sperm (Pease, 1963)

Figure 6 Microtubule doublets split in to A- and B-tubule singlets in mammalian sperm, suggest conserved but unexplored function

A Cartoon of mammalian sperm with distinct regions.

B TEM cross-sections of human spermatozoa end-piece depicting nine doublet microtubules forming eighteen singlet microtubules (Afzelius, 1995).

C End piece of rat spermatozoa with microtubule doublet splitting into A- and B-tubule singlets (Pease *et al.,* 1963)

References

Afzelius, B. A., Dallai, R., Lanzavecchia, S., & Bellon, P. (1995). Flagellar structure in normal human spermatozoa and in spermatozoa that lack dynein arms. *Tissue and Cell*, *27*(3), 241–247.

Barisic, M., & Maiato, H. (2016). The Tubulin Code: A Navigation System for Chromosomes during Mitosis. *Trends in Cell Biology*. http://doi.org/10.1016/j.tcb.2016.06.001

Barr, M. M., DeModena, J., Braun, D., Nguyen, C. Q., Hall, D. H., & Sternberg, P. W. (2001). The Caenorhabditis elegans autosomal dominant polycystic kidney disease gene homologs lov-1 and pkd-2 act in the same pathway. *Current Biology VL -*, *11*(17), 1341–1346. http://doi.org/doi: 10.1016/S0960-9822(01)00423-7

Cearns, M. D., Escuin, S., Alexandre, P., Greene, N. D. E., & Copp, A. J. (2016). Microtubules, polarity and vertebrate neural tube morphogenesis. *Journal of Anatomy*, *229*(1), 63–74. http://doi.org/10.1111/joa.12468

Cleveland, D. W. (1987). The multitubulin hypothesis revisited: what have we learned? *The Journal of Cell Biology*, *104*(3), 381–383. http://doi.org/10.1083/jcb.104.3.381

Cole, D. G., Diener, D. R., Himelblau, A. L., Beech, P. L., Fuster, J. C., & Rosenbaum, J. L. (1998). Chlamydomonas kinesin-II-dependent intraflagellar transport (IFT): IFT particles contain proteins required for ciliary assembly in Caenorhabditis elegans sensory neurons, *141*(4), 993–1008. Retrieved from http://gateway.webofknowledge.com/gateway/Gateway.cgi?GWVersion=2&SrcAuth=mekentosj&SrcApp=Papers&DestLinkType=FullRecord&DestApp=WOS&KeyUT=000073763700013

Cornils, A., Maurya, A. K., Tereshko, L., Kennedy, J., Brear, A. G., Prahlad, V., et al. (2016). Structural and Functional Recovery of Sensory Cilia in C. elegans IFT Mutants upon Aging. *PLoS Genetics*, *12*(12), e1006325. http://doi.org/10.1371/journal.pgen.1006325

Desai, A., & Mitchison, T. J. (1997). MICROTUBULE POLYMERIZATION DYNAMICS. *Annual Review of Cell and Developmental Biology*, *13*(1), 83–117. http://doi.org/10.1146/annurev.cellbio.13.1.83

Doroquez, D. B., Berciu, C., Anderson, J. R., Sengupta, P., Nicastro, D., & Hobert, O. (2014). A high-resolution morphological and ultrastructural map of anterior sensory cilia and glia in Caenorhabditis elegans, *3*. http://doi.org/10.7554/eLife.01948

Dutcher, S. K. (2001). The tubulin fraternity: alpha to eta. *Current Opinion in Cell Biology*, *13*(1), 49–54. http://doi.org/doi: 10.1016/S0955-0674(00)00173-3

Hurd, D. D., Miller, R. M., Núñez, L., & Portman, D. S. (2010). Specific alpha- and beta-tubulin isotypes optimize the functions of sensory Cilia in Caenorhabditis elegans. *Genetics*, *185*(3), 883–896. http://doi.org/10.1534/genetics.110.116996

Janke, C. (2014). The tubulin code: molecular components, readout mechanisms, and functions. *The Journal of Cell Biology*, *206*(4), 461–472. http://doi.org/10.1083/jcb.201406055

Kapitein, L. C., & Hoogenraad, C. C. (2015). Building the Neuronal Microtubule Cytoskeleton. *Neuron*, *87*(3), 492–506. http://doi.org/10.1016/j.neuron.2015.05.046

L I Binder, W. L. D. J. L. R. (1975). Assembly of chick brain tubulin onto flagellar

microtubules from Chlamydomonas and sea urchin sperm. *Proceedings of the National Academy of Sciences of the United States of America*, *72*(3), 1122.

Maguire, J. E., Silva, M., Nguyen, K. C. Q., Hellen, E., Kern, A. D., Hall, D. H., & Barr, M. M. (2015). Myristoylated CIL-7 regulates ciliary extracellular vesicle biogenesis. *Molecular Biology of the Cell*, *26*(15), 2823–2832. http://doi.org/10.1091/mbc.E15-01-0009

McKean, P. G., Vaughan, S., & Gull, K. (2001). The extended tubulin superfamily. *J Cell Sci*, *114*(Pt 15), 2723–2733.

Morsci, N. S. (2011, August 10). *THE ROLE OF KINESIN-LIKE PROTEIN 6 IN STRUCTURE AND FUNCTION OF CILIATED SENSORY NEURONS*. Cell and Molecular Biology Program, University of Wisconsin – Madison, Madison, WI.

Mukai, M., Ikegami, K., Sugiura, Y., Takeshita, K., Nakagawa, A., & Setou, M. (2009). Recombinant Mammalian Tubulin Polyglutamylase TTLL7 Performs both Initiation and Elongation of Polyglutamylation on β-Tubulin through a Random Sequential Pathway †. *Biochemistry*, *48*(5), 1084–1093. http://doi.org/10.1021/bi802047y

Mukhopadhyay, S., Lu, Y., Qin, H., Lanjuin, A., Shaham, S., & Sengupta, P. (2007). Distinct IFT mechanisms contribute to the generation of ciliary structural diversity in C. elegans. *The EMBO Journal*, *26*(12), 2966–2980. http://doi.org/10.1038/sj.emboj.7601717

Pampaloni, F., & Florin, E.-L. (2008). Microtubule architecture: inspiration for novel carbon nanotube-based biomimetic materials. *Trends in Biotechnology*, *26*(6), 302–310. http://doi.org/10.1016/j.tibtech.2008.03.002

Pan, J., Wang, Q., & Snell, W. J. (2005). Cilium-generated signaling and cilia-related disorders. *Laboratory Investigation; a Journal of Technical Methods and Pathology*, *85*(4), 452–463. http://doi.org/10.1038/labinvest.3700253

Peden, E. M., & Barr, M. M. (2005). The KLP-6 kinesin is required for male mating behaviors and polycystin localization in Caenorhabditis elegans. *Current Biology VL -*, *15*(5), 394–404. http://doi.org/10.1016/j.cub.2004.12.073

Perkins, L. A., Hedgecock, E. M., Thomson, J. N., & Culotti, J. G. (1986). Mutant sensory cilia in the nematode Caenorhabditis elegans. *Developmental Biology*, *117*(2), 456–487.

Pigino, G., Geimer, S., Lanzavecchia, S., Paccagnini, E., Cantele, F., Diener, D. R., et al. (2009). Electron-tomographic analysis of intraflagellar transport particle trains in situ. *The Journal of Cell Biology*, *187*(1), 135–148. http://doi.org/10.1083/jcb.200905103

Piperno, G., Siuda, E., Henderson, S., & Segil, M. (1998). Distinct mutants of retrograde intraflagellar transport (IFT) share similar morphological and molecular defects. *The Journal of Cell …*.

Raff, E. C., Fackenthal, J. D., Hutchens, J. A., Hoyle, H. D., & Turner, F. R. (1997). Microtubule Architecture Specified by a β-Tubulin Isoform. *Science (New York, NY)*, *275*(5296), 70–73. http://doi.org/10.1126/science.275.5296.70

Ringo, D. L. (1967). Flagellar motion and fine structure of the flagellar apparatus in Chlamydomonas. *The Journal of Cell Biology*, *33*(3), 543–571.

Roll-Mecak, A. (2014). Intrinsically disordered tubulin tails: complex tuners of microtubule functions? *Seminars in Cell & Developmental Biology*, *37*, 11–19. http://doi.org/10.1016/j.semcdb.2014.09.026

Scholey, J. M. (2012). Kinesin-2 motors transport IFT-particles, dyneins and tubulin subunits to the tips of Caenorhabditis elegans sensory cilia: Relevance to vision research? *Vision Research*, *75*, 44–52. http://doi.org/10.1016/j.visres.2012.06.015

Sorokin, S. (1962). CENTRIOLES AND THE FORMATION OF RUDIMENTARY CILIA BY FIBROBLASTS AND SMOOTH MUSCLE CELLS. *The Journal of Cell Biology*, *15*(2), 363–377. http://doi.org/10.1083/jcb.15.2.363

Stepanek, L., & Pigino, G. (2016). Microtubule doublets are double-track railways for intraflagellar transport trains. *Science (New York, NY)*, *352*(6286), 721–724. http://doi.org/10.1126/science.aaf4594

Topalidou, I., Keller, C., Kalebic, N., Nguyen, K. C. Q., Somhegyi, H., Politi, K. A., et al. (2012). Genetically Separable Functions of the MEC-17 Tubulin Acetyltransferase Affect Microtubule Organization. *Current Biology VL -*, *22*(12), 1057–1065. http://doi.org/10.1016/j.cub.2012.03.066

Verhey, K. J., & Gaertig, J. (2007). The Tubulin Code. *Cell Cycle (Georgetown, Tex.)*, *6*(1538-4101), 2152–2160.

Vincensini, L., Blisnick, T., & Bastin, P. (2012). 1001 model organisms to study cilia and flagella. *Biology of the Cell*, *103*(3), 109–130. http://doi.org/10.1042/BC20100104

Wade, R. H. (2009). On and Around Microtubules: An Overview. *Molecular Biotechnology*, *43*(2), 177–191. http://doi.org/10.1007/s12033-009-9193-5

Wang, J., Kaletsky, R., Silva, M., Williams, A., Haas, L. A., Androwski, R. J., et al. (2015). Cell-Specific Transcriptional Profiling of Ciliated Sensory Neurons Reveals Regulators of Behavior and Extracellular Vesicle Biogenesis. *Current Biology VL -*, *25*(24), 3232–3238. http://doi.org/10.1016/j.cub.2015.10.057

Wang, J., Silva, M., Haas, L. A., Morsci, N. S., Nguyen, K. C. Q., Hall, D. H., & Barr, M. M. (2014). C. elegans ciliated sensory neurons release extracellular vesicles that function in animal communication. *Current Biology : CB*, *24*(5), 519–525. http://doi.org/10.1016/j.cub.2014.01.002

Waters, A. M., & Beales, P. L. (2011). Ciliopathies: an expanding disease spectrum. *Pediatric Nephrology (Berlin, Germany)*, *26*(7), 1039–1056. http://doi.org/10.1007/s00467-010-1731-7

Westermann, S., & Weber, K. (2003). Post-translational modifications regulate microtubule function. *Nature Reviews. Molecular Cell Biology*, *4*(12), 938–948. http://doi.org/10.1038/nrm1260

Williams, C. L., Li, C., Kida, K., Inglis, P. N., Mohan, S., Semenec, L., et al. (2011). MKS and NPHP modules cooperate to establish basal body/transition zone membrane associations and ciliary gate function during ciliogenesis. *The Journal of Cell Biology*, *192*(6), 1023–1041. http://doi.org/10.1083/jcb.201012116

Woolley, D. M., & Nickels, S. N. (1985). Microtubule termination patterns in mammalian sperm flagella. *Journal of Ultrastructure Research*, *90*(3), 221–234. http://doi.org/10.1016/S0022-5320(85)80001-0

Yu, I., Garnham, C. P., & Roll-Mecak, A. (2015). Writing and Reading the Tubulin Code. *The Journal of Biological Chemistry*, *290*(28), 17163–17172. http://doi.org/10.1074/jbc.R115.637447

Part I

Chapter 1

Cell-specific α-tubulin isotype regulates ciliary microtubule ultrastructure, intraflagellar transport, and extracellular vesicle biology

Malan Silva[1, 2], Natalia Morsci[2], Ken C. Q. Nguyen[3], Anza Rizvi[1], Christopher Rongo[1, 2], David H. Hall[3], Maureen M. Barr[1, 2, *]

[1]Department of Genetics and Human Genetics Institute of New Jersey, Rutgers University, Piscataway, NJ 08854

[2]Waksman Institute for Microbiology, Rutgers University, Piscataway, NJ 08854

[3]Center for *C. elegans* Anatomy, Albert Einstein College of Medicine, Bronx, NY 10461

[*]lead contact and corresponding author: barr@dls.rutgers.edu

Published in Current biology in March 2017

Summary

Cilia are found on most non-dividing cells in the human body and, when faulty, cause a wide range of pathologies called ciliopathies. Ciliary specialization in form and function is observed throughout the animal kingdom, yet mechanisms generating ciliary diversity are poorly understood. The "tubulin code" – a combination of tubulin isotypes and tubulin post-translational modifications – can generate microtubule diversity. Using C. elegans, we show that α-tubulin isotype TBA-6 sculpts 18 A- and B-tubule singlets from nine ciliary A-B doublet microtubules in cephalic male (CEM) neurons. In CEM cilia, tba-6 regulates velocities and cargoes of intraflagellar transport (IFT) kinesin-2 motors kinesin-II and OSM-3/KIF17 without affecting kinesin-3 KLP-6 motility. In addition to their unique ultrastructure and accessory kinesin-3 motor, CEM cilia are specialized to produce extracellular vesicles. *tba-6* also influences several aspects of extracellular vesicle biology, including cargo sorting, release, and bioactivity. We conclude that this cell-specific α-tubulin isotype dictates the hallmarks of CEM cilia specialization. These findings provide insight into mechanisms generating ciliary diversity and lay a foundation for further understanding the tubulin code.

Introduction

Microtubules are essential for many cytoskeletal processes including cell division, ciliogenesis, and intracellular trafficking. Microtubules are composed of α+β tubulin heterodimers arranged into protofilaments that form cylinders (Dutcher 2001). These cylinders can also form higher order microtubule structures like A-B tubule doublets and A-B-C triplets found in the axonemes and basal bodies of cilia and flagella (Winey and O'Toole 2014). Eukaryotes express multiple tubulin isotypes that may function redundantly or perform specialized functions (Roll-Mecak 2015, Lockhead, Schwarz et al. 2016). Mutations in certain α and β-tubulin isotypes cause a spectrum of neurological disorders (Tischfield, Cederquist et al. 2011). The mechanisms by which tubulin isotypes contribute to higher order microtubule structural and functional diversity are not well understood.

Cilia are organelles with a microtubule core, called the axoneme, that exhibit a conserved architecture of nine outer doublet microtubules with a variable number of inner singlets (Rosenbaum and Witman 2002, Fisch and Dupuis-Williams 2011). The axoneme has distinct structural regions: the basal body (microtubule triplets), transition zone (microtubule doublets attached to the surrounding membrane via “Y” links), middle segment (microtubule doublets), and distal segment (microtubule singlets). Microtubule doublets consist of complete A-tubules with 13-protofilaments and attached incomplete 10-protofilament B-tubules (Linck, Fu et al. 2014). Axonemal structural variations may arise in the relative length of each region and the presence or absence of the distal segment,

where A-tubule singlets extend and B-tubules terminate (Fisch and Dupuis-Williams 2011). For example, the mammalian kidney displays a variant ciliary axoneme that is composed of a short proximal microtubule doublet and long distal microtubule singlet region (Tsuji, Matsuo et al. 2016) and is reminiscent of *C. elegans* amphid channel cilia (Perkins, Hedgecock et al. 1986, Doroquez, Berciu et al. 2014). Ciliary specialization mechanisms including those regulating microtubule doublet to singlet conversion are unknown.

C. elegans possesses numerous ciliary specializations that can be visualized *in vivo* using fluorescent reporters and examined ultrastructurally using transmission electron microscopy and electron tomography (Perkins, Hedgecock et al. 1986, Doroquez, Berciu et al. 2014, O'Hagan and Barr 2016). Cilia are built by a conserved process called intraflagellar transport (IFT). IFT is a bidirectional microtubule-based motor driven cargo transport system that consist of biochemically separable and functionally distinct IFT-A and -B particles transported by anterograde heterotrimeric kinesin-II and retrograde dynein-2 motors (Rosenbaum and Witman 2002, Taschner and Lorentzen 2016). In some cilia, anterograde IFT transport is modulated by accessory kinesins. In *C. elegans* amphid neurons, homodimeric kinesin-2 OSM-3/KIF17 participates in IFT and is implicated in generating sensory cilia of diverse morphology and function (Mukhopadhyay, Lu et al. 2007). In *C. elegans* cephalic male (CEM) neurons, kinesin-3 KLP-6 modulates velocities of both IFT kinesin-2 motors and also regulates release of ciliary extracellular vesicles (EVs) (Peden and Barr 2005, Morsci and Barr 2011, Wang, Silva et al. 2014).

The “tubulin code” employs tubulin isotypes and tubulin post-translational modifications to orchestrate cytoskeletal functions (Verhey and Gaertig 2007, Janke 2014, Roll-Mecak 2015, Yu, Garnham et al. 2015). The tubulin code is “written” by tubulin isotypes and tubulin modifying enzymes such as tubulin tyrosine ligase-like enzymes (TTLLs) that glutamylate microtubules (Janke, Rogowski et al. 2005). The tubulin code can be erased by tubulin modifying enzymes such as cytosolic carboxypeptidase (CCP) deglutamylases that remove glutamylates from microtubules (Rogowski, van Dijk et al. 2010). The tubulin code is “read” or interpreted by cellular effectors such as molecular motors or microtubule associated proteins. We previously showed that the *C. elegans ccpp-1* deglutamylase regulates stability of B-tubules and controls the velocity of kinesin-3 KLP-6 and kinesin-2 OSM-3/KIF17 without affecting the transport of kinesin-II cargo (O'Hagan, Piasecki et al. 2011).

The *C. elegans* genome encodes nine α-tubulin and six b-tubulins (1998, Gogonea, Gogonea et al. 1999). The CEM neurons express a cell-type specific a-tubulin isoform TBA-6 (Hurd, Miller et al. 2010), suggesting that TBA-6 may contribute to CEM specialization. Using serial transmission electron microscopy and electron tomography of CEM cilia, we discovered a novel axonemal variation whereby doublet microtubules are splayed to form complete A- and B-tubule singlets in middle regions while remaining attached at their proximal and distal ends. a-tubulin TBA-6 was essential for B-tubule singlet formation. In *tba-6* mutants, the CEM axoneme was comprised of a proximal doublet microtubule region followed by a distal A-tubule singlet microtubule region. The coordination of kinesin-2 motors with IFT-A and IFT-B complexes was disrupted in *tba-6* mutant cilia. *tba-6*

was also required for extracellular vesicle (EV) cargo sorting, EV release, and EV bioactivity. Our findings demonstrate that the tubulin code via a-tubulin isotype TBA-6 influences axonemal microtubule architecture, IFT dynamics, and extracellular vesicle biology.

Results

CEM ciliary doublet microtubules splay to form A-tubule and B-tubule singlet microtubules

We characterized the ultrastructure of CEM cilia using transmission electron microscopy and electron tomography. In the male head, four quadrant cephalic sensilla contain the cilia of the male-specific CEM and non-sex specific CEP ciliated sensory neurons and associated glial socket and sheath cells that create a lumen surrounding the cilia (Figure 1A). The CEM ciliary axoneme can be subdivided into distinct segments based on microtubule ultrastructure (Figure 1B), described here in proximal-to-distal order.

The transition zone contains nine doublet microtubules attached to the ciliary membrane by Y-links and arranged in a ring around one to four inner singlet microtubules. Doublet microtubules at the base of the transition zone flare out into the periciliary membrane compartment (PCMC) and terminate at varying lengths (Movie S1). At the anterior end of the transition zone, doublet microtubules became progressively devoid of Y-links. The doublet microtubule region is ~0.5μm and lacks Y-links. After the initial doublet segment, A- and B-tubules of the nine doublet microtubules splay to form discrete A-tubule and B-tubule singlets (Figure 1C). Incomplete B-subfibers separate at inner and outer seams from their partner A-tubules transiently display concave "C" shapes, and then seal to form complete B-tubule singlets (Figure 1F, Figure S1A-B). As a consequence of doublet splaying, the CEM axoneme contains 20±2 singlet microtubules along the length of its middle region (Figure 1B, quantified in 2D).

Some singlet microtubules closely associate with the ciliary membrane via electron-dense bridges (Figure 1D, Movie S2). By tracing A- and B-tubules along the cilia length, we found that A- and B- singlet microtubules eventually fuse to each other in the sub-distal region. The distal region possesses only A-tubule singlets (Figure 1B and E, Figure S1A). The distal-most ciliary region consists of tightly packed A-tubule singlets (Figure 1B also Figure S1B for an oblique view of the CEM cuticle pore). The number of singlets in this region ranged from nine immediately after the sub-distal region to as few as one at the tip. The CEM ciliary tip protrudes to the outside environment via an opening in the cuticle bulge (Figure 1A, Figure S1C). We also observed electron-opaque membrane structures continuous with CEM pore (Figure S1B). In sum, this is the first evidence of doublet microtubules splaying to generate discrete A-tubule and B-tubule singlets microtubules. B-tubule singlets exhibit a transient C-shape conformation during the doublet to singlet microtubule conversion.

α-tubulin isotype tba-6 is required for CEM ciliary ultrastructure.

CEM cilia are approximately 3.5±0.4μm long and have a sinusoid curved shape visible by both transmission electron microscopy in fixed specimens and fluorescent reporters in living animals (Figure 1B, Figure 2A, 2D, 2F). In wild type (WT), 90% of CEM cilia curve outward from the central body axis of the worm (Figure 2A, 2F). Several genes regulate CEM cilia shape including a-tubulin *tba-6*, the IFT kinesin-II subunits *klp-11, klp-20, kap-1*, and the transition zone component *nphp-4* (Jauregui, Nguyen et al. 2008, Hurd, Miller et

al. 2010, Morsci and Barr 2011). *tba-6* expression in the ciliated nervous system is restricted to the 27 ciliated extracellular vesicle (EV) releasing neurons including the four CEMs (Hurd, Miller et al. 2010), while *klp-11, klp-20, kap-1* and *nphp-4* are pan-ciliary genes. A functional GFP-tagged TBA-6 reporter localizes along the length of the curved CEM axoneme (Figure S2C) (Hurd, Miller et al. 2010). We therefore focused on *tba-6* as a potential CEM ciliary specialization factor.

We examined CEM cilia of *tba-6(cxP4018)* loss of function mutants (Figure S2) using fluorescent reporters. To visualize the CEM ciliary axoneme *in vivo*, we expressed GFP-tagged β-tubulin *tbb-4* under the CEM-specific *pkd-2* promoter (Figure 2F, Table S1). *tbb-4* encodes a pan-ciliary β-tubulin isotype (Hao, Thein et al. 2011). In WT CEM cilia, TBB-4::GFP localizes along the sinusoid curved-out axoneme, with reduced GFP intensity at the transition zone and sub-distal region (Figure 2F quantified in 2G). In *tba-6* mutants, 41% of CEM cilia showed an abnormal curved-in morphology that deflected away from the cuticular pore and bent inward adjacent to the CEP cilium (Figure 2B' and 2F). 59% of *tba-6* CEM cilia curved out and terminated before reaching the cuticular pore (Figure 2B).

Using serial transmission electron microscopy and electron tomography, we found that doublet microtubules do not splay into singlets in either curved-out or curved-in *tba-6* CEM cilia (Figure 2C and 2D). Instead, the doublet microtubule region was defined by the abrupt termination of B-tubules, with A-tubule singlets extending distally (Figure 2C-D). As a consequence, the number of singlets was reduced to almost half in *tba-6* males (Figure 2E). The doublet microtubule region was longer in curved-in *tba-6* than curved-out

tba-6 CEM cilia (Figure 2D). We conclude that **α**-tubulin TBA-6 is required for formation of B-tubule singlets and characteristic shape of CEM cilia.

TBA-6 regulates relative ciliary abundance of ciliary kinesin-2 and kinesin-3 motors but only affects ciliary distribution of accessory kinesin motors

To determine whether *tba-6* regulates localization of ciliary proteins, we examined GFP-tagged ciliary kinesin motors and IFT polypeptides in *tba-6* and WT CEM cilia (Figure 3A-C, Table S1). Ciliary fluorescence intensity of all ciliary motors were significantly increased in *tba-6* mutants (Figure 3A-C, Table S1). However, only OSM-3::GFP and KLP-6::GFP ciliary distribution patterns were abnormal in *tba-6* mutant cilia (Figure 3A, quantified in 3B and 3C). CEM ciliary distributions of IFT-A complex component CHE-11::GFP, IFT-B complex proteins OSM-5::GFP and OSM-6::GFP were similar in WT and *tba-6* mutant males (Figure 3A and 3B), while ciliary fluorescence intensity levels of KAP-1::GFP and OSM-5::GFP were slightly elevated in *tba-6* mutants. These results suggest that the loss of TBA-6 selectively affects ciliary distribution patterns of a subset of ciliary motors and IFT proteins, with the most dramatic changes observed for accessory kinesins OSM-3 and KLP-6.

tba-6 regulates anterograde velocity and coordination of IFT kinesin-2 motors but not kinesin-3 KLP-6

To determine whether *tba-6* regulates IFT, we examined anterograde velocity of CHE-11::GFP (IFT-A), OSM-5::GFP (IFT-B), OSM-6::GFP (IFT-B), IFT kinesin-2 motors kinesin-II (KAP-1::GFP) and OSM-3::GFP in WT and *tba-6* CEM cilia (Figure 3D, Table 1) (O'Hagan and Barr 2016). In WT, the velocity ranges of CHE-11::GFP, OSM-5::GFP, OSM-6::GFP, and KAP-

1::GFP overlap at ~0.4µm/sec, while OSM-3::GFP moved at distinctly faster velocity range of ~0.6µm/sec (Figure 3D, Table 1). These observations are consistent with our model in which heterotrimeric kinesin-II but not OSM-3 drives IFT in CEM cilia (Morsci and Barr 2011).

In *tba-6* mutants, IFT-A and IFT-B moved at different velocity ranges. IFT-A protein CHE-11::GFP and KAP-1::GFP moved at ~0.5µm/sec. IFT-B proteins OSM-5::GFP and OSM-6::GFP velocities overlapped with OSM-3::GFP at ~0.7µm/sec (Figure 3D, Table 1). Kinesin-3 KLP-6 velocity was unaffected (Table 1). These data suggest that, in *tba-6* CEM cilia, heterotrimeric kinesin-II transports IFT-A and homodimeric kinesin-2 OSM-3 transports IFT-B.

tba-6 mutants retain ciliary extracellular vesicles (EVs) in the cephalic lumen

CEM neurons shed and release EVs (Wang, Silva et al. 2014, Wang, Kaletsky et al. 2015, Wang and Barr 2016). GFP-tagged TRP polycystin PKD-2 and peripheral membrane protein CIL-7 localize to the CEM ciliary base, cilium, and EVs (Figure 4A-B, 5A) (Maguire, Silva et al. 2015). The ciliary base region includes the periciliary membrane compartment (PCMC) internal to the CEM neuron and the extracellular lumen surrounding the cilium. Ciliary base localization of PKD-2::GFP and CIL-7::GFP may reflect EVs that are shed into the lumen but not environmentally released (Maguire, Silva et al. 2015). In *tba-6* mutants, PKD-2::GFP and CIL-7::GFP accumulated at ciliary base, suggesting an EV release defect (Figure 4A-B).

To resolve whether *tba-6* regulates EV shedding into the lumen and/or EV environmental release, we used serial TEM. We examined the location of EVs, EV numbers, and EV diameters. The WT cephalic lumen contains two discernable EV populations based on location, abundance, and size. The distal lumen contained a few rare and smaller-sized EVs (39±10nm) (Figure 4C-F). The proximal lumen surrounding the PCMC and proximal cilium contained larger-sized EVs (105±29) (Figure 4C-E and, G). Proximally located EVs varied in size and appearance, with some being electron opaque and others translucent (Figure 4C; average distribution of EV sizes quantified in Figure 4G).

In *tba-6* mutants with curved in cilia, EV numbers increased in distal and proximal luminal regions (distal 14±10 and proximal 80±60 EVs in WT versus distal=252±10 and proximal=753±77 EVs in *tba-6* curved in cilia) (Figure 4C; quantified in 4D-G). This increase was primarily due to enrichment of 50-60nm diameter EVs (10-30 fold higher in the cephalic lumen of a curved in *tba-6* cilium) (Figure 4F-G). Lumenal EV accumulation increased exponentially with decreasing environmental access of the CEM ciliary tip (Figure 5H). We conclude that TBA-6 is required for CEM-specific axoneme microtubule ultrastructure, cilia shape and EV release as manifested by abnormally high levels of lumenal EVs.

tba-6 regulates EV release and cargo composition

To confirm that lumenal EV accumulation correlates with an EV environmental release defect, we scored release of PKD-2::GFP-containing EVs in living animals. *tba-6* mutants released fewer PKD-2::GFP-containing EVs and fewer PKD-2::GFP-labeled EV streaks from CEM cilia compared to WT (Figure 5A). In WT, KLP-6::GFP is not EV cargo (Wang, Silva et al. 2014). Surprisingly, in *tba-6* mutants, KLP-6::GFP localized to environmentally released EVs (Figure 5C), which may correlate with KLP-6::GFP abnormal ciliary localization patterns (Figure 3A). GFP-tagged kinesin-2 ciliary motors, IFT-A CHE-11, IFT-B OSM-5 and OSM-6, and TBB-4 were not released in EVs in WT or *tba-6* animals. These results suggest that EV cargo composition is different between *tba-6* and WT animals.

tba-6 is required for EV bioactivity

EVs isolated from WT animals stimulate male tail-chasing behavior, indicating a role in inter-animal communication (Wang, Silva et al. 2014). EVs isolated from *klp-6* animals do not contain PKD-2::GFP and do not stimulate male tail-chasing behavior, suggesting that EV bioactivity is affected by cargo content. We therefore examined whether TBA-6 regulates EV bioactivity.

We isolated EVs from mixed stage, male-enriched cultures of WT and *tba-6* mutants as previously described (Wang, Silva et al. 2014). We compared bioactivity of WT and *tba-6*-isolated EVs by measuring the ability of EV preps to evoke male tail chasing. When exposed to WT EV preparations, 71±0.05% of WT males displayed tail chasing behavior, as

compared to 32 ±0.06% to buffer control (Figure 5D, middle panel). When exposed to EV preparations derived from *tba-6* mutants, 42±0.06% of wild-type males displayed tail chasing behavior which is not significantly different from buffer control (Figure 5D, middle panel). For those males that displayed tail-chasing behavior, the frequency of repetitive tail chasing was more robust in response to WT EVs than to *tba-6*-derived EVs (Figure 5D, right panel). We conclude that a-tubulin TBA-6 is important for EV cargo content and EV bioactivity.

Discussion

α-tubulin isotype TBA-6 sculpts 18 singlet MTs from nine doublet MTs. Flagella of mammalian spermatozoa also display A- and B-tubule singlets extending from microtubule doublets (Woolley and Nickels 1985, Afzelius, Dallai et al. 1995), hinting that a conserved but unexplored mechanism generates this ciliary ultrastructure. How are nine A-tubule and nine B-tubule singlets generated from an axoneme with nine doublets? *In vitro* studies showed that formation of B-tubule based singlets can be energetically stable and persist in partially unwound states (Binder and Rosenbaum 1978, Song and Mandelkow 1995). We observed B-tubules transiently forming C-shapes when separating from partner A tubules and before sealing to form B-tubule singlets (Figure 1C, 1F). In the absence of *tba-6*, the CEM axoneme is composed of proximal microtubule doublets followed by a distal A-tubule microtubule singlet region, resembling *C. elegans* amphid channel cilia (Perkins, Hedgecock et al. 1986, Doroquez, Berciu et al. 2014). We conclude that α-tubulin TBA-6 is essential for architectural remodeling of axonemal MT-doublets into A- and B-tubule singlets (see model in Figure 6).

We propose three potential mechanisms by which TBA-6 and the tubulin code generate A- and B-tubule singlets from doublet microtubules. TBA-6 may directly or indirectly regulate protofilament composition necessary for stabilizing the intermediate C-tubule structure and the transition of B-tubules from doublets to singlets (Figure 1 and 6). Consistent with this hypothesis, b-tubulin β3 regulates protofilament number in flagellar microtubules of Drosophila spermatozoa (Raff, Fackenthal et al. 1997) and α-tubulin MEC-12 and tubulin acetyltransferase MEC-17 generate 15-protofilament neuronal

microtubules in non-ciliated *C. elegans* touch receptor neurons (Akella, Wloga et al. 2010, Cueva, Hsin et al. 2012, Topalidou, Keller et al. 2012).

Alternatively, TBA-6 may act as a buffer to temper against hyperglutamylation and resultant B-tubule instability (Pathak, Obara et al. 2007, O'Hagan, Piasecki et al. 2011). The C-terminus of TBA-6 is an unusually long and positively charged compared to other α-tubulin isotypes (Figure S2B). The C-tail of α-tubulin TBA-6 lacks glutamate residues (Figure S2B) and cannot be glutamylated by a TTLL enzyme. We previously showed that microtubule hyperglutamylation causes B-tubule instability (O'Hagan, Piasecki et al. 2011). While TBA-6 itself may not be a direct substrate of the TTLL glutamylase enzymes, TTLL enzymes glutamylate tubulin in the context of the microtubule. Structural characterization of TTLL7 reveals that TTLL7 binds both α and β tails of tubulin dimers and that this binding is required for glutamylation of β-tubulin (Garnham, Vemu et al. 2015). Hence α-tubulin TBA-6 may impact TTLL activity without itself being a substrate.

Finally, TBA-6 may function in CEM ciliary maturation. CEM neurons are embryonically-derived, yet *tba-6* is not expressed until the L4 stage immediately preceding sexual maturation (Hurd, Miller et al. 2010). In this instance, *tba-6* may be required for extending doublet microtubules, while other factors such as tubulin glutamylases, tubulin deglutamylases, or microtubule-associated proteins may sculpt 18 singlets from nine doublet microtubules. None of these models are mutually exclusive.

tba-6 also regulates IFT. How ciliary motors walk along microtubule tracks is a fundamental and unresolved question in cell biology. In *Chlamydomonas* flagella, anterograde heterotrimeric kinesin-II walks on the B-tubule while retrograde dynein-2 moves on the A-tubule (Stepanek and Pigino 2016). Metazoans such as *C. elegans* acquired an additional accessory IFT kinesin-2 motor, homodimeric KIF17/OSM-3, which depending on the specific cilium type, maybe functionally redundant with kinesin-II or seemingly not involved in IFT at all (Jenkins, Hurd et al. 2006, Morsci and Barr 2011, Zhao, Omori et al. 2012, Williams, McIntyre et al. 2014, Jiang, Tam et al. 2015). How A- and B-tubule ultrastructure relates to microtubule motor coordination in cilia with multiple kinesins is not known. In *C. elegans* amphid and phasmid channel cilia that express two IFT kinesin-2 motors, kinesin-II transports IFT through the transition zone before handing its cargo over to OSM-3 in the proximal cilium (Prevo, Mangeol et al. 2015). Here, kinesin-II is restricted to the region of the cilium that contains microtubule doublets and excluded from the distal A-tubule singlet region (Snow, Ou et al. 2004, Prevo, Mangeol et al. 2015). In the distal region OSM-3 alone moves the entire IFT-A/B complex (Prevo, Mangeol et al. 2015), indicating that OSM-3 utilizes A-tubule singlets (Pan, Ou et al. 2006).

In CEM cilia, anterograde IFT is driven predominantly by kinesin-II with minimal modulation from accessory kinesins OSM-3 and KLP-6 (Morsci and Barr 2011). Based on the above literature and our data, we propose that core IFT motor kinesin-II moves on B-tubules while accessory ciliary kinesins OSM-3 and KLP-6 are restricted to A-tubules (Figure 6). The loss of specialized ciliary ultrastructure in *tba-6* mutants is accompanied by the loss of CEM-specific coordination of the IFT kinesins and IFT-A/B complex transport. In

tba-6 mutants, the inherently faster OSM-3 motor is abnormally recruited into the IFT machinery, resulting in the formation of discrete populations of kinesin-II•IFT-A and OSM-3•IFT-B moving at different velocities. KLP-6 moves independently of the IFT machinery in WT and *tba-6* mutant cilia, consistent with KLP-6 moving on A-tubules. To our knowledge, this is the first *in vivo* demonstration that a tubulin isotype directly affects IFT and ciliary microtubule-based transport.

α-tubulin isotype TBA-6 is required for the cilium's ability to release bioactive EVs. CEM cilia shed and release EVs to the outside environment via the cuticle pore (Wang, Silva et al. 2014). TBA-6 is required for EV environmental release, EV cargo selection, and EV bioactivity. In *tba-6* mutants, environmental access of the ciliary tip inversely correlates with lumenal EV accumulation (Figure 4H). The abnormal inward curvature of the CEM cilia in *tba-6* mutants precludes environmental access to the cuticle pore. This may result in lumenal accumulation of smaller sized 50-60 nm EVs. These data suggest that ciliary EVs may be shed from two sites – larger EVs that are shed at the ciliary base into the lumen and smaller EVs that are shed at the ciliary tip and released into the environment.

Our studies raise several new and interesting questions. What mechanisms drive axonemal remodeling? How do microtubule tracks and the tubulin code control ciliary motors and multiple aspects of EV biology? Our findings reveal the far-reaching effects of the tubulin code and how a specific tubulin isotype can be a defining regulator of the structural and functional identity of a cilium.

Author contributions

Conceptualization: M.S and M.M.B.; Methodology, investigation, and analysis: M.S. N.M, K.Q.C.N, A.R., C.R., D.H.H., and M.M.B.; Writing: M.S, N.M., M.M.B.; Funding Acquisition M.S., C.R., D.H.H., and M.M.B.

Acknowledgements

We thank Leslie Gunther and Geoff Perumal for help in HPF-FS performed at Einstein, and William Rice and Ed Eng at the New York Structural Biology Center (NYSBC), for help in electron tomography; Daniella Nicastro, Antonina Roll-Mecak, Kristen Verhey for insights on the tubulin code; the Barr lab and Rutgers *C. elegans* community somewhere in the swamps of Jersey for discussion and constructive criticisms; Rutgers Human Genetics Institute and Genetics Department for critical bridge funding; WormBase and WormAtlas for online resources. Use of the NYSBC facilities was supported by the Albert Einstein College of Medicine. **Some strains were provided by the** National Bioresource Project and the *Caenorhabditis* Genetics Center **(CGC), which is funded by NIH Office of Research Infrastructure Programs (P40 OD010440).** This work was funded by NIH DK059418 and DK074746 (to M.M.B.), NIH OD 010943 (to D.H.H.), NIH R01GM101972 and R01NS42023 (to C.R.), and Waksman Institute Charles and Johanna Busch Fellowship (to M.S).

Tables and Figures

Table 1 Velocity and frequency of anterograde IFT in CEM cilia

Complex	Reporter	Genotype	Velocity, µm/s Mean[a]	SD*	p value	n = # Cilia	Frequency/30sec Mean	SD
Heterotrimeric kinesin II IFT motor	**KAP-1**	WT	0.39	0.11	2.87E-12	25	5	2
		tba-6	0.46	0.13		28	6	2
Homodimeric kinesin-2 IFT motor	**OSM-3**	WT	0.62	0.18	3.02E-32	55	11	4
		tba-6	0.74	0.24		57	14	4
Kinesin-3 ciliary motor	**KLP-6**	WT	0.67	0.21	0.11	15	11	4
		tba-6	0.64	0.21		28	11	3
IFT-A polypeptide	**CHE-11**	WT	0.37	0.10	8.29E-44	26	9	3
		tba-6	0.52	0.17		16	9	3
IFT-B polypeptide	**OSM-5**	WT	0.43	0.15	8.64E-66	22	7	3
		tba-6	0.69	0.24		21	13	3
IFT-B polypeptide	**OSM-6**	WT	0.45	0.12	1.80E-53	16	9	3
		tba-6	0.65	0.20		22	14	3

Table 1 Velocity and frequency of anterograde IFT in CEM cilia.

Data obtained from *in vivo* imaging of GFP-tagged transgenic reporters. *p*-values indicate results of unpaired two-tailed t-test (with unequal variances) comparing wild type and *tba-6* groups for a given reporter. [a]Mean and Standard Deviation were calculated based on the population of particles. See Figure 3D for frequency histograms of these reporters.

Table S1 Localization of GFP reporters in wild type and tba-6 CEM cilia

	Reporter	Ciliary localization		Sample size (animals, *cilia)		Quantification
		wild type	*tba-6*			
Axonemal structural makers	NPHP-4::GFP	Transition Zone (TZ)	No change	WT	90	
				tba-6	101	No change, **Ci/CB**, *p-value = 0.6078*
		Localizes to TZ with 1.264±0.55µm length	Localizes to TZ with 1.31±0.55µm length	WT	*199	
				tba-6	*202	Mean ± SD. *P*- value = 0.61, by Mann Whitney test for lenth NPHP-4::GFP of localization in *tba-6*
	TBB-4::tagRFP	Along the cilium with gaps in TZ and distal cilium.	Labels cilium uniformly and dimly. Accumulates at cilia base.	WT	83	
				tba-6	102	Levels are reduced in the nose, **Ci/D**, *p-value < 0.0001*
Ciliary motors	KAP-1::GFP	**a** - see legend	**b** - see legend	WT	33	
				tba-6	40	Accumulates, **Ci/D**, *p-value = 0.0045*
	OSM-3::GFP	Along entire cilium	Shows punctuated accumulation along the axoneme.	WT	35	
				tba-6	32	Accumulates, **Ci/CB**, *p-value < 0.0001*
	KLP-6::GFP	Along the entire cilium	Accumulate in cilia and ciliary tips.	WT	25	
				tba-6	55	Accumulates in nose cilia, **Ci/CB**, *p-value = 0.0005*
		In EVs in 7% of the wildtype animals	Ectopically in Evs in 53% of the animals	WT	26	
				tba-6	57	*p*- value < 0.0001 by Mann Whitney test for number of *tba-6* animal with ectopic EVs
IFT polypeptides	CHE-11::GFP	**a** - see legend	No change	WT	38	
				tba-6	25	No change, **Ci/CB**, *p-value = 0.5319*
	OSM-5::GFP	**a** - see legend	**b** - see legend	WT	40	
				tba-6	49	Accumulates, **Ci/CB**, *p-value = 0.0291*
	OSM-6::GFP	**a** - see legend	**b** - see legend	WT	27	
				tba-6	45	No change, **Ci/CB**, *p-value = 0.1219*
Extracellular vesicle cargo	PKD-2::GFP	CEM specific. Dimly lables the cilium with accumulation at ciliary base	Accumulates in the cilium	WT	70	
				tba-6	62	Accumulates, **Ci/CB**, *p-value = 0.0009*
	CIL-7::GFP	Dimly lables the cilium with accumulation at ciliary base	Accumulates in the cilium	WT	56	
				tba-6	60	Accumulates, **Ci/CB**, *p-value < 0.0001*

Table S1 Localization of GFP reporters in wild-type and *tba-6* CEM cilia.

Data obtained from *in vivo* imaging of fluorescent transgenic reporters. *p-values* are based on Mann-Whitney U test of max fluorescence intensity ratio of cilium to dendrite (**Ci/D**) or cilium to cell body (**Ci/CB**) between wild type and *tba-6* mutant animals. **a–** Fluorescence intensity peaks at the base of the cilium where periciliary membrane conpartment (PCMC) is located, and tapers into the cilium. **b–** Fluorescence intensity peaks at the base of the cilium where PCMC is located, but unlike wild type displays a slightly longer span of distribution within the cilium. See Figure 2, 3, 4, and 5 for related widefield images.

Figure 1

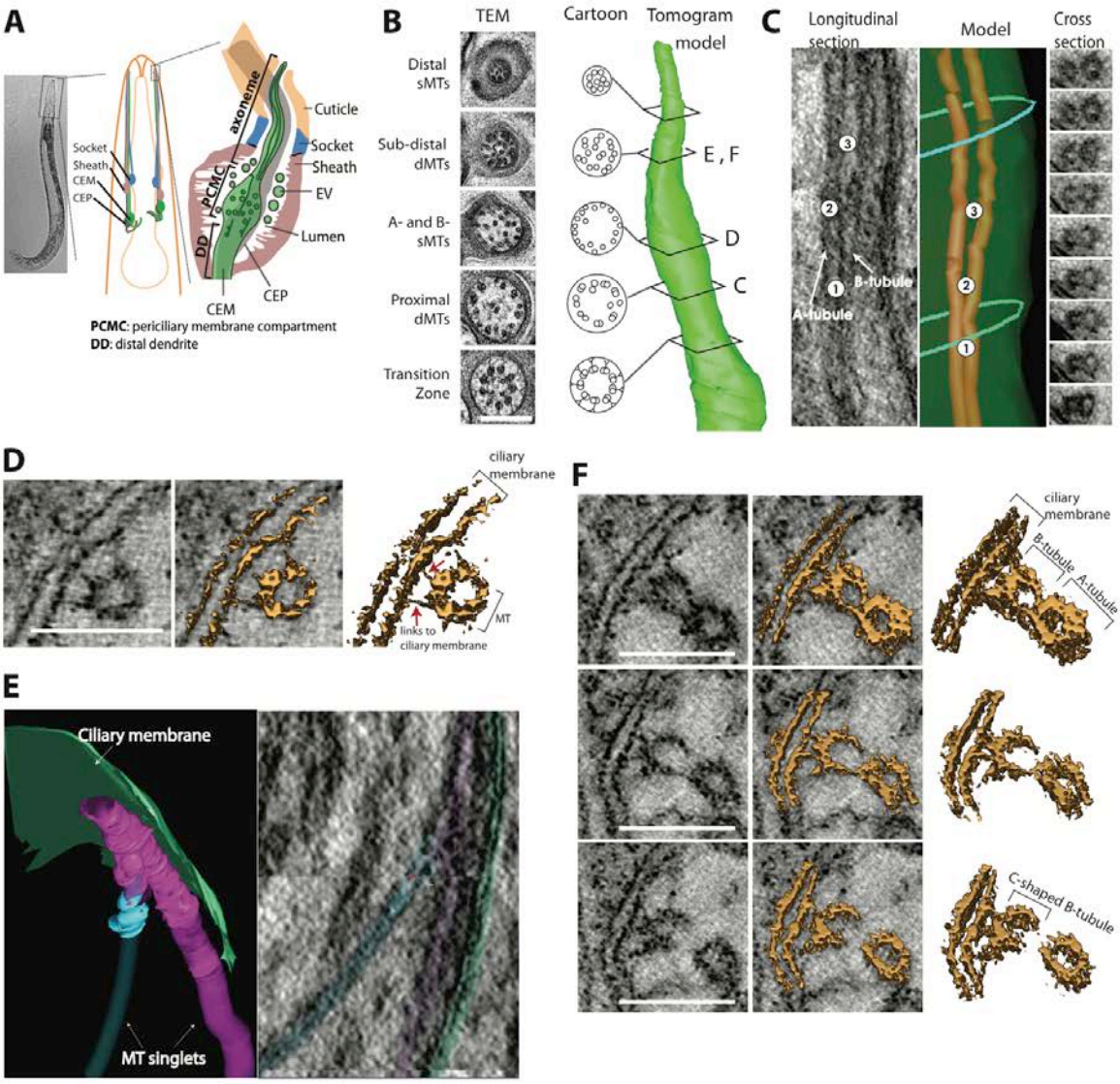

Figure 1 Specialized ultrastructure of adult CEM cilia reveals a novel axonemal microtubule arrangement

A Left: Adult *C. elegans* male DIC image with region of interest boxed. Middle: Each of four quadrant cephalic sensilla contains the endings of CEM and CEP neurons and the socket

and sheath support cells. **Right:** The cephalic sensillum contains cilia of the CEM and CEP neurons surrounded by socket (blue) and sheath (pink) cells. The CEM cilium (green) curves out and the tip protrudes to the environment via a cuticular pore (orange); while CEP cilium (gray) curves in and embeds in the cuticle. The cephalic lumen formed by the sheath and socket cells contains CEM-derived EVs (Wang, Silva et al. 2014).

B The CEM axoneme has five ultrastructurally distinct regions. Right: Serial electron tomogram model shows the relative positions of the five distinguishable regions. Sections labeled C-F correspond to subsequent panels. Left: TEM inserts show the representative microtubule organization. Scale bar, 250nm. dMT, doublet microtubule; sMT, singlet microtubule. Cartoon inserts show a stereotypical microtubule arrangement within each segment and do not directly reflect adjacent TEM sections.

C Tomogram model of A- and B- tubules of a microtubule doublet splitting into an A-tubule and B-tubule singlet. **Left:** Longitudinal section taken from a serial electron tomogram depicting a representative microtubule doublet splitting into A- and B- tubule singlets at the proximal doublet region. **Middle:** segmented tomogram model of the left panel depicting microtubules in orange, and ciliary membrane is green. Teal rings depict the boundary of 500-600nm long region where most microtubule doublets split into two singlets. Numbers correspond to the equivalent regions in the tomogram and model. **Right:** tomogram cross-sections of a representative doublet splitting into two singlets. Refer to Figure S1 for images of all nine microtubules.

D Some microtubules form bridges with the ciliary membrane. **Left**: flat-plane image taken from electron tomogram illustrating a microtubule singlet making three bridges with ciliary membrane. **Right**: density-based isosurface 3D model of this location. **Middle**: overlay. Scale bar, 50nm. Refer to Movie S2 for annotated 3D tomogram. In the 75nm cilia section examined, 5 out of 9 A-tubules, 6 out of 8 B-tubules, and 0 out of 2 inner singlets were connected the ciliary membrane at least at one point. Of those membrane-associated tubules, the number of connections was: 4.4±6.3 for an A-tubule and 11.16±3.9 for a B-tubule (mean±SD). The difference between A-tubule and B-tubule connections did not reach statistical significance

E Tomogram model of the sub-distal region depicting A- and B- tubule singlet fusion. **Left:** segmented electron tomogram model depicting fusion of A-tubule and B-tubule singlets (pink and teal false-colored), and the A-tubule singlet continuing to the distal segment (incomplete). Ciliary membrane is green. **Right:** false-colored longitudinal section from the electron tomogram used to generate the model on the left.

F B-tubules form transient C-shaped structures during the singlet-to-doublet transition in the sub-distal segment (refer to Figure 1B). **Left panel**: successive images from a tomogram. Scale bar, 50nm. **Right panel**: isosurface 3D models corresponding to images on the left. **Middle panel:** overlay.

See also Figure S1, Movies S1 and S2.

Figure 2

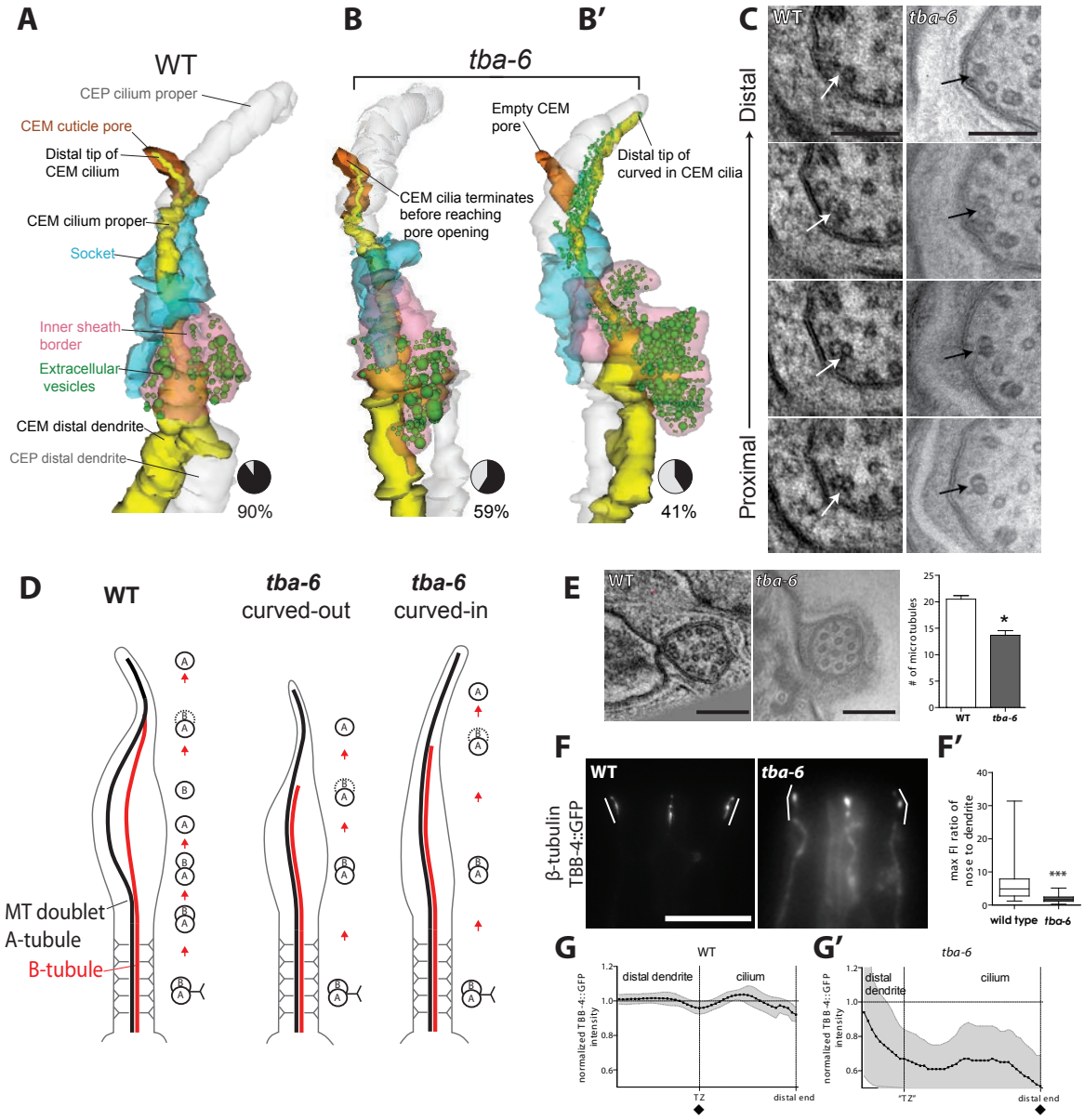

Figure 2 tba-6 is required for CEM cilia curvature, microtubule architecture, and tubulin composition

A, B, B' Serial TEM reconstructions of male cephalic sensilla of WT and *tba-6* males. Pie charts (bottom) indicate the penetrance of the cilia curvature phenotype as assayed by TBB-4::tagRFP (WT N=83, *tba-6* N=102 males).

A In WT, CEM (yellow) and CEP cilia (gray) share a lumen formed by the sheath (inner border in pink) and socket (teal) (refer to Figure 1A). The distal tip of the CEM cilium protrudes to the environment through a cuticular pore (brown) (also, Figure S1C). The CEP cilium curves in and embeds in the cuticle. EVs (green) are located in the proximal region of the cephalic lumen.

B 59% of *tba-6* cilia curve-out but do not protrude through the cuticular pore. EVs were observed inside the cuticular pore (for TEM cross sections of *tba-6*, see Figure 4C).

B' 41% of *tba-6* cilia curve-in, follow the path of the CEP cilium, and embed in the cuticle. EVs were found in the lumen surrounding CEM and CEP cilia.

C In *tba-6*, microtubule doublets terminate and do not form A- and B- tubule singlets. **Right:** Serial TEM images of *tba-6* cilia with A-tubules continuing as singlets and B-tubules terminating (black arrow). **Left:** Cross-sections of WT cilia from a serial tomogram showing a representative A- and B-tubule of a microtubule doublet splitting to form two singlets (white arrow) (refer to Figure 1F and Figure S1A, B). Scale bar, 50nm.

D Cartoon depicting microtubule architectures and cilia shapes.

E Cross sections of sub-distal CEM cilia in WT and *tba-6* animals. Scale bar, 50nm. **Right:** Microtubule singlet quantification: WT= 20±2, *tba-6* curved-out = 14±2 tubules, mean±SD, *p*-value=0.0269 by Mann Whitney, N=3 animals, and n=12 cilia for each genotype.

F, F', G, G' β-tubulin TBB-4::GFP relative ciliary levels and ciliary localization. In WT, TBB-4::GFP localizes to CEM cilia in a stereotypical pattern; lines indicate two of four CEM cilia, quantified in **G**, n= 25 cilia. Ciliary TBB-4::GFP levels were normalized to levels in the CEM dendrite, mean fold intensity ± SD. This pattern is altered in *tba-6* mutants, quantified in **G'**, n=20 cilia. In *tba-6,* TBB-4::GFP ciliary levels are significantly reduced and TBB-4::GFP accumulates at ciliary bases. **F'**, N=86 and 102 animals for WT and *tba-6* respectively, p-value < 0.0001 by Mann-Whitney U test, Scale bar,10µm.
See also Table S1, and Figure S2.

Figure 3

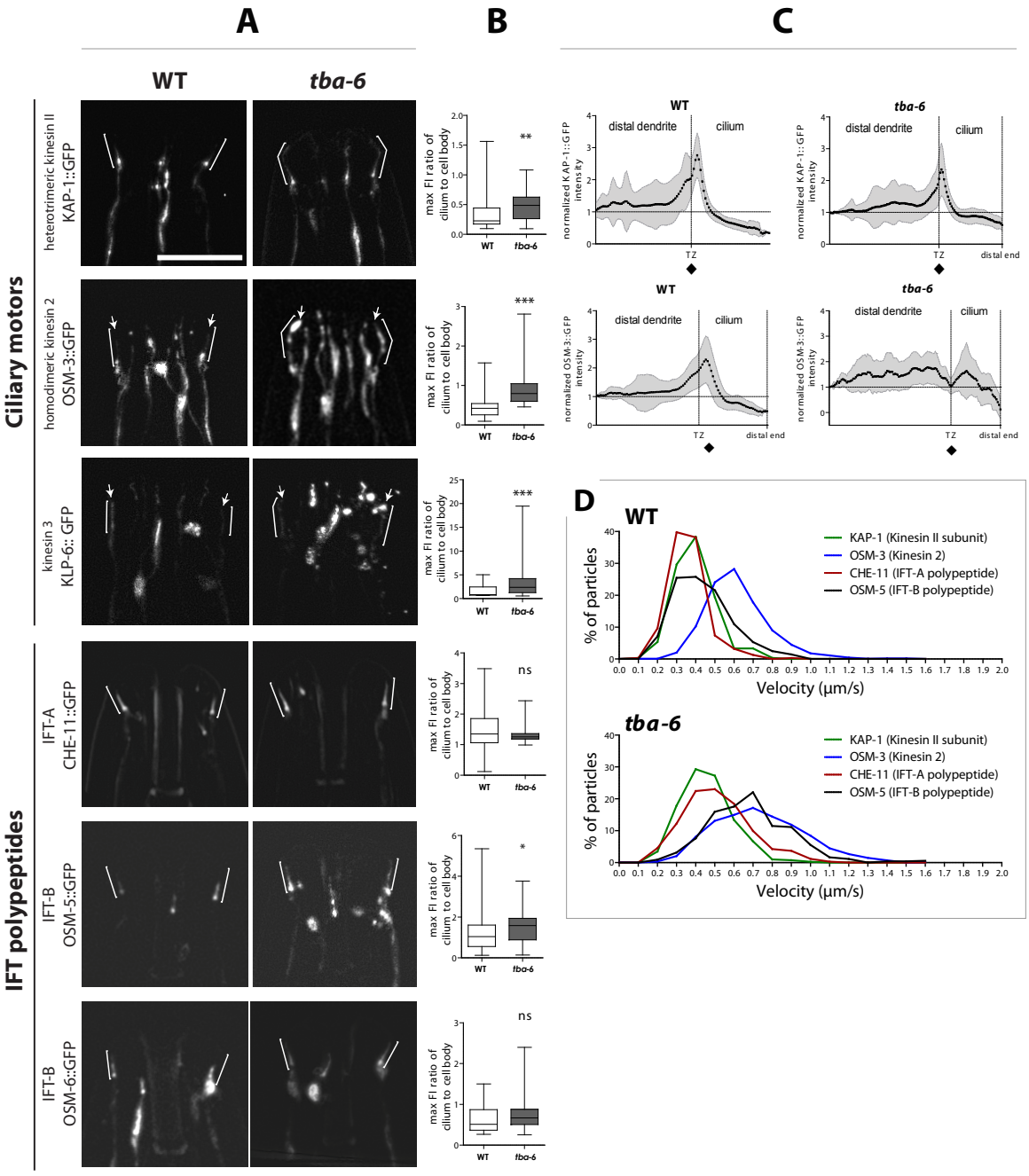
A
B
C
WT
tba-6
Ciliary motors
IFT polypeptides
heterotrimeric kinesin II
KAP-1::GFP
homodimeric kinesin 2
OSM-3::GFP
kinesin 3
KLP-6:: GFP
IFT-A
CHE-11::GFP
IFT-B
OSM-5::GFP
IFT-B
OSM-6::GFP
max FI ratio of cilium to cell body
**
***
***
ns
*
ns
distal dendrite
cilium
TZ
distal end
normalized KAP-1::GFP intensity
normalized OSM-3::GFP intensity
D
% of particles
Velocity (µm/s)
KAP-1 (Kinesin II subunit)
OSM-3 (Kinesin 2)
CHE-11 (IFT-A polypeptide)
OSM-5 (IFT-B polypeptide)

Figure 3 Localization and velocity distributions of IFT motors and polypeptides in CEM cilia of wild type and tba-6 mutant animals

A Widefield fluorescence images of GFP tagged IFT polypeptides and motors. Lines in each image indicate two of the four CEM cilia. OSM-3::GFP and KLP-6 GFP are driven by the *klp-6* promoter and expressed in both CEM (arrows) and IL2 cilia. All other reporters are driven by the *pkd-2* promoter and expressed in CEM cilia. Phenotypes are summarized in Table S1. Scale bar is 10μm and applicable to all panels.

B Comparison of fluorescence levels in cilia of WT and *tba-6* males normalized to cell body. Mean ± SD. '*', '**', '***' indicate *p*-values of <0.01, <0.001 and, <0.0001 respectively by Mann-Whitney U test.

C Average CEM ciliary localization pattern of KAP-1::GFP and OSM-3::GFP in WT and *tba-6* mutant backgrounds. 'u' indicates feature used to align intensity profiles; center-line depicts the mean intensity and the shaded area represent the standard deviation.

D Velocity distributions of GFP-tagged IFT motors and polypeptides in CEM cilia of WT and *tba-6* males. Distribution averages, standard deviations, and statistical analyses are summarized in Table 1.

See also Table S1.

Figure 4

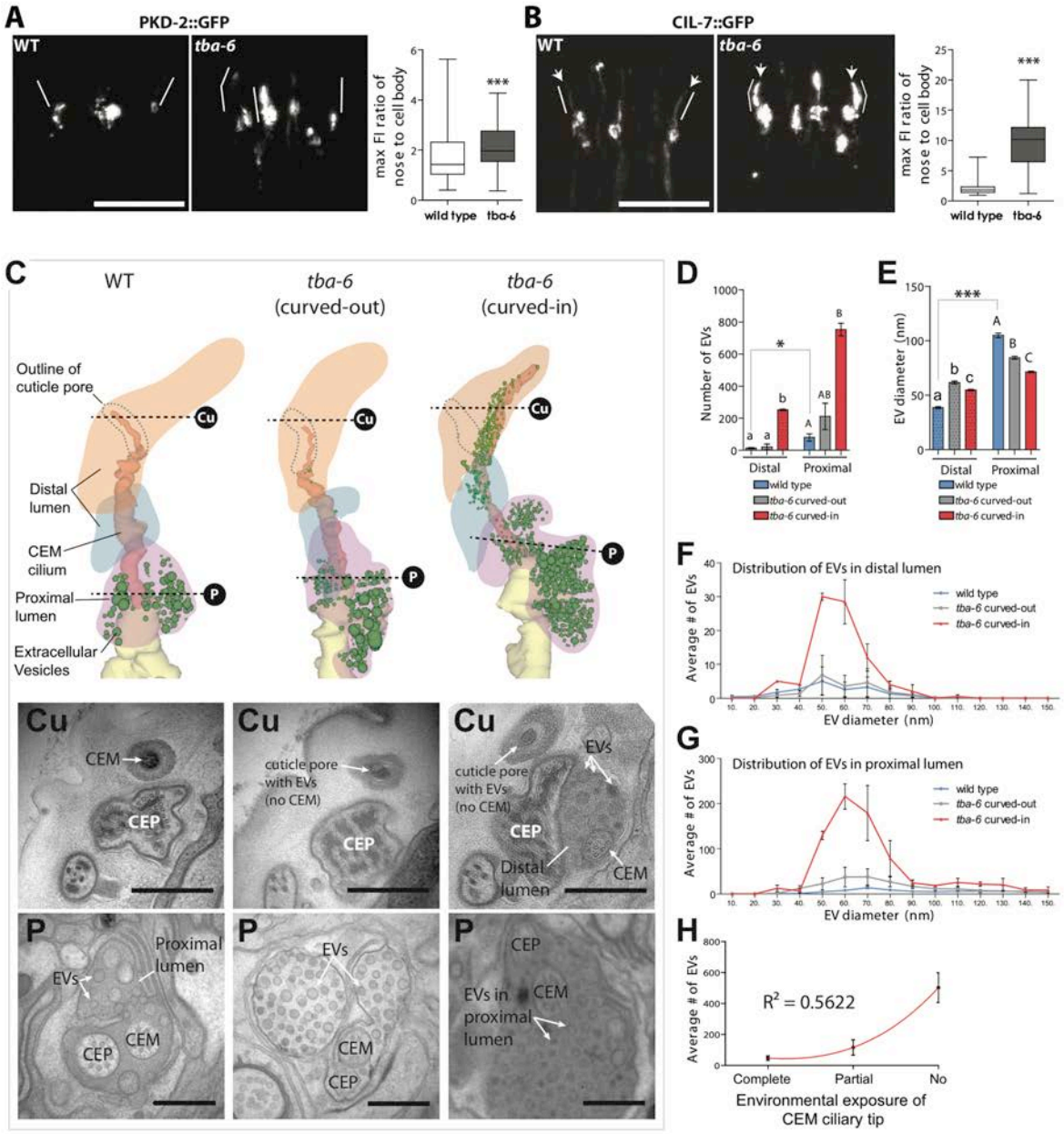

Figure 4 tba-6 regulates EV location, abundance, and size in the cephalic sensilla.

A, B PKD-2::GFP and CIL-7::GFP abnormally accumulate in *tba-6* mutant animals. Quantified on right. See Table S1 for statistical analysis. Lines indicate cilia. Scale bar, 10µm.

C Simplified serial TEM reconstructions depicting relative positions of lumenal EVs. Genotypes are indicated at the top and respective reconstructions and TEM images are arranged vertically. Scale bars in TEM images are 500nm.

C-top row The CEM cilium is red and distal dendrite is yellow. For simplicity, the cuticular pore is outlined using a dotted line and the CEP cilium is not shown. Dashed lines indicated by 'Cu'(cuticular pore) or 'P' (proximal lumen) denote the relative position of the TEM cross sections.

C-middle row TEM cross section at the cuticular pore. The WT distal CEM cilium is present and contains microtubule singlets. The *tba-6* curved out CEM cilium does not reach the cuticular pore. Instead, EVs are seen in the empty pore. *tba-6* curved in cilia are deflected from the pore and embedded in the cuticle lumen next to the CEP cilium. EVs are seen in the cephalic lumen and cuticle pore.

C-bottom row TEM cross-sections from proximal sheath cell level**.** In WT, few EVs are observed in the cephalic lumen. In *tba-6*, EVs abnormally accumulate in the cephalic lumen.

D and **E** Comparison of average number of EVs and average EV diameter in the distal and proximal cephalic lumen. In WT, EVs were more abundant in the proximal lumen (distal=14±10 EVs, proximal=80±60 EVs, *p*-value=0.0087, '*', by Mann-Whitney U test). When present, distally located EVs were significantly smaller than proximally located EVs (distal=36.67±0.63nm, proximal=105±29.14nm, mean±SD, n=8 cilia, *p*-value<0.0001 for size, '***', by Mann-Whitney U test). *tba-6* accumulated significantly more lumenal EVs than WT (distal=252±10 and proximal=753±77 EVs, mean±SD, *p*-value=0.007 for both with WT using Kruskal-Wallis with Dunn's correction). *tba-6* distally located EVs were larger than WT distally located EVs (diameters were 61.65±13.96nm and 54.86±9.76nm for curved out (n=6) and curved in (n= 2) sensilla, *p*-value<0.0001 compared with WT by Kruskal-Wallis with Dunn's correction). *tba-6* proximally located EVs were smaller than WT proximally located EVs (diameters were 84.57±35.21nm and 71.48±19.75nm, mean±SD, for curved-out and curved–in sensilla, *p*-values<0.0001 compared with wild type by Kruskal-Wallis with Dunn's correction).

G and **H** Average histograms of EV diameter within the distal and proximal cephalic lumen in WT and *tba-6*. In *tba-6* curved-in cilia 50-70nm sized EVs accumulate in the lumen (WT distal: 8 50-60nm EVs, *tba-6* curved-in distal: 59 50-60nm EVs; WT proximal: 13 50-60nm EVs, *tba-6* curved-in proximal: 346 50-60nm EVs n=8 sensilla for WT and n=2 sensilla for *tba-6* curved-in, *p*-value<0.0001 by two-way ANOVA).

I Occlusion of the CEM cilia tip correlates with luminal EV accumulation. In WT, CEM cilia tips are environmentally exposed through the cuticular pore (see Figure S1C) and contain 47±53 lumenal EVs, n=7 sensilla. Tips of the *tba-6* curved-out cilia do not reach pore (hence "partial" label), accumulate 116±170 EVs (n=6 sensilla). Tips of *tba-6* curved-in cilia are not environmentally exposed and accumulate on 502±272 lumenal EVs (n=4 sensilla). R^2 indicates 'goodness of fit' of the cubic polynomial line. Number of EVs reflect mean ± SD and n is number of cephalic sensilla analyzed via quantitative serial EM.

See also Table S1

Figure 5

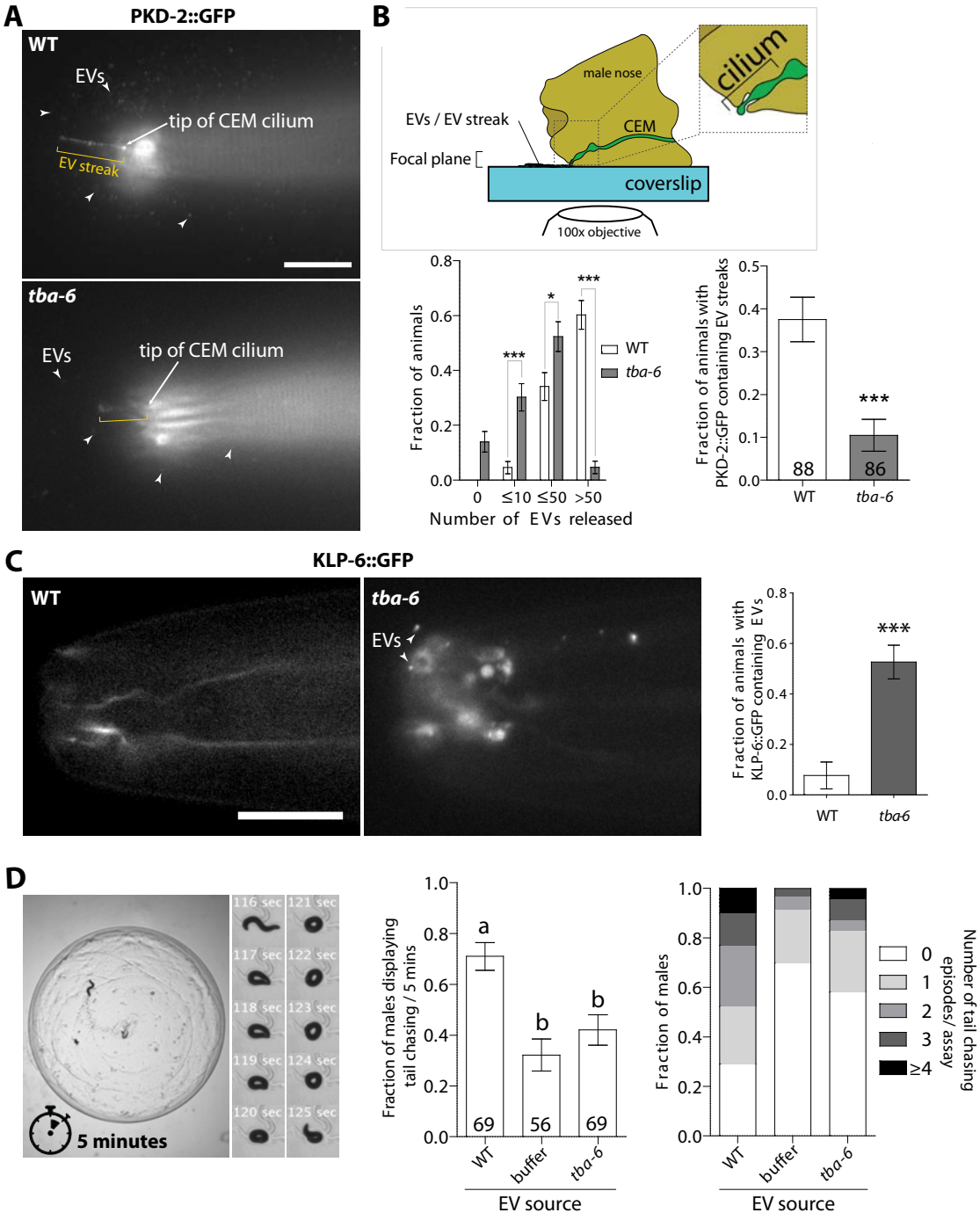

Figure 5 tba-6 is required for ciliary EV cargo composition, release, and bioactivity

A WT and *tba-6* males release PKD-2::GFP containing EVs. **B** Cartoon depicts the single-focal-plane fluorescence image acquired at the surface of the cover slip showing PKD-2::GFP-containing EVs in WT and *tba-6* worms. In **A**, arrowheads point to EVs; yellow brackets mark PKD-2::GFP EV streaks. Abundance of EV streaks is quantified below. Environmental release of PKD-2::GFP-containing EVs is significantly reduced in *tba-6* mutants (WT: '0' = 0, '≤10'= 0.04±21, '≤50,'= 0.34±0.48 , '>50'=0.60±0.49, fraction ± SD, N=88 worms; *tba-6*: '0' = 0.14±35, '≤10'= 0.30±0.46, '≤50'= 0.52±0.50, '>50'=0.05±0.21, fraction ± SD, N=86 worms). WT and *tba-6* mutants are significantly different in '≤10', '≤50' and '>50'catogories, '*' and '***' indicate *p*-values of <0.01 and <0.0001, respectively, using the Kruskal-Wallis test with Dunn's correction for multiple comparisons. Error bars indicate SEM. Fraction of animals with PKD-2::GFP-positive EV streaks was significantly reduced in *tba-6* background (WT = 0.37±0.49, *tba-6* = 0.10±0.34) '***' indicates *p*-value <0.0001 using Mann-Whitney test. Fraction ± SD, N = 88 (WT) and 86 (*tba-6*) animals. Error bars indicate SEM.

C In WT, KLP-6::GFP is excluded from EVs. In *tba-6* mutants, KLP-6::GFP is ectopically shed and released into EVs. Arrowheads point to ectopic EVs (refer Figure 3). Quantified on right. Statistical details are summarized in Table S1. Scale bar is 10µm.

D TBA-6 is required for bioactivity of EVs.

Left: Young adult virgin WT males were individually placed on a freshly made EV-containing bacterial lawn and video recorded for 5 minutes. **Inset** Sample time series of tail-chasing behavior; in this case the male was tail-chasing from 117th to 124th second.

Middle: WT males exhibit a basal level of tail chasing behavior (buffer control). WT-derived EVs increased the fraction of males exhibiting tail chasing (0.71±0.06 events/5 minutes vs buffer control 32±0.06 events/5 minutes, mean ± SEM, N=56 males and N=69 males for WT and buffer control, *p*-value<0.0001 with buffer control). In contrast, tail chasing events were similar with *tba-6* derived EVs and buffer control (0.42±0.05 events/5 minutes, N= 69 *tba-6* males, *p*-value>0.05 with buffer control and *p*-value<0.001 with WT EVs). Number within bars indicates number of animals. Letters indicate statistically distinct groups by Kruskal-Wallis test with Dunn's correction for multiple comparisons. Error bars indicate SEM.

Right: Number of tail chasing episodes per assay increases when WT males are exposed to WT EVs but not *tba-6*-derived EVs.

See also Table S1

Figure 6

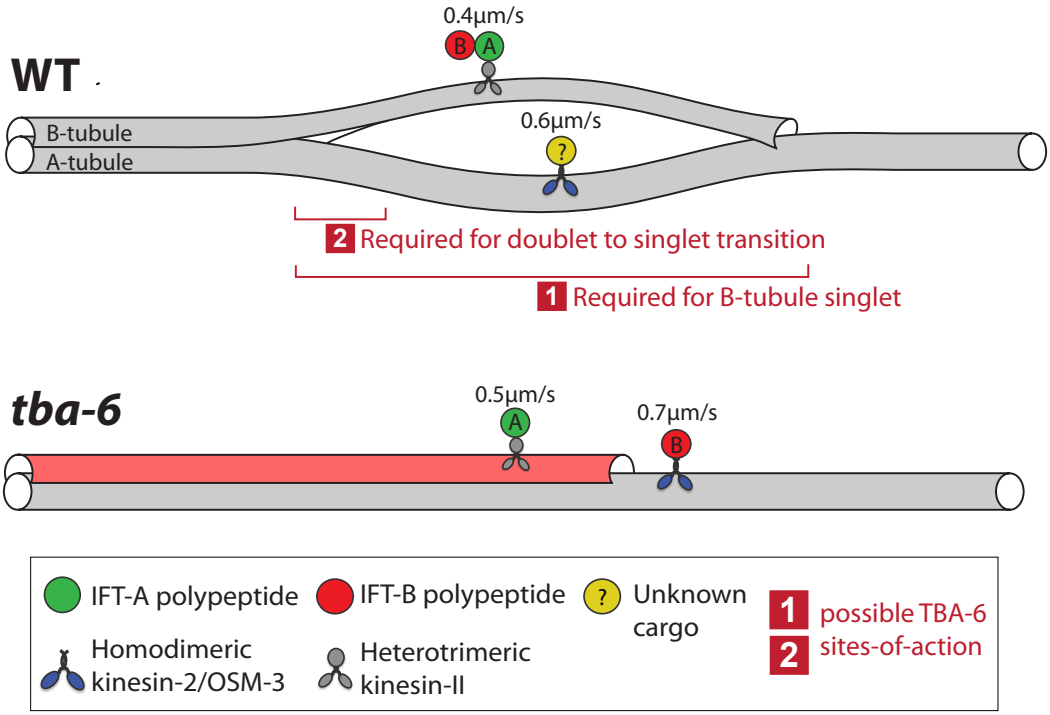

Figure 6 Model of a doublet microtubule, IFT motors and polypeptides in WT and tba-6 CEM cilia

In **WT,** microtubule doublets splay to form A- and B-tubule singlets. Heterotrimeric kinesin-II and IFT A- and B-polypeptides are co-transported at overlapping velocities. Homodimeric kinesin-2 OSM-3 travels at a higher velocity separate from IFT polypeptides, transporting unknown cargo. KLP-6 is not included in this model.

In ***tba-6,*** microtubule doublets do not splay to form A- and B- tubule singlets. The doublet region is elongated and terminates abruptly. Only A-tubule singlets extend. Axonemal

abnormalities accompany changes in IFT. IFT-A and –B polypeptides travel at distinct velocities that overlap with heterotrimeric kinesin-II and OSM-3, respectively.

Red squares indicate possible TBA-6 sites of action. We propose a model where the separation of microtubule doublets into distinct A-tubule and B-tubule singlets acts as a physical substrate for the functional separation of these two conserved IFT kinesins. Alternatively, tubulin composition and post-translational modifications may also impact IFT-motor-cargo dynamics.

References

1. Dutcher, S.K. (2001). The tubulin fraternity: alpha to eta. Current Opinion in Cell Biology *13*, 49-54.
2. Winey, M., and O'Toole, E. (2014). Centriole structure. Phil. Trans. R. Soc. B *369*, 20130457-20130398.
3. Roll-Mecak, A. (2015). Intrinsically disordered tubulin tails: complex tuners of microtubule functions? Semin Cell Dev Biol *37*, 11-19.
4. Lockhead, D., Schwarz, E.M., O'Hagan, R., Bellotti, S., Krieg, M., Barr, M.M., Dunn, A.R., Sternberg, P.W., and Goodman, M.B. (2016). The tubulin repertoire of C. elegans sensory neurons and its context-dependent role in process outgrowth. Mol Biol Cell.
5. Tischfield, M.A., Cederquist, G.Y., Gupta, M.L., Jr., and Engle, E.C. (2011). Phenotypic spectrum of the tubulin-related disorders and functional implications of disease-causing mutations. Curr Opin Genet Dev *21*, 286-294.
6. Rosenbaum, J.L., and Witman, G.B. (2002). Intraflagellar transport. Nat Rev Mol Cell Biol. *3*, 813-825.
7. Fisch, C., and Dupuis-Williams, P. (2011). Ultrastructure of cilia and flagella - back to the future! Biol Cell *103*, 249-270.
8. Linck, R., Fu, X., Lin, J., Ouch, C., Schefter, A., Steffen, W., Warren, P., and Nicastro, D. (2014). Insights into the structure and function of ciliary and flagellar doublet microtubules: tektins, Ca2+-binding proteins, and stable protofilaments. J Biol Chem *289*, 17427-17444.
9. Tsuji, T., Matsuo, K., Nakahari, T., Marunaka, Y., and Yokoyama, T. (2016). Structural basis of the Inv compartment and ciliary abnormalities in Inv/nphp2 mutant mice. Cytoskeleton (Hoboken) *73*, 45-56.
10. Perkins, L.A., Hedgecock, E.M., Thomson, J.N., and Culotti, J.G. (1986). Mutant sensory cilia in the nematode Caenorhabditis elegans. Dev Biol *117*, 456-487.
11. Doroquez, D.B., Berciu, C., Anderson, J.R., Sengupta, P., and Nicastro, D. (2014). A high-resolution morphological and ultrastructural map of anterior sensory cilia and glia in Caenorhabditis elegans. Elife *3*, e01948.
12. O'Hagan, R., and Barr, M.M. (2016). Kymographic Analysis of Transport in an Individual Neuronal Sensory Cilium in Caenorhabditis elegans. Methods Mol Biol *1454*, 107-122.
13. Taschner, M., and Lorentzen, E. (2016). The Intraflagellar Transport Machinery. Cold Spring Harb Perspect Biol *8*.
14. Mukhopadhyay, S., Lu, Y., Qin, H., Lanjuin, A., Shaham, S., and Sengupta, P. (2007). Distinct IFT mechanisms contribute to the generation of ciliary structural diversity in C. elegans. EMBO J *26*, 2966-2980.
15. Peden, E.M., and Barr, M.M. (2005). The KLP-6 kinesin is required for male mating behaviors and polycystin localization in Caenorhabditis elegans. Curr Biol *15*, 394-404.
16. Morsci, N.S., and Barr, M.M. (2011). Kinesin-3 KLP-6 regulates intraflagellar transport in male-specific cilia of Caenorhabditis elegans. Curr Biol *21*, 1239-1244.

17. Wang, J., Silva, M., Haas, L.A., Morsci, N.S., Nguyen, K.C., Hall, D.H., and Barr, M.M. (2014). C. elegans Ciliated Sensory Neurons Release Extracellular Vesicles that Function in Animal Communication. Curr Biol *24*, 519-525.
18. Verhey, K.J., and Gaertig, J. (2007). The tubulin code. Cell Cycle *6*, 2152-2160.
19. Janke, C. (2014). The tubulin code: molecular components, readout mechanisms, and functions. J Cell Biol *206*, 461-472.
20. Yu, I., Garnham, C.P., and Roll-Mecak, A. (2015). Writing and Reading the Tubulin Code. J Biol Chem *290*, 17163-17172.
21. Janke, C., Rogowski, K., Wloga, D., Regnard, C., Kajava, A.V., Strub, J.M., Temurak, N., van Dijk, J., Boucher, D., van Dorsselaer, A., Suryavanshi, S., Gaertig, J., and Edde, B. (2005). Tubulin polyglutamylase enzymes are members of the TTL domain protein family. Science *308*, 1758-1762.
22. Rogowski, K., van Dijk, J., Magiera, M.M., Bosc, C., Deloulme, J.-C., Bosson, A., Peris, L., Gold, N.D., Lacroix, B., Bosch Grau, M., Bec, N., Larroque, C., Desagher, S., Holzer, M., Andrieux, A., Moutin, M.-J., and Janke, C. (2010). A family of protein-deglutamylating enzymes associated with neurodegeneration. Cell *143*, 564-578.
23. O'Hagan, R., Piasecki, B.P., Silva, M., Phirke, P., Nguyen, K.C., Hall, D.H., Swoboda, P., and Barr, M.M. (2011). The tubulin deglutamylase CCPP-1 regulates the function and stability of sensory cilia in C. elegans. Curr Biol *21*, 1685-1694.
24. (1998). Genome sequence of the nematode C. elegans: a platform for investigating biology. The C. elegans Sequencing Consortium. Science *282*, 2012-2018.
25. Gogonea, C.B., Gogonea, V., Ali, Y.M., Merz, K.M., Jr., and Siddiqui, S.S. (1999). Computational prediction of the three-dimensional structures for the Caenorhabditis elegans tubulin family. J Mol Graph Model *17*, 90-100, 126-130.
26. Hurd, D.D., Miller, R.M., Nunez, L., and Portman, D.S. (2010). Specific alpha- and beta-tubulin isotypes optimize the functions of sensory Cilia in Caenorhabditis elegans. Genetics *185*, 883-896.
27. Jauregui, A.R., Nguyen, K.C., Hall, D.H., and Barr, M.M. (2008). The Caenorhabditis elegans nephrocystins act as global modifiers of cilium structure. J Cell Biol *180*, 973-988.
28. Hao, L., Thein, M., Brust-Mascher, I., Civelekoglu-Scholey, G., Lu, Y., Acar, S., Prevo, B., Shaham, S., and Scholey, J.M. (2011). Intraflagellar transport delivers tubulin isotypes to sensory cilium middle and distal segments. Nat Cell Biol *13*, 790-798.
29. Wang, J., and Barr, M.M. (2016). Ciliary Extracellular Vesicles: Txt Msg Organelles. Cell Mol Neurobiol *36*, 449-457.
30. Wang, J., Kaletsky, R., Silva, M., Williams, A., Haas, L.A., Androwski, R.J., Landis, J.N., Patrick, C., Rashid, A., Santiago-Martinez, D., Gravato-Nobre, M., Hodgkin, J., Hall, D.H., Murphy, C.T., and Barr, M.M. (2015). Cell-Specific Transcriptional Profiling of Ciliated Sensory Neurons Reveals Regulators of Behavior and Extracellular Vesicle Biogenesis. Curr Biol *25*, 3232-3238.
31. Maguire, J.E., Silva, M., Nguyen, K.C., Hellen, E., Kern, A.D., Hall, D.H., and Barr, M.M. (2015). Myristoylated CIL-7 regulates ciliary extracellular vesicle biogenesis. Mol Biol Cell *26*, 2823-2832.
32. Woolley, D.M., and Nickels, S.N. (1985). Microtubule termination patterns in mammalian sperm flagella. J Ultrastruct Res *90*, 221-234.

33. Afzelius, B.A., Dallai, R., Lanzavecchia, S., and Bellon, P.L. (1995). Flagellar structure in normal human spermatozoa and in spermatozoa that lack dynein arms. Tissue Cell *27*, 241-247.
34. Binder, L.I., and Rosenbaum, J.L. (1978). The in vitro assembly of flagellar outer doublet tubulin. The Journal of Cell Biology *79*, 500-515.
35. Song, Y.H., and Mandelkow, E. (1995). The anatomy of flagellar microtubules: polarity, seam, junctions, and lattice. The Journal of Cell Biology *128*, 81-94.
36. Raff, E.C., Fackenthal, J.D., Hutchens, J.A., Hoyle, H.D., and Turner, F.R. (1997). Microtubule Architecture Specified by a β-Tubulin Isoform. Science (New York, NY) *275*, 70-73.
37. Akella, J.S., Wloga, D., Kim, J., Starostina, N.G., Lyons-Abbott, S., Morrissette, N.S., Dougan, S.T., Kipreos, E.T., and Gaertig, J. (2010). MEC-17 is an alpha-tubulin acetyltransferase. Nature *467*, 218-222.
38. Cueva, J.G., Hsin, J., Huang, K.C., and Goodman, M.B. (2012). Posttranslational acetylation of alpha-tubulin constrains protofilament number in native microtubules. Curr Biol *22*, 1066-1074.
39. Topalidou, I., Keller, C., Kalebic, N., Nguyen, K.C.Q., Somhegyi, H., Politi, K.A., Heppenstall, P., Hall, D.H., and Chalfie, M. (2012). Genetically Separable Functions of the MEC-17 Tubulin Acetyltransferase Affect Microtubule Organization. Current Biology VL - *22*, 1057-1065.
40. Pathak, N., Obara, T., Mangos, S., Liu, Y., and Drummond, I.A. (2007). The zebrafish fleer gene encodes an essential regulator of cilia tubulin polyglutamylation. Mol Biol Cell *18*, 4353-4364.
41. Garnham, C.P., Vemu, A., Wilson-Kubalek, E.M., Yu, I., Szyk, A., Lander, G.C., Milligan, R.A., and Roll-Mecak, A. (2015). Multivalent Microtubule Recognition by Tubulin Tyrosine Ligase-like Family Glutamylases. Cell *161*, 1112-1123.
42. Stepanek, L., and Pigino, G. (2016). Microtubule doublets are double-track railways for intraflagellar transport trains. Science *352*, 721-724.
43. Jiang, L., Tam, B.M., Ying, G., Wu, S., Hauswirth, W.W., Frederick, J.M., Moritz, O.L., and Baehr, W. (2015). Kinesin family 17 (osmotic avoidance abnormal-3) is dispensable for photoreceptor morphology and function. FASEB J.
44. Jenkins, P.M., Hurd, T.W., Zhang, L., McEwen, D.P., Brown, R.L., Margolis, B., Verhey, K.J., and Martens, J.R. (2006). Ciliary targeting of olfactory CNG channels requires the CNGB1b subunit and the kinesin-2 motor protein, KIF17. Curr Biol *16*, 1211-1216.
45. Williams, C.L., McIntyre, J.C., Norris, S.R., Jenkins, P.M., Zhang, L., Pei, Q., Verhey, K., and Martens, J.R. (2014). Direct evidence for BBSome-associated intraflagellar transport reveals distinct properties of native mammalian cilia. Nat Commun *5*, 5813.
46. Zhao, C., Omori, Y., Brodowska, K., Kovach, P., and Malicki, J. (2012). Kinesin-2 family in vertebrate ciliogenesis. Proc Natl Acad Sci U S A *109*, 2388-2393.
47. Prevo, B., Mangeol, P., Oswald, F., Scholey, J.M., and Peterman, E.J. (2015). Functional differentiation of cooperating kinesin-2 motors orchestrates cargo import and transport in C. elegans cilia. Nat Cell Biol.

48. Snow, J.J., Ou, G., Gunnarson, A.L., Walker, M.R., Zhou, H.M., Brust-Mascher, I., and Scholey, J.M. (2004). Two anterograde intraflagellar transport motors cooperate to build sensory cilia on C. elegans neurons. Nat Cell Biol *6*, 1109-1113.
49. Pan, X., Ou, G., Civelekoglu-Scholey, G., Blacque, O.E., Endres, N.F., Tao, L., Mogilner, A., Leroux, M.R., Vale, R.D., and Scholey, J.M. (2006). Mechanism of transport of IFT particles in C. elegans cilia by the concerted action of kinesin-II and OSM-3 motors. J Cell Biol *174*, 1035-1045.

Supplemental

Figure S1

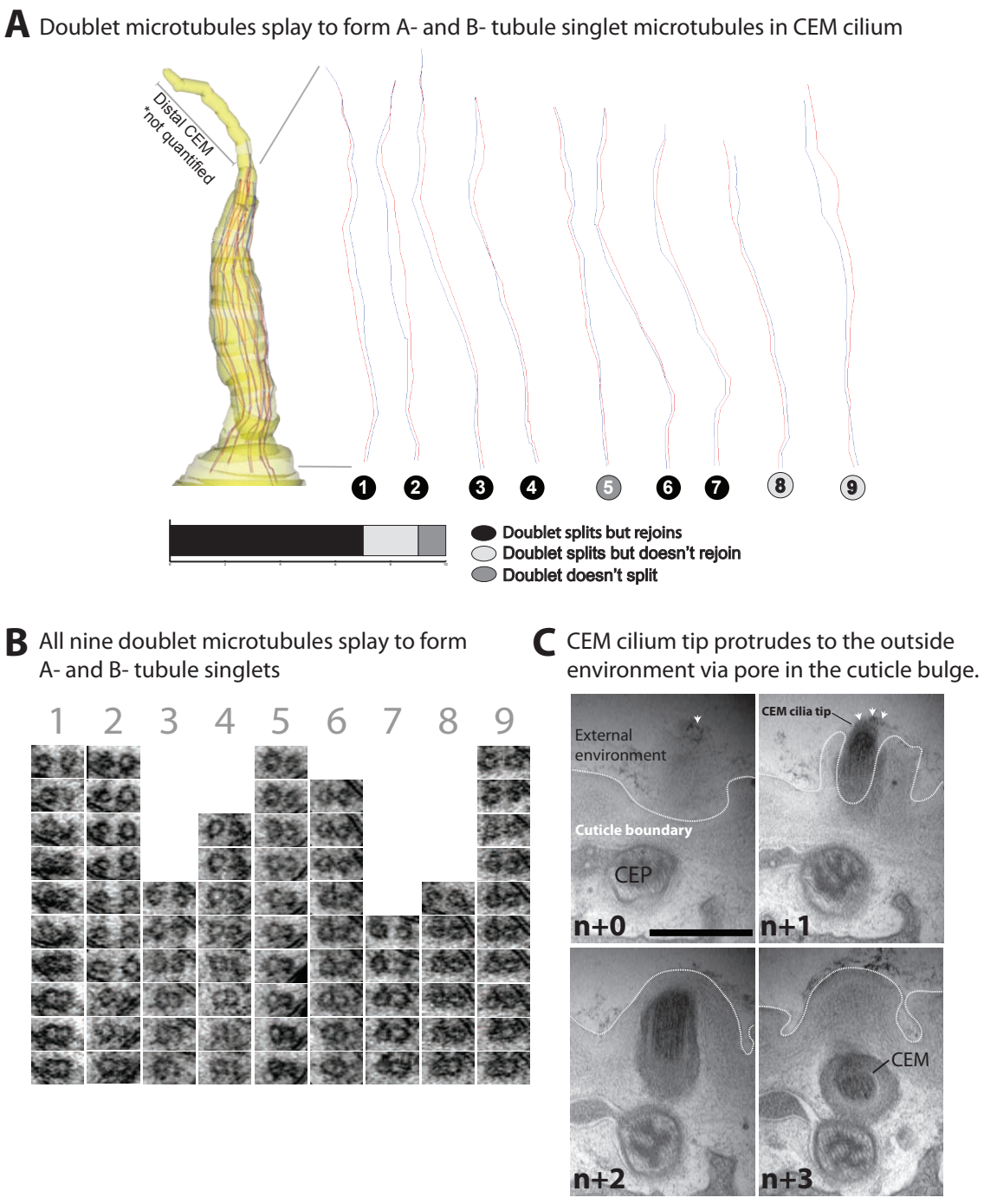

Figure 7 (S1) Specialized ultrastructure of adult CEM cilia

A Doublet microtubules (dMTs) splay to form A-tubule and B-tubule singlet microtubules (sMTs) in CEM cilia. Segmented model of a CEM cilium (yellow) generated via serial TEM reconstruction with false-colored A-tubules and B-tubules (red and blue, respectively). Doublets are individually displayed on the right to illustrate that A-tubule and B-tubule singlets in the A-B-sMT region (Figure 1B) are generated by splaying doublets that are attached at the ends. Microtubule doublets are numbered in no particular order and color-coded to distinguish their A-tubules and B-tubules, which are sorted into three categories depicted below. Microtubules of the distal CEM cilium could not be resolved due to their low contrast in oblique serial TEM images.

B A- and B-tubules of all nine doublet-microtubules splay to form individual singlets at the end of proximal dMT region (refer Figure 1B). Serial cross-sections taken from a tomogram depict all nine microtubule doublets in CEM cilia splitting into A- and B- tubule singlets. Doublets are numbered in no particular order.

C The CEM cilium tip protrudes to the outside environment via a pore in the cuticle bulge. Consecutive serial section TEM images acquired at 75nm thickness. 'n+0' to 'n+4' labeling corresponds to anterior to posterior orientation, respectively. 'n+2' shows the longitudinal view of CEM cilium tip protruding to the outside environment. 'n+4' depicts the cross section of distal CEM cilium immediately prior to making radial turn towards the surface of the animal. 'n+3' shown an oblique intermediate view. Arrowheads point the membranous structures associated with the tip of CEM cilia that could be fragmented EVs. All images are of same scale. Scale bar is 500nm. Related to Figure 1

Figure S2

A *tba-6(cxP4018)* is a loss of function allele

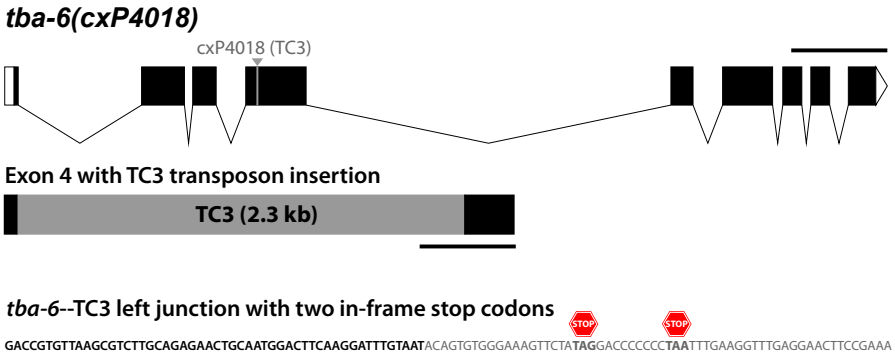

B TBA-6 C-terminal tail is unusual in amino acid composition, overall charge, and length

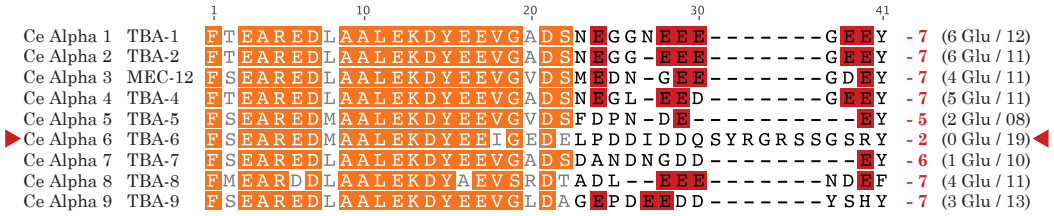

C Localization of TBA-6::GFP from Hurd *et al.* 2010 in CEM cilia and its ability to rescue the curved-in CEM cilia phenotype in *tba-6(cxP4018)* mutants

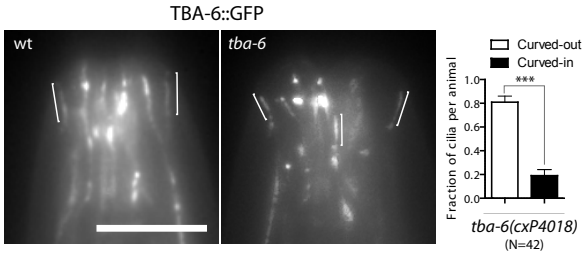

Figure 8 (S2) *tba-6(cxP4018)* is a loss of function allele

A

Top row Gene model of *tba-6(cxP4018)* with TC3 insertion site in the fourth exon indicated by an arrow (TC3 is not drawn to scale).

Middle row TC3 insertion (gray), drawn to scale in the context of fourth exon (black), introduces 2.3kb additional base pairs. Scale bar is 500 base pairs.

Bottom row Sequencing of left *tba-6*—TC3 junction revealed that TC3 introduced two in-frame stop codons in exon four**.**

B TBA-6 C-terminal tail is unusual in number of glutamine residues, overall charge, and length. Alignment of *C. elegans* α-tubulin C-terminal regions based on conserved residues highlighted in orange, C-terminal tail residues are in black letters with glutamate residues highlighted in red. In each C-terminal tail: overall charge is in red, number of glutamate residues and length is in parenthesis.

C TBA-6::GFP transgene from Hurd *et al.* 2010 (Hurd, Miller et al. 2010) can partially rescue the curved-in CEM cilia phenotype in *tba-6* CEM cilia (refer Figure 2). TBA-6::GFP expression in wild type and *tba-6* mutant backgrounds. Brackets indicate the length of the CEM cilia. CEM cilia curvature in *tba-6* animals expressing the TBA-6::GFP transgene is quantified on left: *tba-6* curved-out cilia 80±5, *tba-6* curved-in cilia 19±5, mean± SEM, '***' indicate *p*-value <0.0001 via Mann Whitney test. N= 42 number of animals. Scale bar is 50μm

Related to Figure 2

Supplemental Experimental Procedures

Transmission electron microscopy (TEM)

Age synchronized animals were subjected to high-pressure freeze fixation and freeze substitution in 2% osmium tetroxide and 2% water in acetone as the primary fixative (Weimer 2006). Samples were slowly treated to freeze substitution in an RMC freeze substitution device. Samples were infiltrated with Embed812 plastic resin with progressive change into 100% resin over 24 hours and with several 100% resin changes over two days prior to embedding in blocks. For TEM, plastic serial sections (70 to 80 nm thickness) were collected on copper mesh grids and stained with 4% uranyl acetate in 70% methanol, followed by washing and incubating with aqueous lead citrate. TEM images were captured on a Philips CM10 transmission electron microscope at 80kV with a Morada 11 megapixel TEM CCD camera driven by iTEM software (Olympus Soft Imaging Solutions).

Electron tomography (ET)

For tomography, data were acquired from either thinner (75nm) or thicker sections (250nm) using an FEI Technai20 TEM, using SerialEM software, and collecting 140 images per tilt axis. These data were Fourier processed using iMod software; dual-axis tomograms were generated using either the marker-less back projection method (Kremer, Mastronarde et al. 1996) or simultaneous iterative reconstruction technique (SIRT) (Wolf, Lubk et al. 2014). Up to 20 serial section tomograms were stitched to generate a volume spanning five microns and annotated using iMod software to generate models (Hall and Rice 2015).

Image handling, serial TEM volume reconstruction, annotation and quantitative EM

To quantify EVs and generate 3D models we used serial TEM sections of complete CEM sensilla. These images were stacked, aligned, annotated and measured using trakEM2 suite in FIJI (Schindelin, Arganda-Carreras et al. 2012). To quantify EV radii, abundance, and distribution, "spheres" were manually fitted to the narrowest diameter of each EV in the CEM sensilla. These spheres were then grouped based on their size and location in the sensillum. To generate 3D models of sensilla, the cuticle pore, CEM cilia, socket and inner sheath boundary were annotated using a combination of "pipe" and "arealist" tools. These models were smoothened for several iterations to improve appearance prior to exporting individual components to Adobe Photoshop as a single layer except for the "cuticle group". In Photoshop, background was removed and the "cuticle pore" group was "send to back" prior to generating the final Figure in Adobe Illustrator.

Wide field fluorescent microscopy

All fluorescence images were acquired using a Q-image retina camera attached to a Zeiss Imager microscope with 100x 1.4NA oil Zeiss plan- apochromatic objective. The microscope was controlled by Metamorph 7.1 to acquire Z-stacks and streams. To generate a comparative average distribution of proteins along CEM cilia, Z-stacks were acquired using the method described above, and then converted to maximum intensity-based projections using FIJI. Starting at a region of the distal dendrite with homogeneous fluorescence intensity, each cilium was manually traced using the "segmented line" tool

with a five-pixel diameter. The intensity along these lines was recorded as a string of numbers using the "plot profile" tool. These profiles were imported to Microsoft Excel as columns and aligned using an identified common feature (transition zone or ciliary tip) specific to each fluorescent reporter. Once aligned, values were averaged across rows to generate representative distributions.

In vivo motility assays

To directly measure *in vivo* velocity of IFT components in CEM cilia, we acquired time-lapse image stacks, which were later converted to kymographs using the KymographClear V2.0 plugin in FIJI. Motile particles were traced manually and velocities extracted with KymographDirect as described in (Prevo, Mangeol et al. 2015). We observed ~0.1 µm/s reduction of overall observed velocities as compared to Morsci and Barr (Morsci and Barr 2011). This reduction does not affect our analysis or overall conclusions, as our model is not based on absolute velocities of individual IFT components but rather on their relative changes.

Behavior Analysis

EVs were isolated from *him-5* or *tba-6; him-5* male enriched mixed-stage cultures using the ultracentrifugation method described in (Wang, Silva et al. 2014) with slight alterations. The quantity of EVs isolated from wild type and *tba-6* cultures was equalized before testing for bioactivity. For tail chasing assays, 4µl of EVs or M9 buffer was used to cover a 10µl OP50 bacterial lawn that was seeded within 8 hours of the assay. We observed sharp declines in wild type tail chasing if OP50 bacterial lawns were older than 8 hours. Larval L4

males were isolated the day prior to behavior assays. Virgin young adult males were placed in the center of the EV or M9 buffer (control) spotted lawn and behavior was recorded for 5 minutes with a capture rate of 1 frame/second. Plates were not reused. EV genotypes were rotated every 5 animals. Tail chasing events were scored from recordings. See Figure 5C for time series of the tail chasing behavior.

Statistical Analysis

Microsoft Excel was used to sort and arrange raw data. Statistical analysis was done using GraphPad Prism V5. Comparing two groups of data was done using Mann-Whitney tests. Standard symbols were used to indicate the P value of statistical significance with *<0.05, **<0.005, ***<0.0005. When comparing more than two groups, the Kruskal-Wallis test with Dunn's post-hoc correction was used. We used distinct letters to distinguish groups of statistical significance. P values of these comparisons were indicated in corresponding legends.

Strains

CB1490 *him-5(e1490) V*
PT3049 *tba-6(cxP4018) I; him-5(e1490) V*
UR495 *pha-1(e2123) III; him-5(e1490) V; Ex[Ptba-6::tba-6::yfp + ccYFP + pBX]*
PT3106 *tba-6(cxP4018) I; pha-1(e2123) III; him-5(e1490) V; Ex[Ptba-6::tba-6::yfp + ccYFP + pBX]*
PT443 *myIs1 pkd-2(sy606) IV; him-5(e1490) V*
PT2106 *tba-6(cxP4018) I; myIs1 pkd-2(sy606) IV; him-5(e1490) V*
PT2679 *him-5(e1490)V;myIs23[Pcil-7::gCIL-7::GFP_3'UTR+ccRFP]*
PT2925 *tba-6 (cxP4018) I; him-5(e1490) V; myIs23[Pcil-7::gCIL-7::GFP_3'UTR+ccRFP]*
PT1247 *pha-1(e2123) III; him-5(e1490) V; myEx514[Ppkd-2::NPHP-4::GFP +pBX]*
PT2936 *tba-6(cxP4018) I; pha-1(e2123) III; him-5(e1490) V; myEx514[Ppkd-2::NPHP-4::GFP +pBX]*
PT3099 *him-5(e1490) V; myIs24 myIs24[Ppkd-2::TBB-4::tagRFP +ccRFP]*
PT3083 *tba-6(cxP4018) I; him-5(e1490) V; myIs24[Ppkd-2::TBB-4::tagRFP +ccRFP]*
PT1857 *pha-1(e2123) III; him-5(e1490) V; myEx648[Pklp-6::KLP-6::GFP +pBX]*

PT2928 *tba-6(cxP4018) I; pha-1(e2123) III; him-5(e1490) V; myEx648[GFP::KLP-6 + pBX]*
PT2098 *pha-1(e2123) III; him-5(e1490) V; myEx685 [Pklp-6::OSM-3::GFP + pBX]*
PT3057 *tba-6(cxP4018) I; pha-1(e2123) III; him-5(e1490) V; myEx685 [Pklp-6::OSM-3::GFP + pBX]*
PT2991 *tba-6(cxP4018) I; pha-1(e2123) III; him-5(e1490) V; myEx687 [Ppkd-2::KAP-1::GFP + pBX]*
PT3103 *tba-6(cxP4018) I; pha-1(e2123) III; him-5(e1490) V; myEx687 [Ppkd-2::KAP-1::GFP + pBX]*
PT2102 *pha-1(e2123) III; him-5(e1490) V; myEx686 [Pklp-6::GFP::gKLP-6_3'UTR + pBX]*
PT3066 *tba-6(cxP4018) I; pha-1(e2123) III; him-5(e1490) V; myEx686 [Pklp-6::GFP::gKLP-6_3'UTR + pBX]*
PT1132 *pha-1(e2123) III; him-5(e1490) V; myEx506 [Ppkd-2::OSM-5::GFP + pBX]*
PT3062 *tba-6(cxP4018) I; pha-1(e2123) III; him-5(e1490) V; myEx506 [Ppkd-2::OSM-5::GFP + pBX]*
PT1416 *pha-1(e2123) III; him-5(e1490) V; myEx554 [Ppkd-2::OSM-6::GFP+ pBX]*
PT3063 *tba-6(cxP4018) I; pha-1(e2123) III; him-5(e1490) V; myEx554[Ppkd-2::OSM-6::GFP+ pBX]*
PT2235 *pha-1(e2123) III; him-5(e1490) V; myEx726 [Ppkd-2::CHE-11::GFP + pBX]*
PT3064 *tba-6(cxP4018) I; pha-1(e2123) III; him-5(e1490) V; myEx726 [Ppkd-2::CHE-11::GFP + pBX]*

Supplemental References

S1. Hurd, D.D., Miller, R.M., Nunez, L., and Portman, D.S. (2010). Specific alpha- and beta-tubulin isotypes optimize the functions of sensory Cilia in Caenorhabditis elegans. Genetics *185*, 883-896.

S2. Weimer, R. (2006). Preservation of C. elegans Tissue Via High-Pressure Freezing and Freeze-Substitution for Ultrastructural Analysis and Immunocytochemistry, Volume 351, K. Strange, ed. (New Jersey: Humana Press), pp. 203-221-222.

S3. Kremer, J.R., Mastronarde, D.N., and McIntosh, J.R. (1996). Computer visualization of three-dimensional image data using IMOD. J Struct Biol *116*, 71-76.

S4. Wolf, D., Lubk, A., and Lichte, H. (2014). Weighted simultaneous iterative reconstruction technique for single-axis tomography. Ultramicroscopy *136 IS -*, 15-25.

S5. Hall, D.H., and Rice, W.J. (2015). Electron tomography methods for C. elegans. In C. elegans, Methods and Applications, Volume in press, G. Haspel and D. Biron, eds. (Humana Press).

S6. Schindelin, J., Arganda-Carreras, I., Frise, E., and Kaynig, V. (2012). Fiji: an open-source platform for biological-image analysis. Nature *9*, 676-682.

S7. Prevo, B., Mangeol, P., Oswald, F., Scholey, J.M., and Peterman, E.J. (2015). Functional differentiation of cooperating kinesin-2 motors orchestrates cargo import and transport in C. elegans cilia. Nat Cell Biol.

S8. Morsci, N.S., and Barr, M.M. (2011). Kinesin-3 KLP-6 regulates intraflagellar transport in male-specific cilia of Caenorhabditis elegans. Curr Biol *21*, 1239-1244.

S9. Wang, J., Silva, M., Haas, L.A., Morsci, N.S., Nguyen, K.C., Hall, D.H., and Barr, M.M. (2014). C. elegans Ciliated Sensory Neurons Release Extracellular Vesicles that Function in Animal Communication. Curr Biol *24*, 519-525.

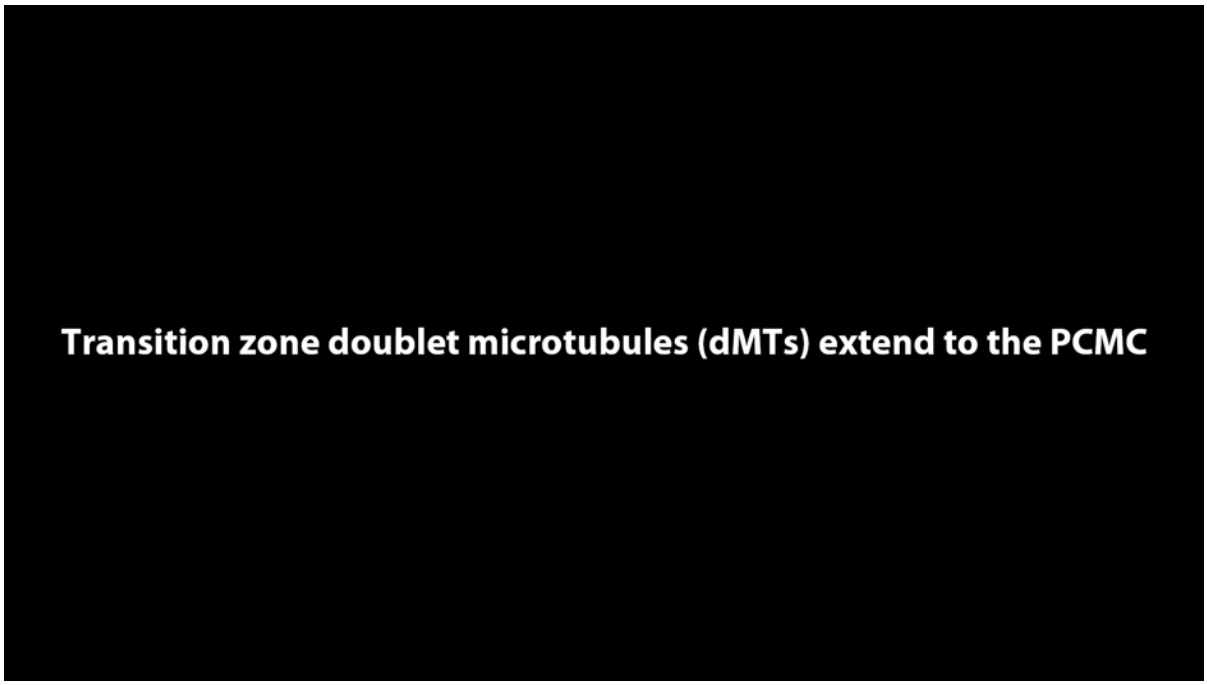

Movies 1 At the base of the CEM transition zone (refer to Figure 1B) doublet microtubules extend to PCMC and terminate at varying lengths.

Low resolution serial tomogram with side by side longitudinal and cross sectional view of the PCMC, transition zone, and bottom of the transition zone. At the base of the CEM transition zone, microtubules extend to the PCMC and terminate at varying lengths. Related to Figure 1.

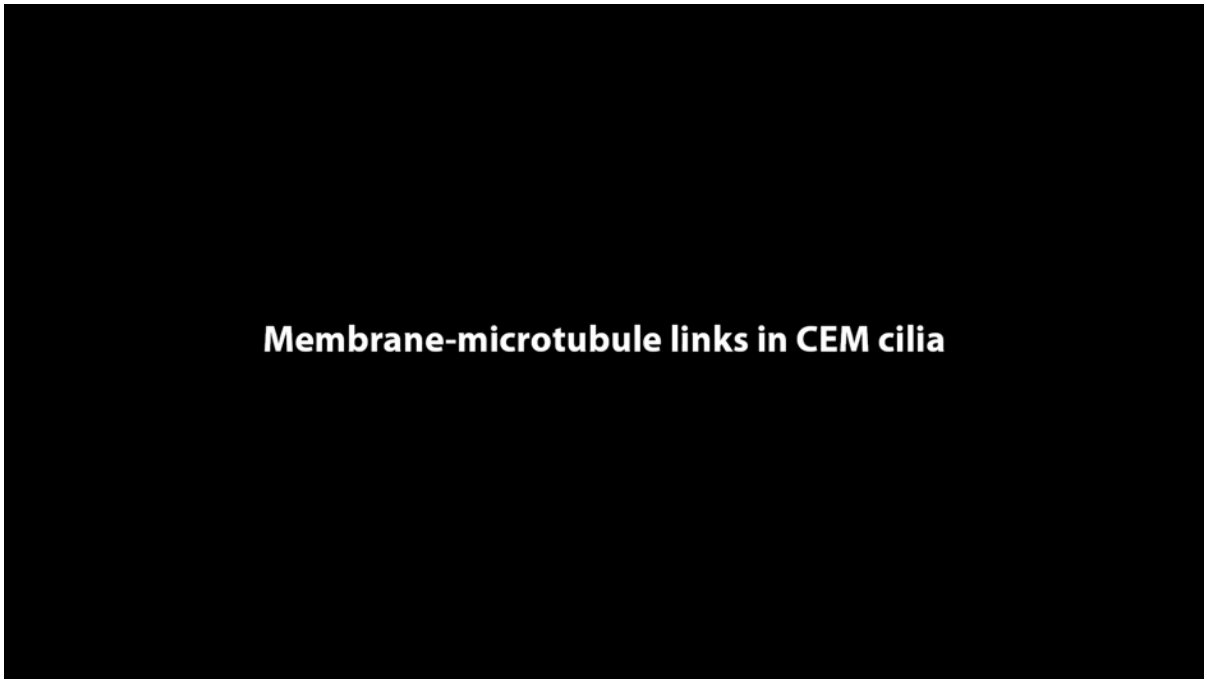

Movies 2 In A-tubule and B-tubule singlet microtubule region of CEM cilia (refer Figure 1B), electron dense links can be seen between the ciliary membrane and microtubules.

High-resolution thin-section tomogram obtained from a serially reconstructed wild-type CEM cilium with annotated A-singlet microtubules (red), B-singlet microtubules (teal), inner singlets (yellow), and inner leaflet of ciliary membrane (green). Electron dense links (white arrows) can be seen between ciliary membrane and singlet microtubules. In the 75nm thin-section electron tomogram examined, 5 out of 9 A-tubules, 6 out of 8 B-tubules, and 0 out of 2 inner singlets had links to the cilia membrane at least once. Of those tubules with connections to the membrane, the number of connections was: 4.4±6.3 for each A-tubule and 11.16±3.9 connections for each B-tubule (mean±SD). Related to Figure 1.

Part II

Chapter 3

The Tubulin Deglutamylase CCPP-1 Regulates the Function and Stability of Sensory Cilia in C. elegans

Modified from Robert O'Hagan, Brian P. Piasecki, Malan Silva , *et al.* 2011, Current Biology

Forward

This was my first project in the Barr lab. After graduating from SUNY Geneseo in May 2008?, and a summer of research with Abbi Cox, I joined Barr lab as a research technician in the Fall of 2009. I collaborated with Robert O'Hagan. At that time he had finished mapping *my22,* one of the mutants from Young Bae's screen to isolate genes required for PKD-2::GFP localization (Bae *et al.* 2008*)*. *my22* is a point mutation in *ccpp-1*. My initial task was to clone *ccpp-1* and test if it could rescue the PKD-2::GFP localization defect in *my22*. After months of trial and error I was unable to amplify the entire genomic region at once. However, after I came across Mehta *et al.* 1999, "Bridge-overlap-extension PCR method for constructing chimeric genes", I repurposed it to amplify *ccpp-1* genomic region in two manageable lengths and then sew them together to finally create the 7.5kB genomic region and microinjected it into *my22* mutants, I learned microinjection from John Haynie, a fly geneticist, whose lab was adjacent to Cox lab at SUNY Geneseo. Microinjection of *ccpp-1* containing PCR rescued the PKD-2::GFP localization phenotype in *my22*. This experiment confirmed *my22* is indeed an allele of *ccpp-1*. Following this, I

continued to work on *ccpp-1* project scoring kymographs generated by Robert O'Hagan, and conducting dye-filling experiments.

In the Fall of 2010, I continued on in the Barr lab as a graduate student in the Molecular Bioscience masters program. A while later, Maureen asked me if I would choose to pursue training in electrophysiology with Robert O'Hagan or electron microscopy in David Hall Lab at Albert Einstein. I chose EM.

In the beginning I would spend hours and hours at the electron microscope just imaging serial sections already cut and processed by Ken Nguyen, Dave Hall's technician. At first, I was essentially a button pusher: move the specimen to the target region at low magnification, increase magnification, adjust focus, adjust exposure, and acquire image. Handling of sensitive specimen-holding grids was all done by Ken Nguyen, a standard practice with all newbies. There I was for the next four months, taking more than 1000 pictures of cephalic region of *C. elegans* males. I focused on amphid and CEM cilia cross-sections, captured images in multiple magnifications and at varying depths from tip of the nose. I compared images of wild type and *ccpp-1* animals and showed that in *ccpp-1* mutants amphid B-tubules seem to unravel and some cilia seem to degenerate. What was surprising is how relatively intact the CEM cilia are in *ccpp-1* mutants. Yes, in some instances, region of the CEM was indistinguishable from a whirlpool of membranes that were electron opaque, but these were rare. Most of the CEM cilia were essentially swollen, and in the sections we examined, singlet microtubules seemed to have drawn away from the ciliary membrane towards the center. I counted those microtubules and compared them to a similar region in wild type specimens and found that number of signets has reduced to 16±2 in *ccpp-1* mutant background as compared to 20±4 in the wild type. It

was then that I asked the question: How can there be 20 singlets in CEM cilia when there are only nine doublets at its transition zone? This suggested that in addition to the known singlet formation of doublet A-tubules, incomplete B-tubules might also be forming singlets.

Highlights

- *C. elegans* CCPP-1 is needed for maintenance of the structure and function of cilia
- Loss of CCPP-1 causes B-tubule defects in ciliary MT structures
- CCPP-1 regulates ciliary kinesin-2 and kinesin-3 motors, but not kinesin-II
- Loss of polyglutamylase TTLL-4 suppresses progressive ciliary defects of *ccpp-1*

Summary

Background

Post-translational modifications (PTMs) such as acetylation, detyrosination, and polyglutamylation have long been considered markers of stable microtubules, and have recently been proposed to guide molecular motors to specific subcellular destinations. Microtubules can be deglutamylated by the cytosolic carboxypeptidase CCP1. Loss of CCP1 in mice causes cerebellar Purkinje cell degeneration. Cilia, which are conserved organelles that play important diverse roles in animal development and sensation, contain axonemes comprised of microtubules that are especially prone to PTMs.

Results

Here, we report that a CCP1 homolog, CCPP-1, regulates the ciliary localization of the kinesin-3 KLP-6 and the polycystin PKD-2 in male-specific sensory neurons in *C. elegans*. In male-specific CEM (cephalic sensilla, male) cilia, *ccpp-1* also controls the velocity of the kinesin-2 OSM-3/KIF17 without affecting the transport of kinesin-II cargo. In the core ciliated nervous system of both males and hermaphrodites, loss of *ccpp-1* causes progressive defects in amphid and phasmid sensory cilia, suggesting that CCPP-1 activity

is required for ciliary maintenance but not ciliogenesis. Affected cilia exhibit defective B-tubules. Loss of TTLL-4, a polyglutamylating enzyme, suppresses progressive ciliary defects in *ccpp-1* mutants.

Conclusions

Our studies suggest that CCPP-1 acts as a tubulin deglutamylase that regulates the localization and velocity of kinesin motors, and the structural integrity of microtubules in sensory cilia of a multicellular, living animal. We propose that the neuronal degeneration caused by loss of CCP1 in mammals may represent a novel ciliopathy in which cilia are formed but not maintained, depriving the cell of cilia-based signal transduction.

Introduction

Cilia are microtubule-based organelles that are present on most non-dividing eukaryotic cells and are essential for vision, olfaction, hearing, and embryonic development [1]. Ciliary axonemes typically have a "9 + 2" or "9 + 0" microtubule (MT) formation (nine outer doublets with two inner singlets, or nine outer doublets, with zero inner singlets), but variations do occur [1].

All motile and non-motile eukaryotic cilia are built by a process called IFT (intraflagellar transport) [2]. Anterograde IFT is driven by heterotrimeric kinesin-II motors that transport IFT-A and IFT-B complexes [2]. This basic IFT machinery can be accompanied by other accessory motors. *C. elegans* amphid channel cilia are built by the cooperative action of two kinesin-2 motors—homodimeric kinesin-2 OSM-3 and heterotrimeric kinesin-II, comprised of KLP-11, KLP-20, and KAP-1 [2, 3]. In *C. elegans* male-specific CEM cilia, the kinesin-3 KLP-6 moves independently of the IFT kinesin-2 motors and reduces the velocity of OSM-3 [4]. In humans, mutations that affect cilia formation or function can cause genetic diseases called ciliopathies that display pleiotropic defects, including cystic kidneys, retinal photoreceptor degeneration, anosmia, and sperm immotility [2].

Ciliary axonemal MTs are subject to post-translational modifications (PTMs). PTMs are considered to be markers of stable microtubules, and can regulate the activities of kinesin and dynein motors [5-8]. For example, kinesin-3/KIF1A localization to axons and dendrites is regulated by the level of MT polyglutamylation [9]. At present, our understanding of the physiological relevance of tubulin PTMs is very limited.

We report here several ciliary defects arising from a mutation in the gene *ccpp-1*, which encodes a cytosolic carboxypeptidase tubulin modifying enzyme. The *ccpp-1(my22)* mutant was isolated in a genetic screen for defective ciliary localization of PKD-2::GFP, a functional fluorescently tagged TRP polycystin ion channel [10]. The murine homolog, CCP1 (also called Nna1 or AGTPBP1) is a deglutamylating enzyme that reduces the polyglutamylation that is added as a side chain to glutamate residues in the C-terminus of tubulin [11]. CCP1 also removes the penultimate amino acid, a glutamate, encoded in the primary sequence of tubulin to produce Δ2-tubulin [11].

C. elegans ccpp-1 mutants also displayed defects in localization of the kinesin-3 KLP-6, and abnormal motility of OSM-3/KIF17 in male-specific cilia required for mating behavior. In amphid and phasmid neurons, loss of CCPP-1 function caused progressive ciliary dye-filling (Dyf) defects, suggesting that ciliary structure is not maintained. The progressive Dyf defect in *ccpp*-1 mutants was dependent on the TTLL-4 polyglutamylase. *ccpp-1* animals also displayed cell-specific defects in ciliary polyglutamylation signals. Our results provide the first demonstration that CCPP-1 regulates the function and stability of neuronal cilia. Loss of function of CCP1 in *pcd* mice causes progressive degeneration of cerebellar Purkinje neurons, thalamic neurons, retinal photoreceptors, and olfactory mitral neurons, as well as sperm immotility [12, 13], phenotypes that are reminiscent of human ciliopathies. We propose that CCPP-1 affects the structure and stability of ciliary MTs, the function of ciliary kinesins, and ciliary localization of their cargoes, by regulating the polyglutamylation state of ciliary MTs.

Results

_my22_ and _ok1821_ are alleles of _ccpp-1,_ which is required for proper localization of PKD-2::GFP

We isolated the *my22* allele in a screen for ciliary PKD-2::GFP localization defective mutants [10]. PKD-2::GFP localizes to cilia located on the distal dendrites of CEMs, RnBs, and HOB male-specific neurons (Fig. 1A, B) [14]. In *my22* males, excessive PKD-2::GFP accumulates in cilia and distal dendrites (hereafter referred to as the Cil phenotype; Fig. 1B) [10].

We mapped *my22* to a region between +0.39 and +0.5 cM on chromosome I. The Cil phenotype in *my22* mutants was rescued by germline injection of fosmid WRM0627dB11, which contains full genomic sequence of seven genes, of which only the *ccpp-1(ok1821)* mutant failed to complement *my22* for the Cil phenotype. *ccpp-1(ok1821)* males also displayed the Cil phenotype, which was rescued by a genomic *ccpp-1(+)* transgene (Fig. 1B). We conclude that both *my22* and *ok1821* are recessive alleles of a single gene, *ccpp-1*.

The _my22_ molecular lesion affects a conserved domain in CCPP-1

The *my22* lesion is a G-A transition encoding a G596R amino acid substitution (Fig. 1C) in the conserved sequence FESGNL (Fig. 1C). The *ccpp-1(ok1821)* mutation encodes a deletion that removes putative 5' regulatory sequences as well as the first 5 exons of the *ccpp-1* locus, and may be a genetic null (Fig. 1C). BLASTs [15] of *C. elegans* CCPP-1 against human sequences revealed several conserved domains, including a zinc carboxypeptidase

domain ([16]; Fig. 1C), and showed that residues 536 – 1015 are 43% identical to human CCP1 residues 573 – 1122. Hence, *ccpp-1* encodes an evolutionarily conserved protein.

CCPP-1::GFP is expressed in the ciliated sensory nervous system

We analyzed expression and localization of a *ccpp-1::gfp* translational reporter. CCPP-1::GFP was neuronally expressed in developing embryos (not shown) through adulthood in amphid and IL2 ciliated sensory neurons of the "core" nervous system, which males and hermaphrodites have in common (Fig. 1D, E). In the male-specific nervous system, CCPP-1::GFP was coexpressed with *pkd-2* in CEM head neurons and the B-type ray (RnB) and HOB hook neurons in the tail (Fig 1E). CCPP-1::GFP was also expressed in some unidentified neurons and the gubernacular erector and retractor muscles in the male tail (Fig. 1E). CCPP-1::GFP was localized diffusely throughout neurons, including cilia, but excluded from the nucleus.

To determine if CCPP-1::GFP was functional, we assayed the mating behavior of transgenic males. *ccpp-1* mutant males are defective in the response substep of mating (Fig. 1F; [10]), in which males sense contact with and begin scanning the body of a potential hermaphrodite mate [17]. Response behavior requires the ray neurons [14, 18]. While 99 ± 1% of wild-type males (7 trials, $n = 70$ animals total assayed) responded to hermaphrodite mates within four minutes, only 38 ± 8% of *ccpp-1(my22)* (4 trials, $n = 40$) and 35 ± 9% of *ccpp-1(ok1821)* males responded (6 trials, $n = 60$) (Fig. 1F). Genomic *ccpp-1(+)* and *ccpp-1::gfp* transgenes rescued the response defect in *ccpp-1* mutant males (Fig. 1F). Hence, the CCPP-1::GFP translational fusion protein was functional in RnB neurons.

***ccpp-1* mutants exhibit a progressive defect in ciliary structure**

We performed dye-filling assays to assess the structural integrity of cilia in the amphid and phasmid sensillae of *ccpp-1* mutants [19]. Wild-type amphid and phasmid ciliated sensory neurons took up a lipophilic fluorescent dye through environmentally exposed ciliated endings (Fig. 2 A, B; [19]). Mutants with ciliary structure defects, such as *osm-3(p802)* and the IFT-B polypeptide mutant *che-13(e1805)* exhibit the Dyf phenotype at all developmental stages [19]. *ccpp-1(ok1821)* hermaphrodites displayed an age-dependent Dyf defect (Fig. 2 A, B). In young *ccpp-1* larvae (L1 or L2), amphid dye-uptake appeared nearly normal (Fig. 2B), while L4 larvae and young adults (YA) showed a severe Dyf phenotype in ciliated sensory neurons in both the amphid and phasmid sensillae. Older adults displayed the most severe Dyf phenotype. *ccpp-1(my22)* hermaphrodites displayed a similar, but less penetrant, age-dependent Dyf defect (Fig. 2 B), consistent with *ok1821* being a loss-of-function and *my22* being a reduction-of-function allele. The Dyf phenotype in *ccpp-1(ok1821)* animals at all ages was rescued by a *ccpp-1(+)* transgene (Fig. 2 B).

C. elegans relies on ciliated sensory neurons of the amphid sensilla to detect and avoid high osmolarity [20]. Cilium structure mutants, such as *che-13(e1805),* are osmotic avoidance defective (the Osm phenotype) at all developmental stages (Fig. 2C; [19, 20]). *ccpp-1* mutants exhibited progressive Osm defects that mirrored the progressive Dyf phenotype (Fig. 2C). *ccpp-1(ok1821)* L1 and L2 larvae were slightly defective (avoidance index, or a.i., of 0.80 ± 0.06; $p < 0.0001$ versus 1.0 ± 0 for wild-type; Fig. 2C), but this defect

became more severe with age (a.i. = 0.23 ± 0.01 of 1-2 day old adults; $p < 0.0001$ versus 0.99± 0.04 for wild type; Fig. 2C). As adults, *ccpp-1(my22)* mutants were also partially defective in osmotic avoidance behavior (Fig. 2D). In all cases, the Osm phenotype of *ccpp-1* mutants was fully rescued by the *ccpp-1::gfp* transgene (Fig. 2D). Based on the results of dye-filling and osmotic avoidance assays, which reflect the structure and function of amphid cilia, we propose that *ccpp-1* mutants are capable of forming but not maintaining sensory cilia.

ccpp-1 mutants display ciliary ultrastructural defects including B-tubule defects, disorganization of MTs, and ciliary fragmentation

To examine the ultrastructure of the CEM and amphid cilia, we used transmission electron microscopy (TEM) and electron tomography of fixed age-matched young adult males. Wild-type CEM cilia typically contained approximately 20 singlet MTs that were distributed spatially, with many singlets closely apposed to the membrane, when viewed in cross section (Fig. 3A; Table 1). CEM cilia in a *ccpp-1(ok1821)* male contained only 16 MT singlets on average, and those that remained were disorganized, residing on average four times farther from the membrane than in wild type (Fig. 3A; Table 1). The average diameter of *ccpp-1(ok1821)* CEM cilia was 66% larger than wild type (Fig. 3A; Table 1).

In wild-type males, the amphid channel middle segment region contained ten axonemes and each contained on average eight visible outer microtubule doublets (Fig. 3B; Table 1). In a *ccpp-1(ok1821)* male, the amphid channel middle segment region contained an average of only eight intact cilia that had on average two outer doublets

and few singlets, which appeared disorganized (Fig. 3B; Table 1). Some of the singlets appeared to have attached remnants of B-tubules. Some missing cilia may have fragmented (Fig. 3B; Table 1). Hence, CCPP-1 function is important for ciliary integrity as well as MT architecture.

CCPP-1 regulates polyglutamylation in sensory cilia

Murine CCP1 removes the penultimate amino acid, a glutamate, of the primary sequence of α-tubulin and shortens side chains of glutamates (polyglutamylation) added to the C-terminus of α- and β-tubulins in stable microtubules [11]. CCPP-6 was reported to reduce polyglutamylation in *C. elegans* sensory cilia [21].

If *ccpp-1* Cil and Dyf defects were caused by excessive glutamylation of ciliary MTs, loss of a polyglutamylase might suppress *ccpp-1* defects. Polyglutamylases—enzymes that oppose deglutamylases—are known as tubulin tyrosine ligase like (TTLL) proteins [22, 23]. The *C. elegans* genome encodes six predicted TTLL homologs [21]. In *C. elegans* core ciliated sensory neurons, *ttll-4* mutants display drastically reduced antibody detection of polyglutamation signals in cilia, while *ttll-9* mutants show a minor reduction [21]. IFT70/DYF-1 positively regulates polyglutamylation in *C. elegans* and zebrafish [24]. To determine if mutations in *ttll-4*, *ttll-9*, or *dyf-1* could suppress *ccpp-1* Cil or Dyf phenotypes, we examined double mutant combinations. Strikingly, *ttll-4(tm3310)* suppressed the progressive Dyf, but not Cil, phenotype of *ccpp-1(ok1821)* mutants (Fig. 4A, B, Fig. S1). *ttll-9(tm3389)* did not suppress *ccpp-1* Cil or Dyf phenotypes (data not shown). Our results indicate that CCPP-1 opposes the activity of TTLL-4 in polyglutamylation of proteins in

amphid and phasmid cilia. Both the *dyf-1(mn335)* single mutant and *dyf-1(mn335) ccpp-1(my22)* double mutant were Dyf and Cil (Fig. S1). Because *dyf-1* and *ccpp-1* single and double mutants display similar Dyf and Cil phenotypes, we cannot draw any conclusion about genetic interactions between them.

To detect polyglutamylation, we stained adult males with the monoclonal antibody GT335 [25]. In wild type, GT335 neuronal staining was most apparent in the middle segments of amphid cilia, IL cilia in the nose, and phasmid cilia in the tail (Fig. 4C). GT335 occasionally stained the CEM cilia in males, as visualized by PKD-2::GFP (Fig. 4D, S2A). GT335 stained the distal tips of male tail ray neuronal cilia (Fig. 4C). *ccpp-1* mutations had cell-type specific effects on polyglutamylation. In general, GT335 immunofluorescence appeared to be more speckled in *ccpp-1* mutants (Fig. 4C). *ccpp-1(my22)* and *ccpp-1(ok1821)* showed an approximately five-fold increase over wild type in the percent of CEM cilia with GT335 staining (Fig. 4D, S2A). Increased polyglutamylation in *ccpp-1* CEM cilia is consistent with CCPP-1 acting as a deglutamylase. Not surprisingly, the increased polyglutamylation in CEM cilia was not suppressed in *ccpp-1(ok1821);ttll-4(tm3310)* or *dyf-1(mn335) ccpp-1(my22)* double mutants (Fig. S2A, B).

In contrast, peak GT335 staining of amphid middle segments in *ccpp-1* adult males was significantly reduced to half or less of wild type (Fig. 4E, S2C). GT335 fluorescence in phasmid cilia of the tail and in male ray neuronal cilia also appeared to be decreased in *ccpp-1* mutants (Fig. 4C). In some cases, ray neurons appeared to retain low polyglutamylation signals, but these signals were in ciliary bases rather than the tips of cilia (Fig. 4C inset). The reduction of polyglutamylation in *ccpp-1* mutants was unexpected, but might reflect the ciliary ultrastructural defects in *ccpp-1* adults. In *ccpp-*

1(ok1821);ttll-4(tm3310) and *dyf-1(mn335) ccpp-1(my22)* double mutants, the reduction in polyglutamylation signals in amphid middle segments was similar to the *ccpp-1* single mutants (Fig. S2B, C). Since both TTLL-4 and DYF-1 positively regulate polyglutamylation, this result was expected.

To determine if *ccpp-1* mutations perturbed other PTMs, we examined polyglycylated tubulin and Δ2-tubulin by antibody staining. The *C. elegans* genome lacks predicted polyglycylating enzymes [21]; as expected, we detected no polyglycylation signals (data not shown). An anti-Δ2-tubulin polyclonal antibody stained pairs of lateral neurites in wild-type males, but did not stain cilia except the phasmids in the tail; Fig. S2D). In *ccpp-1* mutants, the anti-Δ2-tubulin antibody also dimly stained some cilia in the nose (Fig. S2D).

CCPP-1 regulates the kinesin-3 KLP-6 and the kinesin-2 OSM-3

To determine if *ccpp-1* regulates the abundance or localization of ciliary motor proteins, we examined KLP-6, OSM-3/KIF17, and the kinesin-II cargo OSM-6. In wild type, KLP-6::GFP is diffusely localized throughout neuronal cell bodies, axons, dendrites, and cilia of the male-specific CEM, HOB, and RnB neurons and the core IL2 neurons (Fig. 5A; [26]). In *ccpp-1(my22)* mutants, KLP-6::GFP accumulated in cilia (Fig. 5A). We used the *pkd-2* promoter to drive expression of *ccpp-1* in the male-specific CEM, HOB, and RnB neurons [27], which rescued KLP-6::GFP abundance and localization in cilia of these neurons (Fig. 5B, C). We conclude that CCPP-1 acts cell-autonomously to regulate the distribution of KLP-6 and its putative cargo, PKD-2.

Next, we investigated OSM-3 in CEM cilia for two reasons: First, we could observe the effects of *ccpp-1(ok1821)* on OSM-3::GFP motility and localization in a single cilium, whereas the amphid channel contains cilia of 8 different neuronal types [19]. Second, TEM experiments indicated that amphid cilia in *ccpp-1* mutants had variable structural defects (Fig. 3), indicating that individual amphid channel cilia might be affected differently or with different timecourses. In CEM cilia, the majority of OSM-3 moves independently of kinesin-II and IFT complexes [4]. The localization of OSM-3::GFP was similar in wild type and *ccpp-1(ok1821)* CEM cilia (Fig. 6A). However, the apparent velocity of motile OSM-3::GFP puncta in CEM cilia was significantly increased in *ccpp-1(ok1821)* mutants (1.07 ± 0.07 µm/s vs. 0.75 ± 0.03 µm/s; Fig. 6B). Mutation of *ttll*-4 had no effect on OSM-3::GFP localization or velocity in either wild-type or *ccpp*-1 backgrounds (Fig. S3A, B, C), consistent with the failure of *ttll-4* to suppress the Cil phenotype of *ccpp-1*.

OSM-6 is an IFT-B polypeptide that is transported solely by kinesin-II in CEM cilia [4]. *ccpp-1(ok1821)* did not affect abundance, localization, or velocity of OSM-6::GFP (Fig. 6C, D, S3D). We conclude that, in CEM cilia, CCPP-1 regulates the accessory motors OSM-3 and KLP-6, but does not regulate the canonical IFT motor, heterotrimeric kinesin-II.

Discussion

Loss of CCPP-1 function causes ciliary transport defects and progressive deterioration of ciliary structure and function

Here we show that the *C. elegans* carboxypeptidase CCPP-1 plays critical cell-specific roles in maintaining ciliary integrity and function *in vivo*. *ccpp-1* mutants are defective in localization and abundance of the kinesin-3 KLP-6 and its putative cargo PKD-2 in male-specific sensory cilia. Mutant males also have a corresponding mating defect in response behavior, which requires PKD-2 and KLP-6 function [14, 26]. Unlike IFT mutants, *ccpp-1* mutant larvae exhibit amphid cilia that fill with dye and support osmotic avoidance behavior. However, *ccpp-1* mutants display a progressive, age-dependent dye-filling defect of cilia in amphid and phasmid sensory neurons, which correlates with deficits in osmotic avoidance behavior. We propose that CCPP-1 is needed for ciliary maintenance rather than ciliogenesis. Two previous studies have shown that CCP1 requires a functional carboxypeptidase domain to rescue defects in *pcd* mice [28, 29]. The *ccpp-1(my22)* mutation, which encodes a G596R substitution, demonstrates that the FESGNL motif is also essential for full function (Fig. 1B). However, the function of this domain, or indeed, the CCPP-1 protein itself, is not fully understood.

CCPP-1 regulation of the tubulin code affects specific kinesin motors

Our results are consistent with a proposed "tubulin code" model, in which PTMs provide signposts that regulate the localization or activity of motors [5-8]: In male-specific

CEM cilia of *ccpp-1* mutants, ciliary localization of KLP-6 is elevated, and the apparent velocity of OSM-3::GFP is increased. In contrast, the localization and motility of the kinesin-II-driven IFT-B polypeptide OSM-6::GFP are unaffected. We propose that CCPP-1-mediated MT modification normally regulates KLP-6 subcellular distribution and OSM-3 velocity in CEM cilia. Identification of additional roles for CCPP-1, such as regulating dynein-based transport, motor recycling, or cargo-motor binding, await future studies.

CCPP-1 regulates MT polyglutamylation, MT stability, and ciliary stability

In CEM cilia, CCPP-1 regulates polyglutamylation levels independently of TTLL-4 (Fig. 4, S1, S2A, B, S3C). We suggest that polyglutamylation in CEM cilia is normally maintained at a low level by CCPP-1 and an unknown TTLL polyglutamylase. Since misregulation of MT polyglutamylation affects the kinesin-2 OSM-3 and the kinesin-3 KLP-6, we propose that the PKD-2::GFP Cil phenotype could be secondary to motor function defects. Our data strongly suggest that CCPP-1 reduces polyglutamylation of MTs and opposes polyglutamylating enzymes in *C. elegans* cilia.

Our results also predict that CCPP-1 activity depends on cell-specific factors, since loss of TTLL-4 suppresses *ccpp-1* Dyf, but not Cil, defects. Such cell-specific factors may include particular tubulin isoforms or regulators of PTMs. In amphid cilia, mutation of *ccpp-1* decreases polyglutamylation levels (Fig. 4, S2C)—counter to our expectation, considering that mammalian CCP1 deglutamylates MTs, and that loss of the polyglutamylase TTLL-4 suppressed the Dyf phenotype of *ccpp-1* mutants. However, hyperglutamylation destabilizes axonemal MTs in *Tetrahymena* [30]. Degradation of

extensively polyglutamylated MTs, as well as the loss of some amphid cilia, might explain the paradoxical loss of GT335 staining in amphid cilia middle segments in *ccpp-1* adults.

Our ultrastructural studies support this hypothesis (Fig. 3B, Table 1). In *ccpp-1* amphid cilia, the number of both doublets and singlets is reduced by 75% compared to wild type (Table 1). In *Chlamydomonas* ciliary MT doublets, B-tubules are the main site of polyglutamylation [31]. Assuming this is true in *C. elegans*, the B-tubule defects we observed are likely to explain the reduction of GT335 staining in *ccpp-1* amphid cilia. These ultrastructural defects are also consistent with the progressive Dyf phenotype in *ccpp-1* mutants. We propose that the degree of polyglutamylation must be tightly controlled for MT doublet stability.

Does mutation of CCP1 in mammals cause ciliopathic neurodegeneration?

A greater understanding of the function of CCPP-1 is of interest because the mammalian homolog, CCP1, is required for survival of several populations of neurons in the mouse brain [12, 13]. In addition to adult-onset degeneration of cerebellar Purkinje neurons, other defects, such as degeneration of retinal photoreceptors, olfactory bulb mitral neurons, and thalamic neurons, and sperm immotility, result from loss of CCP1 [12, 13]. All of the cell types affected in *pcd* mice are ciliated/flagellated. RNAi-mediated knockdown of CCP1 reduced ciliary length in cultured human cells [32]. We show here, for the first time, that CCPP-1 is required for maintenance of the structure and function of cilia in *C. elegans*.

Consequently, we propose that neurodegeneration and other defects in *pcd* mice could be caused by ciliopathy. Vertebrate primary cilia may be specialized for intercellular

signaling such as Wnt and Hedgehog (reviewed in [33]). In addition to developmental roles, such signaling might be needed for cellular survival and maintenance of cilia in which receptors reside. Hence, further study of *ccpp-1*, tubulin post-translational modification, and ciliary dynamics in *C. elegans* should provide more insight on ciliopathic degenerative diseases.

Experimental Procedures

Strains used:

The genotypes of all strains used are described in Supplemental Experimental Procedures.

PKD-2::GFP Localization

Strains used: PT443, PT1645, PT1931, PT1932, PT2168, PT2169, PT2170, PT2171, PT2172, PT2379, PT2381

We isolated L4 males from hermaphrodites 20 – 24 hours before observation. To score the Cil phenotype, we observed PKD-2::GFP localization on the Zeiss Axioplan2 microscope using the 10X objective. At this magnification, GFP fluorescence was not visible anywhere outside of the cell bodies of the CEM, RnB, or HOB neurons in wild-type males. In *ccpp-1* mutants, PKD-2::GFP was visible in dendrites and cilia, especially in rays. Images of PKD-2::GFP localization were captured using 63X or 100X objectives.

Antibody Staining

Strains used: PT443, PT1645, PT2168, PT2171, PT2172, PT2379, PT2381

Gravid adults were bleached to obtain age-synchronized embryos, which were then fixed as one-day-old adults. We used the fixation and staining method described in [34]). Fixed worms were stored at 4°C for up to one month before antibody staining. Animals were stained overnight at room temperature with a 1:600 dilution in Antibody Buffer A of GT335 (a monoclonal antibody which binds the branch point of both monoglutamylated and polyglutamylated substrates [25]); 1:500 dilution of AB3203 (polyclonal antibody that binds Δ2-tubulin; Millipore; [37]); 1:200 dilution of TAP952 (monoclonal antibody that binds both mono-glycylated and polyglycylated tubulin, a gift from the Drummond laboratory); and a 1:200 dilution of R2302 anti-poly-G (rabbit polyclonal antibody that binds polyglycylated tubulin, a gift from the Gorovsky laboratory). Alexa Fluor-578-conjugated anti-mouse or anti-rabbit secondary antibodies (Invitrogen) were used at a dilution of 1:2000 and incubated for 2 hours at room temp with gentle agitation. See Supplemental Experimental Procedures for details.

Statistical Methods

All data values are expressed as mean ± standard error unless indicated. To determine the statistical significance of differences in experimental results, we conducted statistical tests in IGOR 6 (Wavemetrics, Inc.), Statplus (Analystsoft), or Prism (Graphpad Software).

See Supplemental Experimental Methods:

C. elegans culture, mapping of *my22* mutation, transgenesis, microscopy, KLP-6::GFP localization, OSM-3::GFP and OSM-6::GFP motility, male mating response behavior, dye-filling and osmotic avoidance behavior, and electron microscopy and tomography.

Acknowledgements

This work was supported by: NIH NRSA 5F32NS56540-4 and NJCSCR 10-2951-SCR-E-0 fellowships to RO; a Fulbright Fellowship and a Lars Hiertas Minne Foundation grant to BPP; NIH RO1DK059418 to MBB; grants from the Swedish Research Council, Marcus Borgström Foundation, and the NordForsk Nordic Networks for *C. elegans* and Cilia/Centrosomes Research to PS; NIH RR12596 to DHH; and Einstein funds for access to the NYSBC. We thank Bill Rice and K.D. Derr (New York Structural Biology Center) for help in using the Technai20 microscope, and creating electron tomograms. Some nematode strains used in this work were provided by the Caenorhabditis Genetics Center, which is funded by the NIH National Center for Research Resources (NCRR); The *C. elegans* Gene Knockout Consortium; and the National Bioresource Project for the Nematode (Japan). Thanks to the Drummond and Gorovsky laboratories for the anti-polyglycylation antibodies. We also thank Natalia Morsci, Andrew Jauregui, and Julie Maguire for plasmids and strains, and members of the Barr laboratory for discussions and constructive criticism of this manuscript.

References

1. Fliegauf, M., Benzing, T., and Omran, H. (2007). When cilia go bad: cilia defects and ciliopathies. Nat Rev Mol Cell Biol *8*, 880-893.
2. Scholey, J.M. (2008). Intraflagellar transport motors in cilia: moving along the cell's antenna. J Cell Biol *180*, 23-29.
3. Pan, X., Ou, G., Civelekoglu-Scholey, G., Blacque, O.E., Endres, N.F., Tao, L., Mogilner, A., Leroux, M.R., Vale, R.D., and Scholey, J.M. (2006). Mechanism of transport of IFT particles in *C. elegans* cilia by the concerted action of kinesin-II and OSM-3 motors. J Cell Biol *174*, 1035-1045.
4. Morsci, N.S., and Barr, M.M. (2011). Kinesin-3 KLP-6 Regulates Intraflagellar Transport in Male-Specific Cilia of Caenorhabditis elegans. Curr Biol *21*, 1239-1244.
5. Bulinski, J.C., and Gundersen, G.G. (1991). Stabilization of post-translational modification of microtubules during cellular morphogenesis. BioEssays : news and reviews in molecular, cellular and developmental biology *13*, 285-293.
6. Verhey, K.J., and Gaertig, J. (2007). The tubulin code. Cell Cycle *6*, 2152-2160.
7. Janke, C., and Kneussel, M. (2010). Tubulin post-translational modifications: encoding functions on the neuronal microtubule cytoskeleton. Trends Neurosci *33*, 362-372.
8. Ikegami, K., and Setou, M. (2010). Unique post-translational modifications in specialized microtubule architecture. Cell Struct Funct *35*, 15-22.
9. Ikegami, K., Heier, R.L., Taruishi, M., Takagi, H., Mukai, M., Shimma, S., Taira, S., Hatanaka, K., Morone, N., Yao, I., et al. (2007). Loss of alpha-tubulin polyglutamylation in ROSA22 mice is associated with abnormal targeting of KIF1A and modulated synaptic function. Proc Natl Acad Sci U S A *104*, 3213-3218.
10. Bae, Y.K., Lyman-Gingerich, J., Barr, M.M., and Knobel, K.M. (2008). Identification of genes involved in the ciliary trafficking of *C. elegans* PKD-2. Dev Dyn *237*, 2021-2029.
11. Rogowski, K., van Dijk, J., Magiera, M.M., Bosc, C., Deloulme, J.C., Bosson, A., Peris, L., Gold, N.D., Lacroix, B., Grau, M.B., et al. (2010). A family of protein-deglutamylating enzymes associated with neurodegeneration. Cell *143*, 564-578.
12. Fernandez-Gonzalez, A., La Spada, A.R., Treadaway, J., Higdon, J.C., Harris, B.S., Sidman, R.L., Morgan, J.I., and Zuo, J. (2002). Purkinje cell degeneration *(pcd)* phenotypes caused by mutations in the axotomy-induced gene, Nna1. Science *295*, 1904-1906.
13. Mullen, R.J., Eicher, E.M., and Sidman, R.L. (1976). Purkinje cell degeneration, a new neurological mutation in the mouse. Proc Natl Acad Sci U S A *73*, 208-212.
14. Barr, M.M., DeModena, J., Braun, D., Nguyen, C.Q., Hall, D.H., and Sternberg, P.W. (2001). The *Caenorhabditis elegans* autosomal dominant polycystic kidney disease gene homologs *lov-1* and *pkd-2* act in the same pathway. Curr Biol *11*, 1341-1346.
15. Altschul, S.F., Gish, W., Miller, W., Myers, E.W., and Lipman, D.J. (1990). Basic local alignment search tool. Journal of molecular biology *215*, 403-410.
16. Rodriguez de la Vega, M., Sevilla, R.G., Hermoso, A., Lorenzo, J., Tanco, S., Diez, A., Fricker, L.D., Bautista, J.M., and Aviles, F.X. (2007). Nna1-like proteins are active

metallocarboxypeptidases of a new and diverse M14 subfamily. Faseb J *21*, 851-865.
17. Liu, K.S., and Sternberg, P.W. (1995). Sensory regulation of male mating behavior in *Caenorhabditis elegans*. Neuron *14*, 79-89.
18. Barrios, A., Nurrish, S., and Emmons, S.W. (2008). Sensory regulation of *C. elegans* male mate-searching behavior. Curr Biol *18*, 1865-1871.
19. Perkins, L.A., Hedgecock, E.M., Thomson, J.N., and Culotti, J.G. (1986). Mutant sensory cilia in the nematode *Caenorhabditis elegans*. Dev Biol *117*, 456-487.
20. Culotti, J.G., and Russell, R.L. (1978). Osmotic avoidance defective mutants of the nematode *Caenorhabditis elegans*. Genetics *90*, 243-256.
21. Kimura, Y., Kurabe, N., Ikegami, K., Tsutsumi, K., Konishi, Y., Kaplan, O.I., Kunitomo, H., Iino, Y., Blacque, O.E., and Setou, M. (2010). Identification of tubulin deglutamylase among *Caenorhabditis elegans* and mammalian cytosolic carboxypeptidases (CCPs). J Biol Chem *285*, 22936-22941.
22. Janke, C., Rogowski, K., Wloga, D., Regnard, C., Kajava, A.V., Strub, J.M., Temurak, N., van Dijk, J., Boucher, D., van Dorsselaer, A., et al. (2005). Tubulin polyglutamylase enzymes are members of the TTL domain protein family. Science *308*, 1758-1762.
23. Ikegami, K., Mukai, M., Tsuchida, J., Heier, R.L., Macgregor, G.R., and Setou, M. (2006). TTLL7 is a mammalian beta-tubulin polyglutamylase required for growth of MAP2-positive neurites. J Biol Chem *281*, 30707-30716.
24. Pathak, N., Obara, T., Mangos, S., Liu, Y., and Drummond, I.A. (2007). The zebrafish *fleer* gene encodes an essential regulator of cilia tubulin polyglutamylation. Molecular biology of the cell *18*, 4353-4364.
25. Wolff, A., de Nechaud, B., Chillet, D., Mazarguil, H., Desbruyeres, E., Audebert, S., Edde, B., Gros, F., and Denoulet, P. (1992). Distribution of glutamylated alpha and beta-tubulin in mouse tissues using a specific monoclonal antibody, GT335. European journal of cell biology *59*, 425-432.
26. Peden, E.M., and Barr, M.M. (2005). The KLP-6 kinesin is required for male mating behaviors and polycystin localization in *Caenorhabditis elegans*. Curr Biol *15*, 394-404.
27. Barr, M.M., and Sternberg, P.W. (1999). A polycystic kidney-disease gene homologue required for male mating behaviour in *C. elegans*. Nature *401*, 386-389.
28. Wang, T., Parris, J., Li, L., and Morgan, J.I. (2006). The carboxypeptidase-like substrate-binding site in Nna1 is essential for the rescue of the Purkinje cell degeneration (*pcd*) phenotype. Mol Cell Neurosci *33*, 200-213.
29. Chakrabarti, L., Eng, J., Martinez, R.A., Jackson, S., Huang, J., Possin, D.E., Sopher, B.L., and La Spada, A.R. (2008). The zinc-binding domain of Nna1 is required to prevent retinal photoreceptor loss and cerebellar ataxia in Purkinje cell degeneration (*pcd*) mice. Vision research *48*, 1999-2005.
30. Wloga, D., Dave, D., Meagley, J., Rogowski, K., Jerka-Dziadosz, M., and Gaertig, J. (2010). Hyperglutamylation of tubulin can either stabilize or destabilize microtubules in the same cell. Eukaryotic cell *9*, 184-193.
31. Kubo, T., Yanagisawa, H.A., Yagi, T., Hirono, M., and Kamiya, R. (2010). Tubulin polyglutamylation regulates axonemal motility by modulating activities of inner-arm dyneins. Curr Biol *20*, 441-445.

32. Kim, J., Lee, J.E., Heynen-Genel, S., Suyama, E., Ono, K., Lee, K., Ideker, T., Aza-Blanc, P., and Gleeson, J.G. (2010). Functional genomic screen for modulators of ciliogenesis and cilium length. Nature *464*, 1048-1051.
33. Gerdes, J.M., Davis, E.E., and Katsanis, N. (2009). The vertebrate primary cilium in development, homeostasis, and disease. Cell *137*, 32-45.
34. Lewis, J.A., and Fleming, J.T. (1995). Basic culture methods. Methods Cell Biol *48*, 3-29.
35. Kosugi, S., Hasebe, M., Tomita, M., and Yanagawa, H. (2009). Systematic identification of cell cycle-dependent yeast nucleocytoplasmic shuttling proteins by prediction of composite motifs. Proc Natl Acad Sci U S A *106*, 10171-10176.
36. de Castro, E., Sigrist, C.J., Gattiker, A., Bulliard, V., Langendijk-Genevaux, P.S., Gasteiger, E., Bairoch, A., and Hulo, N. (2006). ScanProsite: detection of PROSITE signature matches and ProRule-associated functional and structural residues in proteins. Nucleic acids research *34*, W362-365.
37. Paturle-Lafanechere, L., Eddé B., Denoulet P., Van Dorsselaer A., Mazarguil H., Le Caer JP, Wehland J., Job D. (1991). Characterization of a major brain tubulin variant which cannot be tyrosinated. Biochemistry *30*, 10523-10528.

Figures

Figure 1

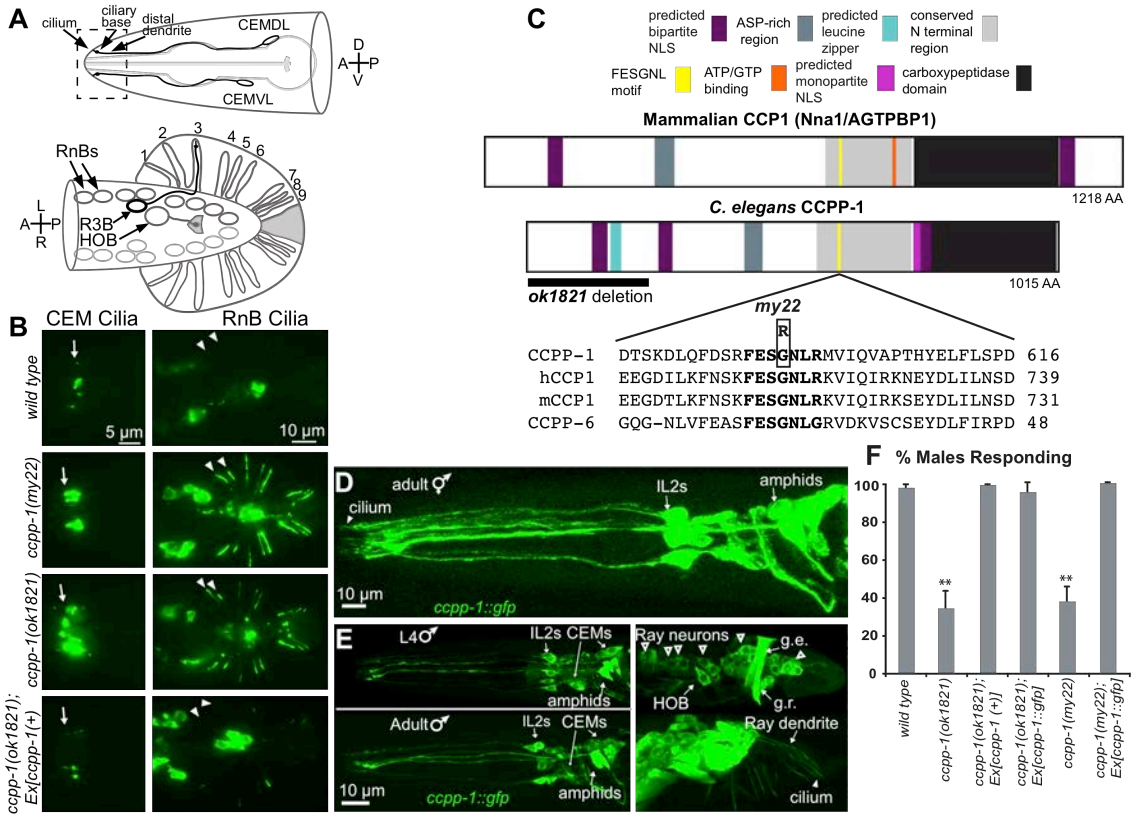

Figure 1 CCPP-1 is required for PKD-2 localization and is expressed in the ciliated sensory nervous system

A Diagram of the male-specific CEM neurons in the head, and HOB and RnB neurons in the tail. Box illustrates the region of CEM cilia and distal dendrites shown in the epifluorescent images. In the ventral-up cartoon of the male tail, the RnBs innervate the tail rays; R3B dendrite is shown as an example. **B** In wild-type males, PKD-2::GFP faintly illuminated cilia of the CEM neurons, the HOB cilium, and the cilia of the ray B-type neurons (RnB, where n = 1 – 9, excluding 6). *ccpp-1*(*my22)* and *ccpp-1(ok1821)* mutants exhibit the Cil phenotype. Arrows point to CEM cilia; arrowheads point to R1B and R2B cilia. Expression of genomic *ccpp-1* rescued the Cil phenotype of *ccpp-1(ok1821)*. **C** CCPP-1 contains several conserved regions, including a zinc carboxypeptidase domain, an aspartic-acid rich domain, a conserved "NT" region [12], and predicted NLS (nuclear localization signal; [35]). CCPP-1 also contains a predicted leucine zipper near the N-terminus (ScanProsite, [36]). The *my22* lesion affects the conserved sequence FESGNL in the NT region of CCPP-1. **D** In adult hermaphrodites, CCPP-1::GFP expression was expressed in amphid and IL2 core ciliated sensory neurons. Cilium containing CCPP-1::GFP is indicated. **E** Confocal projections of CCPP-1::GFP expression in males. Top (L4): CCPP-1::GFP was expressed in (left) amphid, IL2, and CEM neurons and (right) male tail ray and HOB neuronal cell bodies (empty arrowheads). Gubernacular erector (g.e.) and retractor (g.r.) muscles are indicated. Bottom (1 day old adult): CCPP-1::GFP localization in ray neuron dendrites (arrow) and a cilium (arrowhead). **F** *ccpp-1* mutants are defective in response behavior. Number of trials and number of males for each genotype was as follows: wild type, 7 trials, *N* = 70 males; *ok1821*, 6 trials, *N* = 60; *ok1821;Ex[ccpp-1(+)]*, 3 trials, *N* = 29; *ok1821;Ex[ccpp-1::gfp]*, 3 trials,

N = 24; *my22*, 4 trials, *N* = 40; *my22;Ex[ccpp-1::gfp]*, 5 trials, *N* = 39. Error bars indicate SEM; **indicates *ccpp-1* mutants were statistically different ($p < 10^{-4}$, ANOVA/Tukey HSD test) from mutants expressing *ccpp-1* transgenes, which were similar to wild type. See also Fig. S1.

Figure 2

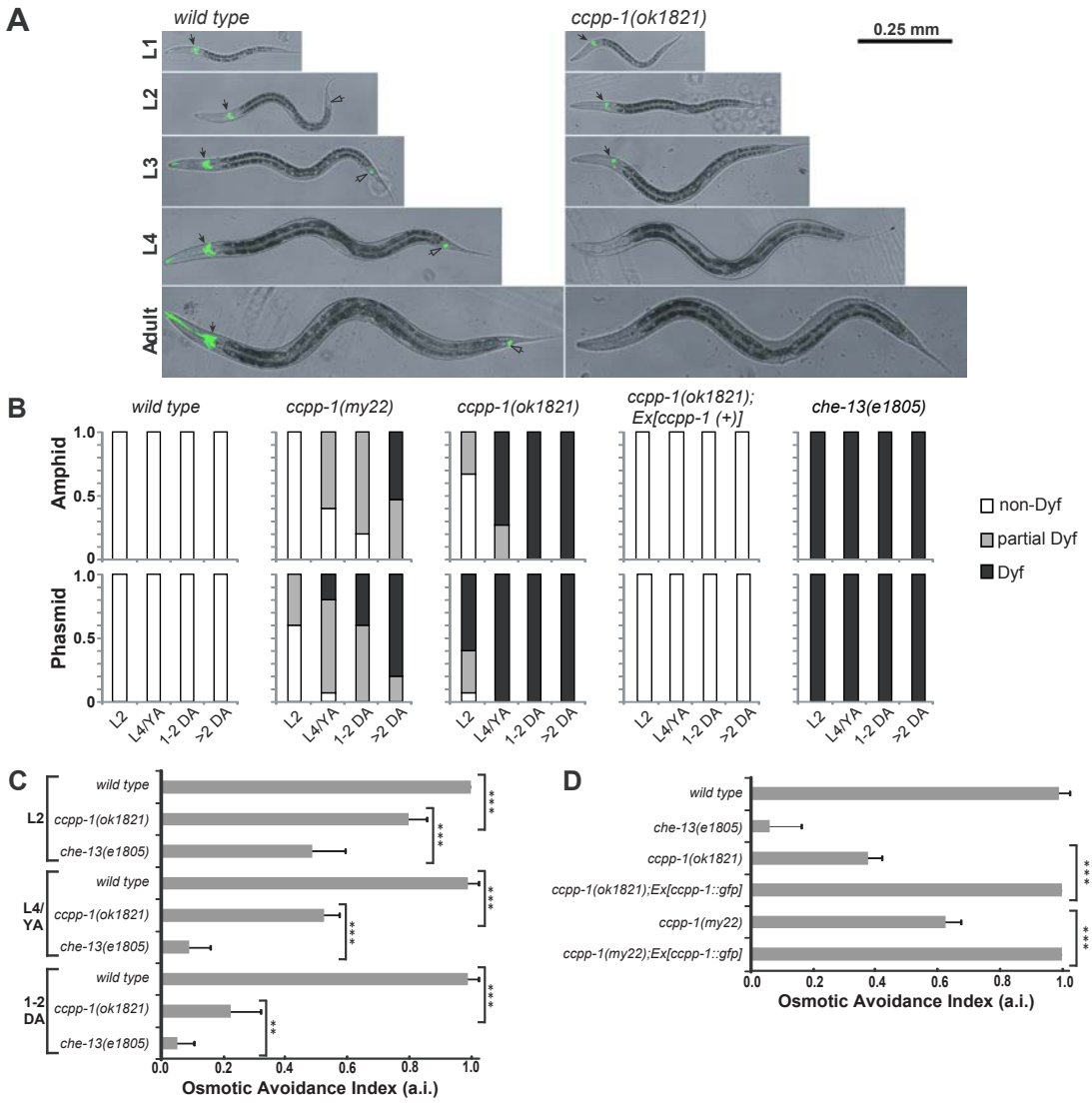

Figure 2 *ccpp-1* mutants exhibited progressive Dyf and Osm defects

A Amphid (solid arrows) and phasmid (hollow arrows) ciliated neurons of wild type hermaphrodites were stained by DiI (pseudocolored green) at all developmental stages. *ccpp-1(ok1821)* amphid cilia in L1 larvae stained normally, but became Dyf in later larval

stages and adults. **B** Dyf defects were scored in amphid and phasmid neurons in wild-type, *my22*, *ok1821*, and *che-13(e1805)* young adults (24 hours post-L4). 15 animals were scored for each stage/genotype. **C** Wild-type animals exhibit osmotic avoidance behavior when challenged with an 8 M glycerol ring. 80 hermaphrodites (8 trials, 10 per trial) were tested for each stage/genotype. Osmotic avoidance index (a.i.) is the fraction of animals that avoided crossing the ring. **D** The *ccpp-1* Osm defect was rescued by the *ccpp-1::gfp* transgene (8 trials, 10 animals per trial tested). (Error bars indicate SEM; ** indicates $p = 0.0022$ with Fischer's Exact Test; *** indicates $p < 0.0001$ with Fischer's Exact Test).

Figure 3

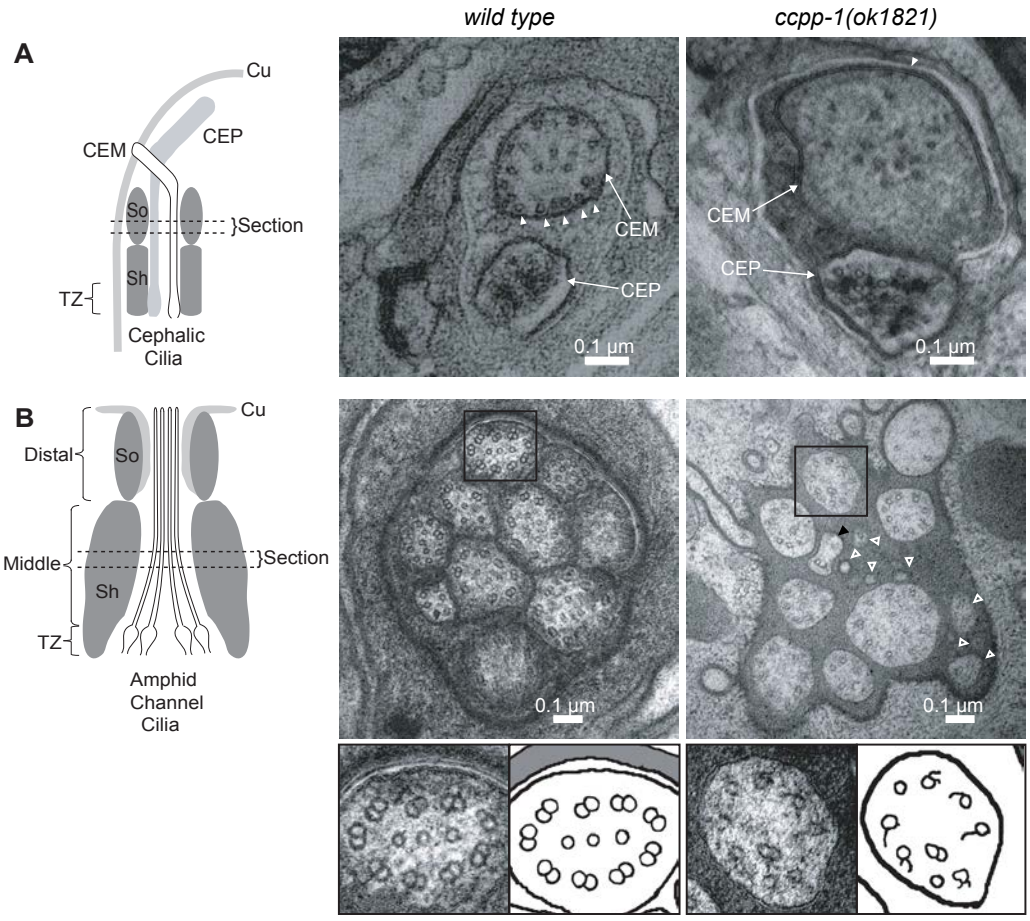

Figure 3 *ccpp-1(ok1821)* mutants exhibit ciliary ultrastructure defects

Left diagrams show regions from which the cephalic (CEM and CEP) and amphid cilia images were taken (Cu = cuticle; Sh = sheath cell; So = socket cell; TZ =transition zone). **A** EM Images of CEM and CEP cilia in wild-type and *ccpp-1(ok1821)* mutant adult males. Wild-type CEM cilia image (taken from a tomogram) contained many singlet MTs (19 singlets in section shown) closely apposed to the membrane (arrowheads). *ok1821* CEM cilia had fewer singlets (15 singlets in section shown), which were more distant from the membrane (arrowhead indicates one singlet near membrane). The *ok1821* CEM cilium

diameter was larger than wild type. **B** Thin sections of amphid cilia in wild-type and *ccpp-1(ok1821)* adult males. Wild-type middle segments contain ten axonemes, each of which typically has nine outer doublets plus a variable number of inner singlets. The *ok1821* middle segment contained only eight intact axonemes plus what appear to be fragments of two cilia (hollow white arrowheads), one of which contains a singlet with attached broken B-tubule (black arrowhead). Most *ok1821* mutant axonemes had fewer MTs, with many doublets replaced by singlets or broken B-tubules. Bottom, boxed wild-type and mutant axonemes accompanied by cartoons. Refer to Table 1 for quantification of images.

Figure 4

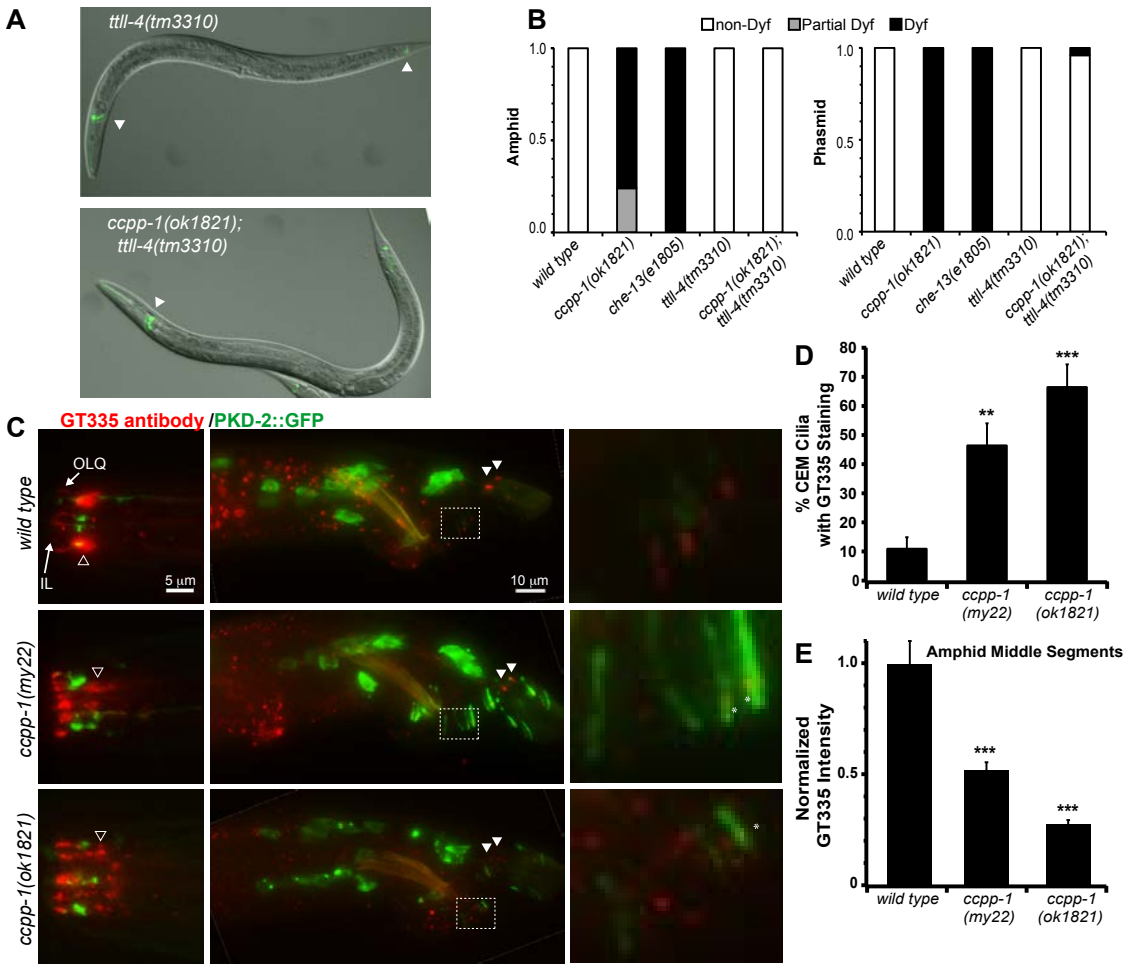

Figure 4 Loss of CCPP-1 results in altered polyglutamylation of sensory cilia

A Dye uptake (pseudocolored green) was normal in young adult hermaphrodite *ttll-4(tm3310)* mutants (left), which were previously reported to lack polyglutamylation in cilia [21]. Deletion of *ttll-4* suppressed the Dyf phenotype of *ccpp-1* (right). Arrowheads indicate dye-filled amphid and phasmid neurons. **B** Penetrance of Dyf defects in amphid and phasmid neurons. 50 young adult hermaphrodites per genotype were tested. **C** Staining of wild-type and *ccpp-1* mutant young adult males with GT335, a monoclonal

antibody that detects polyglutamylation, most prominently in amphid middle segments (hollow arrowhead). An IL and putative OLQ cilium are indicated in the nose. GT335 rarely stained wild-type CEM cilia, which express PKD-2::GFP. In the tail, phasmid cilia (solid arrowheads) were brightly stained. Right, enlarged boxed area containing several ray neuron dendrites and cilia. Asterisks mark polyglutamylation signals that are abnormally localized to the ciliary base in *ccpp-1* mutants. **D** *ccpp-1* mutations increased the incidence of GT335 staining of CEM cilia, which were identified by PKD-2::GFP (** indicates $P < 0.01$, *** indicates $P < 0.001$ vs. wild type, ANOVA/Tukey test; $N = 19 – 22$ males per genotype; scored blindly). **E** The normalized peak pixel value of GT335 staining in the area containing amphid middle segments was significantly lower in mutants (Error bars indicate SEM; *** indicates $p < 10^{-5}$ versus wild type, by ANOVA/Tukey HSD test; $N =$ 10 males per genotype). See also Fig. S2.

Figure 5

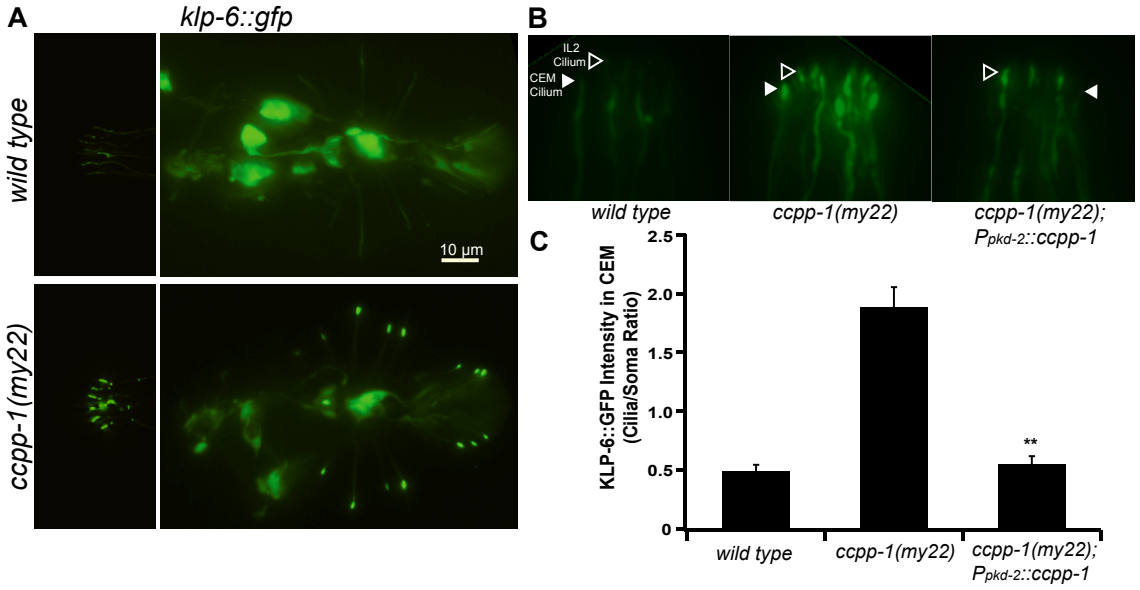

Figure 5 CCPP-1 is needed for proper localization of KLP-6::GFP in IL2 and male-specific neurons

A KLP-6::GFP localization in IL2 and CEM neurons (left) and in HOB and RnB neurons in the tail (right) is diffuse in wild-type males. In contrast, KLP-6::GFP is highly enriched in cilia in *ccpp-1(my22)* mutants. **B** A magnified view of IL2 (hollow arrowheads) and CEM (solid arrowheads) cilia containing KLP-6::GFP in wild-type, *ccpp-1(my22)*, and *ccpp-1(my22)* rescued young adult males. **C** Quantification of KLP-6::GFP fluorescence in cilia/somata of CEM neurons. KLP-6::GFP localization defects in *ccpp-1(my22)* mutant cilia were rescued by $P_{pkd\text{-}2}$*::ccpp-1* in male specific CEM (and RnB, not shown) neurons (Error bars indicate SEM; $N = 9 – 10$ animals per genotype; ** indicates $P < 0.01$ by t-test versus *ccpp-1(my22)*.)

Figure 6

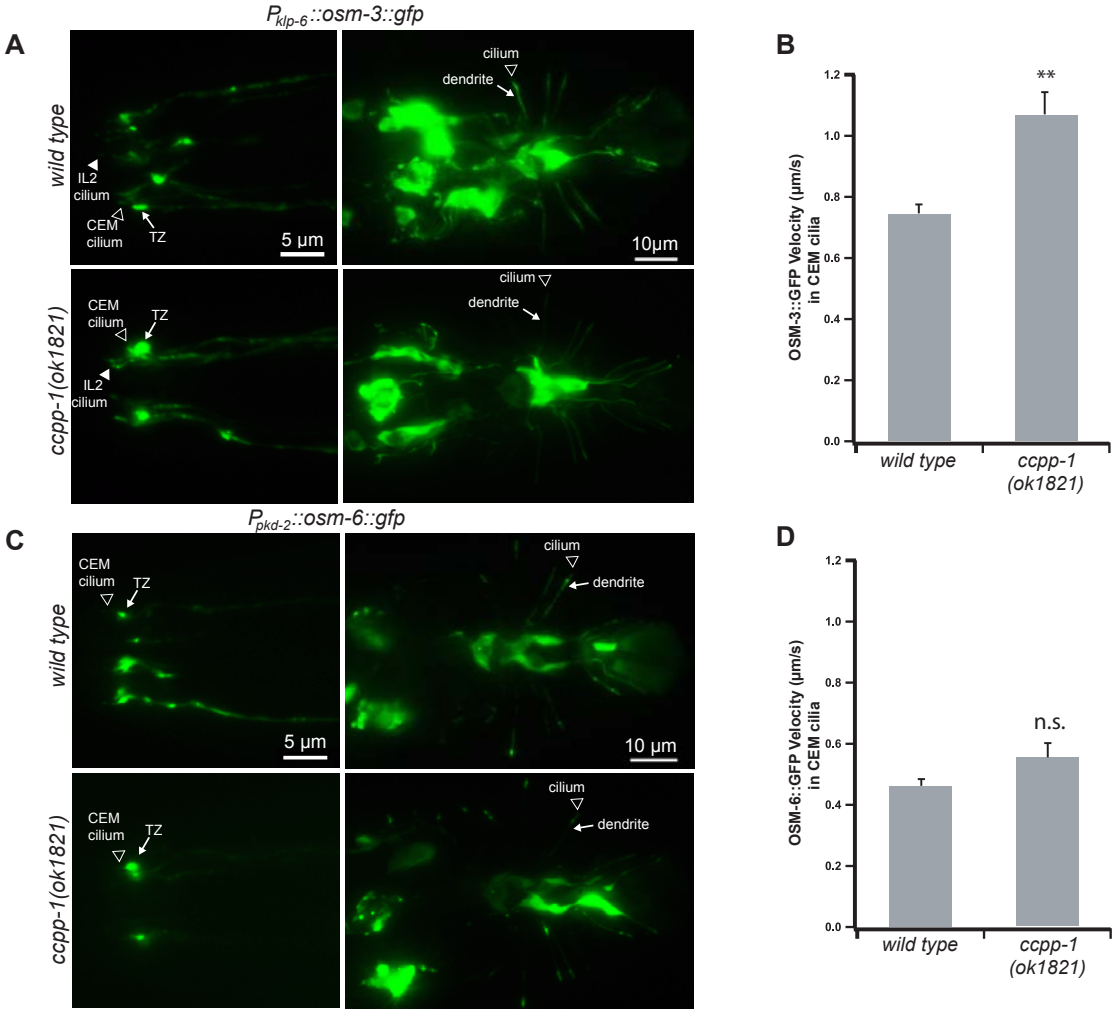

Figure 6 CCPP-1 regulates the velocity of OSM-3::GFP but not kinesin-II-driven IFT-B polypeptide OSM-6::GFP in CEM cilia

A In wild-type and *ccpp-1(ok1821)* young adult males, *klp-6* promoter-driven OSM-3::GFP was visible diffusely in cell bodies, dendrites, and cilia, with some accumulation in transition zones (TZ). **B** OSM-3::GFP particles moved faster in *ccpp-1* CEM cilia (78 particles in 7 wild-type males; 81 particles in 10 *ccpp-1(ok1821)* males; ** indicates $p < 10^{-4}$ by

ANOVA/Tukey test). **C, D** OSM-6::GFP localization and velocity in CEM cilia was similar in wild-type and *ok1821* males (Error bars indicate SEM; 55 particles in 6 wild-type males; 61 particles in 7 *ccpp-1(ok1821)* males; n.s. indicates no significant difference). See also Fig. S3.

Supplemental Figures

Figure S1

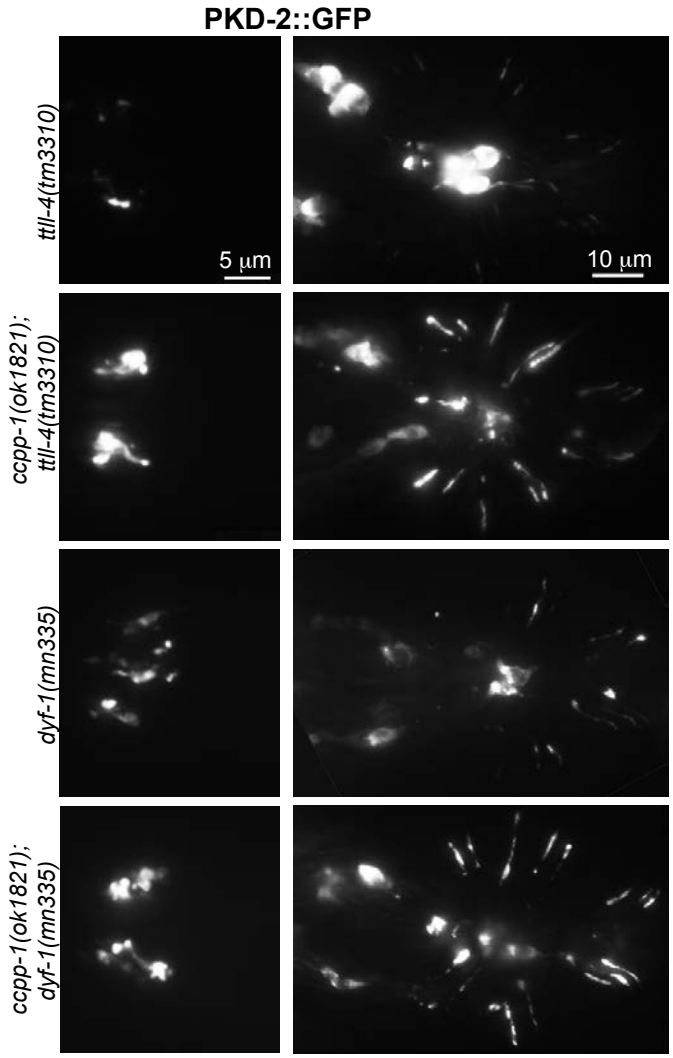

Figure 7 (S1) Mutations in *ttll-4* or *dyf-1* do not suppress the Cil phenotype of *ccpp-1* mutants (Related to Fig. 1)

Fig. S1

Only *ttll-4* males were non-Cil, *ccpp-1; ttll-4* double mutants, *dyf-1* single mutants, and *dyf-1 ccpp-1* double mutants were Cil.

Figure S2

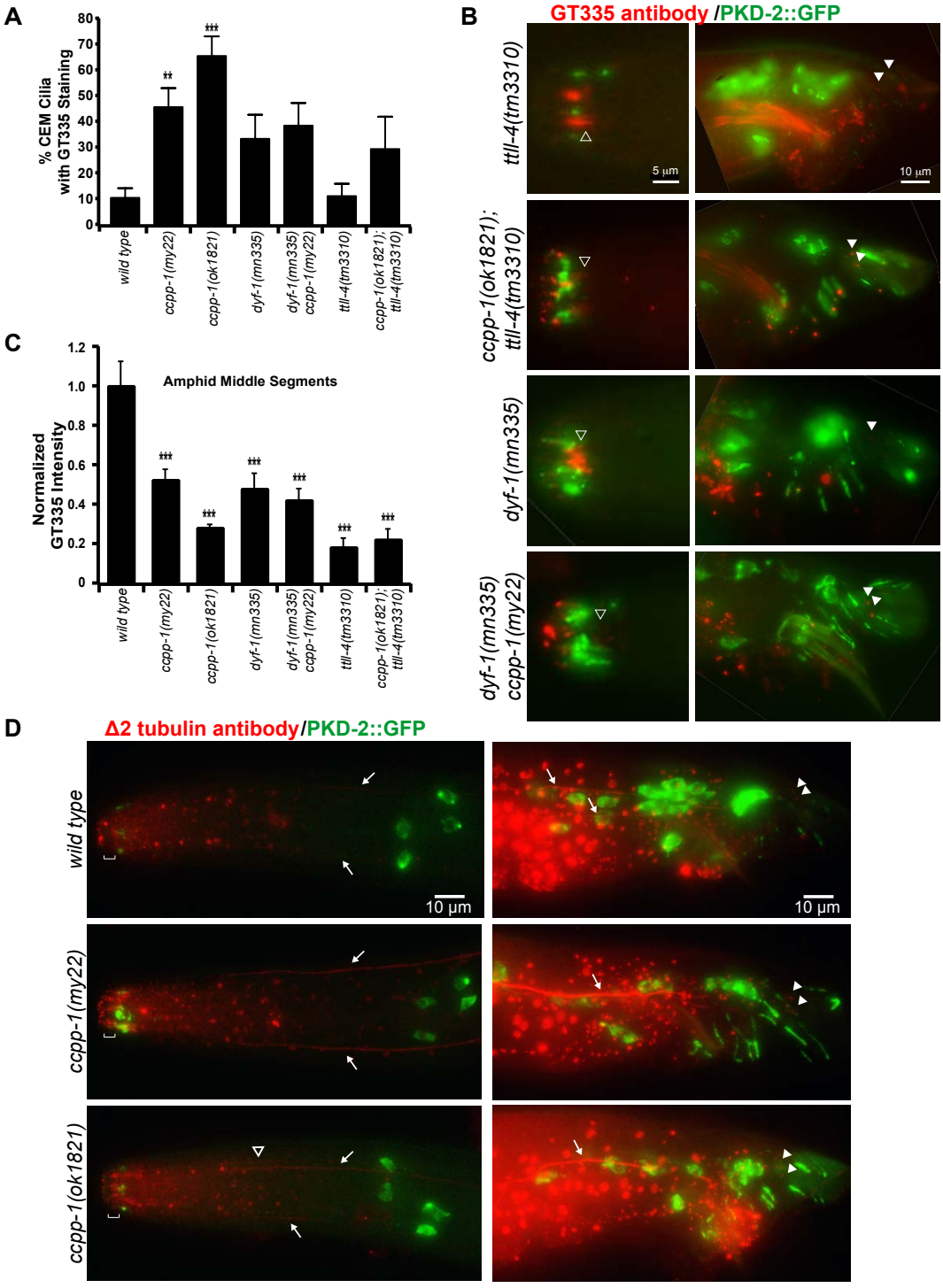
A
% CEM Cilia with GT335 Staining
wild type
ccpp-1(my22)
ccpp-1(ok1821)
dyf-1(mn335)
dyf-1(mn335) ccpp-1(my22)
ttll-4(tm3310)
ccpp-1(ok1821); ttll-4(tm3310)
B
GT335 antibody /PKD-2::GFP
ttll-4(tm3310)
ccpp-1(ok1821); ttll-4(tm3310)
dyf-1(mn335)
dyf-1(mn335) ccpp-1(my22)
5 µm
10 µm
C
Amphid Middle Segments
Normalized GT335 Intensity
D
Δ2 tubulin antibody/PKD-2::GFP
wild type
ccpp-1(my22)
ccpp-1(ok1821)
10 µm

Figure 8 (S2) Mutations in *dyf-1* or *ttll-4* do not suppress increased polyglutamylation in CEM cilia (Related to Fig. 4)

A We performed a blind analysis of GT335 staining in CEM cilia (identified by PKD-2::GFP) and found that while *ccpp-1* mutations increased the incidence of GT335 staining of CEM cilia (** indicates $P < 0.01$, *** indicates $P < 0.001$ vs. wild type, ANOVA/Tukey test), mutations in *ttll-4* or *dyf-1* did not significantly suppress this phenotype ($P > 0.05$, *ttll-4;ccpp-1* or *dyf-1;ccpp-1* double mutants versus *ccpp-1* single mutants; $N = 8 – 22$ animals for each genotype; error bars indicate SEM). **B** Images of adult males expressing PKD-2::GFP stained with GT335 antibody. Empty arrowheads indicate amphid channel cilia middle segments, solid arrowheads indicate phasmid cilia. **C** In amphid middle segments, normalized peak intensity of GT335 staining for all mutant genotypes was significantly different than wild type ($P < 0.001$, ANOVA/Tukey test; $N = 9 – 18$ animals for each genotype; error bars indicate SEM). Since all single mutants decreased GT335 staining in amphid middle segments, suppression of the *ccpp-1* mutant phenotype was not expected. **D** Images of adult males expressing PKD-2::GFP stained with an anti-Δ2-tubulin polyclonal antibody [37]. In wild-type males, the antibody stained unidentified lateral neurites (arrows) but few ciliated neurons (only the phasmid cilia, identified by arrowheads, were stained). In *ccpp-1* mutants, the antibody stained the lateral neurites and dimly stained some cilia in the nose (in the bracketed areas). A hollow arrowhead indicates another neurite that was visible in this *ok1821* male.

Figure S3

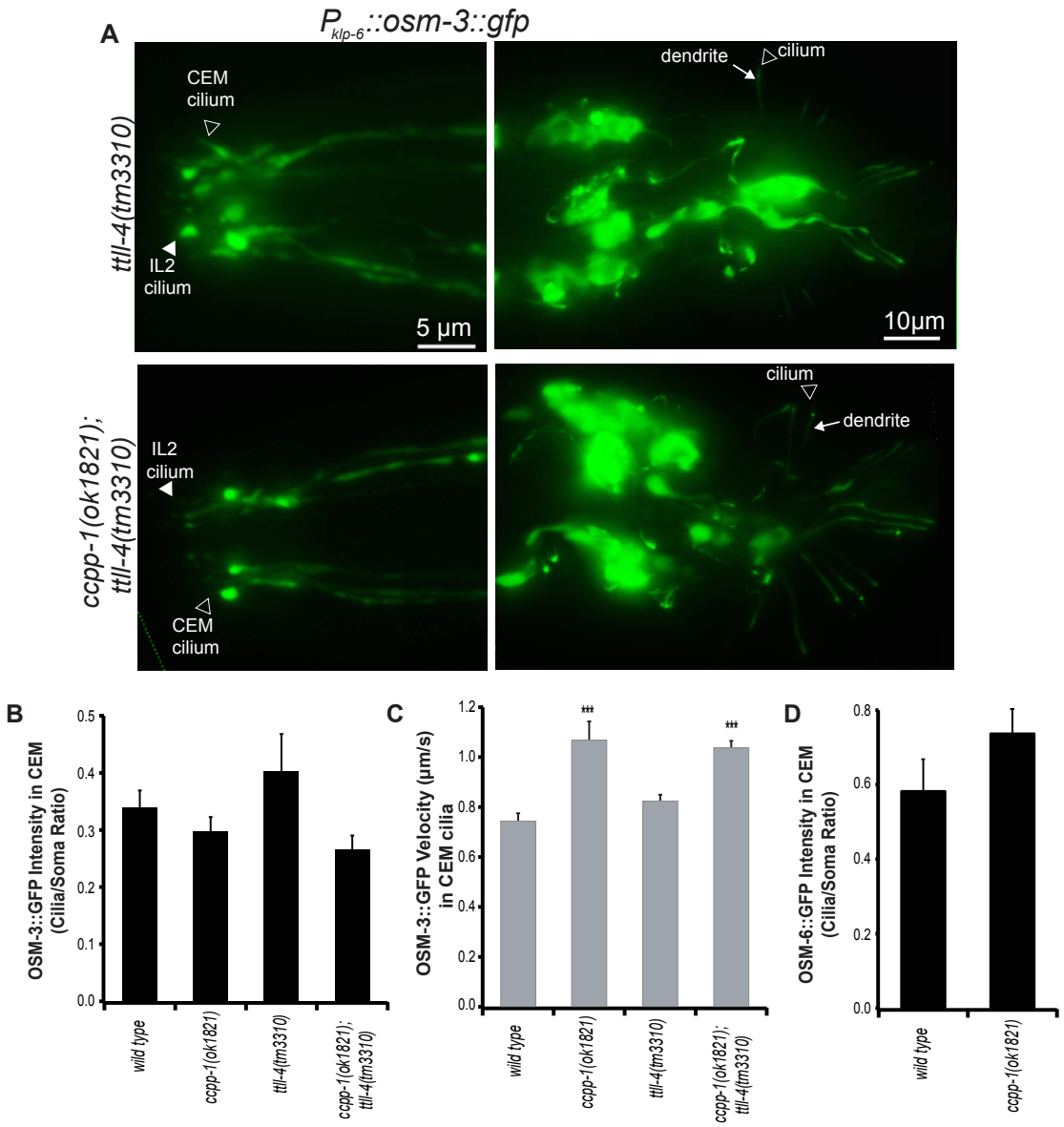

Figure 9 (S3) TTLL-4 does not affect OSM-3::GFP localization or velocity in CEM cilia (Related to Fig. 6)

A Epifluorescent images of OSM-3::GFP in male-specific neurons in *ttll-4(tm3310)* single and *ccpp-1(ok1821);ttll-4(tm3310)* double mutants. Localization of OSM-3::GFP was normal in both backgrounds. **B** The ratio of ciliary to somatic OSM-3::GFP fluorescence was similar

in CEM neurons of wild type, *ccpp-1(ok1821), ttll-4(tm3310),* and *ccpp-1(ok1821);ttll-4(tm3310)* adult males (P> 0.05 by ANOVA). **C** The velocity of motile OSM-3::GFP particles was unchanged by *ttll-4* mutation in both wild-type and *ccpp-1* backgrounds (*** indicates P < 0.01 vs. wild type and *ttll-4* by ANOVA/Tukey test. Wild-type and *ttll-4* velocities were not significantly different; wild type *n* = 78 particles, *N* = 8 animals; *ccpp-1 n* = 81, *N* = 10; *ttll-4 n* = 137, *N* = 13; *ccpp-1;ttll-4 n* = 179, *N* = 17). **D** OSM-6::GFP localization in CEM neurons was similar in wild-type and *ccpp-1(ok1821)* backgrounds (*P* > 0.05 by ANOVA; *N* = 9 – 10 males per genotype). Error bars in panels B, C, and D indicate SEM.

Supplemental Experimental Procedures

Strains used:

CB169: *unc-31(e169) IV*
CB1490: *him-5(e1490) V*
CB3323: *che-13(e1805) I*
CB3687: *che-14(e1960) I*
CB4856: Hawaiian wild isolate strain
DR102: *dpy-5(e61) unc-29(e403) I*
HS634: *rnt-1(os58) I*
JT5010: N2
OE4160: *ccpp-1(ok1821)*
OE4165: *ccpp-1(ok1821) I;ofEx805[ccpp-1 short PCR product + P_{elt-2}::mCherry]*
OE4171: *ccpp-1(ok1821) I;ofEx809[ccpp-1::gfp + P_{elt-2}::mCherry]*
OE4180: *ccpp-1(my22) I;him-5(e1490) V;ofEx809*
PT443: *myIs1[pkd-2::gfp + ccGFP] pkd-2(sy606) IV;him-5(e1490) V*
PT1416: *pha-1(e2123ts) III; him-5(e1490) V; myEx554[P_{pkd-2}::osm-6::gfp + pBx]*
PT1668: *ccpp-1(my22) I; myIs1 pkd-2(sy606) IV;him-5(e1490) V*
PT1931: *dpy-5(e61) unc-29(e403) I; myIs1 pkd-2(sy606) IV;him-5(e1490) V*
PT1932: *dpy-5(e61) ccpp-1(my22) unc-29(e403) I; myIs1 pkd-2(sy606) IV;him-5(e1490) V*
PT2098: *pha-1(e2123ts) III; him-5(e1490) V; myEx685[P_{klp-6}::osm-3::gfp + pBx]*
PT2064: *ccpp-1(ok1821) I; pha-1(e2123ts) III; him-5(e1490) V ; myEx554*
PT2065: *ccpp-1(ok1821) I; pha-1(e2123ts) III; him-5(e1490) V ; myEx685*
PT2168: *ccpp-1(ok1821) I; myIs1 pkd-2(sy606) IV;him-5(e1490) V*
PT2169: *myIs1 pkd-2(sy606) IV; him-5(e1490) ttll-9(tm3889) V*
PT2170: *ccpp-1(ok1821) I;myIs1 pkd-2(sy606) IV; him-5(e1490) ttll-9(tm3889) V*
PT2171: *ttll-4(tm3310) III;myIs1 pkd-2(sy606) IV; him-5(e1490)V*
PT2172: *ccpp-1(ok1821) I;ttll-4(tm3310) III;myIs1 pkd-2(sy606) IV; him-5(e1490)V*
PT2277: *pha-1(e2123ts) III; him-5(e1490) V; myEx647[klp-6::gfp + pBx]*
PT2278: *ccpp-1(my22) I; pha-1(e2123ts) III; him-5(e1490) V ; myEx647*
PT2279: *ccpp-1(my22) I; pha-1(e2123ts) III; him-5(e1490) V; myEx647; myEx708[Ppkd-2::ccpp-1 + pRF4]*
PT2280: *ccpp-1(my22) I;him-5(e1490) V*
PT2281: *ccpp-1(ok1821) I;him-5(e1490) V*
PT2379: *dyf-1(mn335) unc-29(e403) I; myIs1 pkd-2(sy606) IV; him-5(e1490)V*
PT2381: *dyf-1(mn335) ccpp-1(my22) unc-29(e403) I; myIs1 pkd-2(sy606) IV; him-5(e1490)V*
PT2338: *ttll-4(tm3310) III;myIs1 pkd-2(sy606) IV; him-5(e1490)V; myEx685[P_{klp-6}::osm-3::gfp + pBx]*
PT2339: *ccpp-1(ok1821) I;ttll-4(tm3310) III;myIs1 pkd-2(sy606) IV; him-5(e1490)V; myEx685[P_{klp-6}::osm-3::gfp + pBx]*
VC200: *rnt-1(ok351) I*

Culture of *C. elegans* Nematodes

Nematodes were cultured using standard conditions as described in [1]. For generation of transgenic strains, we used several transformation markers. *pBX* denotes a plasmid containing the rescuing *pha-1(+)* transformation marker [2]. *pRF4* denotes a plasmid encoding the dominant *rol-6(su1006)* allele as a transformation marker. A plasmid containing $P_{elt\text{-}2}$*::mCherry* (a gift from Gert Jansen) was also used as a transformation marker.

In *C. elegans*, the predominant gender is hermaphrodite and males spontaneously arise only rarely (less than 1%). Therefore, in all experiments in which males were tested, we used animals in either the *him-5(e1490)* or *myIs1[pkd-2::gfp] pkd-2(sy606);him-5(e1490)* background to generate a supply of male animals. These backgrounds were considered wild type relative to *ccpp-1* mutants. Males with the *him-5(e1490)* mutation exhibit normal mating behaviors and are commonly used as wild-type controls for mating assays. We also used males that were heterozygous for *him-5(e1490)* and made no distinction from homozygous *him-5(e1490)* males.

Mapping of *my22* Mutation

Strains used: PT443, PT1645, PT1931, PT1932, PT2168, DR102, VC200, HS634, CB3687, CB4856

Standard three-factor mapping was performed with *my22* using the *dpy-5* and *unc-29* visible markers, and scoring the Cil phenotype. We used the *CB4856* Hawaiian strain for standard snp-mapping [3]. In addition to *ok1821*, we used *rnt-1* and *che-14* in

complementation tests. Unlike *ok1821*, mutations in *rnt-1* and *che-14* complemented *my22*.

Germline Transformation of *ccpp-1* Mutants With Genomic *ccpp-1* DNA

Strain OE4160 was transformed by germline injection [4] with a PCR amplified genomic *ccpp-1* sequence including an endogenous promoter of 848 bp before the start codon (primer pair: gatcacggatccGTGGACAAGGTATCGAATGG/AGAAAGTAGTGGGGGAAAAGGAC) to create strain OE4165. Alternatively, a full-length translational fusion of *ccpp-1* with green fluorescent protein (GFP) (created by ligating *ccpp-1* genomic sequence [primer pair: gatcacggatccGTGGACAAGGTATCGAATGG/tgcagtaccggtCCAGCTCGCTCAGTCTTGGTC] digested by BamHI/AgeI into the pPD95.75 vector [5]) was injected into OE4160 to create OE4171. For each of these *ccpp-1* constructs, the $P_{elt\text{-}2}$::*mCherry* transformation marker was coinjected to identify transformants. For rescue of the Cil phenotype, we crossed PT2168 males into OE4165 and looked at F1 males expressing *myIs1* and *ofEx805*.

Microscopy

Nematodes were anaesthetized with 10 mM levamisole (except strains with the *unc-29(e403)* background, which are insensitive to levamisole and were immobilized with 25 mM sodium azide) and mounted on agar pads for imaging at room temperature. Epifluorescence images were acquired using a Zeiss Axioplan2 microscope with 10x, 63x (NA 1.4), and 100x (NA 1.4) oil-immersion objectives with a Photometrics Cascade 512B CCD camera using Metamorph software (www.moleculardevices.com). Optical Z-stack projections were stored as TIFF files and manipulated using Adobe PhotoShop.

In preparation for confocal imaging, worms were mounted and anaesthetized on agar pads using 15 mM sodium azide. Images were collected using a Zeiss LSM 510 microscope with a 63X (NA 1.4) oil-immersion objective. Optical Z-stack projections were generated using Zeiss LSM Image Browser, saved as TIFF files, and manipulated using Adobe Photoshop.

KLP-6::GFP Localization

Strains used: PT2277, PT2278, PT2279

klp-6::gfp construction was previously described [4]. The *Ppkd-2::ccpp-1* construct was made by PCR sequence overlap extension (SOE; [S6]). We PCR amplified the genomic sequence of *ccpp-1* and a 1.3 kb *pkd-2* promoter separately, and then fused the PCR products together. Animals were observed using the 63X objective. Localization of KLP-6::GFP was tested by circling a region of interest and using the Integrated Morphometry function in Metamorph. We measured fluorescence intensities in CEM cilia and somata separately, then calculated the ratio of intensity in cilia/soma as a measure of localization.

OSM-3::GFP and OSM-6::GFP Localization and Motility:

Strains used: PT2098, PT2065, PT1416, PT2064, PT2338, PT2339

The P_{klp-6}*::osm-3::gfp* construct, which drives expression of OSM-3::GFP in CEM, RnB, HOB and IL2 neurons, was previously described [4]. We expressed OSM-6::GFP in male-specific neurons using the *pkd-2* promoter. The P_{pkd-2}*::osm-6::gfp* construct was made by restriction cloning (detailed method available by request). Localization of OSM-3::GFP or

OSM-6::GFP were measured in CEM neurons using the method described above for KLP-6::GFP.

IFT velocity experiments were conducted using time-lapse microscopy for 200 frames, each frame being a 150-200 ms exposure. Images were captured on the Zeiss Axioplan2 with a 100X (1.4NA) oil immersion objective using the Cascade camera. We used Metamorph software to convert the streaming video to kymographs and calculate the velocity of moving particles. All moving particles we observed were included in analysis.

Male Mating Response Behavior:

Strains used: CB1490, CB169, PT2280, PT2281, OE4165, OE4171, OE4180,

L4 larval males were moved to a fresh plate approximately 24 hours before mating behavior assays. Males used were either from the strains listed above or were F1 males resulting from crossing PT2281 males with OE4165 or OE4171 hermaphrodites. *unc-31* mutant hermaphrodites were also picked as L4 larvae ~24 hours before experiments. Male mating assays were conducted on a fresh NGM agar plate with a small lawn of *E. coli* (OP50) containing 25 young adult *unc-31* hermaphrodites. One, two, or three males were placed in the center of the lawn and observed for 4 minutes. A response was scored as positive when a male began scanning a hermaphrodite and his tail maintained contact with a mate for at least 10 seconds.

Dye-Filling and Osmotic Avoidance Behavior

Strains used: CB3323, JT5010, PT443, PT1645, PT2169, PT2170, PT2171, PT2172, PT2280, PT2379, PT2381, OE4160, OE4165, OE4171

Standard dye-filling assays were performed [19,20] using DiI (Invitrogen). Osmotic avoidance assays were performed by placing 10 animals in the center of an 8 M glycerol ring, and observing them for 10 minutes. The avoidance index (a.i.) was the ratio of the number of animals that remain in the center to the total number of worms [19,20].

Antibody Staining

Strains used: PT443, PT1645, PT2168, PT2171, PT2172, PT2379, PT2381

Animals were synchronized by bleaching and fixed as 1-day-old adults. Fixation (adapted from [S7]) was accomplished by washing animals off of 3 NGM plates using M9 buffer, then washing animals in a 15 ml conical tube 3 more times with M9 over one hour. Worms were chilled on ice, then washed in ice cold Ruvkun buffer (80mM KCl, 20mM NaCl, 10mM EGTA, 5mM spermidine-HCl, 15mM Pipes, pH 7.4 and 25% methanol) plus 20% formaldehyde in 1.6ml centrifuge tubes. The tubes were immersed in liquid nitrogen, then melted under tap water to crack the worm's cuticles. Worms were then washed with Tris-Triton buffer (100mM Tris-HCl, pH 7.4, 1% Triton X-100 and 1mM EDTA), then suspended in Tris-Triton buffer +1% β-mercaptoethanol and incubated overnight at 37°C. Worms were then washed with 1X BO_3 (50mM H_3BO_3, 025mM NaOH) + 0.01% Triton buffer, and suspended in 1X BO_3 + 0.01% Triton buffer + 0.3% H_2O_2 for 15 minutes with gentle agitation at room temperature. After washing once with 1X BO_3 + 0.01% Triton buffer, worms were washed for 15 minutes in Antibody buffer B (1X PBS, 0.1% BSA, 0.5%

Triton X-100, 0.05% sodium azide and 1mM EDTA) with gentle agitation at room temperature. Fixed worms were stored in Antibody buffer A (1X PBS, 1% BSA, 0.5% Triton X-100, 0.05% sodium azide and 1mM EDTA) at 4°C for up to one month before antibody staining. Animals were stained overnight at room temperature with a 1:600 dilution (in Antibody Buffer A) of GT335, a monoclonal antibody which binds the branch point of both monoglutamylated and polyglutamylated substrates [25]. Stained worms were washed with several changes of Antibody B Buffer with gentle agitation at room temperature over several hours. After rinsing with Antibody Buffer A, the rhodamine-conjugated anti-mouse secondary antibody was added at a dilution (in Antibody A Buffer) of 1:2000 and incubated for 2 hours at room temp with gentle agitation. Worms were then washed with several changes of Antibody Buffer B over several hours before mounting on 2% agarose pads for viewing on the Zeiss Axioplan2. Manual scoring of GT335 staining in CEM cilia was performed blind to the genotype using ImageJ. A positive was scored when GT335 staining (red) occupied the same voxel as ciliary PKD-2::GFP (green) in a color-combined Z-stack.

Serial Section Transmission Electron Microscopy and Electron Tomography

Strains used: CB1490, PT2280, PT2281

Young adult animals were subjected to high-pressure freeze fixation and freeze substitution, using 2% osmium tetroxide + 2% water in acetone as the primary fixative [S8]. Samples were slowly treated to freeze substitution in an RMC freeze sub device, before infiltration with Embed812 plastic resin. Serial sections (80 nm thickness) of fixed animals were collected on copper slot grids and stained with 4% uranyl acetate in 70%

methanol, followed by washing and incubating with aqueous lead citrate. Images were captured on a Philips CM10 transmission electron microscope at 80kV with a Morada 11 megapixel TEM CCD camera driven by iTEM software (Olympus Soft Imaging Solutions). Some of the EM pictures were still frames exported from tomograms. For electron tomography, animals were fixed identically and sections of 250 nm were collected on Pioloform coated slot grids. Sections were post-stained with aqueous uranyl acetate, and viewed in a FEI Technai20 TEM to collect about 200 tilt images per thick section using the SerialEM software package [S9], using the dual axis tilt method. Fourier processing using Protomo software and a markerless backprojection method was used for tomogram production [S10]. Dual axis tomograms from serial thick section were stitched together to produce larger tomograms spanning up to 20 serial sections (e.g. about 5 microns in the Z-axis). Model annotation was performed using IMOD [S11].

Supplemental References

S1. Brenner, S. (1974). The genetics of *Caenorhabditis elegans*. Genetics *77*, 71-94.

S2. Miyabayashi, T., Palfreyman, M.T., Sluder, A.E., Slack, F., and Sengupta, P. (1999). Expression and function of members of a divergent nuclear receptor family in *Caenorhabditis elegans*. Developmental Biology *215*, 314-331.

S3. Wicks, S.R., Yeh, R.T., Gish, W.R., Waterston, R.H., and Plasterk, R.H. (2001). Rapid gene mapping in *Caenorhabditis elegans* using a high density polymorphism map. Nature Genetics *28*, 160-164.

S4. Mello, C., and Fire, A. (1995). DNA transformation. Methods Cell Biol *48*, 451-482.

S5. Fire, A., Ahnn, J., Kelly, W., Harfe, B., Kostas, S., Hsieh, J., Hsu, M., and Xu, S. (1998). Green fluorescent protein : properties, applications, and protocols, (New York: Wiley-Liss).

S6. Horton, R.M., Cai, Z.L., Ho, S.N., and Pease, L.R. (1990). Gene splicing by overlap extension: tailor-made genes using the polymerase chain reaction. Biotechniques *8*, 528-535.

S7. Epstein, H.F., and Shakes, D.C. (1995). *Caenorhabditis elegans*: Modern Biological Analysis Of An Organism, (San Diego: Academic Press).

S8. Weimer, R.M. (2006). Preservation of *C. elegans* tissue via high-pressure freezing and freeze-substitution for ultrastructural analysis and immunocytochemistry. Methods Mol Biol *351*, 203-221.

S9. Mastronarde, D.N. (2005). Automated electron microscope tomography using robust prediction of specimen movements. Journal of Structural Biology *152*, 36-51.

S10. Winkler, H., and Taylor, K.A. (2006). Accurate marker-free alignment with simultaneous geometry determination and reconstruction of tilt series in electron tomography. Ultramicroscopy *106*, 240-254.

S11. Kremer, J.R., Mastronarde, D.N., and McIntosh, J.R. (1996). Computer visualization of three-dimensional image data using IMOD. Journal of Structural Biology *116*, 71-76.

Chapter 4

C. elegans ciliated sensory neurons release extracellular vesicles that function in animal communication.

Modified from Juan Wang, Malan Silva, *et al.* 2014 Current Biology

Forward

By 2014, it had almost a been a decade since myIs1 strain was made, outcrossed, imaged, characterized, and used in screens; but it was Juan Wang who noticed that several microns above perhaps the most imaged of focal planes in the Barr lab was a sea of bright fluorescent foci: PKD-2::GFP containing vesicles. These vesicles escape the tips of cilia, float upwards, and accumulate underneath the coverslip. It is possible that others have transiently noticed this phenomenon, but it was Juan who was smitten with the idea that these PKD-2::GFP-containing extracellular vesicles (EVs) coming out of the CEM and RnB cilia underlie a deeply conserved biological phenomenon and not an artifact of PKD-2::GFP overexpression. She isolated these vesicles from culture plates enriched for males via ultracentrifugation and together with Natalia Morsci and Lenny Hass, developed an assay that showed that these EVs could induce male tail chasing behavior.

During this time, Ken Nguyen and I were finishing up processing four serial tomograms of wild type CEM sensilla. The goal was to capture the entire length of axoneme microtubules to resolve the mystery of 20 signets in CEM cilia. In these

tomograms, I noticed that the membrane below the CEM cilia was forming omega structures, characteristic of membrane budding and CEM cilia were surrounded by EVs contained in the cephalic lumen. These EVs were of different diameters. Some of their lumens were electron opaque, others translucent. These findings corroborated nicely to establish CEM cilia as a model to study extracellular vesicle biology. Later I characterized extracellular vesicles in *cil-7* mutant to extend these findings in Maguire *et al.* 2014 and further in Silva *et al.* 2016 (Chapter 1) to demonstrate that there are two distinct populations of EVs in the CEM sensilla.

Highlights

- In vivo imaging reveals that *C. elegans* ciliated neurons release ECVs.
- The polycystins LOV-1 and PKD-2 are ECV cargo.
- IFT and kinesin-3 KLP-6 are required for PKD-2::GFP ECV release.
- Isolated ECVs trigger cargo-dependent behavioral changes in males.

Summary

Cells release extracellular vesicles (ECVs) that play important roles in intercellular communication and may mediate a broad range of physiological and pathological processes. Many fundamental aspects of ECV biogenesis and signaling have yet to be determined, with ECV detection being a challenge and obstacle due to their small size (100nm). We developed an *in vivo* system to visualize the dynamic release of GFP-labeled ECVs. We show here that specific *Caenorhabdidits elegans* ciliated sensory neurons shed and release ECVs containing GFP-tagged polycystins LOV-1 and PKD-2. These ECVs are also abundant in the lumen surrounding the cilium. Electron tomography and genetic analysis indicate that ECV biogenesis occurs via budding from the plasma membrane at the ciliary base and not via fusion of multivesicular bodies (MVBs). Intraflagellar transport (IFT) and kinesin-3 KLP-6 are required for environmental release of PKD-2::GFP-containing ECVs. ECVs isolated from wild-type animals induce male tail chasing behavior, while ECVs isolated from *klp-6* animals and lacking PKD-2::GFP do not. We conclude that environmentally released ECVs play a role in animal communication and mating related behaviors.

Results

Ciliated sensory neurons shed and release polycystin-containing extracellular vesicles (ECVs)

Caenorhabditis elegans ciliated sensory neurons monitor internal and external conditions. The hermaphrodite has 60 ciliated sensory neurons, the male possesses an additional 52 (Sulston, Albertson et al. 1980, Perkins, Hedgecock et al. 1986). Six IL2 (inner labial type 2) and 21 male-specific B-type sensory neurons are unique in that their sensory cilia protrude into the environment via a cuticular pore (Ward, Thomson et al. 1975, Sulston, Albertson et al. 1980, Perkins, Hedgecock et al. 1986). The *C. elegans* polycystins LOV-1 and PKD-2 are expressed exclusively in 21 male-specific B-type sensory neurons that include four CEM (cephalic male) neurons in the head, and HOB (hook B-type) and bilateral ray B-type neurons ("RnB" where n=1~9 but not 6) in the tail (Figure 1) (Barr and Sternberg 1999, Barr, DeModena et al. 2001).

GFP-tagged LOV-1 and PKD-2 extracellular vesicles (ECVs) are released from the tip of the nose where CEM cilia are exposed, and from the tips of the male tail rays, where the RnB cilia are exposed in late larval L4 and adult males (Fig. 1 A-D). PKD-2::GFP labeled ECVs are shed and released by late L4 males and trapped in the L4 molted cuticle (Supplemental Movie 1). Another cilia-enriched protein CWP-1 (co-expressed with polycystin-1, (Miller and Portman 2010)) is abundantly shed and released by male-specific B type sensory neurons (Fig. 1 E, F) and from the IL2 neurons in both hermaphrodites and males throughout development (data not shown). We can observe GFP-tagged ECV release from individual RnB ciliated neurons (see inset of Fig. 1B, D, F). Inner labial sensilla, male cephalic sensilla, male ray sensilla, and the male hook sensillum are similar in that

each contain two ciliated dendrites, with the tips of the IL2, CEM, RnB, and HOB cilia completely penetrating the cuticle (Perkins, Hedgecock et al. 1986) and releasing ECVs (Figure 1, Table 1).

pkd-2 is required for male mating behavior, therefore we asked if PKD-2::GFP containing ECVs are produced in a hermaphrodite-dependent manner. Adult males shed and release PKD-2::GFP ECVs whether cultured as single males (virgin) or in mixed populations (mated), suggesting that ECV production is constitutive in these conditions (Fig. 2A).

ECVs were harvested by washing off from culture plates and purified by repeated centrifugations and filtering, as described in Supplemental Methods. Supplemental Movie 1 shows isolated PKD-2::GFP containing vesicles. Negative staining of the ECV preparation reveals vesicle sizes averaging 91.7± 92.5 nm (average ± standard deviation; n=329). By staining with a monoclonal LOV-1 antibody and using ultra-small (<0.8nm) gold labeled secondary antibody detection followed by silver enhancement (Wood, Huang et al. 2013), we observe endogenous LOV-1 containing ECVs (Fig. 1 G-J) that are 111.2± 31.1 nm in diameter (n=210; see Supplemental Table 1 for ECV size comparison). These results confirm that *C. elegans* ECVs contain endogenous LOV-1, and that ECV shedding is not a consequence of overexpressed GFP-tagged proteins.

To test for cargo specificity of the shed vesicles, we examined GFP-tagged reporters of known ciliary components (Table 1). We do not observe environmental release of GFP-tagged b-tubulin TBB-4, IFT-A polypeptide IFT140/CHE-11, IFT-B polypeptide IFT52/OSM-6, motors (kinesin-II, kinesin-2, and kinesin-3 KLP-6), or soluble GFP from B-type, IL2, or any other ciliated sensory neurons. Therefore, in contrast to the

polycystins LOV-1 and PKD-2, cilium structural components, intraflagellar transport (IFT) polypeptides, and ciliary motors are not ECV cargo. Likewise, a GFP-labeled GPCR ODR-10::GFP that is expressed in AWA (amphid wing A) neurons is not shed.

Lysosome-associated membrane protein 1 (LAMP1) is a marker of both exosomes and microvesicles, types of ECVs (Flaumenhaft, Dilks et al. 2009, Logozzi, De Milito et al. 2009). LMP-1::GFP is shed and released from male B-type ciliated neurons but not other ciliated sensory neurons. Hence, ECV shedding and release is selective, constitutive, and abundant in IL2 and male-specific B-type ciliated sensory neurons, and not a consequence of simply breakage from the cilium.

MVB biogenesis components are not essential for ECV release of PKD-2::GFP

Exosomes and microvesicles/ectosomes are two main types of ECVs that differ in size and origin (Mathivanan, Ji et al. 2010, Raposo and Stoorvogel 2013). Exosomes are 40-100 nm in diameter and released by fusing of the multivesicular body (MVB) with the plasma membrane. Microvesicles (also known as ectosomes) are 100-1000 nm in diameter and generated by pinching off of the plasma membrane. To investigate if components of the MVB pathway regulate PKD-2::GFP ECV biogenesis, we examined PKD-2::GFP shedding and release in animals lacking the function of MVB biogenesis components. The endosomal sorting complexes required for transport (ESCRT-0, I, II and III), are vital components for MVB biogenesis (Henne, Buchkovich et al. 2011). The signal transducing adaptor molecule STAM-1 is a component of ESCRT-0, binds ubiquitinated PKD-2 and is required for PKD-2 downregulation (Hu, Wittekind et al. 2007). MVB-12 is a conserved core component of ESCRT-I (Audhya, McLeod et al. 2007). ALX-1 is required for

endosomal intralumenal vesicle formation (Shi, Pant et al. 2007). PKD-2::GFP ECV shedding and release is not reduced in *stam-1, mvb-12* or *alx-1* mutants as determined by imaging PKD-2::GFP release from individual males, or by visualizing PKD-2::GFP in isolated ECV preparations (Fig. 2B, Supplemental Fig. 1, and data not shown).

IFT and kinesin-3 KLP-6 are required for PKD-2::GFP ECV release

In MDCK cell lines, IFT88 is required for polycystin 2 apical secretion (Hurd, Zhou et al. 2010). In *C. elegans* B-type neurons, IFT regulates PKD-2 ciliary abundance (Qin, Rosenbaum et al. 2001, Bae, Qin et al. 2006). IFT-B IFT88/*osm-5* and IFT-A IFT122/*daf-10* are required for PKD-2::GFP ECV release into the environment (Fig. 2C). In contrast, Bardet-Biedl-Syndrome gene 7 homolog *bbs-7* is not required for PKD-2::GFP release. These results indicate that polycystin release in both mammalian kidney cells and *C. elegans* B-type ciliated neurons relies on IFT88 and intact cilia.

In *C. elegans* amphid channel and phasmid cilia, two IFT motors, homodimeric kinesin-2 OSM-3 and the heterotrimeric Kinesin II, encoded by *klp-11, klp-20* and *kap-1,* act redundantly (Scholey 2008). The B-type neurons employ the kinesin-3 KLP-6 to regulate IFT and PKD-2 ciliary localization, but *klp-6*, *osm-3*, or kinesin-II alone is not essential for CEM ciliogenesis (Peden and Barr 2005, Morsci and Barr 2011). Neither *osm-3* nor *klp-11* is required for shedding and release of PKD-2::GFP containing ECVs (Fig. 2B). However, the *osm-3;klp-11* double mutant is defective in PKD-2::GFP release (Fig. 2B), indicating that the two anterograde IFT motors act redundantly in this process (Fig. 2B). *klp-6* mutant males do not release PKD-2::GFP ECVs to the environment (Fig. 2B, C), suggesting that PKD-2::GFP accumulation at the ciliary base (Peden and Barr 2005) may reflect an ECV shedding

or environmental release defect. We conclude that intact cilia and the kinesin-3 *klp-6* are required for PKD-2::GFP-ECV shedding and/or release.

ECVs are abundant in the cephalic lumen surrounding the CEM cilium

We performed electron tomography (ET) of the wild-type cephalic sense organ, or sensillum, that houses the CEM neuron (Fig. 1K). The CEM cilium and ciliary base are surrounded by an extracellular lumen that is formed by the glial sheath cell, socket cell and the cuticle, with the ciliary tip exposed through the cuticular opening. ECVs are observed in the lumen surrounding the CEM cilium and cilium base (Fig. 2C, Supplemental Movie 2). We observed one ECV connected to the ciliary base membrane with a long stalk, indicating that this ECV was either budding off or fusing with the membrane (data not shown). Consistent with our finding that MVB components are not required for PKD-2::GFP ECV shedding or release (Fig. 2B, Supplemental Fig. 1), we did not observe MVB structures spanning the CEM neuron from the distal dendrite to the ciliary tip (Supplemental Movie 3 and data not shown).

In the four CEM neurons, we observed a range of 62 to 259 vesicles per lumen (Fig. 2C, Supplemental Movie 2). The average ECV size was 104.7±46.7 nm (average±SD; Supplemental Table 1, Fig. 2C). Therefore, *C. elegans* ECVs are similar in size to both microvesicles/ectosomes (100 - 1000 nm) and exosomes (40-100nm)(Gyorgy, Szabo et al.). In males, the cephalic lumen surrounds the ciliated endings of both the CEM and CEP neurons. In hermaphrodites, the cephalic lumen contains only the CEP neuronal cilium and lacks ECVs (Ward, Thomson et al. 1975), suggesting that luminal ECVs are produced by the male-specific CEM neurons.

To determine if ECVs are native to other ciliated sensilla, we examine the amphid sensilla (major sensory organs in the anterior of the nematode) and the outer labial sensilla. Each amphid sensillum contains 12 cilia surrounded by a lumen that formed by a sheath cell, a socket cell, and the cuticle (Ward, Thomson et al. 1975). Although extensive TEM analysis has been done on the amphids, no luminal ECVs have been reported. We performed ET on the amphid sensillum of adult males. From two tomograms, we found only one vesicle in one and nine vesicles in the other amphid channel lumen (Supplemental Figure 2). By contrast, we observed an average of 162 ECVs in the male-specific cephalic lumen. Furthermore, the location of the ECVs in the cephalic and amphid lumen was different. In the cephalic sensillum, ECVs are found near the ciliary base of CEM neurons (Fig. 1K, 2C) whereas in the amphid sensillum, rare ECVs are in close proximity to amphid channel cilia distal segments (Supplemental Fig. 2). In the outer labial sensillum, the OLQ cilium is surrounded by an extracellular lumen that lacks ECVs (data not shown). Combined, these data suggest that the abundant ECVs found in the cephalic lumen are shed by male-specific CEM ciliated sensory neurons.

***klp-6* is required for PKD-2::GFP release**

klp-6 mutant males are defective in PKD::GFP ECV release (Fig 2B) and accumulate PKD-2::GFP in ciliary regions (Fig. 2F) (Peden and Barr 2005), which may correlate with defects in ECV biogenesis, shedding into the lumen, or release from the lumen to the exterior of the animal. We therefore examined the cephalic sensillum of the *klp-6* mutant by serial thin section TEM. *klp-6* mutant males accumulate a large number of luminal ECVs (Fig. 2D) and possess an extracellular lumen doubled in volume compared to wild type (Fig. 2E).

ECVs in the lumen surrounding the CEM cilia may be the source of the ECVs released outside of the worm. These results also indicate that *klp-6* is not required for ECV biogenesis or shedding. Rather, *klp-6* may regulate ECV environmental release from the lumen. We can isolate ECVs from *klp-6* mutants via ultracentrifugation. These ECVs contain endogenous LOV-1 but not PKD-2::GFP (data not shown), indicating that *klp-6* may play a role in ECV cargo selection.

Isolated ECVs induce male tail chasing behavior

Functions of ECVs include protein disposal and cell-cell communication. As IL2 and B-type neurons release ECVs to the environment, we hypothesized that ECVs may play a role in animal-animal communication. To test this, we developed two behavioral assays. First, we performed a choice assay, to determine if males can distinguish between ECVs versus M9 buffer alone (Fig. 3A). Males display no chemotactic preference for spots containing ECVs from wild-type worms, ECVs from *klp-6* worms, or M9 buffer (Fig. 3B). We conclude that ECVs do not act as a long-range chemotactic cue. However, males did alter locomotion by increasing reversal frequency in ECV spots but not M9 spots (Fig. 3C). Males exhibit similar reversal frequency on both wild-type and the *klp-6* ECV preparations. We noticed three instances of tail chasing behavior (in 27 recordings) in the wild-type ECV spot, in which the male tail curls to contact its own head and moves in a backward circle. Tail curling enables the male to contact and circle around the hermaphrodite body during mating (Sherlekar, Janssen et al. 2013). Tail curling behavior may also culminate in male-self or male-male contact (Gems and Riddle 2000). Male-male contact is called clumping behavior (Gems and Riddle 2000), in which *pkd-2* males are defective (Kaletta, Van Der

Craen et al. 2003). Clumping is a population-based behavior and assays would be confounded by ECVs produced by the population versus purified ECVs. We therefore developed an assay to measure individual male-self contact or tail chasing behavior.

In the "tail chasing assay," a large spot of ECVs from wild-type animals, *klp-6* mutants, or M9 buffer was placed and dried on a seeded agar plate (Fig. 3D). A single male was placed on each spot directly. On wild-type ECV spots, males exhibited a high frequency of tail chasing behavior (Fig. 3E, Supplemental Movie 3). In contrast, *klp-6* ECV spots were not significantly different than M9 control spots in inducing tail chasing behavior (Fig. 3E). We conclude that environmentally released ECVs and ECV-cargo play a role in animal communication and mating behavior.

Discussion

Here, we use *C. elegans* as a new model system to visualize ECVs release in vivo. We identify ECV cargo and demonstrate animal behavior changes due to purified ECVs and ECV cargo alone. ECV shedding from ciliated cells is an evolutionarily conserved phenomenon.

Membrane bound ECVs containing ciliary proteins including PKD2 have been reported in *Chlamydomonas* and human urine (Hogan, Manganelli et al. 2009, Hurd, Zhou et al. 2010, Wood, Huang et al. 2013).

From where are ciliary released ECVs derived? Recently Rosenbaum and colleagues showed that *Chlamydomonas* releases ectosomes from the flagellar tip, and that ectosomes contain an enzyme required to digest the mother cell wall and release newly born daughter cells free (Wood, Huang et al. 2013). In rat biliary epithelium, polycystin containing exosome-like vesicles may be extruded by the MVB at the base of the cilium (Hogan, Manganelli et al. 2009). In earlier work, Bloodgood showed that antibody crosslinked flagellar membrane glycoproteins are enriched at the flagellar tip, transported back to the cell body, and released from the base of the *Chlamydomonas* flagella (Bloodgood, Woodward et al. 1986). In *C. elegans* cephalic sensillia, ECVs are abundant at the CEM ciliary base of wild-type and *klp-6* males (Figure 2C, D, Supplemental Figure 1). In amphid sensilla, we observe rare ECVs at the distal ciliary region of amphid sensillum (Supplemental Figure 2). Combined, these results indicate that ciliary-derived ECVs may be generated and released by multiple pathways.

ECVs are released from most mammalian cell types and carry specific protein and RNA cargo that may be transferred between donor and recipient cells without requiring

direct contact. ECVs function in protein degradation and intercellular communication, and mediate a broad range of physiological and pathological processes (Cocucci, Racchetti et al. 2009, Gyorgy, Szabo et al. 2011). Here we show that *C. elegans* ECVs act as a local sensory cue by promoting male reversal behavior and tail chasing behavior (Figure 3 and Supplemental Movie 4). The cue(s) provided by ECVs are different than ascaroside cues, which were removed by washing in the ECV centrifugation and isolation procedure (Ludewig and Schroeder 2013). Moreover, specific ECV cargo are required for tail chasing behavior: ECVs isolated from *klp-6* animals and lacking PKD-2::GFP do not trigger this male-specific locomotory behavior. In natural populations, males are rare and capable of sensing and responding to numerous cues from potential mates (reviewed by (Chasnov 2013)). We speculate that ECV-triggered reversals and tail chasing behavior may represent components of a male behavioral repertoire aimed optimizing reproductive success with self-fertilizing hermaphrodites. Consistent with the idea of sexual arms race, *C. elegans* males secrete unidentified compounds that shorten the life span of hermaphrodites (Maures, Booth et al. 2013). Whether male-released ECVs play a role in male-induced demise of hermaphrodites is not known. We propose that ECVs and ECV-cargo composition modulates animal-to-animal communication, which to our knowledge, is a new radically function for ECVs.

An important and unresolved question is how ECVs interact with recipient cells. ECVs are closely associated with mammalian cilia (Hogan, Manganelli et al. 2009, Masyuk, Huang et al. 2010, Pampliega, Orhon et al. 2013), yet the physiological relevance remains elusive. Bodily fluids such as breast milk, urine, and seminal fluid are rich in ECVs (Cocucci, Racchetti et al. 2009, Hogan, Manganelli et al. 2009) and may play a role animal

communication. For example, breast milk plays a role in development of newborn immunity (Admyre, Johansson et al. 2007). We propose that ECVs play important and unexplored roles in animal communication and behavior.

Experimental procedures

All nematodes were grown under standard conditions (Brenner 1974). The following strain was used to image ECV release and considered wild-type: PT621 *him-5(e1490) myIs4 [PKD-2::GFP +Punc-122::GFP]V* (Bae, Qin et al. 2006). Additional methods are provided in Supplemental Experimental methods and strains in Supplemental Table 2.

Supplemental Information

Supplemental information includes supplemental experimental procedures, two supplemental figures, four supplemental movies, and two supplemental tables.

Acknowledgements. We are grateful to Joel Rosenbaum for ongoing encouragement and constant challenge to decipher ECV roles, and Christopher Wood for protocol for ultra-small gold immuno-EM labeling. We thank Christopher Ward, Barth Grant, Monica Driscoll, and Barr lab members for ongoing discussions, and to Robert O'Hagan, Nathan Schroeder, and Simon Warburton-Pitt for constructive criticism of the manuscript. This work was supported by NIH RO1DK059418 and NIH R01DK074746 to MBB, and by NIH OD010943 to DHH. We thank William Rice at the New York Structural Biology Center for

ET help, and Valentine Starovoytov (Rutgers) for TEM assistance. Access to equipment at the NYSBC was supported by funds from Albert Einstein College of Medicine. Some nematode strains were provided by the *Caenorhabditis* Genetics Center, which is funded by the NIH National Center for Research Resources (P40 OD010440), the *C. elegans* Gene Knockout Consortium, and the National Bioresource Project for the Nematode.

Figures

Figure 1

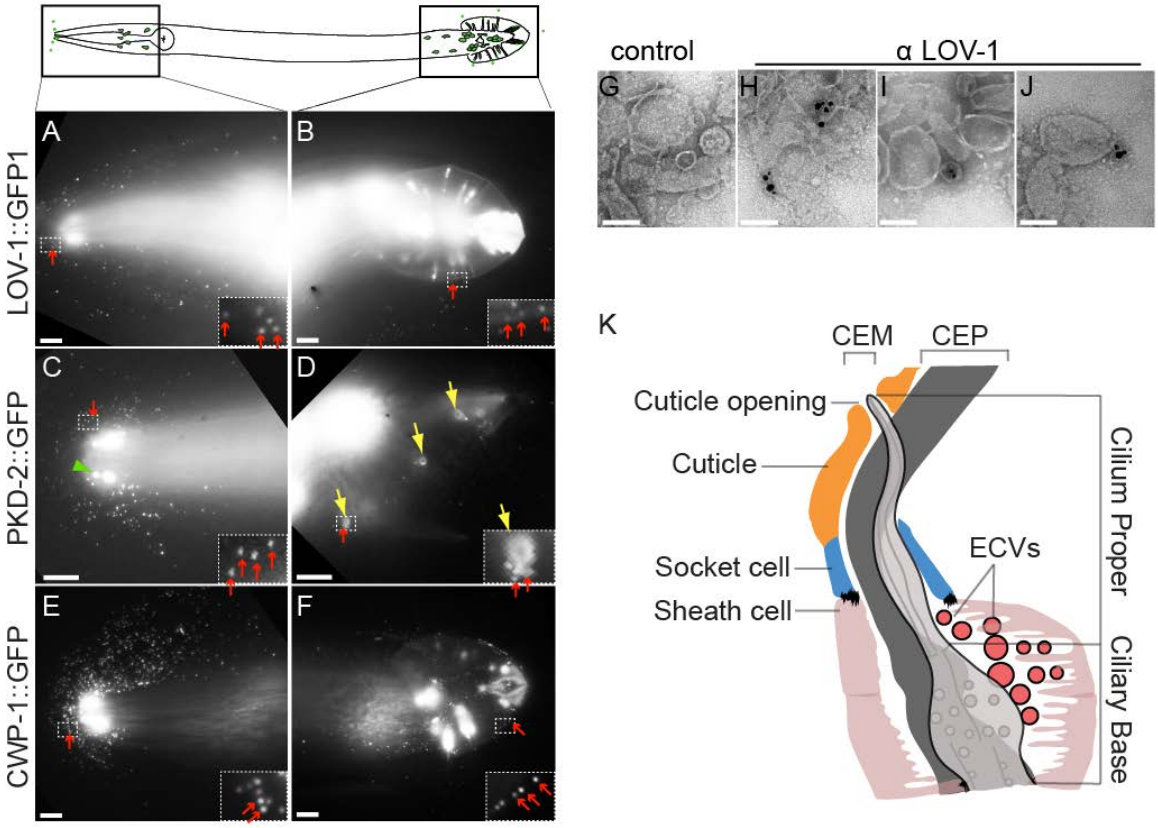

Figure 1 IL2 and male-specific B-type ciliated neurons release GFP-labeled ECVs.

Top panel, cartoon of six IL2 and B-type sensory neurons in adult *C. elegans* male (in the head, four CEM neurons, and in the tail, one HOB and 16 RnB neurons). (A, B) Male head and tail images of LOV-1::GFP reporter (N-terminal extracellular domain of LOV-1 (1-991 aa) fused to GFP). In all panels, red arrows point to ECVs surrounding the head and the tail. Insets show framed area zoomed to 4X, and increased brightness to show GFP-labeled ECVs. (C, D) Male head and tail images of PKD-2::GFP reporter. Green arrow head points to

a CEM cilium with PKD-2::GFP enriched at the tip. Yellow arrows point to the cuticular pore of the ray neurons and PKD-2::GFP release around the pore. (E, F) CWP-1::GFP release from the head and the tail. (G-J) Negatively stained ECVs. (G) ECVs with no primary antibody control. (H, I and J) Different images of LOV-1 antibody labeling endogenous LOV-1 on ECVs purified from wild-type hermaphrodites and males without a GFP transgene, detection by 0.8 nm ultrasmall gold, followed by silver enhancement. Scale bar of A-F is 10 μm, of G-J is 100 nm. (K) Model based on electron tomography (ET) of the distal end of the CEM neuron and its surroundings. The glial sheath cell and socket cell form a continuous lumen surrounding the CEM neuron cilium, which is exposed to the environment directly through a cuticular opening. The lumen is shared by CEM and CEP neurons. The CEM neuron is more centrally located in the lumen, while the CEP neuron is closer to the side of the lumen. ECVs are observed in the lumen (161.8 ± 82.8 nm, Average ±SD of vesicles in each lumen).

Figure 2

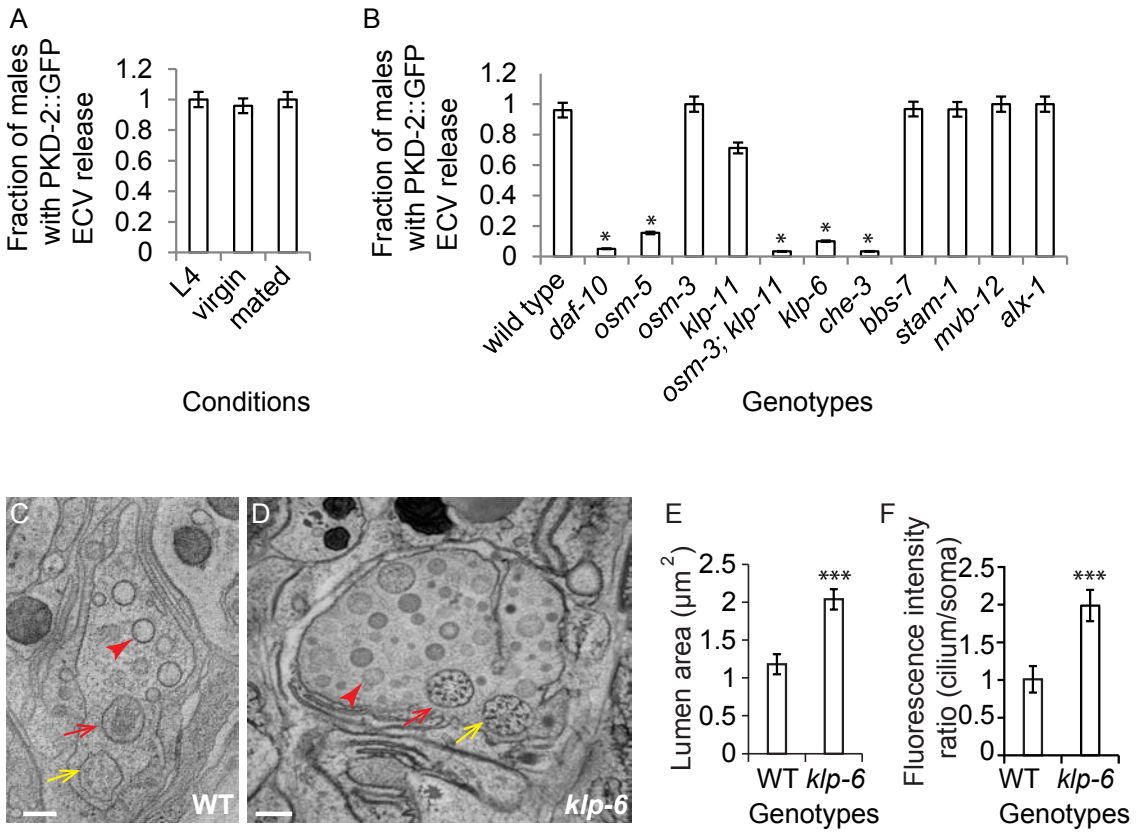

Figure 2 ECV release is constitutive, independent of ESCRT-0 and -I components, and dependent on IFT and the kinesin-3 *klp-6*.

(A) Wild-type L4 larvae, virgin males and mated males equally shed and release PKD-2::GFP ECVs. (B) PKD-2::GFP ECV release is impaired in *daf-10* (IFT-A), *osm-5* (IFT-B), *osm-3;klp-11* (redundant anterograde kinesin-2 motors), *klp-6* (kinesin-3) and *che-3* (dynein heavy chain, retrograde motor). *osm-3*, *klp-11*, and *bbs-7* and MVB biogenesis pathway single mutants are not defective in PKD-2::GFP release. Error bar indicates 95% confident intervals, * Different from wild type, Fisher's exact test, Bonferroni-Holm corrected $P < 0.05$). (C-D) Cross sections of the cephalic sensillum at CEM transition zone level in wild

type and *klp-6* mutant. Yellow arrows point to the CEP neuron; red arrows point to the CEM neuron; red arrowheads point to the ECVs. Scale bar is 200 nm. (E) Quantification of the lumen cross-sectional area in wild-type and *klp-6* mutant males. (F) *klp-6* mutants accumulate PKD-2::GFP at the ciliary region, and the ratio of total fluorescence intensity of cilium to soma is significantly greater than wild type (in E-F, error bar indicates Stdev, *** $p<0.001$ by Mann-Whitney test).

Figure 3

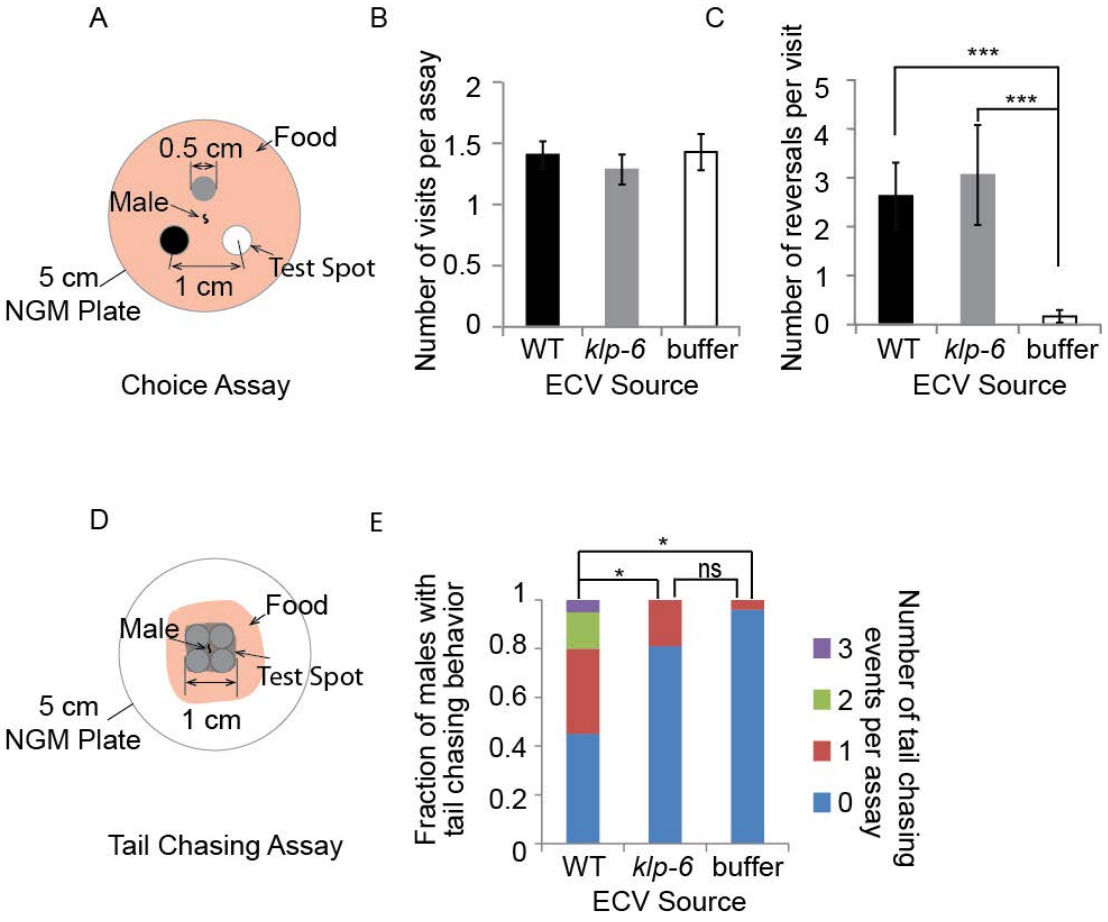

Figure 3 Purified ECVs promote adult male-specific behaviors.

(A) Diagram of choice assay plate. Three spots of M9 (negative control), wild-type ECV suspension, and *klp-6* ECV suspension were placed equidistance apart on a 5 cm seeded NGM plate. A male was placed in the center of the plate and his behavior recorded for five minutes. (B) The number of times the male visited each test spot is not significantly different. (C) Males exhibit more reversals on either the wild-type or the *klp-6* ECV spot than on the M9 buffer (minus ECV) control spot ($p<0.001$). The number of reversals is not different between the wild-type and *klp-6* ECV samples. Statistical analysis was done by Kruskal-Wallis test, six independent trials with 10 assays per trials. (D) To measure tail

chasing behavior, the male was placed in a bigger spot comprised of four smaller drops of the ECV preparation, with small food lawn to restrict the male from wandering too far away from the spot. (E) Males displayed tail chasing behavior only on wild-type ECVs (Supplemental Movie 3) but not on *klp-6* ECVs or M9 buffer control. Six independent trials with 20, 21, and 25 individual male assays for wild-type ECV, *klp-6* ECV and M9 buffer control respectively were performed. * Different from wild type, Fisher's exact test, Bonferroni-Holm corrected $P < 0.05$).

References:

1. Perkins, L.A., Hedgecock, E.M., Thomson, J.N., and Culotti, J.G. (1986). Mutant sensory cilia in the nematode *Caenorhabditis elegans*. Dev Biol *117*, 456-487.
2. Sulston, J.E., Albertson, D.G., and Thomson, J.N. (1980). The *Caenorhabditis elegans* male: postembryonic development of nongonadal structures. Dev Biol *78*, 542-576.
3. Ward, S., Thomson, N., White, J.G., and Brenner, S. (1975). Electron microscopical reconstruction of the anterior sensory anatomy of the nematode *Caenorhabditis elegans*. J Comp Neurol *160*, 313-337.
4. Barr, M.M., DeModena, J., Braun, D., Nguyen, C.Q., Hall, D.H., and Sternberg, P.W. (2001). The *Caenorhabditis elegans* autosomal dominant polycystic kidney disease gene homologs *lov-1* and *pkd-2* act in the same pathway. Curr Biol *11*, 1341-1346.
5. Barr, M.M., and Sternberg, P.W. (1999). A polycystic kidney-disease gene homologue required for male mating behaviour in *C. elegans*. Nature *401*, 386-389.
6. Miller, R.M., and Portman, D.S. (2010). A latent capacity of the *C. elegans* polycystins to disrupt sensory transduction is repressed by the single-pass ciliary membrane protein CWP-5. Dis Model Mech *3*, 441-450.
7. Wood, C.R., Huang, K., Diener, D.R., and Rosenbaum, J.L. (2013). The cilium secretes bioactive ectosomes. Curr Biol *23*, 906-911.
8. Logozzi, M., De Milito, A., Lugini, L., Borghi, M., Calabro, L., Spada, M., Perdicchio, M., Marino, M.L., Federici, C., Iessi, E., Brambilla, D., Venturi, G., Lozupone, F., Santinami, M., Huber, V., Maio, M., Rivoltini, L., and Fais, S. (2009). High levels of exosomes expressing CD63 and caveolin-1 in plasma of melanoma patients. PLoS One *4*, e5219.
9. Flaumenhaft, R., Dilks, J.R., Richardson, J., Alden, E., Patel-Hett, S.R., Battinelli, E., Klement, G.L., Sola-Visner, M., and Italiano, J.E., Jr. (2009). Megakaryocyte-derived microparticles: direct visualization and distinction from platelet-derived microparticles. Blood *113*, 1112-1121.
10. Mathivanan, S., Ji, H., and Simpson, R.J. (2010). Exosomes: extracellular organelles important in intercellular communication. J Proteomics *73*, 1907-1920.
11. Raposo, G., and Stoorvogel, W. (2013). Extracellular vesicles: exosomes, microvesicles, and friends. J Cell Biol *200*, 373-383.
12. Henne, W.M., Buchkovich, N.J., and Emr, S.D. (2011). The ESCRT pathway. Dev Cell *21*, 77-91.
13. Hu, J., Wittekind, S.G., and Barr, M.M. (2007). STAM and Hrs Down-Regulate Ciliary TRP Receptors. Mol Biol Cell *18*, 3277-3289.
14. Audhya, A., McLeod, I.X., Yates, J.R., and Oegema, K. (2007). MVB-12, a fourth subunit of metazoan ESCRT-I, functions in receptor downregulation. PLoS One *2*, e956.
15. Shi, A., Pant, S., Balklava, Z., Chen, C.C., Figueroa, V., and Grant, B.D. (2007). A novel requirement for *C. elegans* Alix/ALX-1 in RME-1-mediated membrane transport. Curr Biol *17*, 1913-1924.
16. Hurd, T., Zhou, W., Jenkins, P., Liu, C.J., Swaroop, A., Khanna, H., Martens, J., Hildebrandt, F., and Margolis, B. (2010). The retinitis pigmentosa protein RP2

interacts with polycystin 2 and regulates cilia-mediated vertebrate development. Hum Mol Genet *19*, 4330-4344.

17. Qin, H., Rosenbaum, J.L., and Barr, M.M. (2001). An autosomal recessive polycystic kidney disease gene homolog is involved in intraflagellar transport in *C. elegans* ciliated sensory neurons. Curr Biol *11*, 457-461.
18. Bae, Y.K., Qin, H., Knobel, K.M., Hu, J., Rosenbaum, J.L., and Barr, M.M. (2006). General and cell-type specific mechanisms target TRPP2/PKD-2 to cilia. Development *133*, 3859-3870.
19. Scholey, J.M. (2008). Intraflagellar transport motors in cilia: moving along the cell's antenna. J Cell Biol *180*, 23-29.
20. Morsci, N.S., and Barr, M.M. (2011). Kinesin-3 KLP-6 regulates intraflagellar transport in male-specific cilia of *Caenorhabditis elegans.* Curr Biol *21*, 1239-1244.
21. Peden, E.M., and Barr, M.M. (2005). The KLP-6 Kinesin Is Required for Male Mating Behaviors and Polycystin Localization in *Caenorhabditis elegans*. Current Biology *15*, 394-404.
22. Gyorgy, B., Szabo, T.G., Pasztoi, M., Pal, Z., Misjak, P., Aradi, B., Laszlo, V., Pallinger, E., Pap, E., Kittel, A., Nagy, G., Falus, A., and Buzas, E.I. (2011). Membrane vesicles, current state-of-the-art: emerging role of extracellular vesicles. Cell Mol Life Sci *68*, 2667-2688.
23. Ward, S., Thomson, N., White, J.G., and Brenner, S. (1975). Electron microscopical reconstruction of the anterior sensory anatomy of the nematode *Caenorhabditis elegans*. J Comp Neurol *160*, 313-337.
24. Sherlekar, A.L., Janssen, A., Siehr, M.S., Koo, P.K., Caflisch, L., Boggess, M., and Lints, R. (2013). The *C. elegans* male exercises directional control during mating through cholinergic regulation of sex-shared command interneurons. PLoS One *8*, e60597.
25. Gems, D., and Riddle, D.L. (2000). Genetic, behavioral and environmental determinants of male longevity in *Caenorhabditis elegans*. Genetics *154*, 1597-1610.
26. Kaletta, T., Van Der Craen, M., Van Geel, A., Dewulf, N., Bogaert, T., Branden, M., King, K.V., Buechner, M., Barstead, R., Hyink, D., Li, H.P., Geng, L., Burrow, C., and Wilson, P. (2003). Towards understanding the polycystins. Nephron *93*, E9-E17.
27. Hogan, M.C., Manganelli, L., Woollard, J.R., Masyuk, A.I., Masyuk, T.V., Tammachote, R., Huang, B.Q., Leontovich, A.A., Beito, T.G., Madden, B.J., Charlesworth, M.C., Torres, V.E., LaRusso, N.F., Harris, P.C., and Ward, C.J. (2009). Characterization of PKD protein-positive exosome-like vesicles. J Am Soc Nephrol *20*, 278-288.
28. Bloodgood, R.A., Woodward, M.P., and Salomonsky, N.L. (1986). Redistribution and shedding of flagellar membrane glycoproteins visualized using an anti-carbohydrate monoclonal antibody and concanavalin A. J Cell Biol *102*, 1797-1812.
29. Cocucci, E., Racchetti, G., and Meldolesi, J. (2009). Shedding microvesicles: artefacts no more. Trends Cell Biol *19*, 43-51.
30. Ludewig, A.H., and Schroeder, F.C. (2013). Ascaroside signaling in *C. elegans*. WormBook, 1-22.
31. Chasnov, J.R. (2013). The evolutionary role of males in *C. elegans*. Worm *2*, e21146.
32. Maures, T.J., Booth, L.N., Benayoun, B.A., Izrayelit, Y., Schroeder, F.C., and Brunet, A. (2013). Males Shorten the Life Span of *C. elegans* Hermaphrodites via Secreted Compounds. Science.

33. Masyuk, A.I., Huang, B.Q., Ward, C.J., Gradilone, S.A., Banales, J.M., Masyuk, T.V., Radtke, B., Splinter, P.L., and LaRusso, N.F. (2010). Biliary exosomes influence cholangiocyte regulatory mechanisms and proliferation through interaction with primary cilia. Am J Physiol Gastrointest Liver Physiol *299*, G990-999.
34. Pampliega, O., Orhon, I., Patel, B., Sridhar, S., Diaz-Carretero, A., Beau, I., Codogno, P., Satir, B.H., Satir, P., and Cuervo, A.M. (2013). Functional interaction between autophagy and ciliogenesis. Nature *502*, 194-200.
35. Admyre, C., Johansson, S.M., Qazi, K.R., Filen, J.J., Lahesmaa, R., Norman, M., Neve, E.P., Scheynius, A., and Gabrielsson, S. (2007). Exosomes with immune modulatory features are present in human breast milk. J Immunol *179*, 1969-1978.
36. Brenner, S. (1974). The genetics of *Caenorhabditis elegans*. Genetics *77*, 71-94.

Chapter 5

Cell-Specific Transcriptional Profiling of Ciliated Sensory Neurons Reveals Regulators of Behavior and Extracellular Vesicle Biogenesis.

Modified from Juan Wang, Rachel Kaletsky, Malan Silva *et al.* 2014 Current Biology

Forward

I enthusiastically tested candidates from RNAseq list for genes expressed in extracellular vesicles-releasing neurons. This list was a result of experiments done during Maureen Barr's sabbatical research year at Coleen Murphy's lab at Princeton. I fixed, sectioned, imaged, and reconstructed *trf-1*, *trf-2*, *lov-1*, *pkd-2*, *tag-232,* and *pmk-1* mutants at low resolution. Of these TEM data only *pmk-1* was included in the manuscript. This was perhaps due to several reasons. *Pmk-1* had an unusual defect in EV biology. Most mutants defective in proper PKD-2::GFP localization show accumulation of EVs in CEM ciliary base and proper, perhaps as a consequence of defective in release of PKD-2::GFP containing EVs into the outside environment. In *pmk-1* mutant background, reduced levels of PKD-2::GFP release didn't go hand-in-hand with their accumulation within the sensillum. Instead, overall levels of PKD-2::GFP at ciliary base was reduced. My TEM data corroborated the lack of accumulation of PKD-2::GFP at the base of the cilia with less than wildtype levels of vesicles seen in the *pmk-1* ciliary base. Concurrently I have been characterizing the developing CEM cilia to understand how the splayed doublets seen in the adults are formed. I noticed that similar to the developing CEM cilia, *pmk-1* mutants

contained incomplete ring of doublets at the cilia transition zone, suggesting that CEM cilia found in the adult *pmk-1* mutants were immature. This hypothesis was consistent with the delayed and reduced onset of PKD-2::GFP expression seen in *pmk-1* mutants.

Summary

Cilia and extracellular vesicles (EVs) are signaling organelles(Wood and Rosenbaum 2015). Cilia act as cellular sensory antennae, with defects resulting in human ciliopathies. Cilia both release and bind to EVs(Wood and Rosenbaum 2015). EVs are submicron-sized particles released by cells and function in both short and long range intercellular communication. In *C. elegans* and mammals, the Autosomal Dominant Polycystic Kidney Disease (ADPKD) gene products polycystin-1 and polycystin-2 localize to both cilia and EVs, act in the same genetic pathway, and function in a sensory capacity, suggesting ancient conservation(O'Hagan, Wang et al. 2014). A fundamental understanding of EV biology and the relationship between the polycystins, cilia, and EVs is lacking. To define properties of a ciliated EV-releasing cell, we performed RNAseq on 27 GFP-labeled EV releasing neurons (EVNs) isolated from adult *C. elegans*. We identified 335 significantly overrepresented genes, of which 61 were validated by GFP reporters. The EVN transcriptional profile uncovered new pathways controlling EV biogenesis and polycystin signaling and also identified EV cargo, which included an antimicrobial peptide and ASIC channel. Tumor necrosis associated factor (TRAF) homologues *trf-1* and *trf-2* and the p38 mitogen-activated protein kinase (MAPK) *pmk-1* acted in polycystin signaling pathways controlling male mating behaviors. *pmk-1* was also required for EV biogenesis, independent of the innate immunity MAPK signaling cascade. This first high-resolution transcriptome profile of a subtype of ciliated sensory neurons isolated from adult animals reveals the functional components of an EVN.

Results and Discussion

The cilium both releases and binds to extracellular vesicles (EVs), suggesting that cilia may be essential in EV-mediated communication as both senders and receivers of information(Tanaka, Okada et al. 2005, Hogan, Manganelli et al. 2009, Bakeberg, Tammachote et al. 2011, Pampliega, Orhon et al. 2013, Wood, Huang et al. 2013, Wang, Silva et al. 2014). EVs carry specific protein and RNA cargoes that can be transferred between donor and recipient cells without requiring direct contact(Raposo and Stoorvogel 2013). EVs mediate a broad range of physiological and pathological processes(S, Mager et al. 2013).

The mammalian polycystins localize to cilia as well as urinary EVs released from renal epithelial cells(Pazour, San Agustin et al. 2002, Yoder, Hou et al. 2002, Pisitkun, Shen et al. 2004, Hogan, Manganelli et al. 2009), and polycystin ciliary trafficking defects may be an underlying cause of ADPKD(Cai, Fedeles et al. 2014). In an amazing display of evolutionary conservation, we recently showed that the *C. elegans* cilium is a source of bioactive polycystin-containing EVs(Wang, Silva et al. 2014). The mechanisms controlling EV biogenesis, shedding, and release are poorly understood, largely due to technical difficulties in visualizing, isolating, and characterizing these sub-micrometer-sized particles. Here, we defined the unique features of a ciliated extracellular vesicle releasing neuron (EVN).

C. elegans shed and release EVs from 27 ciliated extracellular vesicle releasing neurons (EVNs) including six inner labial type 2 (IL2) neurons and 21 male-specific polycystin-expressing EVNs in the head (four CEM neurons) and tail (16 ray B-type RnB

neurons and one hook B-type HOB neuron) (Fig. 1A, B)(Wang, Silva et al. 2014). In these male-specific EVNs, the polycystins *lov-1* and *pkd-2* are required for male sex drive, response to mate contact, and vulva location(Barr and Sternberg 1999, Barr, DeModena et al. 2001, Barrios, Nurrish et al. 2008). The kinesin-3 protein KLP-6 is exclusively expressed in the 27 EVNs and is required for release of bioactive PKD-2::GFP containing EVs that function in reproductive animal-to-animal communication(Wang, Silva et al. 2014). Intact cilia but not multivesicular body components are required for EV release, suggesting that PKD-2 containing EVs are not exosomes but rather ectosomes that bud from the plasma membrane at the ciliary base(Wang, Silva et al. 2014). In addition to *klp-6* and the polycystins, only a handful of genes (coexpressed with polycystin genes *cwp-1* to *-5*, alpha-tubulin *tba-6*, and the EV release regulator *cil-7*) are exclusively expressed in the EVNs(Portman and Emmons 2004, Hurd, Miller et al. 2010, Miller and Portman 2010, Maguire, Silva et al. 2015).

To decipher the biology of a polycystin-expressing EVN in its native environment, we isolated *klp-6p*::GFP labeled neurons from age-synchronized adult animals by mechanical and proteolytic disruption, filtration, and FACS sorting(Kaletsky, Williams et al. in review) (Fig. 1C). Animals were alive until the moment they were processed. Therefore samples are as close to the *in vivo* state as one can get (as opposed to the re-differentiated and fixed cells that other labs have used), which makes profiling results more biologically accurate. RNA from two replicates (8,000 and 11,000 EVNs) was purified and amplified for RNAseq (Methods). RNAseq libraries from the amplification products of EVN cell populations and whole worm lysate control samples were sequenced. Total reads were downsampled in silico to a depth of $4.2–6.7 \times 10^6$ reads per library and tested for

expression and differential expression (Supplemental Fig. 1C, D). DEseq software identified 9,922 genes expressed in EVNs, 14,455 genes in whole worm (Table S2), and 335 genes significantly overrepresented two to 11-fold in EVNs (Fig. 1D, Table S1). Cluster analysis of the total 14,455 genes expressed between sorted EVNs and whole worm showed high intragroup homogeneity (Supplemental Fig. 1A). Principle Components Analysis showed clear separation between sorted EVNs and whole worm lysates (Supplemental Fig. 1B). Volcano plot of the differential RNAseq transcriptome analysis showed close linearization of log2 fold change and the log 10 p value, indicating most data points were consistently represented in both replicates (Fig. 1D).

To uncover the functions of the 335 overrepresented genes, we used gene ontology (GO) term annotation analysis. Among the GO terms in the 335 overrepresented genes were neuropeptide signaling, ciliogenesis, neuron projection, ion channel activity, and synaptic transmission, which are consistent with the neuronal and ciliated characters of the EVNs (Table S3). Over half of the overrepresented genes including 70 in the top 100 have no assigned name or described RNAi phenotype, likely because global RNAi screens do not examine adult male phenotypes. Thus, many of these EVN signature genes may function specifically in the adult male. 61 of 335 signature genes were expressed in EVNs as demonstrated by published GFP expression analysis or described herein (Table S1). The EVN restricted genes *klp-6, lov-1*, *pkd-2*, *cil-7* and the five *cwp* genes(Barr and Sternberg 1999, Portman and Emmons 2004, Peden and Barr 2005, Miller and Portman 2010, Maguire, Silva et al. 2015) were up-regulated 5.8-fold or higher. We identified 20 new genes that were exclusively expressed in all EVNs, similar to the EVN release regulators *klp-*

6 and *cil-7* (Fig. 2A); in all male-specific EVNs, similar to *pkd-2* and *lov-1* (Fig. 2B); or in a subset of the EVNs (Fig. 2C, D), including Y70G10A.2 that was expressed in a single EVN (Fig. 2D). Combined, these results indicate that our RNAseq dataset is reliable and highly enriched for EVN genes, and demonstrate the sensitivity of our profiling method.

TNF receptor associated factors (TRAFs) act as signaling adaptors for the TNFR superfamily, Toll like receptor and many other receptors(Xie 2013). We found that the *C. elegans* TRAF homologues *trf-1* and *trf-2* were overrepresented 8.6 fold in EVNs (Table S1) and exclusively expressed in the male-specific EVNs (Fig. 3A-D). TRF-1 is a canonical TRAF, with a RING domain, a TRAF zinc finger domain, and a MATH (meprin-associated TRAF homology) domain, while *trf-2* (Y110A7.2) encodes a MATH domain only protein (Fig. 3A, C). GFP-tagged TRF-1 and TRF-2 localized through out male-specific EVNs including cilia, dendrites, cell bodies, and axons, but were excluded from nuclei (Fig. 3B, D). We did not observe TRF-1::GFP or TRF-2::GFP released in the extracellular environment, indicating that, unlike the polycystins LOV-1 and PKD-2, TRF-1 and TRF-2 are not EV-cargo.

trf-1 and *trf-2* were required for all polycystin-mediated male behaviors: sex drive, response and vulva location (Fig. 3E-F, 4G). Neither *trf-1* nor *trf-2* was required for PKD-2::GFP localization to cilia or EVs, or for ciliogenesis in EVNs. The *trf-2; trf-1* double mutant was not more response or location of vulva (Lov) defective than the *trf-1* single mutant, indicating that *trf-1* and *trf-2* act non-redundantly. The *lov-1; pkd-2; trf-1* triple mutant and *lov-1; trf-1* and *trf-1; pkd-2* doubles were indistinguishable from each other, indicating that polycystins and TRAFs act in the same genetic pathway (Fig. 3F). *tol-1* (the sole Toll-like receptor in *C. elegans*) and *ikb-1* (inhibitor of kappa beta homologue) were not overrepresented in EVNs and were not required for response or vulva location (Fig. 3E).

These data indicate that the *C. elegans* TRAFs but not other components of the Toll pathway act in polycystin-mediated sensory signaling.

In addition to the TRAFs, a significant number of EVN signature genes were implicated in cellular stress or innate immune responses (Table S4). The stress-activated p38 MAPK homologue *pmk-1* was overrepresented in EVNs. *pmk-1* mutant males were defective in EV biogenesis and release (Fig. 4A-E). 100% of wild-type late L4 larval and adult males released PKD-2::GFP-containing EVs from the ciliated sensory neurons in the head (CEMs) and tail (RnBs and HOB) (Fig. 4A-B). In contrast, less than 10% of L4 *pmk-1* and 50% of adult *pmk-1* mutant males released PKD-2::GFP labeled EVs (Fig. 4B). Ciliary localization of PKD-2::GFP appeared similar between wild-type and *pmk-1* males (Fig. 4A). We conclude that *pmk-1* regulates release of PKD-2::GFP-containing EVs but not ciliary localization of PKD-2::GFP.

To examine *pmk-1* ciliary and EV ultrastructure, we used serial thin cut transmission electron microscopy. In the wild-type cephalic sensillum, EVs are found in the lumen formed by glial-like support cells and surrounding the CEM and CEP cilia(Wang, Silva et al. 2014) (Fig. 4C-D). In the *pmk-1* cephalic sensillum, EVs were largely absent from the lumen and CEM cilia had fewer doublets than the expected nine (Fig. 4C). The quantity of lumen EVs in *pmk-1* mutant males was significantly reduced, indicating an EV biogenesis defect (Fig. 4D-E). *pmk-1* mutant males were also response and Lov defective but displayed normal sex drive (Fig. 4F). Similarly, the EV release regulators *klp-6* and *cil-7* are required for response and vulva location behaviors but not sex drive(Maguire, Silva et al. 2015). For the EVN-specific genes regulating mating behaviors, response and vulva location depended on EV biogenesis or cilia-EV interactions, while sex drive was independent.

These results also suggest that polycystin-mediated behaviors involve different signaling networks (Fig 4G).

In the innate immune response *pmk-1* is the most downstream component in a MAP kinase cascade pathway(Ewbank 2006). However, expression of only *pmk-1* but not the upstream kinase cascade genes *tir-1, nsy-1* and *sek-1* was overrepresented in EVNs. We examined *tir-1, nsy-1* and *sek-1* mutant males for mating behaviors and release of PKD-2::GFP containing-EVs and observed no defects (Table S4), indicating that *pmk-1* acts via an unknown EV biogenesis pathway. In cultured mammalian cells, p38 MAPK is implicated in the production of EVs from macrophages after exposure to tobacco smoke, from aortic endothelial cells induced by TNF-a, and from glial cells (Bianco, Perrotta et al. 2009, Curtis, Wilkinson et al. 2009, Li, Liu et al. 2013). We conclude that *pmk-1* is a conserved regulator of EV biogenesis that acts independent of the innate immune MAPK cascade. These data also reveal the potential of EVN signature gene dataset to uncover new pathways in EV biology.

Our EVN-profile identified many transmembrane (TM) proteins (Table S1 with annotation of signal peptide + TM domains containing proteins) and several channels (Fig. 2E, Table S1), including two acid sensing/amiloride sensitive ion channels (ASICs). *asic-2* and *egas-1,* are expressed in the shared IL2 neurons (Fig.2C). Neither *asic-2* nor *egas-1* was required for remodeling of IL2 neurons in the reproductively-arrested dauer state(Schroeder, Androwski et al. 2013) or for male mating behaviors (Table S5). ASIC-2::GFP localized to IL2 cilia and EVs secreted from IL2 neurons in reproductively growing animals. Hence, our EVN-profile also identified EV cargo, including the known (LOV-1,

PKD-2, CWP-1, and CIL-7)(Wang, Silva et al. 2014, Maguire, Silva et al. 2015) and new cargoes.

GFP-tagged F14D7.11 was also EV cargo, found in cilia and EVs released from all 27 EVNs (Fig. 2A), similar to the EV biogenesis regulator CIL-7 (Maguire, Silva et al. 2015). F14D7.11 resembles an antimicrobial peptide (AMP) and contains a CYSTM (cysteine rich transmembrane) module proposed to play a role in stress tolerance(Venancio and Aravind 2010). Our EVN-profile identified 13 AMPs, with F14D7.11 being the most highly overrepresented (Tables S1 and S4). Intriguingly, human urinary exosomes contain AMPs that have bactericidal activity(Hiemstra, Charles et al. 2014). An intriguing possibility is that EVs possess antimicrobial activity and play protective roles during the mating process. Alternatively, *C. elegans* could release EVs that have deleterious effects on other organisms. Consistent with this idea, unidentified *C. elegans* male secretions reduce hermaphrodite lifespan(Maures, Booth et al. 2014) and parasitic nematodes use EVs to transfer small RNAs to mammalian cells and modulate host innate immunity(Buck, Coakley et al. 2014).

Several EVN signature genes encode lectins or adhesion molecules (Fig. 2E, Table S4). In our dataset, 13 *clec* genes were significantly overrepresented and do not overlap with those upregulated upon infection or expressed at higher levels in the bodies of adult males compared to hermaphrodites (Tables S1, S4). To determine whether these lectins or adhesion molecules play a role in polycystin-mediated behaviors, we examined their expression patterns (Fig. 2A-D) and functions in sex drive, response, and vulva location for available mutants (Fig. 3C, 4G). *clec-164* was specifically expressed in the four CEMs and required for male sex drive (Fig. 2C, 3C). The single transmembrane (TM) protein F28A12.3

resembles an adhesion receptor with a cysteine-rich extracellular domain and was expressed in all 27 EVNs (Fig. 2A, 2E), yet mutant males displayed normal mating behaviors (Table S5). F25D7.5 and its paralog Y70G10A.2 are predicted to encode a long extracellular region containing a C-type lectin fold and EGF domain, followed by five TM spanning domains (Fig. 2E). F25D7.5 was expressed in 21 male-specific EVNs (Fig. 2B) and may negatively regulate sex drive, as its mutation suppressed *pkd-2* sex drive but not response or Lov defects (Fig. 3E, Table S5). Y70G10A.2 was expressed exclusively in the HOB EVN (Fig. 2D) but not required for HOB-mediated vulva location behavior (Table S5). F26C11.3 and F59A6.3 encode secreted mucin-like serine-threonine rich proteins that contain a complement control protein (CCP) domain at their C-termini. F26C11.3 was expressed in 21 male-specific EVNs (Fig. 2B) while F59A6.3 was only expressed in the CEMs (Fig. 2C). F59A6.3 and F26C11.3 single mutants displayed decreased sex drive (Fig. 3E); the latter were also Lov (Table S5). F31F7.2, a predicted two TM protein with a von Willebrand factor type A domain, was expressed in all 27 EVNs (Fig. 2A) but required only for vulva location and not sex drive or response behavior (Table S5).

C. elegans EVNs, EVs, and EVN-expressed genes serve male reproductive signaling functions (Fig. 4G). The polycystin-expressing, male specific EVNs are required for sex drive, response, and vulva location. Some EVN-expressed genes (the TRAFs *trf-1* and *trf-2*) were required for all polycystin-mediated behaviors, while other played more specific behavioral functions (Fig. 4G). For example, CEM-expressed *clec-164* was required only for sex drive and pan EVN-expressed F31F7.2 only for vulva location. The p38 MAPK *pmk-1* was required for response and vulva location behavior, but not sex drive. Intriguingly, the known regulators of EV biogenesis: *pmk-1*, *cil-7*, and *klp-6* display this property(Maguire,

Silva et al. 2015), suggesting that luminal EVs may be required for the integrity of the male sensory organs mediating these behavioral functions. EVs play diabolical roles in the spread of toxic cargo in cancer, infectious diseases, and neurodegenerative disorders(S, Mager et al. 2013, Vader, Breakefield et al. 2014). We speculate that EVs may play a similar role ADPKD and other ciliopathies, We conclude that *C. elegans* polycystin-mediated signaling pathways are genetically separable, and that our EVN-expressed gene list identified new components and pathways regulating mating behavior as well as EV biogenesis, EV cargo sorting, and EV signaling.

Supplemental Information

Supplemental information includes supplemental document (legends, experimental procedure, strain list, and references), one supplemental figure, five supplemental tables (two of which are data sets).

Acknowledgements

We thank WormBase; the National Bioresource Project for strains; Christina DeCoste for assistance with FACS; Ken Nguyen, Leslie Gunther and Geoff Perumal for help in HPF-FS, embedding and serial section protocols performed at Einstein, and William Rice and Ed Eng at the New York Structural Biology Center (NYSBC), for help in electron tomography; Lillian Hunter for assistance with strain construction; members of the Barr and Murphy labs and Rutgers *C. elegans* community for discussion and insight, more than we ever learned in school; Dr. Emily Troemel for critical reading of the manuscript; Rutgers Genetics Department for sabbatical time and critical bridge funding. Use of the NYSBC facilities was supported by the Albert Einstein College of Medicine. Some strains were provided by the *Caenorhabditis* Genetics Center **(**CGC), which is funded by NIH Office of Research Infrastructure Programs (P40 OD010440). This work was funded by NIH DK059418 and DK074746 (to M.M.B.), NIH OD 010943 (to D.H.H.), and the Medical Research Council (to M.G.-N. and J.H.).

Figures

Figure 1

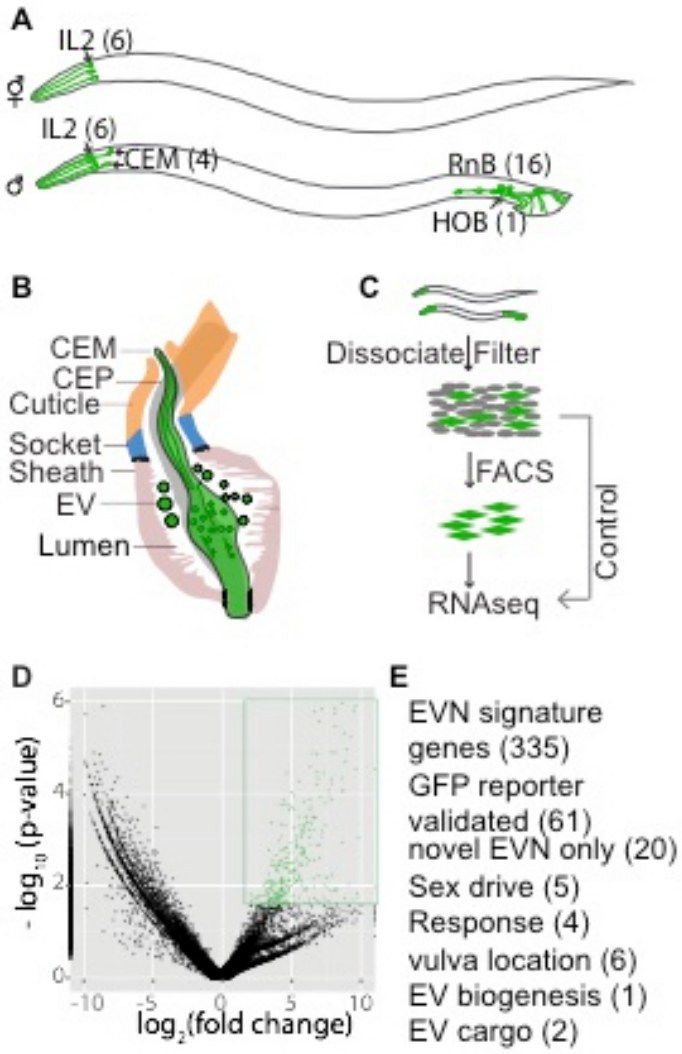

Figure 1 Cell-type RNAseq to define the EVN transcriptome.

(A) The ciliated EVNs, six in the hermaphrodite (top) and 27 in male (bottom). (B) The male cephalic sensillum. Glial sheath and socket cells form a continuous lumen surrounding the CEM neuronal cilium, which is exposed to the environment directly through a cuticular

opening. The lumen is shared by CEM and CEP neurons. EVs are observed in the lumen. (C) Schematic illustration of the differential RNAseq experiment. EVNs were FACS purified from dissociated and filtered cells isolated from synchronized *klp-6p*::GFP expressing young adult males and hermaphrodites, followed by mRNA extraction, library construction, and RNAseq. Refer to Supplemental Figure 1 for heat map, principal component analysis, and downsampling *in silico*. (D) Volcano plot showing 335 genes differentially overrepresented in sorted EVNs (colored and boxed in green) compared to whole worms at a false discovery rate of 10%. (E) 335 EVN gene signature genes were validated by GFP expression pattern and functional analysis (for available mutants). The number of genes for each category is listed in parentheses. Refer to Supplemental Tables S1 and S2 for full list of 335 signature genes and original DEseq data, respectively. See Supplemental Table S3 for GO Analysis of EVN overrepresented genes.

Figure 2

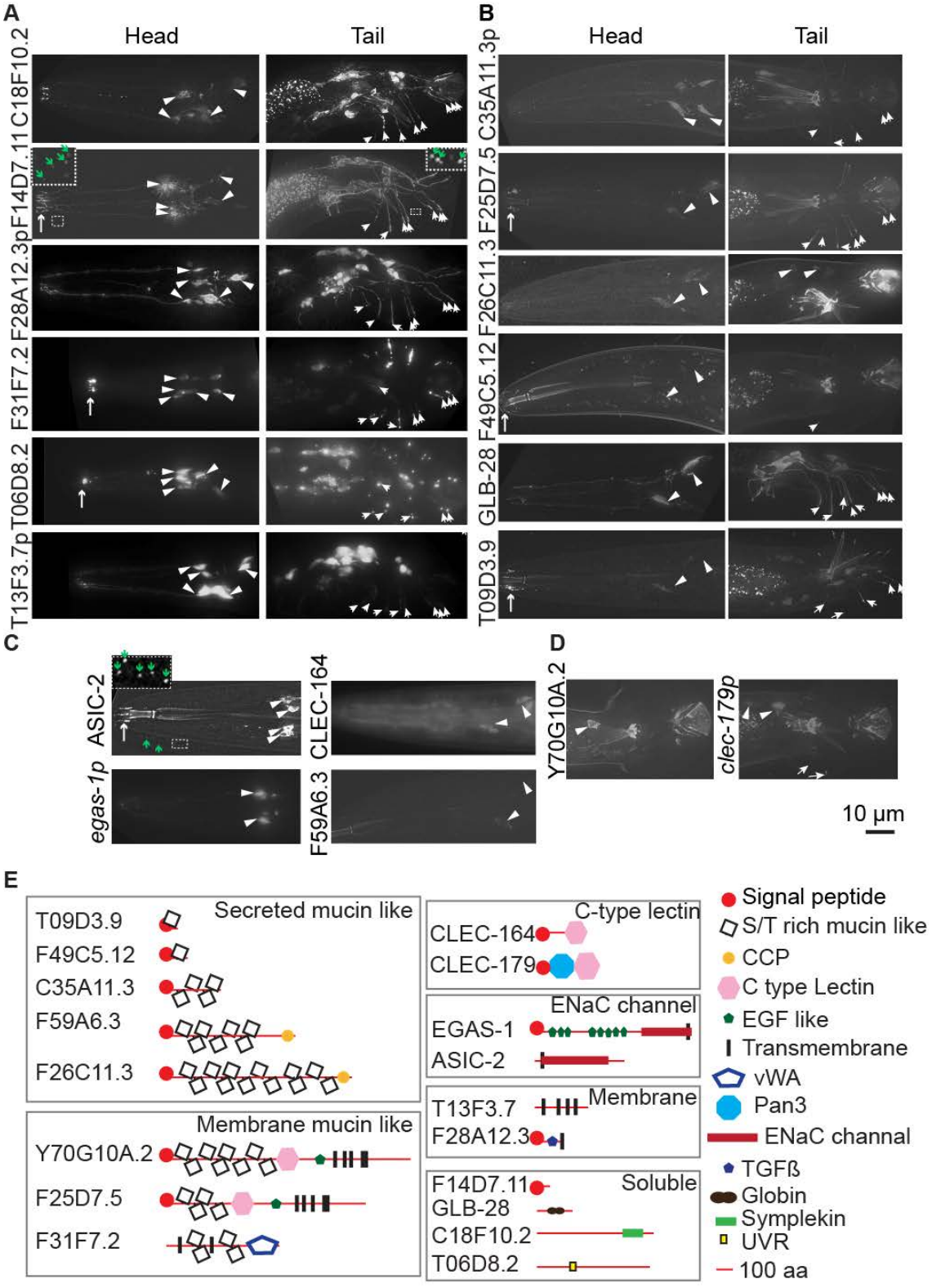
A
Head
Tail
C18F10.2
D7.11
F14D7.3p
F28A12.3p
F31F7.2
T06D8.2
T13F3.7p
B
Head
Tail
C35A11.3p
F25D7.5
F26C11.3
F49C5.12
GLB-28
T09D3.9
C
ASIC-2
egas-1p
CLEC-164
F59A6.3
D
Y70G10A.2
clec-179p
10 µm
E
Secreted mucin like
T09D3.9
F49C5.12
C35A11.3
F59A6.3
F26C11.3
Membrane mucin like
Y70G10A.2
F25D7.5
F31F7.2
C-type lectin
CLEC-164
CLEC-179
ENaC channel
EGAS-1
ASIC-2
Membrane
T13F3.7
F28A12.3
Soluble
F14D7.11
GLB-28
C18F10.2
T06D8.2
Signal peptide
S/T rich mucin like
CCP
C type Lectin
EGF like
Transmembrane
vWA
Pan3
ENaC channal
TGFß
Globin
Symplekin
UVR
100 aa

Figure 2 EVN signature genes were expressed in all 27 EVNs

(A), the 21 polycystin-expressing EVNs (B), or a subset thereof (C, D). (A) Head IL2 and CEM (left) and tail HOB and RnB (right) images of GFP reporters that were expressed exclusively in all 27 EVNs. (B) A subset of EVN signature genes showed expression in only the male-specific head CEM (left) and tail HOB and RnB (right) neurons. In a and b, arrowheads point to cell bodies in the head and to ray dendrites in the tail. Scale bar, 10 µm. (C) *asic-2* was expressed in the six IL2 neurons, *egas-1* in four IL2 quadrant (IL2Q) neurons, *clec-164* and F59A6.3 in CEM neurons. (D) Y70G10A.2 was expressed only in the HOB EVN and *clec-179* in HOB and a few ray EVNs. In all panels, translational GFP reporters are shown by gene name or open reading frame number, transcriptional (promoter) GFP reporters are shown by gene name or ORF followed by *p*. For translational reporters, arrows point to ciliary localization. In A and C, dashed line boxes were 4X scaled with enhanced contrast and brightness to visualize EVs (green arrows). F14D7.11::GFP localized in cilia and secreted EVs from all 27 EVNs and ASIC-2::GFP localized in IL2 cilia and secreted EVs. (E) Domain analysis of validated genes. Signal peptide sequences were predicted by SignalP 4.1 Server (http://www.cbs.dtu.dk/services/SignalP/). Mucin-domain containing proteins are predicted to be secreted and extensively O-glycosylated in the Serine (S) or Threonine (T) rich domain. Transmembrane domains were predicted by the TM Pred server (http://www.ch.embnet.org/software/TMPRED_form.html). CCP, C-type lectin (CLEC), Pan3, TGFβ, EGF-like, DEG/ENaC channel, vWA (Von Willebrand factor type A), globin, and UVR domains were predicted by Wormbase. Refer to Supplemental Table S4 listing EVN

signature genes with predicted or demonstrated function in stress response or innate immunity.

Figure 3

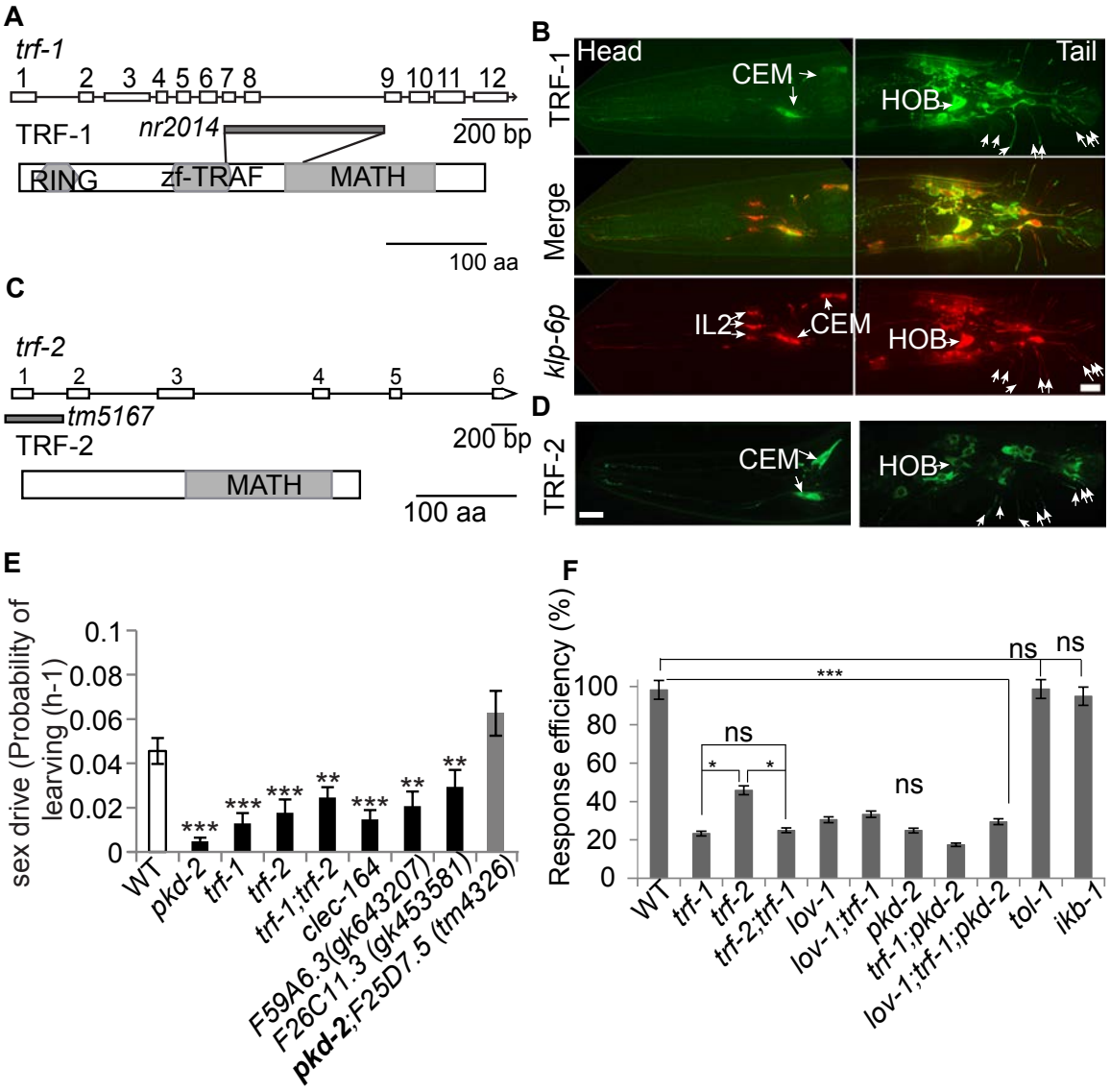

Figure 3 *trf-1* and *trf-2* coexpressed in male-specific EVNs and acted in the polycystin-signaling pathways.

(A, C) Schematic of *trf-1* and *trf-2* genomic and protein structure, with molecular lesions indicated in genomic structure. (A) The *trf-1* locus encodes all common domains shared by mammalian TRAFs: a RING finger domain that may act as an E3 ubiquitin-ligase; a TRAF zinc finger and MATH domain that may mediate protein-protein interaction or

oligomerization. The *trf-1 (nr2041)* mutation deletes part of the zf-TRAF domain and part of the MATH domain and may affect mRNA splicing. (C) TRF-2 has only a MATH domain. The *trf-2(tm5167)* deletion removes upstream of first exon to the end of the first intron. (B) *trf-1* was co-expressed with *klp-6* in male-specific, but not IL2, EVNs. (D) TRF-2::GFP was expressed and localized in the same pattern as TRF-1::GFP. (E) TRAF, lectins, and adhesion molecules were required for male sex drive. The *tm4326* deletion allele of F25D7.5 suppresses the sex drive defect of *pkd-2* mutant males (in bold). The probability of the male leaving the food lawn per hour PL(h-1) is indicated on the Y-axis, the male's genotype on the X-axis. Data was analyzed by Kruskal-Wallis test. * $p<0.05$, ** $p<0.01$, *** $p<0.001$. (F) Response Efficiency (RE) of *lov-1, pkd-2, trf-1, trf-2* and Toll pathway genes *tol-1* and *ikb-1*. Data was analyzed with Fisher's exact test, Bonferroni-Holm corrected. * $p<0.05$, *** $p<0.001$. *ns* not significant. The minimum number (n) of individual males analyzed per genotype was 37 for sex drive and 59 for response behavior.

Figure 4

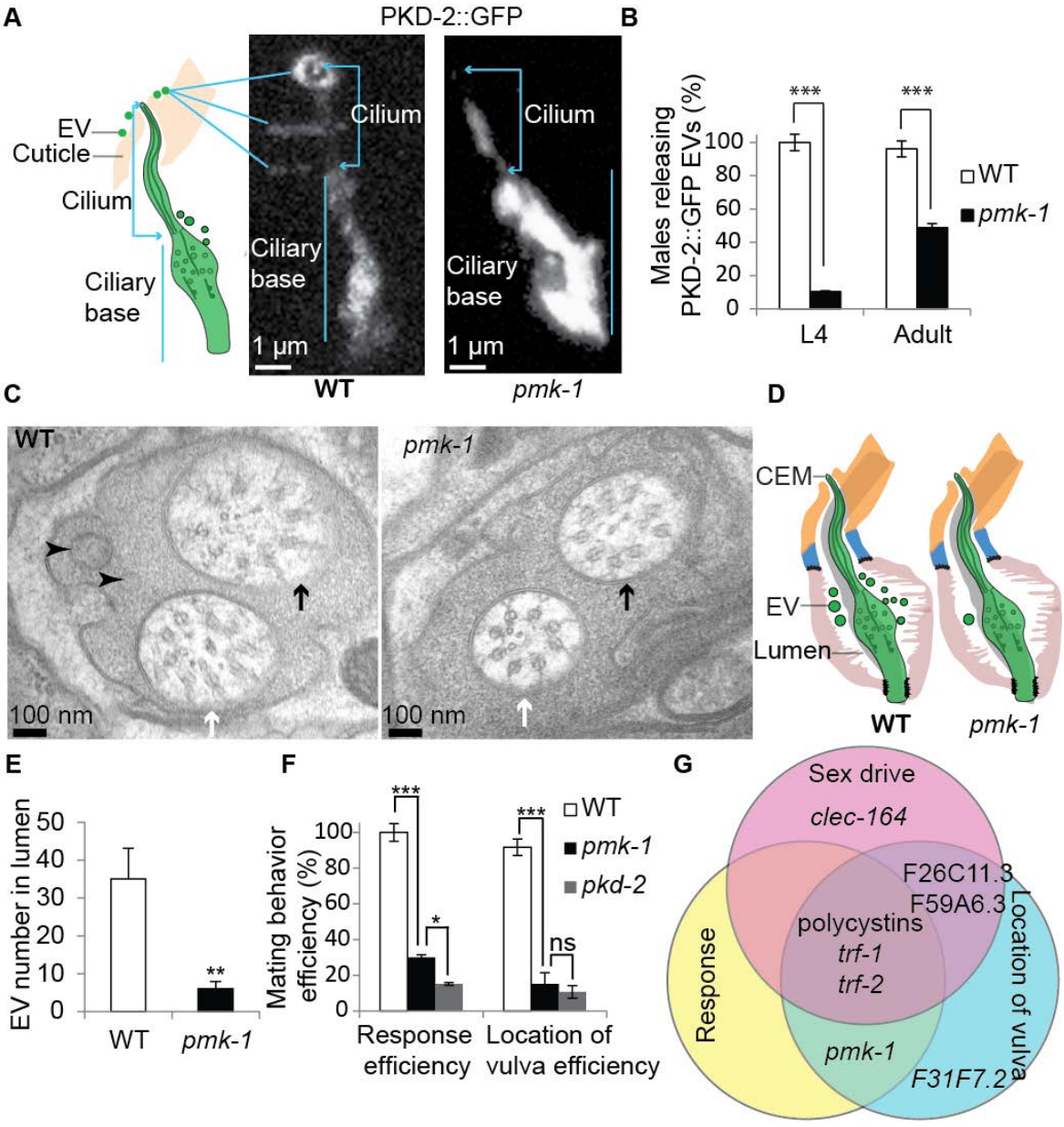

Figure 4 The *p38* MAPK *pmk-1* was required for EV biogenesis and polycystin-mediated response and vulva location behaviors.

(A) PKD-2::GFP CEM ciiary localization in wild-type and *pmk-1* males. Cartoon shows the CEM cilium protruding from the cuticular pore and EVs surrounding the cuticle. In wild type, PKD-2::GFP localized to the ciliary base, cilium, and EVs released outsjde the male's

nose. Note in wild type, EVs accumulated and surrounded the ciliary pore and cuticle. In *pmk-1* males PKD-2::GFP localized normally to the ciliary base and cilium, but was absent from EVs. To show the full length of PKD-2::GFP labeled cilia and the EVs, images of wild type and *pmk-1* males were taken with different exposure times, and adjusted with different brightness and contrast. The original images were enlarged six times by the Photoshop CS5 image transformation tool. Scale bar = 1 μm (B) *pmk-1* mutant males were defective in PKD-2::GFP labeled EV release in both L4 (n=20 for wild-type, n=29 for *pmk-1*) and adult stage (n=52 for wild-type and n=43 for *pmk-1*). Data was analyzed with Fisher's exact test, Bonferroni-Holm corrected; *** $p<0.001$. (C, D) TEM and cartoon of wild-type and *pmk-1* cephalic sensillum at the level of the ciliary transition zone. In wild type, EVs were present in the extracellular lumen. In *pmk-1* males, EVs numbers are significantly reduced in the cephalic lumen. In *pmk-1* males, the CEM axoneme contained eight rather then nine doublet microtubules of wild-type males. Black arrowheads = EVs, white arrows = CEM transition zone, black arrows = CEP transition zone. Scale bar = 100nm. (E) Bar graph of number of EVs (mean $\pm$ SEM) in wild-type and *pmk-1*. Mann-Whitney test was used for statistical analysis; n=7 cephalic sensillae for wild type from two worms, n=4 cephalic sensillae for *pmk-1* from one worm. ** $p=0.01$. (F) *pmk-1* mutant males are response and Lov defective. Statistical analysis was done by Fisher's exact test, Bonferroni-Holm corrected for response efficiency, RE (n=184 for wild type, 60 for *pmk-1* and 264 for *pkd-2*), and one-way ANOVA for location of vulva efficiency, LE (n=20 for wild type, 20 for *pmk-1* and 18 for *pkd-2).* * $p<0.05$, *** $p<0.001$. ns = not significant. (F) The *C. elegans* polycystins function in a multi-layered signaling network. Venn diagram showing polycystin-mediated mating behaviors are genetically separable. *lov-1*, *pkd-2*, and the

TRAFs played a central role in sex drive, response, and vulva location while other genes act in specific behavioral pathways. Refer to Supplemental Table S5 for RE and LE of mutants corresponding to new EVN signature genes and pathways.

References

1. Wood, C.R., and Rosenbaum, J.L. (2015). Ciliary ectosomes: transmissions from the cell's antenna. Trends Cell Biol *25*, 276-285.

2. O'Hagan, R., Wang, J., and Barr, M.M. (2014). Mating behavior, male sensory cilia, and polycystins in Caenorhabditis elegans. Semin Cell Dev Biol *33*, 25-33.

3. Hogan, M.C., Manganelli, L., Woollard, J.R., Masyuk, A.I., Masyuk, T.V., Tammachote, R., Huang, B.Q., Leontovich, A.A., Beito, T.G., Madden, B.J., Charlesworth, M.C., Torres, V.E., LaRusso, N.F., Harris, P.C., and Ward, C.J. (2009). Characterization of PKD protein-positive exosome-like vesicles. J Am Soc Nephrol *20*, 278-288.

4. Wood, C.R., Huang, K., Diener, D.R., and Rosenbaum, J.L. (2013). The cilium secretes bioactive ectosomes. Curr Biol *23*, 906-911.

5. Pampliega, O., Orhon, I., Patel, B., Sridhar, S., Diaz-Carretero, A., Beau, I., Codogno, P., Satir, B.H., Satir, P., and Cuervo, A.M. (2013). Functional interaction between autophagy and ciliogenesis. Nature *502*, 194-200.

6. Wang, J., Silva, M., Haas, L.A., Morsci, N.S., Nguyen, K.C., Hall, D.H., and Barr, M.M. (2014). C. elegans Ciliated Sensory Neurons Release Extracellular Vesicles that Function in Animal Communication. Curr Biol *24*, 519-525.

7. Bakeberg, J.L., Tammachote, R., Woollard, J.R., Hogan, M.C., Tuan, H.F., Li, M., van Deursen, J.M., Wu, Y., Huang, B.Q., Torres, V.E., Harris, P.C., and Ward, C.J. (2011). Epitope-tagged Pkhd1 tracks the processing, secretion, and localization of fibrocystin. J Am Soc Nephrol *22*, 2266-2277.

8. Tanaka, Y., Okada, Y., and Hirokawa, N. (2005). FGF-induced vesicular release of Sonic hedgehog and retinoic acid in leftward nodal flow is critical for left-right determination. Nature *435*, 172-177.

9. Raposo, G., and Stoorvogel, W. (2013). Extracellular vesicles: exosomes, microvesicles, and friends. J Cell Biol *200*, 373-383.

10. EL Andaloussi, S., Mager, I., Breakefield, X.O., and Wood, M.J. (2013). Extracellular vesicles: biology and emerging therapeutic opportunities. Nat Rev Drug Discov *12*, 347-357.

11. Yoder, B.K., Hou, X., and Guay-Woodford, L.M. (2002). The polycystic kidney disease proteins, polycystin-1, polycystin-2, polaris, and cystin, are co-localized in renal cilia. J Am Soc Nephrol *13*, 2508-2516.

12. Pazour, G.J., San Agustin, J.T., Follit, J.A., Rosenbaum, J.L., and Witman, G.B. (2002). Polycystin-2 localizes to kidney cilia and the ciliary level is elevated in orpk mice with polycystic kidney disease. Curr Biol *12*, R378-R380.

13. Pisitkun, T., Shen, R.F., and Knepper, M.A. (2004). Identification and proteomic profiling of exosomes in human urine. Proc Natl Acad Sci U S A *101*, 13368-13373.

14. Cai, Y., Fedeles, S.V., Dong, K., Anyatonwu, G., Onoe, T., Mitobe, M., Gao, J.D., Okuhara, D., Tian, X., Gallagher, A.R., Tang, Z., Xie, X., Lalioti, M.D., Lee, A.H., Ehrlich, B.E., and Somlo, S. (2014). Altered trafficking and stability of polycystins underlie polycystic kidney disease. J Clin Invest. *124*, 5129-44.

15. Barr, M.M., DeModena, J., Braun, D., Nguyen, C.Q., Hall, D.H., and Sternberg, P.W. (2001). The Caenorhabditis elegans autosomal dominant polycystic kidney disease gene homologs lov-1 and pkd-2 act in the same pathway. Curr Biol *11*, 1341-1346.

16. Barr, M.M., and Sternberg, P.W. (1999). A polycystic kidney-disease gene homologue required for male mating behaviour in C. elegans. Nature *401*, 386-389.

17. Barrios, A., Nurrish, S., and Emmons, S.W. (2008). Sensory Regulation of C. elegans Male Mate-Searching Behavior. *18*, 1865-1871.

18. Portman, D.S., and Emmons, S.W. (2004). Identification of C. elegans sensory ray genes using whole-genome expression profiling. Dev Biol *270*, 499-512.

19. Miller, R.M., and Portman, D.S. (2010). A latent capacity of the C. elegans polycystins to disrupt sensory transduction is repressed by the single-pass ciliary membrane protein CWP-5. Dis Model Mech *3*, 441-450.

20. Maguire, J.E., Silva, M., Nguyen, K.C., Hellen, E., Kern, A.D., Hall, D.H., and Barr, M.M. (2015). Myristoylated CIL-7 Regulates Ciliary Extracellular Vesicle Biogenesis. Mol Biol Cell.

21. Hurd, D.D., Miller, R.M., Nunez, L., and Portman, D.S. (2010). Specific alpha- and beta-tubulin isotypes optimize the functions of sensory Cilia in Caenorhabditis elegans. Genetics *185*, 883-896.

22. Kaletsky, R., Williams, A.B., Arey, R., Lakhina, V., Landis, J.L., and Murphy, C.T. (in review). Transcriptional profiling of isolated adult C. elegans neurons identifies the neuronal IIS/FOXO transcriptome and a new regulator of axon regeneration

23. Peden, E.M., and Barr, M.M. (2005). The KLP-6 kinesin is required for male mating behaviors and polycystin localization in Caenorhabditis elegans. Curr Biol *15*, 394-404.

24. Xie, P. (2013). TRAF molecules in cell signaling and in human diseases. J Mol Signal *8*, 7.

25. Ewbank, J.J. (2006). Signaling in the immune response. WormBook, 1-12.

26. Li, C.J., Liu, Y., Chen, Y., Yu, D., Williams, K.J., and Liu, M.L. (2013). Novel proteolytic microvesicles released from human macrophages after exposure to tobacco smoke. Am J Pathol *182*, 1552-1562.

27. Curtis, A.M., Wilkinson, P.F., Gui, M., Gales, T.L., Hu, E., and Edelberg, J.M. (2009). p38 mitogen-activated protein kinase targets the production of proinflammatory endothelial microparticles. J Thromb Haemost *7*, 701-709.

28. Bianco, F., Perrotta, C., Novellino, L., Francolini, M., Riganti, L., Menna, E., Saglietti, L., Schuchman, E.H., Furlan, R., Clementi, E., Matteoli, M., and Verderio, C. (2009). Acid sphingomyelinase activity triggers microparticle release from glial cells. EMBO J *28*, 1043-1054.

29. Schroeder, N.E., Androwski, R.J., Rashid, A., Lee, H., Lee, J., and Barr, M.M. (2013). Dauer-Specific Dendrite Arborization in C. elegans Is Regulated by KPC-1/Furin. Curr Biol *23*, 1527-1535.

30. Venancio, T.M., and Aravind, L. (2010). CYSTM, a novel cysteine-rich transmembrane module with a role in stress tolerance across eukaryotes. Bioinformatics *26*, 149-152.

31. Hiemstra, T.F., Charles, P.D., Gracia, T., Hester, S.S., Gatto, L., Al-Lamki, R., Floto, R.A., Su, Y., Skepper, J.N., Lilley, K.S., and Karet Frankl, F.E. (2014). Human Urinary Exosomes as Innate Immune Effectors. J Am Soc Nephrol. *25*, 2017-27.

32. Maures, T.J., Booth, L.N., Benayoun, B.A., Izrayelit, Y., Schroeder, F.C., and Brunet, A. (2014). Males shorten the life span of C. elegans hermaphrodites via secreted compounds. Science *343*, 541-544.

33. Buck, A.H., Coakley, G., Simbari, F., McSorley, H.J., Quintana, J.F., Le Bihan, T., Kumar, S., Abreu-Goodger, C., Lear, M., Harcus, Y., Ceroni, A., Babayan, S.A., Blaxter, M., Ivens, A., and Maizels, R.M. (2014). Exosomes secreted by nematode parasites transfer small RNAs to mammalian cells and modulate innate immunity. Nat Commun *5*, 5488.

34. Vader, P., Breakefield, X.O., and Wood, M.J. (2014). Extracellular vesicles: emerging targets for cancer therapy. Trends Mol Med. *20*,385-93

Chapter 6

The Glutamylase TTLL-11 Regulates Ciliary Trafficking, Microtubule Structural Specialization, and Extracellular Vesicle Release in *C. elegans* Sensory Neurons

Modified from Robert O'Hagan, Malan Silva *et al.,* in preparation

Forward

I previously discovered that, in *ccpp-1* mutants, where axonemal microtubules of CEM cilia are hyperglutamylated, distance between the ciliary membrane and microtubules is increased while axoneme ultrastructure and ciliary morphology was superficially unchanged (Chapter 4 Figure 3). In *ccpp-1* mutants, adult amphid cilia degenerate while CEM cilia were relatively intact. I found the discrepancy of fates between CEM and amphid cilia fascinating! What were the differences between amphid and CEM microtubules that bestow them these dramatically different fates in *ccpp-1* mutant background? This led me to focus on characterizing the wild type CEM cilia ultrastructure using TEM and electron tomography, where in I discovered the unique CEM axoneme ultrastructure (Chapter 2 Figure 1). In order to develop this finding into a complete story, I was on the hunt for a mutant that disrupted the splayed doublet microtubule ultrastructure. During this time Dr. Robert O'Hagan and Winnie Zhang have been testing *ttll* genes as candidates that could rescue *ccpp-1* amphid dye filing defects due to their reported glutamylase activity *in vitro*. On April 2012, I enthusiastically fixed all these *ttll* single mutant and *ttll* and *ccpp-1*

doublet mutant combinations totaling nine genotype groups. Subsequently, I serial sectioned *ttll-11* which is one of the two *ttll* candidates (*ttll-4* was the other) that consistently suppressed defiling defects *ccpp-1* amphid cilia in Winnie Zhang's dye filling experiments. My TEM studies lead to the discovery that in *ttll-11* mutant background doublet microtubules are ectopically stabilized in both CEM and amphid cilia- alas the type of mutant I have been looking for! Invigorated by the finding, I quickly moved on to identify a gene beyond the immediate PTM landscape that required for splayed doublet microtubule ultrastructure in CEM cilia. Two year later, with a well-timed suggestion from Chris, discovered alpha tubulin *tba-6*.

For the following manuscript, I used a tannic acid based fixative in combination with high-pressure freeze (HPF) in order to better highlight microtubules. I noticed that in the degenerating amphid B-tubules seen in *ccpp-1* mutant background, microtubules were stained non-homogeneously. These animals were fixed without tannic acid. I hypothesized that these observations were due to the change in overall negative change in *ccpp-1* microtubules interfering with how they interact with OsO_4. I serial sectioned and imaged two *ccpp-1; him-5* animals, one *ttll-11*; *him-5* animal, eight *ttll-11; ccpp-1; him-5* animals in order to generate Figure 7. These data provided first direct evidence to support that glutamylation play a role in sculpting B-tubules. In the case of excessive glutamylation in *ccpp-1* mutant background CEM ciliary doublet B-tubules are completely detached from the A-tubules while reduced levels of microtubule glutamylation in *ttll-11* background lead to ectopic stabilization of the B-tubules in doublet configuration. These results parallel my finding in amphid cilia.

In summary, splayed doublets architecture seen in wild type CEM cilia requires a goldilocks state of glutamylation level. This is altered in both *ccpp-1* and *ttll-11* mutant backgrounds. What about the loss of splayed doublets in TBA-6 (Chapter 1)? C-terminal sequence of TBA-6 does not contain glutamate residues that have demonstrated *in vitro* as a requirement for seed glutamate side chain. So perhaps TBA-6 buffer the microtubules against TTLL-11 and CCPP-1 and act as a neutralizer with its long positive C terminal tail. In order to test this hypothesis, I analyzed the CEM microtubule ultrastructure of CEM cilia in *ttll11; tba-6; him-6* background and found it to be similar to that of *ttll-11* CEM cilia. This suggested that at least in terms of microtubule ultrastructure, *ttll-11* is epistatic to *tba-6*. These experiments establish the first known genetic neighborhood for splayed doublet ultrastructure.

Abstract

Ciliary microtubules (MTs) are extensively decorated with post-translational modifications (PTMs). PTMs, such as glutamylation, combined with a diversity of tubulin isotypes are proposed to form a "Tubulin Code" that regulates cytoskeletal functions including ciliary specialization. In *C. elegans*, α-tubulin TBA-6 is required for generating 18 A-tubule and B-tubule singlets from nine A-B doublet MTs in cephalic male (CEM) neuronal cilia while the MT deglutamylase CCPP-1 regulates B-tubule stability.

Here we show that the MT glutamylase TTLL-11 is essential for doublet MTs splaying into A-tubule and B-tubule singlets. A balance of TTLL-11 and CCPP-1 function fine-tunes glutamylation to control velocity of kinesin-2 OSM-3/KIF17 and kinesin-3 KLP-6 without affecting the IFT kinesin-II. TTLL-11 and CCPP-1 are required for the function of male-specific ciliated neurons and regulate environmental release of ciliary extracellular vesicles (EVs). We suggest that MT glutamylation is a common mechanism to specialize ciliary ultrastructure, motor-based transport, and function.

Introduction

Cilia and flagella serve essential sensory and motility functions in development, physiology, and human health, and have a conserved core or "axoneme." The axoneme is composed of MTs that form a ring of nine outer A-B doublets surrounding a variable number of inner singlets (Fliegauf, Benzing et al.). However, cilia and flagella also adopt morphological and functional specializations. For example, the rods and cones of the retina are elaborately shaped cilia (Insinna and Besharse), while sperm cells have simple whip-like flagella that vary in length and axoneme structure (Phillips). The molecular underpinnings of most ciliary specializations are unknown.

Ciliary MTs are marked by PTMs, which combined with a variety of tubulin isotypes might act as a "Tubulin Code" that is "read" by molecular motors and MT-associated proteins (Verhey and Gaertig , Hammond, Cai et al. , Janke and Bulinski , Sirajuddin, Rice et al.) to generate ciliary diversity. Glutamylases of the tubulin-tyrosine ligase-like (TTLL) family add or elongate glutamate side-chains on MTs (van Dijk, Miro et al.) while M14D cytosolic carboxypeptidases (CCPs) remove or shorten glutamate side-chains (Rodriguez de la Vega, Sevilla et al. , Rogowski, van Dijk et al. , Rodriguez de la Vega Otazo, Lorenzo et al. , Yu, Garnham et al.). Hence, a balance of glutamylase and deglutamylase activity by writers and erasers of the Tubulin Code fine-tune tubulin glutamylation (Janke).

CCPP-1, a homolog of the mammalian deglutamylase Ccp1 (O'Hagan, Piasecki et al.), is required in *C. elegans* sensory neuronal cilia to regulate MT stability: in nematodes lacking CCPP-1, B-tubules degenerate in amphid chemosensory cilia, while cephalic male-specific CEM cilia contain fewer MTs (O'Hagan, Piasecki et al.). In CEM cilia, CCPP-1 regulates localization of the ciliary receptor PKD-2 and the kinesin-3 KLP-6, and the

velocity of homodimeric kinesin-2 OSM-3/KIF17 without affecting the anterograde heterotrimeric kinesin-II motor (O'Hagan, Piasecki et al.). These pleiotropic defects are likely to result from MT hyperglutamylation.

Here, we focus on the TTLL-11 glutamylase that opposes CCPP-1 activity in cilia of *C. elegans* male-specific neurons that express PKD-2 (Barr and Sternberg , Barr, DeModena et al.)—specifically, four CEM neurons in the head; the HOB (Hook B-type) neuron in the tail, and 16 RnB (Ray B-type, where n=1-9, excluding ray 6) neurons that innervate the copulatory fan structure of the male tail. We demonstrate that TTLL-11, like CCPP-1, is required for localization of PKD-2. Loss of TTLL-11 suppresses the *ccpp-1* increased ciliary velocity of the kinesin-2 OSM-3, and slows the kinesin-3 KLP-6. Intriguingly, TTLL-11 moves at rates similar to OSM-3, suggesting that TTLL-11 is both cargo and regulator of OSM-3. Neither CCPP-1 nor TTLL-11 affects the heterotrimeric kinesin-II component KAP-1, suggesting that kinesin-II ignores MT glutamylation.

CEM cilia display an ultrastructural specialization in which nine MT doublets splay into A-tubule and B-tubule singlets in middle regions, but remain joined in distal and proximal regions (Silva, Morsci et al. 2017). α-tubulin isotype TBA-6 is essential for B-tubule singlet formation, hence the tubulin code is implicated in generating this specialized cilium (Silva, Morsci et al. 2017). Here we show that TTLL-11 is essential for conversion of doublet MTs to singlets. In *ttll-11* mutants, CEM axonemal doublets fail to splay and remain as doublet MTs throughout the length of the cilium. Conversely, in *ccpp-1* mutants, B-tubule singlets are unstable and are not joined with partner A-tubules in distal segments.

CEM cilia are functionally specialized to shed and release EVs (Wang, Silva et al. , Wang, Kaletsky et al.). We find that CCPP-1 and TTLL-11 are required for environmental release of EVs from ciliated neurons in *C. elegans* males and TTLL-11 itself is an EV cargo. Our results suggest that CCPP-1 and TTLL-11 fine-tune glutamylation to regulate ciliary transport, EVs, and axonemal structure in cilia.

Results

The putative tubulin glutamylase TTLL-11B regulates PKD-2::GFP ciliary localization in EV-releasing neurons

We hypothesized that loss of a glutamylase might suppress defective localization of the ciliary polycystin receptor PKD-2::GFP caused by hyperglutamylation in *ccpp-1* mutants. We tested deletion alleles for each predicted glutamylase encoded in the *C. elegans* genome—TTLL-4, TTLL-5, TTLL-9, TTLL-11, and TTLL-15. (We did not test TTLL-12 because it is not neuronally expressed (www.wormbase.org) and its mammalian ortholog lacks glutamylase activity (Yu, Garnham et al.)). None of these mutations suppressed the *ccpp-1* PKD-2::GFP localization defect (data not shown). However, *ttll-11* mutants displayed defective localization and abundance of PKD-2::GFP (Fig. 1).

ttll-11 encodes a long TTLL-11B and short TTLL-11A isoform (Fig. 2a) (www.wormbase.org , Kimura, Kurabe et al.). Human TTLL11A (amino acids 213 – 742) is approximately 35% identical and 58% similar to *C. elegans* TTLL-11B (amino acids 119 – 642) by BLAST alignment (Altschul, Madden et al.). TTLL-11B contains a putative myristoylation sequence at its N-terminus (Eisenhaber, Eisenhaber et al.). The *ttll-11(tm4059)* deletion is presumably a null allele for both *ttll-11* isoforms, and is predicted to

produce an early stop codon after 90 amino acids in TTLL-11A and 190 amino acids in TTLL-11B (Fig. 2a; (www.wormbase.org)), ablating most of a predicted ATP-grasp_4 domain (Marchler-Bauer, Derbyshire et al. 2015). The *gk482* deletion allele affects the coding region of only TTLL-11B (Fig. 2a; (www.wormbase.org , Kimura, Kurabe et al.)).

Both alleles produced a PKD-2::GFP mislocalization phenotype (Fig. 1). Therefore, at least TTLL-11B is required for normal PKD-2 localization. Hereafter, unless the *ttll-11b(gk482)* allele is specified, reference to mutation of *ttll-11* indicates the *tm4059* allele, which affects both isoforms.

GFP driven by a *ttll-11b* promoter was observed in the IL2 ciliated sensory neurons in males and hermaphrodites, and in male-specific PKD-2-expressing neurons (CEMs in the head; HOB and RnBs in the tail; Fig. 2b, c). The IL2, CEM, HOB, and RnB neurons shed and release EVs into the environment (Wang, Silva et al.), we call them the EVNs (EV-releasing neurons). Expression of *ttll-11b* in EVNs is consistent with RNAseq profiling (Wang, Kaletsky et al.).

GFP driven by a *ttll-11a* promoter was not expressed in the EVNs, but was visible in a distinct set of ciliated sensory neurons including the IL1s, OLQs, CEPs, amphids, and phasmids, and in the male tail, HOA and the RnAs (Ray A-type neurons) but not the HOB and RnB neurons (Fig. 2d-e).

PKD-2 and the male-specific EVNs mediate male mating behaviors in *C. elegans* (Liu and Sternberg , Barr and Sternberg). *ttll-11* males were impaired in locating the hermaphrodite vulva during mating behavior. This Lov (location of vulva defective) phenotype suggests that *ttll-11* is required for the function of male-specific neurons (Supplementary Fig. 1).

TTLL-11 is essential for MT glutamylation in EVNs

To determine if *ttll-11* mutations reduced glutamylation, we stained fixed animals with the monoclonal antibody GT335, which binds the branch point of glutamylate side-chains on tubulin C-terminal tails (O'Hagan, Piasecki et al.). The *ttll-11* mutation, which affects both TTLL-11B and A, virtually abolished staining in neuronal cilia, including those in male-specific RnB and CEM neurons (Fig. 3). In *ttll-11b(gk482)* mutant males, GT335 still stained cilia, consistent with TTLL-11A-mediated glutamylation of ciliary MTs in amphid, phasmid, CEP, and RnA cilia when *ttll-11b* isoform is mutated (Fig. 3).

Mammalian TTLL11 prefers to elongate glutamate side chains *in vitro* (van Dijk, Miro et al.). Therefore, we also analyzed glutamylation state using a polyclonal polyglutamylation (polyE) antibody (IN105) that recognizes chains of 3 or more glutamates (van Dijk, Rogowski et al. 2007). Loss of both TTLL-11B and TTLL-11A abolished or severely decreased polyE staining of cephalic cilia (CEM and CEP; Supplementary Fig. 2). However, in *ttll-11b(gk482)* mutant males, some ciliary polyE staining remained.

Taken together, our immunofluorescence data and isoform expression patterns (Fig. 2) suggest that TTLL-11B is an EVN-specific glutamylase, and TTLL-11A functions in distinct neurons including amphid, phasmid, CEP, HOA, and RnA neurons.

***ccpp-1* and *ttll-11* coordinate the localization and velocity of specific ciliary kinesins**

In CEM cilia, anterograde IFT is driven predominantly by kinesin-II with minimal modulation from accessory kinesin-2 OSM-3/KIF17 and kinesin-3 KLP-6 (Morsci and Barr). Hyperglutamylation of ciliary MTs in *ccpp-1* mutants causes abnormal accumulation of the

kinesin-3 motor KLP-6 in EVNs (O'Hagan, Piasecki et al.). However, GFP::KLP-6 localization was normal in *ttll-11* males, and loss of TTLL-11 suppressed the GFP::KLP-6 accumulation defect in *ccpp-1* mutants (Fig. 4).

To determine if glutamylation affected KLP-6 velocity, we analyzed motility of GFP::KLP-6 puncta in CEM cilia of young adult males. In wild-type CEM cilia, GFP::KLP-6 moved at 0.80 µm/s (Table 1). In *ccpp-1* CEM cilia, GFP::KLP-6 mean velocity was increased to 0.88 ($p<0.05$ vs. wild type) while in *ttll-1,* GFP::KLP-6 velocity decreased to 0.71 ($p<0.05$ vs. wild type; Table 1). GFP::KLP-6 velocity was similar to wild type in the *ccpp-1;ttll-11* double mutant. To date, perturbing glutamylation is the only genetic manipulation found to affect KLP-6 motility *in vivo* (Morsci and Barr 2011); (Silva, Morsci et al. 2017).

OSM-3::GFP moves abnormally fast in *ccpp-1* CEM cilia (O'Hagan, Piasecki et al.) We examined OSM-3::GFP in *ttll-11*, and found that although *ttll-11* mutants had normal OSM-3::GFP velocity, *ttll-11* suppressed abnormally fast OSM-3::GFP motility in *ccpp-1* mutants (Table 1).

In *C. elegans,* heterotrimeric kinesin-II comprises motor subunits KLP-11 and KLP-20 and accessory subunit KAP-1 (Snow, Ou et al.). Mutations in *ccpp-1* or *ttll-11* had no significant effect on the velocity of KAP-1::GFP in CEM cilia *in vivo* (Morsci and Barr), suggesting that kinesin-II is not regulated by glutamylation (Table 1).

CCPP-1 and TTLL-11 regulates shedding and release of EVs; TTLL-11 is an EV cargo

EVs from the CEMs and RnBs contain the polycystin PKD-2::GFP (Wang, Silva et al.). EVs shed by these ciliated neurons occupy extracellular space in the lumen formed by glial support cells, and are released through pores in the cuticle to the environment, where EVs

can signal locally to conspecifics (Wang, Silva et al.). Kinesin-3 KLP-6 and α-tubulin TBA-6 regulate release of ciliary EVs, with mutants accumulating EVs in the cephalic lumen surrounding the CEM cilium (Wang, Silva et al. , Silva, Morsci et al.). Likewise, *ccpp-1* and *ttll-11* mutants contained almost ten-fold more lumenal EVs than wild type, as examined by transmission electron microscopy (TEM; Table 2). The lumen surrounding CEM cilia in *ccpp-1;ttll-11* double-mutant males, in contrast, contained a similar number of EVs as wild type.

Both *ccpp-1* and *ttll-11* mutants were also defective in environmental release of PKD-2::GFP-labeled EVs (Fig. 5, Supplementary Fig. 3). In wild-type males, 102 ± 12 PKD-2::GFP-labeled EVs surrounded the nose, and 100 ± 11 surrounded the tails. In contrast, the *ccpp-1* and *ttll-11* single mutants and the *ccpp-1;ttll-11* double mutant released few PKD-2::GFP-labeled EVs. *ttll-11b(gk482)* adult males also released few PKD-2::GFP-labeled EVs. Counts of PKD-2::GFP-labeled EVs trapped in the molting cuticles of L4 male tails were also reduced in *ccpp-1, ttll-11,* and *ccpp-1;ttll-11* mutants (Supplementary Fig. 3).

To observe the subcellular localization of TTLL-11 in EVNs, we expressed TTLL-11::GFP driven by the *pkd-2* promoter. TTLL-11::GFP localized to cilia, dendrites, and EVs (Fig. 6a-c). Hence, TTLL-11 is both a regulator of EV release and an EV cargo.

TTLL-11::GFP moved bi-directionally in dendrites and cilia of CEM neurons (Fig. 6d,e). In dendrites, TTLL-11::GFP puncta moved at a mean velocity of 0.87 µm/s and 0.97 µm/s, in anterograde and retrograde directions, respectively. In CEM cilia, the mean velocity of anterograde TTLL-11::GFP transport was 0.73 µm/s, consistent with transport by OSM-3 (Table 1). The average retrograde velocity of TTLL-11::GFP in CEM cilia was 0.80 µm/s.

TTLL-11 sculpts CEM axonemal MT architecture

The structure of the CEM axoneme is distinctive (Fig. 7a-c; (Silva, Morsci et al. 2017)). Like typical ciliary axonemes, the CEM ciliary transition zone contains a ring of nine doublet MTs, connected to the membrane by Y-link structures, followed by a proximal region with nine doublet MTs without Y-links. In the middle region, the nine doublet MTs splay into 18 singlets (Silva, Morsci et al. 2017). Many A-tubule and B-tubule singlets remain adjacent to the ciliary membrane (Fig. 7b). In the sub-distal region, A- and B-tubule singlets remain joined as doublets, and A-tubules extend to the distal-most ciliary tip (Fig. 7a). Therefore, doublet B-tubules detach from A-tubules and form B-tubule singlets in the middle of CEM cilia to create a region of A- and B-tubule singlets.

Serial section TEM of *ttll-11* CEM cilia revealed that MT doublets extended along the entire cilium without splaying into singlets (Fig. 7a-c). We previously reported that *ccpp-1* mutants have fewer singlets that are no longer adjacent to the CEM ciliary membrane (Fig. 7b) (O'Hagan, Piasecki et al.). Here, we observed two additional *ccpp-1* phenotypes using high-pressure freeze tannic acid staining: B-tubules that are fully detached from A-tubules and a region of hyper-stabilized open C-shaped configuration in the middle segment (Fig. 7d). Consistent with our previous findings, end of these B-tubules are exposed to the ciliary lumen and may degenerate stochastically. In *ccpp-1;ttll-11* double mutant males, CEM ciliary MTs resembled those in *ttll-11* single mutants. These results suggest that MT glutamylation controls splaying of MT doublets into A- and B-tubule singlets.

Discussion

The Tubulin Code hypothesis proposes that, in conjunction with tubulin isotypes, PTMs encode information needed for specific cytoskeletal functions (Verhey and Gaertig , Janke). In many organisms, ciliary MTs are decorated with PTMs, including polyglutamylation and polyglycylation (Janke). *C. elegans* lacks MT polyglycylation and polyglycylase homologs (www.wormbase.org , O'Hagan, Piasecki et al. , Yu, Garnham et al.), and therefore may use a simplified Tubulin Code. We demonstrate here that writers and erasers of the tubulin code–positive and negative regulators of glutamylation–specialize the form and function of sensory cilia in *C. elegans*.

TTLL-11, CCPP-1, and glutamylation regulate localization of the ciliary receptor PKD-2 and MT-based motor transport

A surprising result of this study was that loss of the tubulin glutamylase TTLL-11, which is expected to have hypoglutamylated MTs, results in a PKD-2::GFP mislocalization defect similar to *ccpp-1,* which has hyperglutamylated MTs. In fact, attempts to "balance" glutamylation by creating *ccpp-1*;*ttll-11* double mutants demonstrated that these genes interact for some, but not all, functions in male-specific sensory cilia (Table 3). We suggest that exquisitely balanced regulation of PTMs is essential for specialization of EVN cilia.

The influence of the Tubulin Code on ciliary motor traffic is not well understood (Verhey and Gaertig). Our data indicate that tubulin isotype and MT glutamylation regulate ciliary motors in specific manners. a-tubulin TBA-6 regulates the velocities and cargo of the IFT kinesin-2 motors kinesin-II and OSM-3/KIF17 without affecting kinesin-3

KLP-6 velocity. Conversely, glutamylation regulates the velocity of KLP-6 and OSM-3/KIF17 without impacting heterotrimeric kinesin-II.

B-tubules are considered to be the predominant site of glutamylation (Lechtreck and Geimer , Kubo, Yanagisawa et al.) and exclusively navigated by heterotrimeric kinesin-II in *Chlamydomonas* (Stepanek and Pigino). However, MT glutamylation impacts OSM-3, which can travel on A-tubules (Snow, Ou et al. , Prevo, Mangeol et al.). Preferences of particular motors for A- or B-tubules are controversial: in *C. elegans* phasmid chemosensory cilia, localization of heterotrimeric kinesin-II and kinesin-2 OSM-3 was attributed motor turnaround frequencies rather than MT composition or structure (Prevo, Mangeol et al.).

Might B-tubule glutamylation affect A-tubule-mediated transport indirectly? Polyglutamylation can seemingly exert structural effects on different doublets. For example, loss of the glutamylase TTLL9 in mouse sperm flagella causes reduction of glutamylation on doublet 5 but selective loss of doublet 7 (Konno, Ikegami et al.). Alternatively, minimal A-tubule glutamylation may be sufficient to regulate A-tubule-mediated transport, or A-tubule glutamylation may be more prevalent in sensory cilia than previously appreciated from studies in motile cilia. MT glutamylation may regulate motors both directly and indirectly, for example, by altering the charge of tubulin C-terminal tails and motor affinities, and by sculpting the ultrastructure of MTs.

TTLL-11, CCPP-1, and glutamylation regulate ciliary ultrastructure

A striking finding in this work is that TTLL-11 and MT glutamylation regulate axonemal structure at a fundamental level. In wild-type CEM cilia, MT doublets splay into

singlets in middle ciliary regions while remaining joined together proximally and distally (Silva, Morsci et al. 2017). MT hyperglutamylation in *ccpp-1* mutant CEM cilia leads to abnormally aggressive detachment of B-tubules from the A-tubules, resulting in C-shaped B-tubule singlets that fail to close, with concomitant loss of some singlets (O'Hagan, Piasecki et al.). In contrast, *ttll-11* and *ccpp-1; ttll-11* mutants contain hypoglutamylated doublet MTs that fail to splay, indicating that mutation of *ttll-11* acts epistatically to *ccpp-1* when both positive and negative regulation of MT glutamylation is lost. We propose that MT glutamylation promotes the splaying of A-B doublets to A-tubule and B-tubule singlets in CEM cilia. Considering that the velocity of TTLL-11 in cilia matches that of OSM-3, we suggest that TTLL-11, a writer of the code, is carried by a kinesin reader of the code to sculpt the MTs on which the kinesins move.

TTLL enzymes and tubulin glutamylation may be associated with structural specialization of other types of cilia and flagella. For example, separation of axonemal doublets into singlets has been described in mammalian sperm (Afzelius, Dallai et al.). TTLLs and tubulin glutamylation are required for normal sperm MT structure and motility in mice (Vogel, Hansen et al. , Lee, He et al.). TTLL9 (Konno, Ikegami et al.) and TTLL5 (Lee, He et al.) are required for normal mammalian sperm flagellar ultrastructure. Because MT glutamylation is tightly regulated in human sperm (Prigent, Kann et al.), we speculate that mutations affecting glutamylation may be a common cause of human infertility.

What are the MT substrates of glutamylation? The most highly enriched tubulins in the EVNs are α-tubulin TBA-6 and β-tubulin TBB-4 (Wang, Kaletsky et al.). TBA-6 is essential for normal morphology and MT ultrastructure of the CEM cilia (Hurd, Miller et al. 2010) (Silva, Morsci et al. 2017). In *tba-6* mutants, the CEM cilium has a middle segment

with nine doublet microtubules followed by abrupt termination of the B-tubule and extension of nine A-tubule singlets distally. Whereas the sequence of TBB-4 suggests it may be a substrate for glutamylation, TBA-6 might be a non-glutamylatable tubulin subunit due to its unusual C-terminal tail that lacks glutamate residues. Possibly, TBA-6 insertion into the MT lattice in CEM cilia fine-tunes glutamylation to regulate the doublet-to-singlet transition. Therefore, both PTMs and particular tubulin isotypes may sculpt axonemes for diverse forms and functions. Further research is needed to determine which tubulins are true substrates for glutamylation *in vivo*.

Glutamylation regulates release of EVs to the external environment

In addition to TBA-6 and KLP-6, CCPP-1 and TTLL-11 regulate EV release, suggesting that writers, erasers, and readers of the Tubulin Code regulate EV-based signaling. EVs are sub-micron sized membrane-enclosed packages of proteins, lipids, and nucleic acids (Wang and Barr). Particular molecules are sorted and packaged into EVs (Wang, Silva et al. , Lener, Gimona et al.) for intercellular communication. EVs are found in every human bodily fluid and their contents change in pathological states (Wang, Silva et al. , Lener, Gimona et al.). EV signaling regulates normal processes, such as stem cell maintenance, tissue repair, and immunity, as well as pathological processes, such as viral infection and neurodegeneration (S, Mager et al.). Packaging of polycystin receptors into EVs is evolutionarily conserved: PKD2-containing EVs in human urine might provide "urocrine" signaling (Hogan, Manganelli et al.).

Loss of either the TTLL-11 glutamylase or the CCPP-1 deglutamylase virtually abolished release of PKD-2::GFP-labeled EVs. Both *ccpp-1* and *ttll-11* mutants harbor an

overabundance of EVs in the cephalic lumen formed by glial cells that surround the CEM dendrite and cilium. Neuronal EVs might be shed from the ciliary base into this lumen before being transported along cilia for environmental release (Maguire, Silva et al. , Wang and Barr). In *ccpp-1* and *ttll-11* mutants, EVs shed into the lumen may accumulate due to inefficient transport to the ciliary tip for environmental release. Release, but not lumenal shedding, of PKD-2::GFP-labeled EVs in *C. elegans* depends on the kinesin-3 KLP-6 (Wang, Silva et al.). In *ccpp-1* mutants, GFP::KLP-6 localization is defective, suggesting that KLP-6 may not be fully functional in hyperglutamylated cilia (O'Hagan, Piasecki et al.). Furthermore, GFP::KLP-6 velocity is affected by both *ccpp-1* and *ttll-11* single mutants. Therefore, the effect of *ccpp-1* and *ttll-11* single mutants on PKD-2::GFP labeled EV release may depend on KLP-6 function.

Alternatively, environmentally released PKD-2::GFP EVs and lumenal EVs might represent two separate EV biogenesis pathways. In this case, CCPP-1 and TTLL-11 enzymes might positively regulate environmental EV release and negatively regulate lumenal EV shedding (Maguire, Silva et al. , Wang and Barr). The *ccpp-1;ttll-11* double mutant fails to release PKD-2::GFP-labeled EVs to the environment, but lumenal EVs do not accumulate. Therefore, EV shedding into the lumen might also be perturbed when both positive and negative regulation of MT glutamylation are lost.

EV release might also be regulated by TTLL-11-mediated glutamylation of non-tubulin substrates. For example, glutamylation of $RPGR^{ORF15}$, rather than tubulin, causes retinal dystrophy, consistent with glutamylases and deglutamylases having both tubulin and non-tubulin substrates (Rogowski, van Dijk et al. , Rao, Anand et al. , Sun, Park et al.). Because TTLL-11::GFP is an EV cargo, TTLL-11 could act locally in EVs in addition to its role

within cilia. N-myristoylation can anchor proteins to membranes and target proteins to cilia or EVs (Maric, McGwire et al. , Shen, Wu et al. , Wright, Baye et al. , Maguire, Silva et al.). TTLL-11B, which is expressed in the EVNs and possesses a predicted myristoylation site, is likely to be the isoform packaged into EVs.

Glutamylation and human ciliopathy

Tubulin glutamylation is an emerging factor in ciliopathic diseases. A cause of Joubert syndrome was proposed to be hypoglutamylation of ciliary MTs, indirectly caused by mutation of the CEP41, which is needed for trafficking of the glutamylase TTLL6 into cilia (Lee, Silhavy et al.). Mutations in the deglutamylase AGBL5 are associated with retinal degeneration (Kastner, Thiemann et al. , Astuti, Arno et al. , Nisha Patel PhD). Loss of Ccp1, the mouse homolog of *C. elegans* CCPP-1, causes progressive neurodegeneration and sperm immotility (Mullen, Eicher et al. , Fernandez-Gonzalez, La Spada et al.). Hypoglutamylation in mice also causes defects in both synaptic function (Ikegami, Heier et al.) and sperm tail structure (Campbell, Waymire et al.). Recent work also identified TTLL5 mutation as a cause of recessive retinal dystrophy in humans (Sergouniotis, Chakarova et al.) and sperm immotility in mice (Lee, He et al.). We predict that the writers and erasers of the Tubulin Code such as the TTLL glutamylases and Ccp deglutamylases, as well as molecules that read the Tubulin Code, are likely to have important impacts on human health.

Acknowledgments

We thank members of the Barr lab and the Rutgers *C. elegans* community for helpful discussions, Leslie Gunther and Geoff Perumal for help in HPF-FS performed at Einstein. This work was funded by NJCSCR postdoctoral fellowship 10-2951-SCR-E-0 and NJCSCR Grant CSCR15IRG014 to R.O.; NIH OD 10943 to D.H.H.; NIH DK059418 and DK074746 to M.M.B., and Waksman Institute Charles and Johanna Busch Fellowship to M.S. Some strains were provided by the CGC, which is funded by NIH Office of Research Infrastructure Programs (P40 OD010440), or by the Mitani Lab through the National Bio-Resource Project of the MEXT, Japan.

Tables and Figures

Table 1

	Genetic Background	Anterograde IFT velocity ($\mu ms^{-1} \pm sd$)	N worms/ n particles
Kinesin-3 GFP::KLP-6	Wild type	0.80 ± 0.15	9/51
	ccpp-1(vs wt)*	0.88 ± 0.15	5/48
	*ttll-11 (*vs wt;***vs ccpp-1)*	0.71 ± 0.13	6/41
	*ccpp-1; ttll-11(***vs ccpp-1)*	0.77 ± 0.14	8/43
Kinesin-2 OSM-3::GFP	Wild type	0.74 ± 0.21	7/53
	ccpp-1 (*** vs wt)	0.92 ± 0.24	6/46
	ttll-11 (*** vs *ccpp-1)*	0.67 ± 0.22	8/63
	ccpp-1; ttll-11 (*** vs *ccpp-1)*	0.65 ± 0.21	6/60
Heterotrimeric Kinesin-II KAP-1::GFP	Wild type	0.55 ± 0.08	16/125
	ccpp-1	0.57 ± 0.13	20/133
	ttll-11	0.56 ± 0.11	10/79
	ccpp-1; ttll-11	0.63 ± 0.17	14/154

Table 1: CCPP-1 and TTLL-11 Regulate Velocities of GFP-tagged Kinesin-2 (OSM-3), Kinesin-3 (KLP-6), but not Heterotrimeric Kinesin-II, in CEM cilia. We used ANOVA and post-hoc Tukey comparisons to determine the statistical significance of velocity differences. * represents $P<0.05$; *** represents $P<0.001$.

Table 2

Genotype	Total # EVs per cilium	# EVs above TZ	# EVs below TZ
wild type	75 ± 28	21 ±10	53 ± 24
ccpp-1	503 ± 118	402 ± 113	102 ± 35
ttll-11	602 ± 121	287 ± 140	314 ± 48
ccpp-1;ttll-11	71 ± 48	28 ± 16	43 ± 32

Table 2: Serial section TEM analysis of lumenal EVs surrounding CEM cilia. EVs CEM cilia in the lumen formed by sheath and socket support cells were counted to determine the average total number of EVs associated with individual cilia of each genotype; number EVs above and below the transition zone (TZ. Data represents AVG ± SEM; N = 1 animal serial section TEM analyzed per genotype; n = 3 cilia for *ttll-11*; 4 for all other genotypes.

Table 3

Mutant	Glutamylation of CEM/RnB Cilia (GT335)	Cilia/Ciliary Base PKD-2::GFP Localization	GFP::KLP-6 Localization	GFP::KLP-6 Vel.	OSM-3::GFP Vel.	MT Structure	Released PKD-2::GFP EVs	Lumenal EVs (TEM)
ccpp-1	+ or é*	é	-	é	é	Reduced # singlets	ê	é
ttll-11	ê	é	+	ê	+	Stabilized doublets	ê	é
ccpp-1; ttll-11	ê	é	+	+	+	Stabilized doublets	ê	+

Table 3: Summary of mutants and phenotypes examined.

Wild-type phenotype indicated by +, mutant phenotype indicated by -,

reduction in intensity, velocity or amount indicated by ê, increase indicated by é.

*indicates that under experimental conditions used here, GT335 staining was not

increased relative to WT, however previous experiments detected an increase in GT335

staining in CEM neurons in *ccpp-1* mutants relative to wild type.

Figure 1

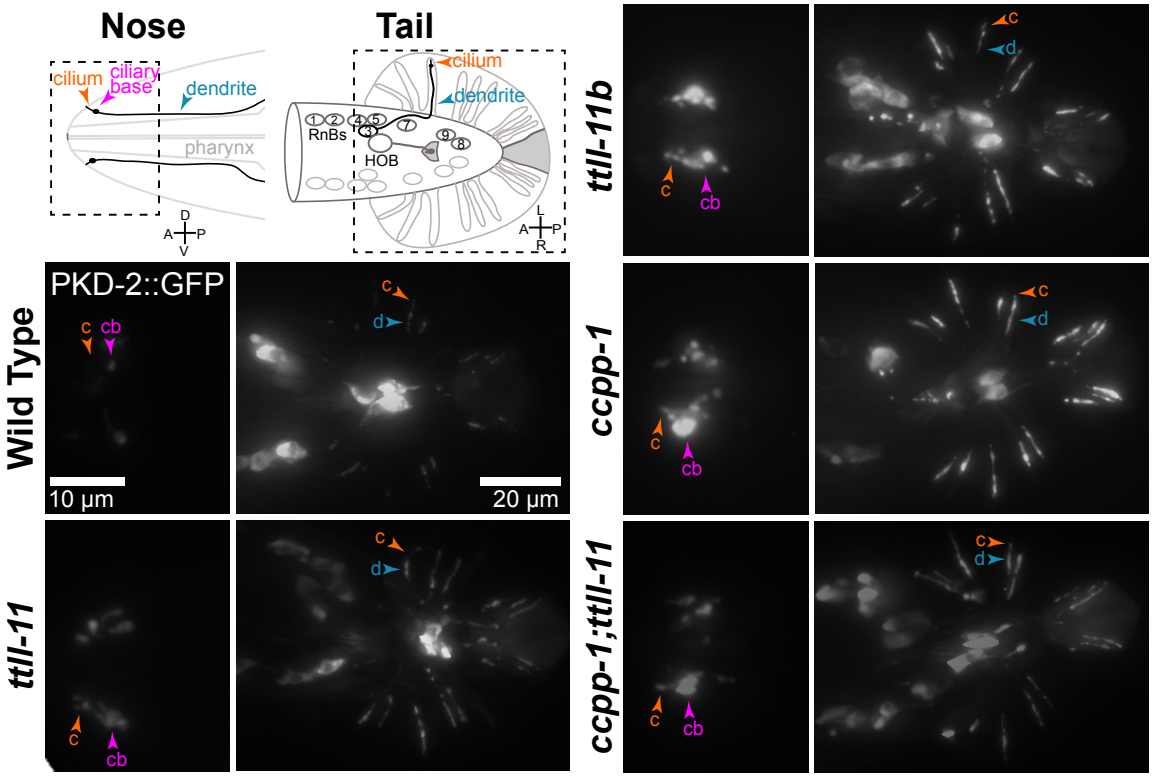

Figure 1 Dysregulation of MT glutamylation caused polycystin accumulation in male-specific ciliated sensory neurons.

Diagrams (adapted from O'Hagan *et al* 2011) of male-specific neurons (CEMs in head, HOB and RnBs in tail), which express PKD-2::GFP. In the diagram of the nose, only the left side CEM neurons of the two bilateral pairs is shown. Boxed area, indicating region shown in micrographs, depicts the distal-most dendrite (d), ciliary base (cb), and cilium (c); somata are further posterior, out of view. In the tail, each ray is innervated by a single RnB neuron; the dendrite and cilium of R3B are shown as an example. In wild type, PKD-2::GFP localized to ciliary base and ciliary regions. PKD-2::GFP dramatically accumulated in cilia and

dendrites in *ttll-11(tm4059)* or *ttll-11b(gk482)* mutants. Male-specific sensory neurons showed a similar PKD-2 accumulation phenotype in *ccpp-1* mutants, which contain hyperglutamylated ciliary MTs, and in *ccpp-1;ttll-11* double mutants.

Figure 2

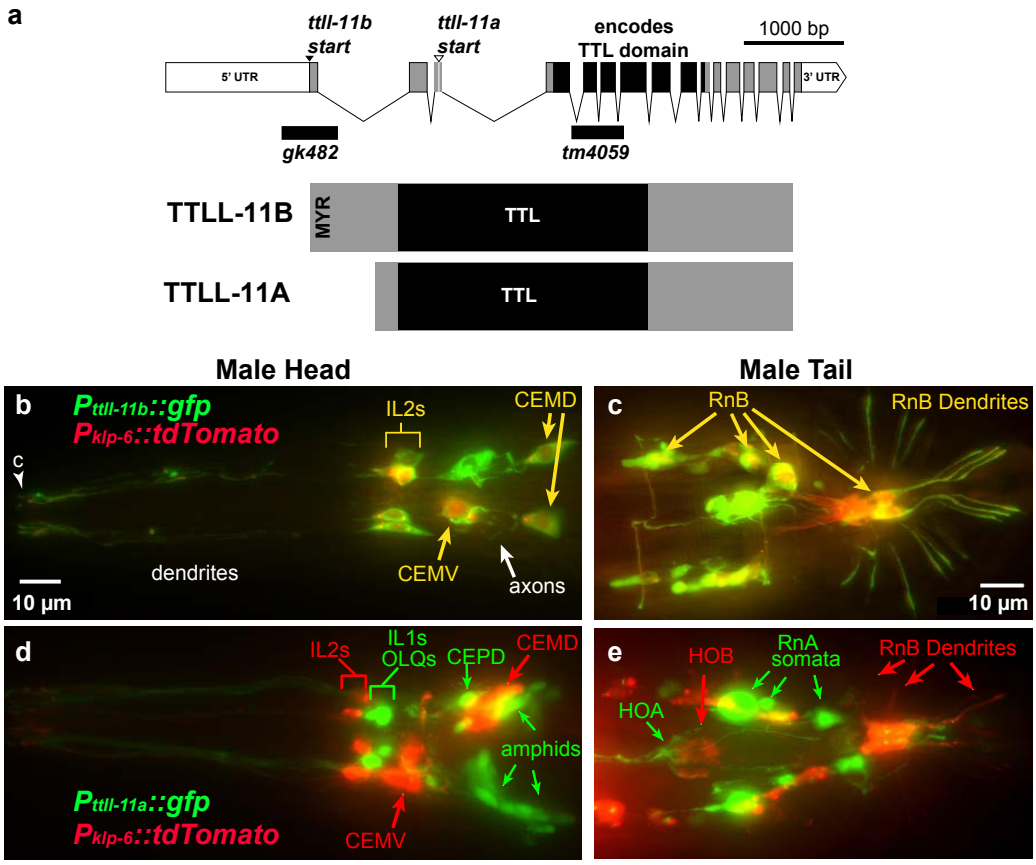

Figure 2 Genomic structure of *ttll-11* isoforms and mutants and expression of $P_{ttll\text{-}11b}$::gfp and $P_{ttll\text{-}11a}$::gfp.

a. *ttll-11b*, which encodes a 707 amino-acid protein, is affected by both *gk482* and *tm4059* deletions. *gk482* eliminates the entire first exon of *ttll-11b*, and the *tm4059* deletion introduces an early stop codon at amino acid 191 of the predicted TTLL-11B product. *ttll-11a*, which encodes a 607 amino acid protein, is affected only by the *tm4059* deletion, which introduces an early stop codon at amino acid 91 of the predicted product. Both TTLL-11B and TTLL-11A contain a TTL domain of 364 amino acids (black region). MYR indicates a predicted myristoylation site (Eisenhaber, Eisenhaber et al.) in TTLL-11B. By

analogy with other TTLL proteins, the C-terminal gray area is expected to bind microtubules. **b**-**c.** Co-expression of GFP by the *ttll-11b* promoter and tdTomato by the *klp-6* promoter was observed in the extracellular vesicle-releasing neurons (EVNs), including the male-specific ciliated CEM sensory neurons and the shared IL2 neurons in the head; and the HOB and RnB neurons in the tail. Expression of both transgenes was somewhat mosaic, and therefore did not completely overlap; for example, one of the CEM ventral neurons in the head was not labeled by tdTomato. **d-e.** A *ttll-11a* promoter drives expression of GFP in the amphid neurons, as well as neurons identified as the IL1 and OLQ neurons in the head and RnA and HOA neurons in the tail. *ttll-11a* was not expressed in the EVNs, marked by expression of P_{klp-6}*::tdTomato*.

Figure 3

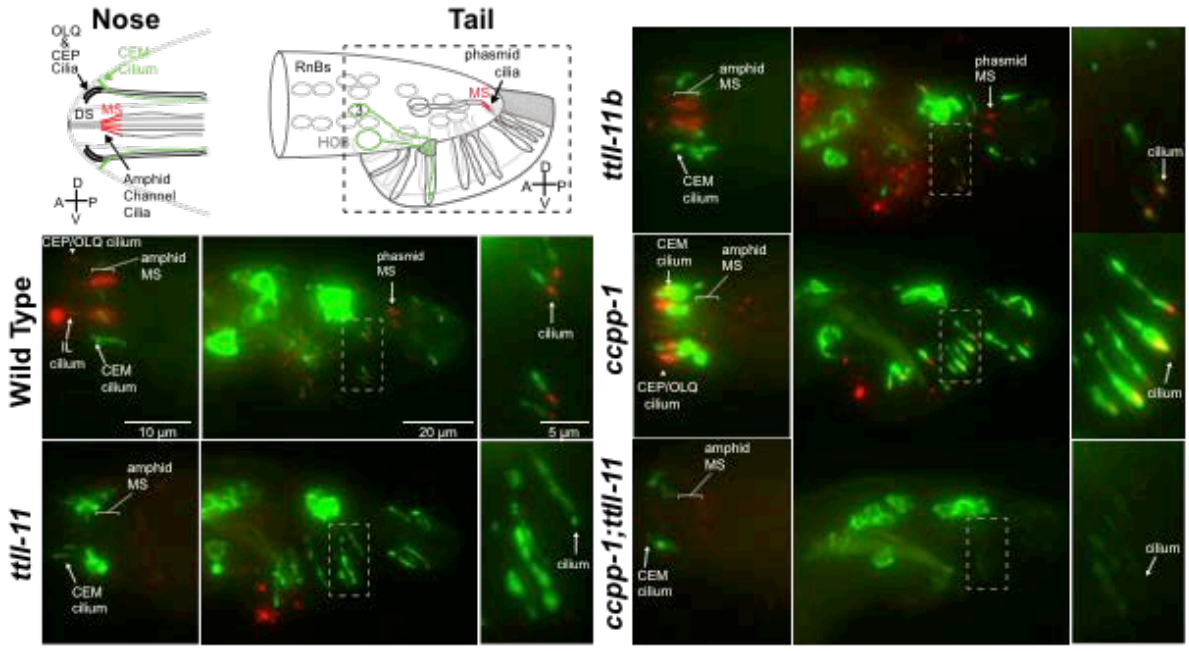

Figure 3 TTLL-11 was required for ciliary MT glutamylation.

Fixed young adult males expressing PKD-2::GFP (green) stained with monoclonal antibody GT335 (red), which detects MT glutamylation, shown in red. Left column: ciliated endings in the tip of the nose; middle column: male tail fan; right column: enlargements of the boxed areas in tails to show ray cilia. In wild type panel, GT335 staining of amphid ciliary MS (middle segments), CEP cilia, and IL cilia in the head, and phasmid cilia in the tail, are indicated. GT335 staining of *ttll-11b* mutants appeared similar to wild type in OLQ and IL cilia.

A deletion affecting both *ttll-11a & b* isoforms eliminated detection of ciliary MT glutamylation by GT335. In *ttll-11b* mutants, GT335 staining was still visible in amphid, phasmid, cephalic, and ray neuronal cilia, suggesting that TTLL-11A activity glutamylates

ciliary MTs in amphid, phasmid, CEP, and RnA cilia when *ttll-11b* isoform is mutated. Loss of the deglutamylase CCPP-1 increased GT335 staining in CEM and RnB cilia. Loss of TTLL-11 function appeared to be epistatic to CCPP-1 in GT335 staining of *ccpp-1;ttll-11* mutant males.

Figure 4

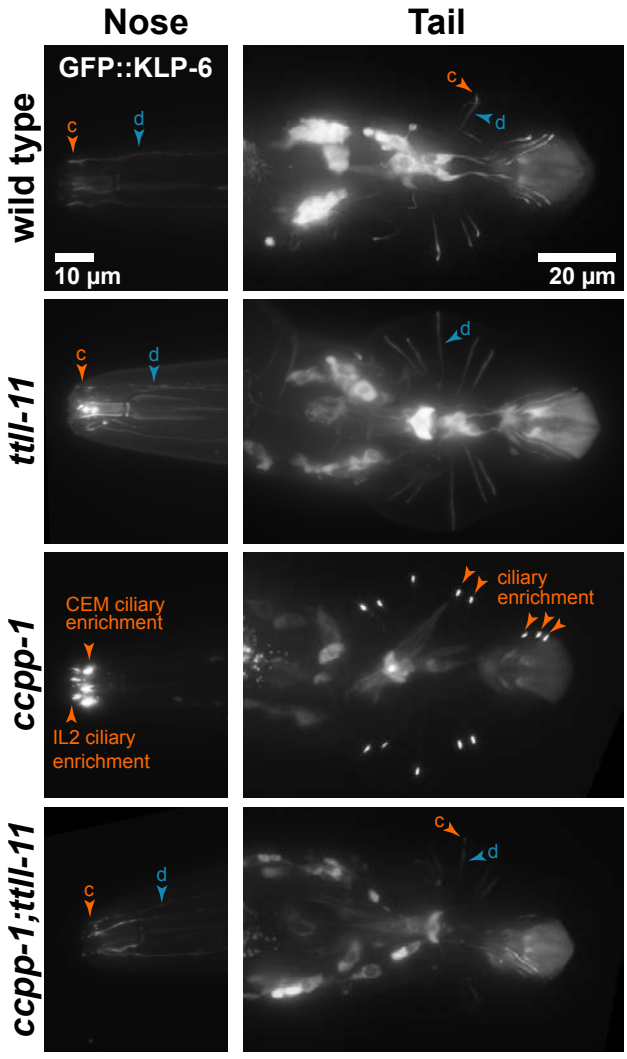

Figure 4 Loss of TTLL-11 function suppressed GFP::KLP-6 kinesin-3 ciliary accumulation of *ccpp-1* mutants.

Localization of the kinesin-3 motor GFP::KLP-6 was diffuse in wild type and *ttll-11* single mutants. In *ccpp-1* mutants, GFP::KLP-6 accumulated in cilia of EVNs in the head (CEMs and IL2s) and tail (HOB and RnBs). Mutation of *ttll-11* suppressed the abnormal ciliary enrichment of GFP::KLP-6 in *ccpp-1* mutants. (Tail images were normalized so that

brightness of autofluorescent posterior tip of acellular tail fan was similar across genotypes. c, cilium; d, dendrite.)

Figure 5

Fig. 5 TTLL-11 required for release of PKD-2::GFP-labeled EVs

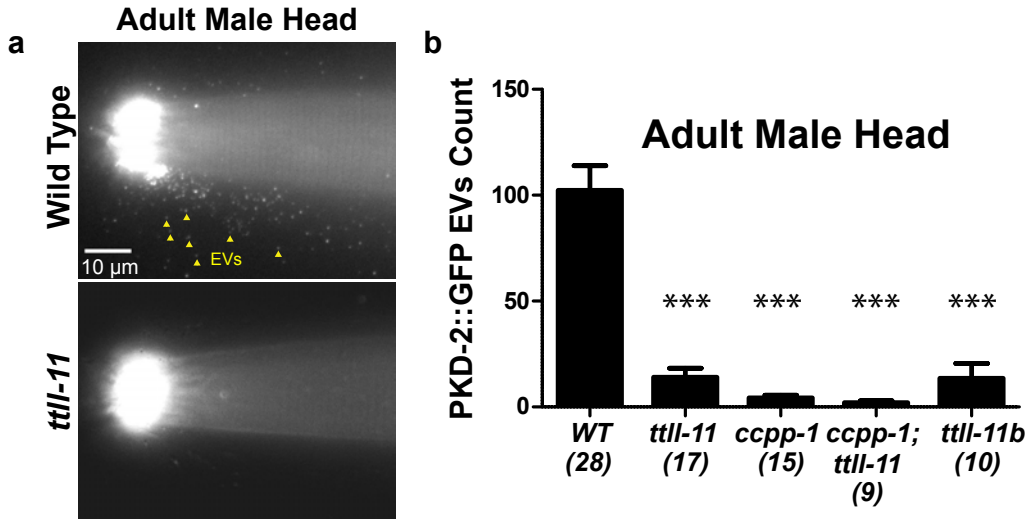

Figure 5 The MT glutamylase TTLL-11 and deglutamylase CCPP-1 were required for release of PKD-2::GFP-labeled extracellular vesicles (EVs).

a. EVs were abundantly released outside from CEM ciliated sensory neurons in wild-type adult males (several EVs indicated by arrowheads). Bottom panel shows *ttll-11* mutant with few PKD-2::GFP-labeled EVs. See Supplementary Figure 3 for images of additional genotypes, as well as images of PKD-2::GFP-labeled EVs released by neurons in the male tail in adults and L4 larvae. **b.** Quantification of EVs released to the local environment by sensory ciliated CEM neurons in adult male head. *ttll-11* (also shown here), *ccpp-1*, and *ccpp-1;ttll-11* mutants (shown in Supplementary Fig. 3) were severely defective in release of EVs to the environment. (AVG ± SEM; **p<0.001, ***p<0.0001 by ANOVA and post-hoc Tukey tests. N animals scored in parentheses for each genotype.)

Figure 6

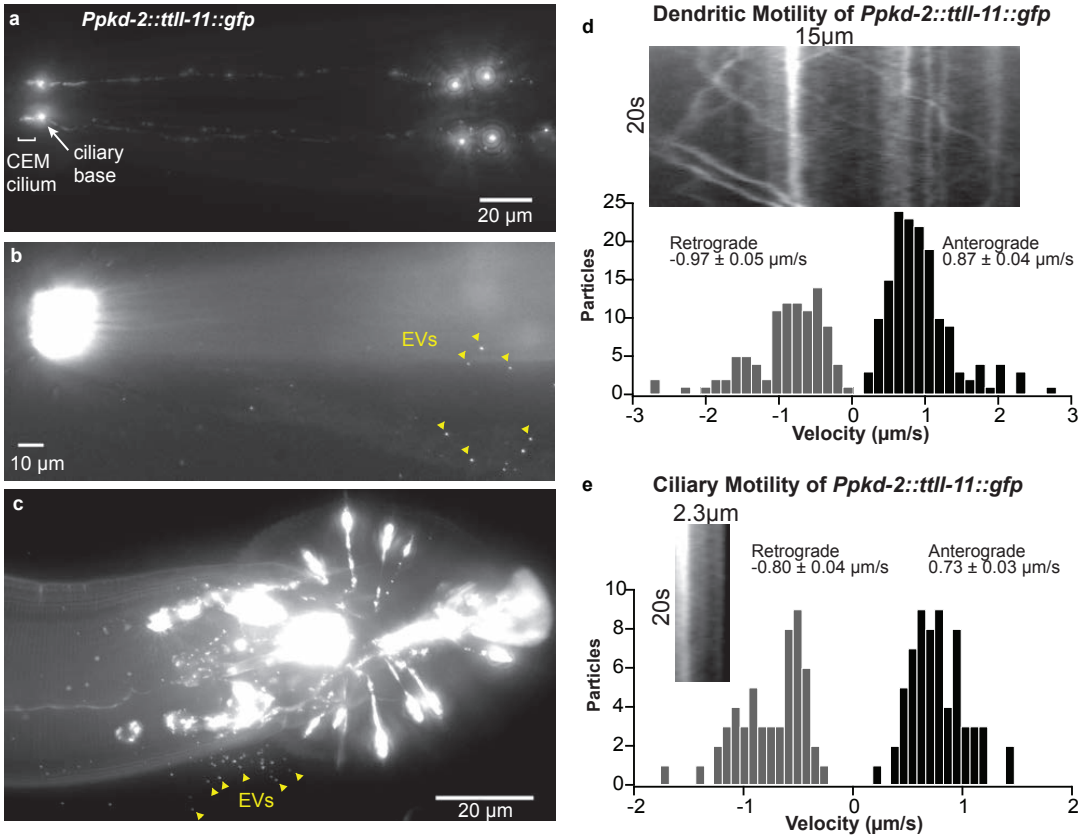

Figure 6 TTLL-11::GFP was enriched in cilia and packaged in released EVs

a.TTLL-11::GFP expressed under the *pkd-2* promoter was enriched in CEM cilia and ciliary bases, suggesting TTLL-11 may act in these locations. TTLL-11::GFP appeared in puncta in dendrites and cell bodies of *C. elegans* males. CEM cilia and ciliary base are indicated by a bracket and arrow, respectively. **b-c.** TTLL-11::GFP was observed in EVs released from CEM neurons in the head (**b**) and RnB neurons in the tail (**c**). In b and c, yellow arrowheads point to TTLL-11::GFP-labeled EVs. **d, e.** Kymograph and histograms of TTLL-11::GFP movement in dendrites and cilia. Mean ± SEM dendritic velocities shown for 15 animals, 153 anterograde particles; 98 retrograde particles. Mean ± SEM ciliary velocities shown for 13 animals, 64 anterograde events; 54 retrograde particles.

Figure 7

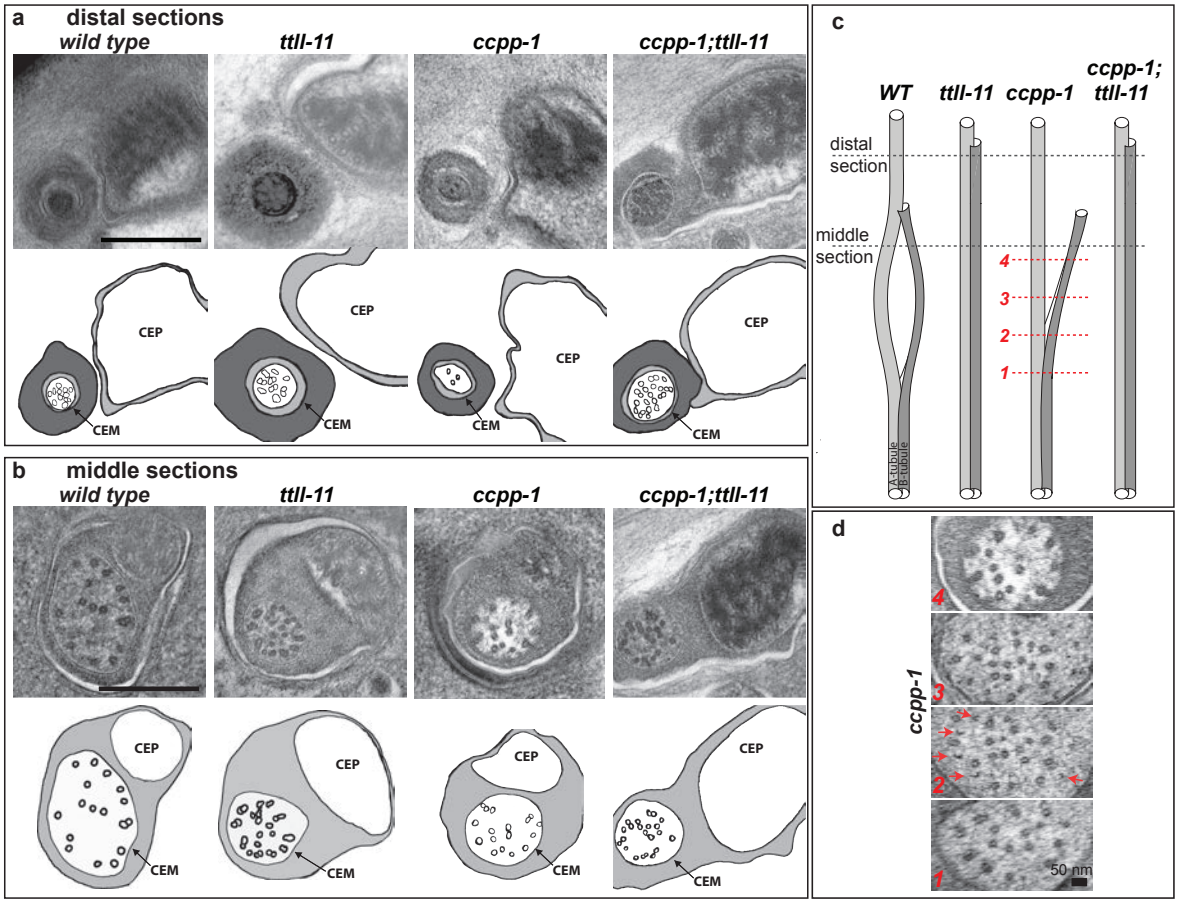

Figure 7 CCPP-1 and TTLL-11 regulators of MT glutamylation are required for normal CEM neuronal ciliary ultrastructure.

TEM sections and corresponding illustrations through CEM cilia in distal region (**a**) and middle region (**b**). **a.** In all genetic backgrounds, the distal-most CEM ciliary tip (white in illustration) and lumen (light gray) extends through the cuticular pore (dark gray halo in illustration). In WT, only singlets are present, while *ttll-11* and *ccpp-1; ttll-11* ciliary tips possess doublets and *ccpp-1* ciliary tips have fewer singlets. **b.** In middle regions, WT CEM cilia contained A- and B- tubule singlets, most of which are closely associated with the ciliary membrane. In *ttll-11* mutants, MTs in this region were doublet-like structures. *ccpp-*

1;ttll-11 CEM cilia resembled cilia in the *ttll-11* single mutant. Scale bar = 500nm. **c.** Cartoon representation of one of nine microtubules along the ciliary length in wild type (WT), *ttll-11* single, *ccpp-1* single, and *ccpp-1; ttll-11* double mutants. In wild type, ciliary microtubules are splayed to from separate A- and B-tubule singlets in middle regions, and the A-tubule extends to the distal-most tip. In *ttll-11*, doublets fail to splay into singlets, and B-tubules are abnormally stabilized and extend far into the distal-most region. In *ccpp-1*, doublets split, but do not remain joined in distal regions. *ccpp-1;ttll-11* double mutants resemble *ttll-11* single mutants. **d.** A series of CEM middle sections from *ccpp-1* mutants revealed open "C-shaped" tubules (arrows in section 2 of panel 7d) that likely correspond to free B-tubules detached from their A-tubule partner. (Approximate locations of sections shown by red dotted lines in **c.)** Scale bar = 50nm. *ccpp-1* A-tubule singlets have 13 protofilaments and B-tubule singlets have 10 protofilaments (**d,** section 4).

Figure S1

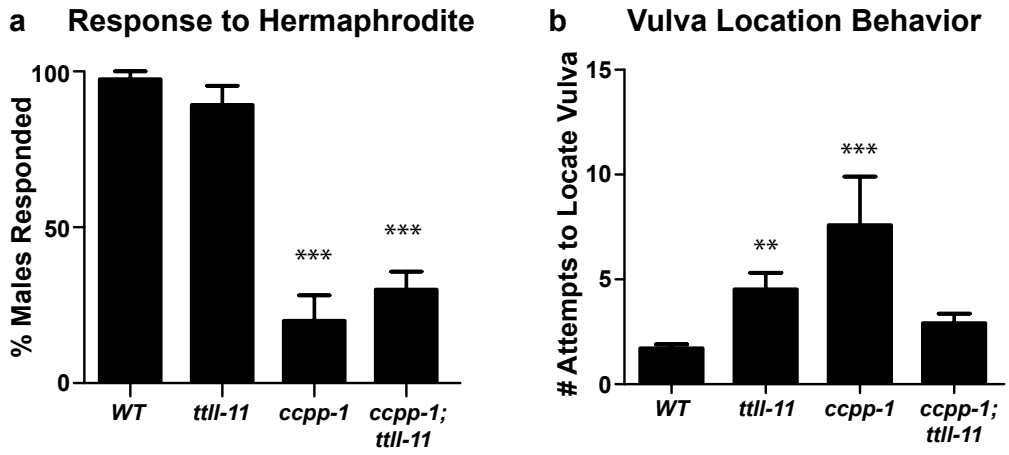

Figure 8 (S1) TTLL-11 was required for Location of Vulva sub-step of male mating behavior.

Appropriate function and localization of PKD-2 is required for male mating behavioral sub-steps: "Response," in which the male responds to contact with a hermaphrodite partner and moves backwards along the hermaphrodite while pressing his tail against her body; and "Location of Vulva," in which males stop at the hermaphrodite vulva and prod with their spicules. **a.** The percentage of *ttll-11* males responding to hermaphrodite contact in mating assays was not significantly different than wild type. However, *ccpp-1* and *ccpp-1;ttll-11* mutant males responded significantly less frequently than wild-type. Data represents AVG ± SEM; N = 4 or 5 assays, n = 51(wt); *61 (ttll-11)*; 35 *(ccpp-1*); 50 *(ccpp-1;ttll-11)* males tested.. ***indicates $p<0.0001$ by ANOVA and Tukey post-hoc tests. **b.** Both *ttll-11* and *ccpp-1* mutant males were impaired in vulva location behavior. However, *ccpp-1;ttll-11* males behaved similarly to wild-type. For vulva location, n males scored = 25 (wt);

19 (*ttll-11*); 10 (*ccpp-1*); 12 (*ccpp-1;ttll-11*). ** p<0.001, *** p<0.0001 by Kruskal-Wallis and Dunn's Multiple Comparison Test.

Figure S2

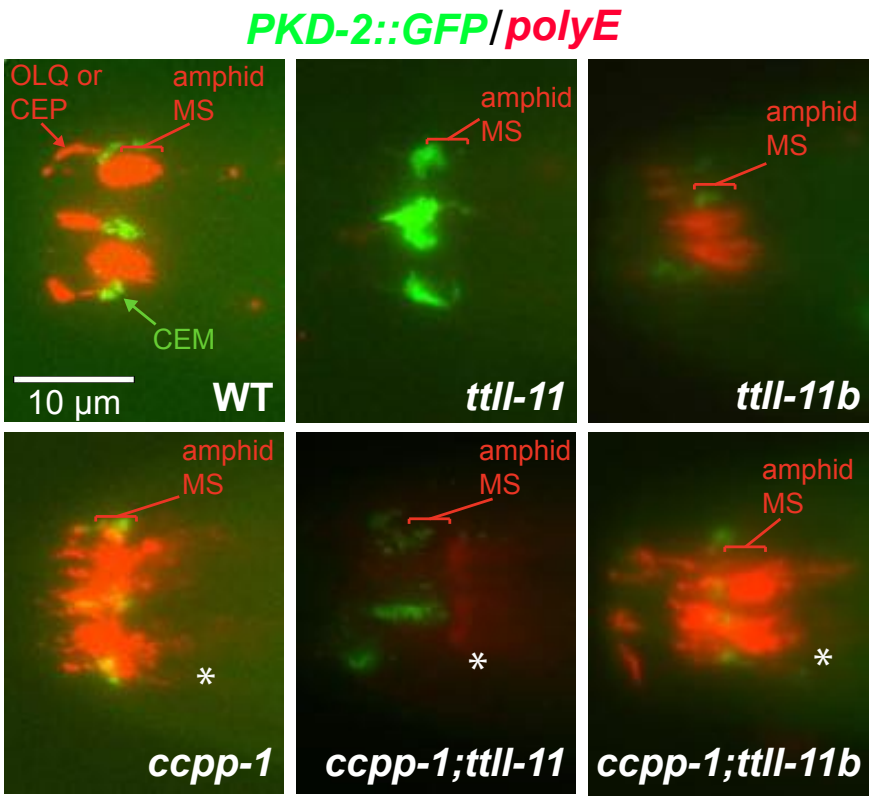

Figure 9 (S2) Detection of long glutamate side chains by indirect immunofluorescence.

The IN105 polyE antibody recognizes linear side-chains of 3 or more glutamates (van Dijk, Rogowski et al. 2007). We stained males on the first day of adulthood and found that, in wild type males, the amphid channel ciliary middle segments and OLQ or CEP cilia were brightly stained. Loss of both TTLL-11 isoforms in *ttll-11(tm4059)* mutants abolished polyglutamylation side-chains from neuronal sensory cilia. However, in *ttll-11b* mutants, polyE detected amphid ciliary middle segments, although possibly less abundantly than in wild type. In *ccpp-1* mutants, polyE staining was seen in more sensory neuronal cilia in

the nose. In *ccpp-1,* polyE staining abnormally localized posterior to amphid middle segment regions in a diffuse trail marked by speckles (*). In *ccpp-1;ttll-11* double mutants, polyE staining of sensory cilia was virtually abolished but the speckled trail of staining posterior to the amphid middle segment was still visible (*). In *ccpp-1;ttll-11b* mutants, amphid ciliary middle segments and other cilia were illuminated by polyE staining. The trailing region of speckled polyE staining was also visible (*).

Figure S3

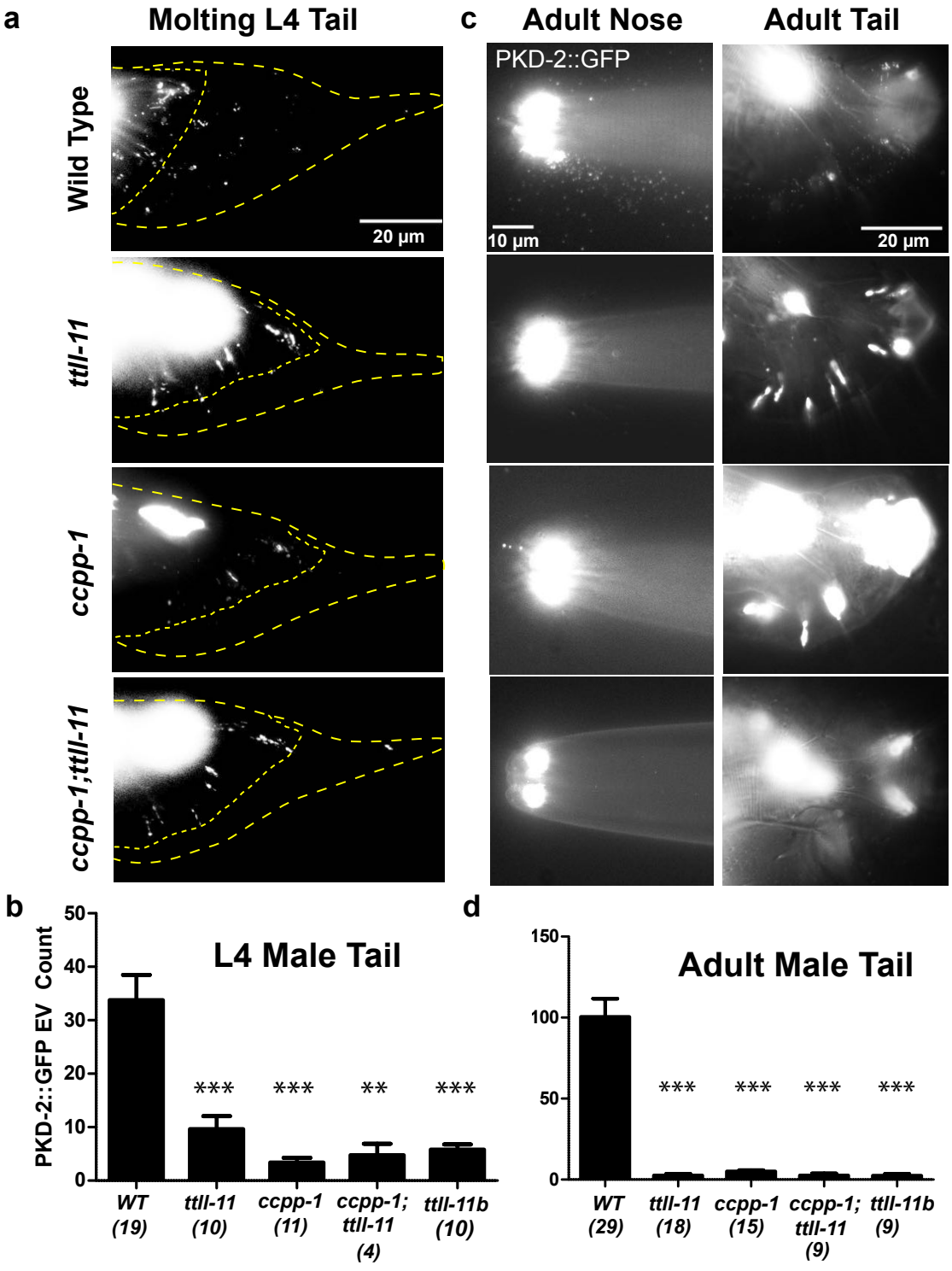

Figure 10 (S3) PKD-2::GFP-labeled EVs in L4 and adult males.

a. In late wild-type L4 males, abundant EVs released from RnB ciliated neurons were trapped in the molting L4 cuticle in the tail. *ttll-11, ccpp-1,* and *ccpp-1;ttll-11* had few EVs in molting L4 cuticles. Yellow dotted lines indicate outline of molting L4 cuticle. **b.** Quantification of EVs trapped in L4 cuticles. **c.** Abundant EVs were also released by adult males ciliated sensory neurons into the environment surrounding the nose and tail in wild type. *ttll-11, ccpp-1,* and *ccpp-1;ttll-11* adult males had few EVs surrounding the nose and tail. **d.** Quantification of EVs released by the adult male tail. (AVG ± SEM; **p<0.001, ***p<0.0001 by ANOVA and post-hoc Tukey tests. N animals scored in parentheses for each genotype.)

References

(1998). "Genome sequence of the nematode C. elegans: a platform for investigating biology. The C. elegans Sequencing Consortium." Science **282**(5396): 2012-2018.
Admyre, C., S. M. Johansson, K. R. Qazi, J. J. Filen, R. Lahesmaa, M. Norman, E. P. Neve, A. Scheynius and S. Gabrielsson (2007). "Exosomes with immune modulatory features are present in human breast milk." J Immunol **179**(3): 1969-1978.
Afzelius, B. A., R. Dallai, S. Lanzavecchia and P. L. Bellon (1995). "Flagellar structure in normal human spermatozoa and in spermatozoa that lack dynein arms." Tissue Cell **27**(3): 241-247.
Akella, J. S., D. Wloga, J. Kim, N. G. Starostina, S. Lyons-Abbott, N. S. Morrissette, S. T. Dougan, E. T. Kipreos and J. Gaertig (2010). "MEC-17 is an alpha-tubulin acetyltransferase." Nature **467**(7312): 218-222.
Altschul, S. F., T. L. Madden, A. A. Schaffer, J. Zhang, Z. Zhang, W. Miller and D. J. Lipman (1997). "Gapped BLAST and PSI-BLAST: a new generation of protein database search programs." Nucleic Acids Res **25**(17): 3389-3402.
Astuti, G. D., G. Arno, S. Hull, L. Pierrache, H. Venselaar, K. Carss, F. L. Raymond, R. W. Collin, S. M. Faradz, L. I. van den Born, A. R. Webster and F. P. Cremers (2016). "Mutations in AGBL5, Encoding alpha-Tubulin Deglutamylase, Are Associated With Autosomal Recessive Retinitis Pigmentosa." Invest Ophthalmol Vis Sci **57**(14): 6180-6187.
Audhya, A., I. X. McLeod, J. R. Yates and K. Oegema (2007). "MVB-12, a fourth subunit of metazoan ESCRT-I, functions in receptor downregulation." PLoS One **2**(9): e956.
Bae, Y. K., H. Qin, K. M. Knobel, J. Hu, J. L. Rosenbaum and M. M. Barr (2006). "General and cell-type specific mechanisms target TRPP2/PKD-2 to cilia." Development **133**(19): 3859-3870.
Bakeberg, J. L., R. Tammachote, J. R. Woollard, M. C. Hogan, H. F. Tuan, M. Li, J. M. van Deursen, Y. Wu, B. Q. Huang, V. E. Torres, P. C. Harris and C. J. Ward (2011). "Epitope-tagged Pkhd1 tracks the processing, secretion, and localization of fibrocystin." J Am Soc Nephrol **22**(12): 2266-2277.
Barr, M. M., J. DeModena, D. Braun, C. Q. Nguyen, D. H. Hall and P. W. Sternberg (2001). "The Caenorhabditis elegans autosomal dominant polycystic kidney disease gene homologs lov-1 and pkd-2 act in the same pathway." Curr Biol **11**(17): 1341-1346.
Barr, M. M., J. DeModena, D. Braun, C. Q. Nguyen, D. H. Hall and P. W. Sternberg (2001). "The Caenorhabditis elegans autosomal dominant polycystic kidney disease gene homologs lov-1 and pkd-2 act in the same pathway." Curr Biol **11**(17): 1341-1346.
Barr, M. M. and P. W. Sternberg (1999). "A polycystic kidney-disease gene homologue required for male mating behaviour in C. elegans." Nature **401**(6751): 386-389.
Barr, M. M. and P. W. Sternberg (1999). "A polycystic kidney-disease gene homologue required for male mating behaviour in C. elegans." Nature **401**(6751): 386-389.
Barrios, A., S. Nurrish and S. W. Emmons (2008). "Sensory Regulation of C. elegans Male Mate-Searching Behavior." **18**(23): 1865-1871.
Bianco, F., C. Perrotta, L. Novellino, M. Francolini, L. Riganti, E. Menna, L. Saglietti, E. H. Schuchman, R. Furlan, E. Clementi, M. Matteoli and C. Verderio (2009). "Acid sphingomyelinase activity triggers microparticle release from glial cells." EMBO J **28**(8): 1043-1054.

Binder, L. I. and J. L. Rosenbaum (1978). "The in vitro assembly of flagellar outer doublet tubulin." The Journal of Cell Biology **79**(2 Pt 1): 500-515.
Bloodgood, R. A., M. P. Woodward and N. L. Salomonsky (1986). "Redistribution and shedding of flagellar membrane glycoproteins visualized using an anti-carbohydrate monoclonal antibody and concanavalin A." J Cell Biol **102**(5): 1797-1812.
Brenner, S. (1974). "The genetics of Caenorhabditis elegans." Genetics **77**(1): 71-94.
Buck, A. H., G. Coakley, F. Simbari, H. J. McSorley, J. F. Quintana, T. Le Bihan, S. Kumar, C. Abreu-Goodger, M. Lear, Y. Harcus, A. Ceroni, S. A. Babayan, M. Blaxter, A. Ivens and R. M. Maizels (2014). "Exosomes secreted by nematode parasites transfer small RNAs to mammalian cells and modulate innate immunity." Nat Commun **5**: 5488.
Cai, Y., S. V. Fedeles, K. Dong, G. Anyatonwu, T. Onoe, M. Mitobe, J. D. Gao, D. Okuhara, X. Tian, A. R. Gallagher, Z. Tang, X. Xie, M. D. Lalioti, A. H. Lee, B. E. Ehrlich and S. Somlo (2014). "Altered trafficking and stability of polycystins underlie polycystic kidney disease." J Clin Invest.
Campbell, P. K., K. G. Waymire, R. L. Heier, C. Sharer, D. E. Day, H. Reimann, J. M. Jaje, G. A. Friedrich, M. Burmeister, T. J. Bartness, L. D. Russell, L. J. Young, M. Zimmer, D. E. Jenne and G. R. MacGregor (2002). "Mutation of a novel gene results in abnormal development of spermatid flagella, loss of intermale aggression and reduced body fat in mice." Genetics **162**(1): 307-320.
Chasnov, J. R. (2013). "The evolutionary role of males in C. elegans." Worm **2**(1): e21146.
Cocucci, E., G. Racchetti and J. Meldolesi (2009). "Shedding microvesicles: artefacts no more." Trends Cell Biol **19**(2): 43-51.
Cueva, J. G., J. Hsin, K. C. Huang and M. B. Goodman (2012). "Posttranslational acetylation of alpha-tubulin constrains protofilament number in native microtubules." Curr Biol **22**(12): 1066-1074.
Curtis, A. M., P. F. Wilkinson, M. Gui, T. L. Gales, E. Hu and J. M. Edelberg (2009). "p38 mitogen-activated protein kinase targets the production of proinflammatory endothelial microparticles." J Thromb Haemost **7**(4): 701-709.
Doroquez, D. B., C. Berciu, J. R. Anderson, P. Sengupta and D. Nicastro (2014). "A high-resolution morphological and ultrastructural map of anterior sensory cilia and glia in Caenorhabditis elegans." Elife **3**: e01948.
Dutcher, S. K. (2001). "The tubulin fraternity: alpha to eta." Current Opinion in Cell Biology **13**(1): 49-54.
Eisenhaber, F., B. Eisenhaber, W. Kubina, S. Maurer-Stroh, G. Neuberger, G. Schneider and M. Wildpaner (2003). "Prediction of lipid posttranslational modifications and localization signals from protein sequences: big-Pi, NMT and PTS1." Nucleic Acids Res **31**(13): 3631-3634.
Ewbank, J. J. (2006). "Signaling in the immune response." WormBook: 1-12.
Fernandez-Gonzalez, A., A. R. La Spada, J. Treadaway, J. C. Higdon, B. S. Harris, R. L. Sidman, J. I. Morgan and J. Zuo (2002). "Purkinje cell degeneration (pcd) phenotypes caused by mutations in the axotomy-induced gene, Nna1." Science **295**(5561): 1904-1906.
Fisch, C. and P. Dupuis-Williams (2011). "Ultrastructure of cilia and flagella - back to the future!" Biol Cell **103**(6): 249-270.
Flaumenhaft, R., J. R. Dilks, J. Richardson, E. Alden, S. R. Patel-Hett, E. Battinelli, G. L. Klement, M. Sola-Visner and J. E. Italiano, Jr. (2009). "Megakaryocyte-derived

microparticles: direct visualization and distinction from platelet-derived microparticles." Blood **113**(5): 1112-1121.
Fliegauf, M., T. Benzing and H. Omran (2007). "When cilia go bad: cilia defects and ciliopathies." Nat Rev Mol Cell Biol **8**(11): 880-893.
Garnham, C. P., A. Vemu, E. M. Wilson-Kubalek, I. Yu, A. Szyk, G. C. Lander, R. A. Milligan and A. Roll-Mecak (2015). "Multivalent Microtubule Recognition by Tubulin Tyrosine Ligase-like Family Glutamylases." Cell **161**(5): 1112-1123.
Gems, D. and D. L. Riddle (2000). "Genetic, behavioral and environmental determinants of male longevity in Caenorhabditis elegans." Genetics **154**(4): 1597-1610.
Gogonea, C. B., V. Gogonea, Y. M. Ali, K. M. Merz, Jr. and S. S. Siddiqui (1999). "Computational prediction of the three-dimensional structures for the Caenorhabditis elegans tubulin family." J Mol Graph Model **17**(2): 90-100, 126-130.
Gyorgy, B., T. G. Szabo, M. Pasztoi, Z. Pal, P. Misjak, B. Aradi, V. Laszlo, E. Pallinger, E. Pap, A. Kittel, G. Nagy, A. Falus and E. I. Buzas (2011). "Membrane vesicles, current state-of-the-art: emerging role of extracellular vesicles." Cell Mol Life Sci **68**(16): 2667-2688.
Hall, D. H. and W. J. Rice (2015). Electron tomography methods for C. elegans. C. elegans, Methods and Applications. G. Haspel and D. Biron, Humana Press. **in press**.
Hammond, J. W., D. Cai and K. J. Verhey (2008). "Tubulin modifications and their cellular functions." Curr Opin Cell Biol **20**(1): 71-76.
Hao, L., M. Thein, I. Brust-Mascher, G. Civelekoglu-Scholey, Y. Lu, S. Acar, B. Prevo, S. Shaham and J. M. Scholey (2011). "Intraflagellar transport delivers tubulin isotypes to sensory cilium middle and distal segments." Nat Cell Biol **13**(7): 790-798.
Henne, W. M., N. J. Buchkovich and S. D. Emr (2011). "The ESCRT pathway." Dev Cell **21**(1): 77-91.
Hiemstra, T. F., P. D. Charles, T. Gracia, S. S. Hester, L. Gatto, R. Al-Lamki, R. A. Floto, Y. Su, J. N. Skepper, K. S. Lilley and F. E. Karet Frankl (2014). "Human Urinary Exosomes as Innate Immune Effectors." J Am Soc Nephrol.
Hogan, M. C., L. Manganelli, J. R. Woollard, A. I. Masyuk, T. V. Masyuk, R. Tammachote, B. Q. Huang, A. A. Leontovich, T. G. Beito, B. J. Madden, M. C. Charlesworth, V. E. Torres, N. F. LaRusso, P. C. Harris and C. J. Ward (2009). "Characterization of PKD protein-positive exosome-like vesicles." J Am Soc Nephrol **20**(2): 278-288.
Hogan, M. C., L. Manganelli, J. R. Woollard, A. I. Masyuk, T. V. Masyuk, R. Tammachote, B. Q. Huang, A. A. Leontovich, T. G. Beito, B. J. Madden, M. C. Charlesworth, V. E. Torres, N. F. LaRusso, P. C. Harris and C. J. Ward (2009). "Characterization of PKD protein-positive exosome-like vesicles." Journal of the American Society of Nephrology : JASN **20**(2): 278-288.
Hu, J., S. G. Wittekind and M. M. Barr (2007). "STAM and Hrs Down-Regulate Ciliary TRP Receptors." Mol Biol Cell **18**(9): 3277-3289.
Hurd, D. D., R. M. Miller, L. Nunez and D. S. Portman (2010). "Specific alpha- and beta-tubulin isotypes optimize the functions of sensory Cilia in Caenorhabditis elegans." Genetics **185**(3): 883-896.
Hurd, T., W. Zhou, P. Jenkins, C. J. Liu, A. Swaroop, H. Khanna, J. Martens, F. Hildebrandt and B. Margolis (2010). "The retinitis pigmentosa protein RP2 interacts with polycystin 2 and regulates cilia-mediated vertebrate development." Hum Mol Genet **19**(22): 4330-4344.

Ikegami, K., R. L. Heier, M. Taruishi, H. Takagi, M. Mukai, S. Shimma, S. Taira, K. Hatanaka, N. Morone, I. Yao, P. K. Campbell, S. Yuasa, C. Janke, G. R. Macgregor and M. Setou (2007). "Loss of alpha-tubulin polyglutamylation in ROSA22 mice is associated with abnormal targeting of KIF1A and modulated synaptic function." Proc Natl Acad Sci U S A **104**(9): 3213-3218.
Insinna, C. and J. C. Besharse (2008). "Intraflagellar transport and the sensory outer segment of vertebrate photoreceptors." Dev Dyn **237**(8): 1982-1992.
Janke, C. (2014). "The tubulin code: molecular components, readout mechanisms, and functions." The Journal of cell biology **206**(4): 461-472.
Janke, C. (2014). "The tubulin code: molecular components, readout mechanisms, and functions." J Cell Biol **206**(4): 461-472.
Janke, C. and J. C. Bulinski (2011). "Post-translational regulation of the microtubule cytoskeleton: mechanisms and functions." Nature reviews. Molecular cell biology **12**(12): 773-786.
Janke, C., K. Rogowski, D. Wloga, C. Regnard, A. V. Kajava, J. M. Strub, N. Temurak, J. van Dijk, D. Boucher, A. van Dorsselaer, S. Suryavanshi, J. Gaertig and B. Edde (2005). "Tubulin polyglutamylase enzymes are members of the TTL domain protein family." Science **308**(5729): 1758-1762.
Jauregui, A. R., K. C. Nguyen, D. H. Hall and M. M. Barr (2008). "The Caenorhabditis elegans nephrocystins act as global modifiers of cilium structure." J Cell Biol **180**(5): 973-988.
Jenkins, P. M., T. W. Hurd, L. Zhang, D. P. McEwen, R. L. Brown, B. Margolis, K. J. Verhey and J. R. Martens (2006). "Ciliary targeting of olfactory CNG channels requires the CNGB1b subunit and the kinesin-2 motor protein, KIF17." Curr Biol **16**(12): 1211-1216.
Jiang, L., B. M. Tam, G. Ying, S. Wu, W. W. Hauswirth, J. M. Frederick, O. L. Moritz and W. Baehr (2015). "Kinesin family 17 (osmotic avoidance abnormal-3) is dispensable for photoreceptor morphology and function." FASEB J.
Kaletsky, R., A. B. Williams, R. Arey, V. Lakhina, J. L. Landis and C. T. Murphy (in review). "Transcriptional profiling of isolated adult C. elegans neurons identifies the neuronal IIS/FOXO transcriptome and a new regulator of axon regeneration

."
Kaletta, T., M. Van Der Craen, A. Van Geel, N. Dewulf, T. Bogaert, M. Branden, K. V. King, M. Buechner, R. Barstead, D. Hyink, H. P. Li, L. Geng, C. Burrow and P. Wilson (2003). "Towards understanding the polycystins." Nephron **93**(1): E9-E17.
Kastner, S., I. J. Thiemann, G. Dekomien, E. Petrasch-Parwez, S. Schreiber, D. A. Akkad, W. M. Gerding, S. Hoffjan, S. Gunes, S. Gunes, H. Bagci and J. T. Epplen (2015). "Exome Sequencing Reveals AGBL5 as Novel Candidate Gene and Additional Variants for Retinitis Pigmentosa in Five Turkish Families." Invest Ophthalmol Vis Sci **56**(13): 8045-8053.
Kimura, Y., N. Kurabe, K. Ikegami, K. Tsutsumi, Y. Konishi, O. I. Kaplan, H. Kunitomo, Y. Iino, O. E. Blacque and M. Setou (2010). "Identification of tubulin deglutamylase among Caenorhabditis elegans and mammalian cytosolic carboxypeptidases (CCPs)." J Biol Chem **285**(30): 22936-22941.
Konno, A., K. Ikegami, Y. Konishi, H. J. Yang, M. Abe, M. Yamazaki, K. Sakimura, I. Yao, K. Shiba, K. Inaba and M. Setou (2016). "Doublet 7 shortening, doublet 5-preferential poly-Glu reduction, and beating stall of sperm flagella in Ttll9-/- mice." J Cell Sci.

Kremer, J. R., D. N. Mastronarde and J. R. McIntosh (1996). "Computer visualization of three-dimensional image data using IMOD." J Struct Biol **116**(1): 71-76.
Kubo, T., H. A. Yanagisawa, T. Yagi, M. Hirono and R. Kamiya (2010). "Tubulin polyglutamylation regulates axonemal motility by modulating activities of inner-arm dyneins." Current biology : CB **20**(5): 441-445.
Lechtreck, K. F. and S. Geimer (2000). "Distribution of polyglutamylated tubulin in the flagellar apparatus of green flagellates." Cell motility and the cytoskeleton **47**(3): 219-235.
Lee, G. S., Y. He, E. J. Dougherty, M. Jimenez-Movilla, M. Avella, S. Grullon, D. S. Sharlin, C. Guo, J. A. Blackford, Jr., S. Awasthi, Z. Zhang, S. P. Armstrong, E. C. London, W. Chen, J. Dean and S. S. Simons, Jr. (2013). "Disruption of Ttll5/stamp gene (tubulin tyrosine ligase-like protein 5/SRC-1 and TIF2-associated modulatory protein gene) in male mice causes sperm malformation and infertility." J Biol Chem **288**(21): 15167-15180.
Lee, J. E., J. L. Silhavy, M. S. Zaki, J. Schroth, S. L. Bielas, S. E. Marsh, J. Olvera, F. Brancati, M. Iannicelli, K. Ikegami, A. M. Schlossman, B. Merriman, T. Attie-Bitach, C. V. Logan, I. A. Glass, A. Cluckey, C. M. Louie, J. H. Lee, H. R. Raynes, I. Rapin, I. P. Castroviejo, M. Setou, C. Barbot, E. Boltshauser, S. F. Nelson, F. Hildebrandt, C. A. Johnson, D. A. Doherty, E. M. Valente and J. G. Gleeson (2012). "CEP41 is mutated in Joubert syndrome and is required for tubulin glutamylation at the cilium." Nat Genet **44**(2): 193-199.
Lener, T., M. Gimona, L. Aigner, V. Borger, E. Buzas, G. Camussi, N. Chaput, D. Chatterjee, F. A. Court, H. A. Del Portillo, L. O'Driscoll, S. Fais, J. M. Falcon-Perez, U. Felderhoff-Mueser, L. Fraile, Y. S. Gho, A. Gorgens, R. C. Gupta, A. Hendrix, D. M. Hermann, A. F. Hill, F. Hochberg, P. A. Horn, D. de Kleijn, L. Kordelas, B. W. Kramer, E. M. Kramer-Albers, S. Laner-Plamberger, S. Laitinen, T. Leonardi, M. J. Lorenowicz, S. K. Lim, J. Lotvall, C. A. Maguire, A. Marcilla, I. Nazarenko, T. Ochiya, T. Patel, S. Pedersen, G. Pocsfalvi, S. Pluchino, P. Quesenberry, I. G. Reischl, F. J. Rivera, R. Sanzenbacher, K. Schallmoser, I. Slaper-Cortenbach, D. Strunk, T. Tonn, P. Vader, B. W. van Balkom, M. Wauben, S. E. Andaloussi, C. Thery, E. Rohde and B. Giebel (2015). "Applying extracellular vesicles based therapeutics in clinical trials - an ISEV position paper." Journal of extracellular vesicles **4**: 30087.
Li, C. J., Y. Liu, Y. Chen, D. Yu, K. J. Williams and M. L. Liu (2013). "Novel proteolytic microvesicles released from human macrophages after exposure to tobacco smoke." Am J Pathol **182**(5): 1552-1562.
Linck, R., X. Fu, J. Lin, C. Ouch, A. Schefter, W. Steffen, P. Warren and D. Nicastro (2014). "Insights into the structure and function of ciliary and flagellar doublet microtubules: tektins, Ca2+-binding proteins, and stable protofilaments." J Biol Chem **289**(25): 17427-17444.
Liu, K. S. and P. W. Sternberg (1995). "Sensory regulation of male mating behavior in Caenorhabditis elegans." Neuron **14**(1): 79-89.
Lockhead, D., E. M. Schwarz, R. O'Hagan, S. Bellotti, M. Krieg, M. M. Barr, A. R. Dunn, P. W. Sternberg and M. B. Goodman (2016). "The tubulin repertoire of C. elegans sensory neurons and its context-dependent role in process outgrowth." Mol Biol Cell.
Logozzi, M., A. De Milito, L. Lugini, M. Borghi, L. Calabro, M. Spada, M. Perdicchio, M. L. Marino, C. Federici, E. Iessi, D. Brambilla, G. Venturi, F. Lozupone, M. Santinami, V. Huber, M. Maio, L. Rivoltini and S. Fais (2009). "High levels of exosomes expressing CD63 and caveolin-1 in plasma of melanoma patients." PLoS One **4**(4): e5219.

Ludewig, A. H. and F. C. Schroeder (2013). "Ascaroside signaling in C. elegans." WormBook: 1-22.
Maguire, J. E., M. Silva, K. C. Nguyen, E. Hellen, A. D. Kern, D. H. Hall and M. M. Barr (2015). "Myristoylated CIL-7 regulates ciliary extracellular vesicle biogenesis." Mol Biol Cell **26**(15): 2823-2832.
Maguire, J. E., M. Silva, K. C. Nguyen, E. Hellen, A. D. Kern, D. H. Hall and M. M. Barr (2015). "Myristoylated CIL-7 Regulates Ciliary Extracellular Vesicle Biogenesis." Mol Biol Cell.
Marchler-Bauer, A., M. K. Derbyshire, N. R. Gonzales, S. Lu, F. Chitsaz, L. Y. Geer, R. C. Geer, J. He, M. Gwadz, D. I. Hurwitz, C. J. Lanczycki, F. Lu, G. H. Marchler, J. S. Song, N. Thanki, Z. Wang, R. A. Yamashita, D. Zhang, C. Zheng and S. H. Bryant (2015). "CDD: NCBI's conserved domain database." Nucleic Acids Res **43**(Database issue): D222-226.
Maric, D., B. S. McGwire, K. T. Buchanan, C. L. Olson, B. T. Emmer, C. L. Epting and D. M. Engman (2011). "Molecular determinants of ciliary membrane localization of Trypanosoma cruzi flagellar calcium-binding protein." J Biol Chem **286**(38): 33109-33117.
Masyuk, A. I., B. Q. Huang, C. J. Ward, S. A. Gradilone, J. M. Banales, T. V. Masyuk, B. Radtke, P. L. Splinter and N. F. LaRusso (2010). "Biliary exosomes influence cholangiocyte regulatory mechanisms and proliferation through interaction with primary cilia." Am J Physiol Gastrointest Liver Physiol **299**(4): G990-999.
Mathivanan, S., H. Ji and R. J. Simpson (2010). "Exosomes: extracellular organelles important in intercellular communication." J Proteomics **73**(10): 1907-1920.
Maures, T. J., L. N. Booth, B. A. Benayoun, Y. Izrayelit, F. C. Schroeder and A. Brunet (2013). "Males Shorten the Life Span of C. elegans Hermaphrodites via Secreted Compounds." Science.
Maures, T. J., L. N. Booth, B. A. Benayoun, Y. Izrayelit, F. C. Schroeder and A. Brunet (2014). "Males shorten the life span of C. elegans hermaphrodites via secreted compounds." Science **343**(6170): 541-544.
Miller, R. M. and D. S. Portman (2010). "A latent capacity of the C. elegans polycystins to disrupt sensory transduction is repressed by the single-pass ciliary membrane protein CWP-5." Dis Model Mech **3**(7-8): 441-450.
Morsci, N. S. and M. M. Barr (2011). "Kinesin-3 KLP-6 regulates intraflagellar transport in male-specific cilia of Caenorhabditis elegans." Curr Biol **21**(14): 1239-1244.
Morsci, N. S. and M. M. Barr (2011). "Kinesin-3 KLP-6 regulates intraflagellar transport in male-specific cilia of Caenorhabditis elegans." Current biology : CB **21**(14): 1239-1244.
Mukhopadhyay, S., Y. Lu, H. Qin, A. Lanjuin, S. Shaham and P. Sengupta (2007). "Distinct IFT mechanisms contribute to the generation of ciliary structural diversity in C. elegans." EMBO J **26**(12): 2966-2980.
Mullen, R. J., E. M. Eicher and R. L. Sidman (1976). "Purkinje cell degeneration, a new neurological mutation in the mouse." Proceedings of the National Academy of Sciences of the United States of America **73**(1): 208-212.
Nisha Patel PhD, M. A. A. P., Hisham Alkuraya MD, Shamsa Anazi MSc, Hadeel Alsharif BSc, Arif O. Khan MD, Asma Sunker BSc, Saleh Al-mohsen MD, Emad B. Abboud MD, Sawsan R. Nowilaty MD, Mohammed Alowain MD, Hamad Al-Zaidan MD, Bandar Al-Saud MD, Ali Alasmari MD, Ghada M. H. Abdel-Salam MD, Mohamed Abouelhoda PhD, Firdous M. Abdulwahab BSc, Niema Ibrahim BSc, Ewa Naim BPharm, Banan Al-Younes MSc, Abeer E. AlMostafa BSc, Abdulelah AlIssa

BSc, Mais Hashem BSc, Olga Buzovetsky PhD, Yong Xiong PhD et al. (2016). "Expanding the clinical, allelic, and locus heterogeneity of retinal dystrophies." Genetics in Medicine **18**(6): 554-562.
O'Hagan, R. and M. M. Barr (2016). "Kymographic Analysis of Transport in an Individual Neuronal Sensory Cilium in Caenorhabditis elegans." Methods Mol Biol **1454**: 107-122.
O'Hagan, R., B. P. Piasecki, M. Silva, P. Phirke, K. C. Nguyen, D. H. Hall, P. Swoboda and M. M. Barr (2011). "The tubulin deglutamylase CCPP-1 regulates the function and stability of sensory cilia in C. elegans." Current biology : CB **21**(20): 1685-1694.
O'Hagan, R., B. P. Piasecki, M. Silva, P. Phirke, K. C. Nguyen, D. H. Hall, P. Swoboda and M. M. Barr (2011). "The tubulin deglutamylase CCPP-1 regulates the function and stability of sensory cilia in C. elegans." Curr Biol **21**(20): 1685-1694.
O'Hagan, R., J. Wang and M. M. Barr (2014). "Mating behavior, male sensory cilia, and polycystins in Caenorhabditis elegans." Semin Cell Dev Biol **33**: 25-33.
Pampliega, O., I. Orhon, B. Patel, S. Sridhar, A. Diaz-Carretero, I. Beau, P. Codogno, B. H. Satir, P. Satir and A. M. Cuervo (2013). "Functional interaction between autophagy and ciliogenesis." Nature **502**(7470): 194-200.
Pan, X., G. Ou, G. Civelekoglu-Scholey, O. E. Blacque, N. F. Endres, L. Tao, A. Mogilner, M. R. Leroux, R. D. Vale and J. M. Scholey (2006). "Mechanism of transport of IFT particles in C. elegans cilia by the concerted action of kinesin-II and OSM-3 motors." J Cell Biol **174**(7): 1035-1045.
Pathak, N., T. Obara, S. Mangos, Y. Liu and I. A. Drummond (2007). "The zebrafish fleer gene encodes an essential regulator of cilia tubulin polyglutamylation." Mol Biol Cell **18**(11): 4353-4364.
Pazour, G. J., J. T. San Agustin, J. A. Follit, J. L. Rosenbaum and G. B. Witman (2002). "Polycystin-2 localizes to kidney cilia and the ciliary level is elevated in orpk mice with polycystic kidney disease." Curr Biol **12**: R378-R380.
Peden, E. M. and M. M. Barr (2005). "The KLP-6 kinesin is required for male mating behaviors and polycystin localization in Caenorhabditis elegans." Curr Biol **15**(5): 394-404.
Peden, E. M. and M. M. Barr (2005). "The KLP-6 Kinesin Is Required for Male Mating Behaviors and Polycystin Localization in Caenorhabditis elegans." Current Biology **15**(5): 394-404.
Perkins, L. A., E. M. Hedgecock, J. N. Thomson and J. G. Culotti (1986). "Mutant sensory cilia in the nematode Caenorhabditis elegans." Dev Biol **117**(2): 456-487.
Phillips, D. M. (1969). "Exceptions to the prevailing pattern of tubules (9 + 9 + 2) in the sperm flagella of certain insect species." J Cell Biol **40**(1): 28-43.
Pisitkun, T., R. F. Shen and M. A. Knepper (2004). "Identification and proteomic profiling of exosomes in human urine." Proc Natl Acad Sci U S A **101**(36): 13368-13373.
Portman, D. S. and S. W. Emmons (2004). "Identification of C. elegans sensory ray genes using whole-genome expression profiling." Dev Biol **270**(2): 499-512.
Prevo, B., P. Mangeol, F. Oswald, J. M. Scholey and E. J. Peterman (2015). "Functional differentiation of cooperating kinesin-2 motors orchestrates cargo import and transport in C. elegans cilia." Nat Cell Biol.
Prevo, B., P. Mangeol, F. Oswald, J. M. Scholey and E. J. Peterman (2015). "Functional differentiation of cooperating kinesin-2 motors orchestrates cargo import and transport in C. elegans cilia." Nat Cell Biol **17**(12): 1536-1545.

Prigent, Y., M. L. Kann, H. Lach-Gar, I. Pechart and J. P. Fouquet (1996). "Glutamylated tubulin as a marker of microtubule heterogeneity in the human sperm flagellum." Mol Hum Reprod **2**(8): 573-581.
Qin, H., J. L. Rosenbaum and M. M. Barr (2001). "An autosomal recessive polycystic kidney disease gene homolog is involved in intraflagellar transport in C. elegans ciliated sensory neurons." Curr Biol **11**(6): 457-461.
Raff, E. C., J. D. Fackenthal, J. A. Hutchens, H. D. Hoyle and F. R. Turner (1997). "Microtubule Architecture Specified by a β-Tubulin Isoform." Science (New York, NY) **275**(5296): 70-73.
Rao, K. N., M. Anand and H. Khanna (2016). "The carboxyl terminal mutational hotspot of the ciliary disease protein RPGRORF15 (retinitis pigmentosa GTPase regulator) is glutamylated in vivo." Biol Open **5**(4): 424-428.
Raposo, G. and W. Stoorvogel (2013). "Extracellular vesicles: exosomes, microvesicles, and friends." J Cell Biol **200**(4): 373-383.
Rodriguez de la Vega, M., R. G. Sevilla, A. Hermoso, J. Lorenzo, S. Tanco, A. Diez, L. D. Fricker, J. M. Bautista and F. X. Aviles (2007). "Nna1-like proteins are active metallocarboxypeptidases of a new and diverse M14 subfamily." Faseb J **21**(3): 851-865.
Rodriguez de la Vega Otazo, M., J. Lorenzo, O. Tort, F. X. Aviles and J. M. Bautista (2013). "Functional segregation and emerging role of cilia-related cytosolic carboxypeptidases (CCPs)." FASEB J **27**(2): 424-431.
Rogowski, K., J. van Dijk, M. M. Magiera, C. Bosc, J.-C. Deloulme, A. Bosson, L. Peris, N. D. Gold, B. Lacroix, M. Bosch Grau, N. Bec, C. Larroque, S. Desagher, M. Holzer, A. Andrieux, M.-J. Moutin and C. Janke (2010). "A family of protein-deglutamylating enzymes associated with neurodegeneration." Cell **143**(4): 564-578.
Rogowski, K., J. van Dijk, M. M. Magiera, C. Bosc, J. C. Deloulme, A. Bosson, L. Peris, N. D. Gold, B. Lacroix, M. B. Grau, N. Bec, C. Larroque, S. Desagher, M. Holzer, A. Andrieux, M. J. Moutin and C. Janke (2010). "A family of protein-deglutamylating enzymes associated with neurodegeneration." Cell **143**(4): 564-578.
Roll-Mecak, A. (2015). "Intrinsically disordered tubulin tails: complex tuners of microtubule functions?" Semin Cell Dev Biol **37**: 11-19.
Rosenbaum, J. L. and G. B. Witman (2002). "Intraflagellar transport." Nat Rev Mol Cell Biol. **3**(11): 813-825.
S, E. L. A., I. Mager, X. O. Breakefield and M. J. Wood (2013). "Extracellular vesicles: biology and emerging therapeutic opportunities." Nat Rev Drug Discov **12**(5): 347-357.
Schindelin, J., I. Arganda-Carreras, E. Frise and V. Kaynig (2012). "Fiji: an open-source platform for biological-image analysis." Nature **9**(7): 676-682.
Scholey, J. M. (2008). "Intraflagellar transport motors in cilia: moving along the cell's antenna." J Cell Biol **180**(1): 23-29.
Schroeder, N. E., R. J. Androwski, A. Rashid, H. Lee, J. Lee and M. M. Barr (2013). "Dauer-Specific Dendrite Arborization in C. elegans Is Regulated by KPC-1/Furin." Curr Biol **23**(16): 1527-1535.
Sergouniotis, P. I., C. Chakarova, C. Murphy, M. Becker, E. Lenassi, G. Arno, M. Lek, D. G. MacArthur, U. C.-E. Consortium, S. S. Bhattacharya, A. T. Moore, G. E. Holder, A. G. Robson, U. Wolfrum, A. R. Webster and V. Plagnol (2014). "Biallelic variants in TTLL5, encoding a tubulin glutamylase, cause retinal dystrophy." Am J Hum Genet **94**(5): 760-769.

Shen, B., N. Wu, J. M. Yang and S. J. Gould (2011). "Protein targeting to exosomes/microvesicles by plasma membrane anchors." J Biol Chem **286**(16): 14383-14395.
Sherlekar, A. L., A. Janssen, M. S. Siehr, P. K. Koo, L. Caflisch, M. Boggess and R. Lints (2013). "The C. elegans male exercises directional control during mating through cholinergic regulation of sex-shared command interneurons." PLoS One **8**(4): e60597.
Shi, A., S. Pant, Z. Balklava, C. C. Chen, V. Figueroa and B. D. Grant (2007). "A novel requirement for C. elegans Alix/ALX-1 in RME-1-mediated membrane transport." Curr Biol **17**(22): 1913-1924.
Silva, M., N. S. Morsci, K. C. Nguyen, A. Rizvi, C. Rongo, D. H. Hall and M. M. Barr (2017). "α-tubulin isotype orchestrates ciliary microtubule architecture, IFT, and extracellular vesicle biogenesis and bioactivity." Current Biology **in press**.
Sirajuddin, M., L. M. Rice and R. D. Vale (2014). "Regulation of microtubule motors by tubulin isotypes and post-translational modifications." Nat Cell Biol **16**(4): 335-344.
Snow, J. J., G. Ou, A. L. Gunnarson, M. R. Walker, H. M. Zhou, I. Brust-Mascher and J. M. Scholey (2004). "Two anterograde intraflagellar transport motors cooperate to build sensory cilia on C. elegans neurons." Nat Cell Biol **6**(11): 1109-1113.
Snow, J. J., G. Ou, A. L. Gunnarson, M. R. Walker, H. M. Zhou, I. Brust-Mascher and J. M. Scholey (2004). "Two anterograde intraflagellar transport motors cooperate to build sensory cilia on C. elegans neurons." Nature cell biology **6**(11): 1109-1113.
Song, Y. H. and E. Mandelkow (1995). "The anatomy of flagellar microtubules: polarity, seam, junctions, and lattice." The Journal of Cell Biology **128**(1-2): 81-94.
Stepanek, L. and G. Pigino (2016). "Microtubule doublets are double-track railways for intraflagellar transport trains." Science **352**(6286): 721-724.
Sulston, J. E., D. G. Albertson and J. N. Thomson (1980). "The *Caenorhabditis elegans* male: postembryonic development of nongonadal structures." Dev Biol **78**(2): 542-576.
Sun, X., J. H. Park, J. Gumerson, Z. Wu, A. Swaroop, H. Qian, A. Roll-Mecak and T. Li (2016). "Loss of RPGR glutamylation underlies the pathogenic mechanism of retinal dystrophy caused by TTLL5 mutations." Proc Natl Acad Sci U S A **113**(21): E2925-2934.
Tanaka, Y., Y. Okada and N. Hirokawa (2005). "FGF-induced vesicular release of Sonic hedgehog and retinoic acid in leftward nodal flow is critical for left-right determination." Nature **435**(7039): 172-177.
Taschner, M. and E. Lorentzen (2016). "The Intraflagellar Transport Machinery." Cold Spring Harb Perspect Biol **8**(10).
Tischfield, M. A., G. Y. Cederquist, M. L. Gupta, Jr. and E. C. Engle (2011). "Phenotypic spectrum of the tubulin-related disorders and functional implications of disease-causing mutations." Curr Opin Genet Dev **21**(3): 286-294.
Topalidou, I., C. Keller, N. Kalebic, K. C. Q. Nguyen, H. Somhegyi, K. A. Politi, P. Heppenstall, D. H. Hall and M. Chalfie (2012). "Genetically Separable Functions of the MEC-17 Tubulin Acetyltransferase Affect Microtubule Organization." Current Biology VL - **22**(12): 1057-1065.
Tsuji, T., K. Matsuo, T. Nakahari, Y. Marunaka and T. Yokoyama (2016). "Structural basis of the Inv compartment and ciliary abnormalities in Inv/nphp2 mutant mice." Cytoskeleton (Hoboken) **73**(1): 45-56.

Vader, P., X. O. Breakefield and M. J. Wood (2014). "Extracellular vesicles: emerging targets for cancer therapy." Trends Mol Med.
van Dijk, J., J. Miro, J. M. Strub, B. Lacroix, A. van Dorsselaer, B. Edde and C. Janke (2008). "Polyglutamylation is a post-translational modification with a broad range of substrates." The Journal of biological chemistry **283**(7): 3915-3922.
van Dijk, J., K. Rogowski, J. Miro, B. Lacroix, B. Edde and C. Janke (2007). "A targeted multienzyme mechanism for selective microtubule polyglutamylation." Molecular cell **26**(3): 437-448.
Venancio, T. M. and L. Aravind (2010). "CYSTM, a novel cysteine-rich transmembrane module with a role in stress tolerance across eukaryotes." Bioinformatics **26**(2): 149-152.
Verhey, K. J. and J. Gaertig (2007). "The tubulin code." Cell Cycle **6**(17): 2152-2160.
Vogel, P., G. Hansen, G. Fontenot and R. Read (2010). "Tubulin tyrosine ligase-like 1 deficiency results in chronic rhinosinusitis and abnormal development of spermatid flagella in mice." Vet Pathol **47**(4): 703-712.
Wang, J. and M. M. Barr (2016). "Ciliary Extracellular Vesicles: Txt Msg Organelles." Cell Mol Neurobiol **36**(3): 449-457.
Wang, J., R. Kaletsky, M. Silva, A. Williams, L. A. Haas, R. J. Androwski, J. N. Landis, C. Patrick, A. Rashid, D. Santiago-Martinez, M. Gravato-Nobre, J. Hodgkin, D. H. Hall, C. T. Murphy and M. M. Barr (2015). "Cell-Specific Transcriptional Profiling of Ciliated Sensory Neurons Reveals Regulators of Behavior and Extracellular Vesicle Biogenesis." Curr Biol **25**(24): 3232-3238.
Wang, J., M. Silva, L. A. Haas, N. S. Morsci, K. C. Nguyen, D. H. Hall and M. M. Barr (2014). "C. elegans ciliated sensory neurons release extracellular vesicles that function in animal communication." Current biology : CB **24**(5): 519-525.
Wang, J., M. Silva, L. A. Haas, N. S. Morsci, K. C. Nguyen, D. H. Hall and M. M. Barr (2014). "C. elegans Ciliated Sensory Neurons Release Extracellular Vesicles that Function in Animal Communication." Curr Biol **24**(5): 519-525.
Ward, S., N. Thomson, J. G. White and S. Brenner (1975). "Electron microscopical reconstruction of the anterior sensory anatomy of the nematode *Caenorhabditis elegans*." J Comp Neurol **160**(3): 313-337.
Ward, S., N. Thomson, J. G. White and S. Brenner (1975). "Electron microscopical reconstruction of the anterior sensory anatomy of the nematode Caenorhabditis elegans.?2UU." J Comp Neurol **160**(3): 313-337.
Weimer, R. (2006). Preservation of C. elegans Tissue Via High-Pressure Freezing and Freeze-Substitution for Ultrastructural Analysis and Immunocytochemistry. K. Strange. New Jersey, Humana Press. **351:** 203-221-222.
Williams, C. L., J. C. McIntyre, S. R. Norris, P. M. Jenkins, L. Zhang, Q. Pei, K. Verhey and J. R. Martens (2014). "Direct evidence for BBSome-associated intraflagellar transport reveals distinct properties of native mammalian cilia." Nat Commun **5**: 5813.
Winey, M. and E. O'Toole (2014). "Centriole structure." Phil. Trans. R. Soc. B **369**(1650): 20130457-20130398.
Wolf, D., A. Lubk and H. Lichte (2014). "Weighted simultaneous iterative reconstruction technique for single-axis tomography." Ultramicroscopy **136 IS -**: 15-25.
Wood, C. R., K. Huang, D. R. Diener and J. L. Rosenbaum (2013). "The cilium secretes bioactive ectosomes." Curr Biol **23**(10): 906-911.

Wood, C. R. and J. L. Rosenbaum (2015). "Ciliary ectosomes: transmissions from the cell's antenna." Trends Cell Biol **25**(5): 276-285.
Woolley, D. M. and S. N. Nickels (1985). "Microtubule termination patterns in mammalian sperm flagella." J Ultrastruct Res **90**(3): 221-234.
Wright, K. J., L. M. Baye, A. Olivier-Mason, S. Mukhopadhyay, L. Sang, M. Kwong, W. Wang, P. R. Pretorius, V. C. Sheffield, P. Sengupta, D. C. Slusarski and P. K. Jackson (2011). "An ARL3-UNC119-RP2 GTPase cycle targets myristoylated NPHP3 to the primary cilium." Genes Dev **25**(22): 2347-2360.
http://www.wormbase.org. from http://www.wormbase.org.
Xie, P. (2013). "TRAF molecules in cell signaling and in human diseases." J Mol Signal **8**(1): 7.
Yoder, B. K., X. Hou and L. M. Guay-Woodford (2002). "The polycystic kidney disease proteins, polycystin-1, polycystin-2, polaris, and cystin, are co-localized in renal cilia." J Am Soc Nephrol **13**(10): 2508-2516.
Yu, I., C. P. Garnham and A. Roll-Mecak (2015). "Writing and Reading the Tubulin Code." J Biol Chem **290**(28): 17163-17172.
Zhao, C., Y. Omori, K. Brodowska, P. Kovach and J. Malicki (2012). "Kinesin-2 family in vertebrate ciliogenesis." Proc Natl Acad Sci U S A **109**(7): 2388-2393.

Key findings

Chapter One and Appendix A

Adult CEM ciliary axoneme composed of microtubule doublets that splay to form both A- and B-tubule singlets

Alpha tubulin TBA-6 is required for splayed doublet architecture of CEM axoneme

TBA-6 is required for CEM specific IFT motor cargo coordination.

TBA-6 is required for extracellular vesicle release, composition, and bioactivity.

Chapter Two and Appendix A

Splayed doublets in adult CEM axoneme is generated by first generating intact doublets and then unzipping

At least some of the nine doublets in the CEM cilia transition zone are generated *de novo* in the absence of centrosome microtubules

Microtubule doublets are generated by first forming complete A-tubule singlet subsequent addition of the incomplete B-tubules.

Developing CEM cilia length is established via a few pioneer microtubules in at L3

Axoneme maturation coincide with CEM morphogenesis and sexual maturation of the male

Chapter Three, Six and Appendix B

Posttranslational glutamylation regulate ciliary B-tubule architecture and stability in both CEM and amphid cilia. Lower levels of glutamylation (resulting from loss of *ttll-11*) leads to B-tubule stability while excessive levels (resulting from *ccpp-1* mutation) leads to instability.

In terms of B-tubule ultrastructure *ttll-11* is epistatic to *ccpp-1*

Chapter Four, Five, and Appendix C

In wild type CEM cilia contain vesicles in periciliary membrane compartment (PCMC) at the base of the cilium and in the region surrounding it.

In *pmk-1* mutant background CEM cilia transition zone contain less than nine microtubule doublets and resemble an immature cilium

Timeline of Findings